The Effects of Tyrosine Kinase Inhibition on Bone Remodelling

Kate Vandyke

Myeloma Research Laboratory
Bone and Cancer Laboratories
Department of Haematology
Institute of Medical and Veterinary Science
&
Department of Medicine
Faculty of Health Sciences
The University of Adelaide

A thesis submitted to the University of Adelaide
for the degree of Doctor of Philosophy
July 2010

Table of Contents

Abstract

Imatinib is a rationally-designed tyrosine kinase inhibitor that is a highly-successful treatment for chronic myeloid leukaemia (CML) and gastrointestinal stromal tumours. In a retrospective study, it was previously shown that imatinib therapy is associated with an increase in trabecular bone volume. In this current study, a prospective analysis of bone indices in imatinib-treated CML patients was carried out to determine the mechanism responsible for this altered bone remodelling. Imatinib therapy resulted in an increase in trabecular bone volume and trabecular thickness in iliac crest trephines, relative to prior to treatment. This was associated with a significant decrease in osteoclast numbers, assessed histologically, and in serum levels of a marker of osteoclast activity. Osteoblast numbers were not altered by up to 12 months of treatment. These data suggest that imatinib dysregulates bone remodelling by inhibiting osteoclast activity.

It was next examined whether a second-generation tyrosine kinase inhibitor, dasatinib, which is successfully used to treat CML in imatinib-resistant patients, could similarly alter bone remodelling. Dasatinib treatment significantly increased trabecular bone volume and trabecular thickness in a rat model of normal bone remodelling. This was primarily attributable to inhibition of osteoclast activity, at least in part through inhibition of Fms. These studies show for the first time that dasatinib treatment is associated with a decrease in osteoclast formation and activity *in vitro* and *in vivo*, suggesting that decreased bone resorption is a likely side-effect of dasatinib therapy. Additionally, these studies highlight the possibility that both imatinib and dasatinib may represent potential treatments for diseases characterised by aberrant bone loss.

While imatinib is well-tolerated in children, emerging data suggest that long-term therapy may result in decelerated growth in juvenile CML patients. To date, there are no reports suggesting a mechanism for altered growth in imatinib-treated paediatric patients. In a normal mature rat model, we found that daily treatment with imatinib or dasatinib significantly decreased growth plate thickness at the proximal tibia, with a complete fusion of the growth plate by 12 weeks of treatment in imatinib-treated animals. Furthermore, chondrocyte proliferation and activity were significantly decreased by imatinib and dasatinib treatment *in vitro*, through a mechanism that may involve inhibition of PDGFRβ. The dramatic effect of imatinib and dasatinib on growth plate morphology in rats suggests that growth plate closure should be investigated as a potential mechanism for inhibited growth in pre-pubescent patients receiving imatinib.

Declaration

This work contains no material which has been accepted for the award of any other degree or diploma in any university or other tertiary institution and, to the best of my knowledge and belief, contains no material previously published or written by another person, except where due reference has been made in the text. I give consent to this copy of my thesis, when deposited in the University Library, being made available for loan and photocopying, subject to the provisions of the Copyright Act 1968. I also give permission for the digital version of my thesis to be made available on the web, via the University's digital research repository, the Library catalogue, the Australasian Digital Theses Program (ADTP) and also through web search engines, unless permission has been granted by the University to restrict access for a period of time.

Signed

……

Kate Vandyke

Acknowledgements

First I would like to thank my wonderful supervisors A/Prof. Andrew Zannettino, Dr Stephen Fitter and Dr Andrea Dewar. Thanks to Andrew Zannettino for his unending optimism, praise and support throughout this project and for generally being the best supervisor I could hope for. I am very grateful to Steve Fitter for always being available to bounce ideas off and to answer my many inane questions. I very much appreciate him taking the time to go through the nitty gritty details of all my writing, picking up on the smallest possible errors. Any mistakes that have made it into this thesis are entirely my own! Thanks also must go to Dr Andrea Dewar for always being there to offer guidance and support throughout my PhD, even at the times when I'm sure she would rather have forgotten all about science!

I am forever grateful to all my colleagues in the Bone and Cancer Laboratories for being such wonderful bunch of people and for making work a happy, fun and, sometimes, crazy place to be. Special thanks need to go to a few of you: Dr Peter "don't you know who I am?" Diamond for all his help with animal experiments, particularly for stepping in and helping scan my rats on those days when I'd been going non-stop all day and really needed to break for noodles; to Jenny Drew for conducting beautiful histology on the patient bone samples; to Dr Sally "the font of all knowledge" Martin for always being there with the answer to any possible question (she is truly all-knowing); and to Danijela "Danni-Julia" Menicanin for all her help with histology and for love, hugs and good will going through the crazy write-up time together with me - it has helped tremendously to have someone to share this process with. I also must give a big thanks to Dr Tony Cambareri for all his help with printing my thesis; his expertise helped everything go a whole lot more smoothly. Thank you also to the rest of the lab members, past and present: Dr Agnes Arthur, Amanda Davis, Catherine Gan, Dr Jim Cakouros, Jimin Xiong, Kate Pilkington, Dr Kim Hynes, Krzysztof Mrozik, Locky Cooper, Mary Matthews, Dr Naohisa Wada, Penny Kostakis, Dr Peter Psaltis, Romana Panagopoulos, Sandra Isenmann, Dr Sharon Williams, Sharon Paton and A/Prof. Stan Gronthos; I truly could not have asked for a better group to work with.

Among the many other people I am indebted to for help with this project, I must single out a few individuals: Peter McNeil and Rebecca Sawyer for teaching me the ins and outs of methacrylate embedding; Peter Self at Adelaide Microscopy for always being available

with help and advice when μ-CT wasn't going as it should; Chris Schultz from the Royal Adelaide Hospital for carrying out all the DXA scans of my rats and patients; Natalie Sims at St Vincent's Institute for passing on her not inconsiderable knowledge of bone histomorphometry and for letting me hole myself up in her microscope room on several occasions to analyse slides for days on end. Cheers also to all the staff at Veterinary Services, IMVS, especially Brian Lewis, Brigitt Hines, Kelly Wicks, Briony Gliddon, Dr Tim Kuchel and of course to Behzad Baradaran who did such a great job gavaging my rats. I'd also like to thank the staff at Haematology Clinical Trials, in particular Lisa Carne and Christine Hoare, who did a tremendous job organising the TIDEL II study. Particular thanks must also go to all the patients who donated their time and body parts to my study: you are all amazing.

Thanks to my parents Tina and John and Mel for all your love, support and generosity throughout the past 8 years of university. Without your help I never could have made it this far and I am eternally grateful for it. To my sister Jen for letting me stay on her couch in Melbourne, for being available for hours of telephone calls when I needed to unwind and for understanding when I didn't have the time to call. I also need to give a heartfelt thanks to my substitute parents in Adelaide, Julie and Tony Atkins, for doing such a great job caring for and, particularly, feeding James, Joe and I, when I haven't had the time to do it! I am so very lucky to have such wonderful in-laws.

The biggest thank you must go to my incomparable partner James for his inexhaustible patience, encouragement and support (among rather a lot else).

Thank you

Abbreviations

ABC	adenosine triphosphate-binding cassette transporter
Abl	Abelson kinase
AHSA1	activator of heat shock 90 kDa protein ATPase homologue 1
ALL	acute lymphoblastic leukaemia
α-MEM	α-modified Eagle's medium
ANOVA	analysis of variance
APS	ammonium persulphate
ARG	Abl-related gene
ATCC	American Type Culture Collection
ATP	adenosine triphosphate
ATPase	adenosine triphosphatase
bALP	bone-specific alkaline phosphatase
Bcr	breakpoint cluster region
BCRP	breast cancer resistance protein
BFR	bone formation rate
BID	*bis in die*
BM	bone marrow
BMC	bone mineral content
BMD	bone mineral density
BMP	bone morphogenetic protein
BMU	basic multicellular unit
B.Pm	bone perimeter
BS	bone surface
BSA	bovine serum albumin
BV	bone volume
CA	carbonic anhydrase
c-α-MEM	complete α-modified Eagle's medium
CBF-β	core-binding factor-β
Cbl	Cas-Br-M ecotropic retroviral transforming sequence
c-DMEM	complete Dulbecco's modified Eagle's medium
C/EBP	CCAAT/enhancer binding protein
CML	chronic myeloid leukaemia

CPC	cetyl pyridinyl chloride
CSA	chondroitin sulphate A
CSF1	colony stimulating factor 1
CSF1R	colony stimulating factor 1 receptor
Ct.BV	cortical bone volume
Ct.Th	cortical thickness
CTX-1	C-terminal collagen crosslinks
DDR	collagen-induced discoiddin domain receptor
Dkk	Dickkopff family member
DMEM	Dulbecco's modified Eagle's medium
DMSO	dimethyl sulphoxide
DTT	dithiothreitol
DXA	dual energy X-ray absorptiometry
ECF	enhanced chemifluorescence
EDTA	ethylenediaminetetraacetic acid
EGFR	epidermal growth factor receptor
ELISA	enzyme-linked immunosorbent assay
ERK	extracellular signal-regulated kinase
FAK	focal adhesion kinase
FCS	foetal calf serum
FGF	fibroblast growth factor
Fms	McDonough feline sarcoma viral oncogene homologue
FOS	Finkel-Biskis-Jinkins murine osteosarcoma viral oncogene homologue
FOXO	forkhead box class O
GAG	glycosaminoglycan
GFR	glomerular filtration rate
GH	growth hormone
GIST	gastrointestinal stromal tumours
Grb2	growth factor receptor-bound protein 2
GSK-3β	glycogen synthase kinase-3β
HBSS	Hanks' buffered saline solution
HCl	hydrochloric acid
HEPES	N-2-hydroxyethylpiperazine-N'-2-ethanesulfonic acid

HLA	human leukocyte antigen
HPLC	high-performance liquid chromatography
HSP90	heat shock protein 90 kDa
IC_{50}	inhibitory concentration, 50%
Ig	immunoglobulin
IGF	insulin-like growth factor
Ihh	Indian hedgehog
IKK	IκB kinase
IL	interleukin
IP	intraperitoneally
IRIS	International Randomized Study of Interferon and STI571
JNK	Jun N-terminal kinase
Kit	stem cell factor receptor
Lef	lymphoid enhancer-binding factor
LRP	low density lipoprotein receptor-related protein
MAP2K	mitogen-activated protein kinase kinase
MAR	mineral apposition rate
mBM	mouse bone marrow monocyte
M-CSF	macrophage colony stimulating factor
μ-CT	micro-computed tomography
MDR1	multidrug resistance-1
MEK	extracellular signal-regulated kinase kinase
min.BV	mineralised bone volume
Mitf	microphthalmia-associated transcription factor
mRNA	messenger ribonucleic acid
MS	mineralised surface
NBF	neutral buffered formalin
NFAT	nuclear factor for activated T cells
NF-κB	nuclear factor of κ light polypeptide gene enhancer in B-cells
N.Ob	number of osteoblasts
N.Oc	number of osteoclasts
NQO2	nicotinamide adenine dinucleotide phosphate-oxidase:quinone oxidoreductase 2
NTX	N-telopeptide of collagen crosslinks

Ob.S	osteoblast surface
Oc.S	osteoclast surface
OCT-1	organic cation transporter-1
OPG	osteoprotegerin
OS	osteoid surface
O.Th	osteoid thickness
OV	osteoid volume
P1NP	pro-collagen type I amino-terminal propeptide
PBS	phosphate buffered saline
PDGF	platelet-derived growth factor
PDGFR	platelet-derived growth factor receptor
PEG	polyethylene glycol
PI3K	phosphoinositide-3-kinase
PMSF	phenylmethylsulphonyl fluoride
pQCT	peripheral quantitative computed tomography
PTH	parathyroid hormone
PTHrP	parathyroid hormone-related protein
PVDF	polyvinylidene difluoride
Rac	Ras-related C3 botulinum toxin substrate 1
RANK	receptor activator of nuclear factor-κB
RANKL	receptor activator of nuclear factor-κB ligand
rBM	rat bone marrow monocyte
rBMSC	rat bone marrow stromal cell
rh	recombinant human
RO	reverse osmosis
Runx2	runt-related transcription factor 2
RXR	retinoic acid X receptor
SCF	stem cell factor
SD	standard deviation
SDS	sodium dodecyl sulphate
SDS-PAGE	sodium dodecyl sulphate polyacrylamide gel electrophoresis
SEM	standard error of the mean
sf-α-MEM	serum-free α-modified Eagle's medium
sf-DMEM	serum-free Dulbecco's modified Eagle's medium

sFRP	secreted Frizzled-related protein
Smad	mothers against decapentaplegic homologues
SMI	structure model index
Sox	sex determining region Y box
SPI1	spleen focus forming virus proviral integration oncogene
sRANKL	soluble receptor activator of nuclear factor-κB ligand
Src	sarcoma viral oncogene homologue
Tb.BMD	trabecular BMD
Tb.N	trabecular number
Tb.Pf	trabecular pattern factor
TBS	Tris-buffered saline
Tb.Sp	trabecular spacing
TBS-Tween	Tris-buffered saline with 1% Tween 20
Tb.Th	trabecular thickness
Tcf	T-cell-specific transcription factor
TEMED	N,N,N,N-tetramethylethylenediamine
TGF-β	transforming growth factor-β
TIDEL	Therapeutic Intensification in *de Novo* Leukaemia
TmP	maximum tubular resorption of phosphate
TNF	tumour necrosis factor
TRAF6	tumour necrosis factor receptor-associated factor 6
TRAP	tartrate-resistant acid phosphatase 5
TV	total volume
UV	ultraviolet
VDR	vitamin D receptor
Wif	Wnt inhibitory factor
Wnt	wingless-type mouse mammary tumour virus integration type family member
WST-1	4-[3-(4-iodophenyl)-2-(4-nitrophenyl)-2H-5-tetrazolio]-1,3-benzene disulphonate

Publications

Scientific Manuscripts

1. **Vandyke K.**, Fitter S., Dewar A.L., Drew J., Shultz C.G., Sims N.A., Zannettino A.C.W. (2010). Prospective evaluation of bone remodelling in imatinib-treated CML patients. *Manuscript in preparation*.

2. **Vandyke K.**, Fitter S., Zannettino A.C.W. (2010). The tyrosine kinase inhibitor dasatinib (Sprycel™) inhibits chondrocyte activity and proliferation. *Manuscript submitted to Bone*.

3. Fitter S., **Vandyke K.**, Shultz C.G., White D., Hughes T.P., Zannettino A.C.W. (2010). Plasma Adiponectin Levels Are Markedly Elevated in Imatinib-Treated Chronic Myeloid Leukemia (CML) Patients: A Mechanism for Improved Insulin Sensitivity in Type 2 Diabetic CML Patients? *Journal of Clinical Endocrinology and Metabolism*, 95(8):3763-3767.

4. **Vandyke K.**, Dewar A.L., Diamond P., Fitter S., Shultz C.G., Sims N.A., Zannettino A.C.W. (2010). The tyrosine kinase inhibitor dasatinib dysregulates bone remodelling through inhibition of osteoclasts *in vivo*. *Journal of Bone and Mineral Research*, 25(8):1759-1770.

5. **Vandyke K.**, Dewar A.L., Fitter S., Hughes T.P., Zannettino A.C.W. (2010). Dysregulation of bone remodelling by imatinib mesylate. *Blood*, 115(4):766-774.

6. **Vandyke K.**, Dewar A.L., Fitter S., Menicanin D., To L.B., Hughes T.P., Zannettino A.C.W. (2009). Imatinib mesylate causes growth plate closure *in vivo*. *Leukemia*, 23(11):2155-2159.

7. **Vandyke K.**, Dewar A.L., Farrugia A.N., Fitter S., To L.B., Hughes T.P., Zannettino A.C.W. (2009). Therapeutic concentrations of dasatinib inhibit *in vitro* osteoclastogenesis. *Leukemia*, 23(5):994-7.

Conference Proceedings

1. **Vandyke K.**, Dewar A.L., Menicanin D., Fitter S., Zannettino A.C.W. Imatinib causes growth plate closure *in vivo*. *Haematology Society of Australia and New Zealand 2009 Annual Scientific Meeting*, Adelaide, Australia, October 2009.

2. **Vandyke K.**, Dewar A.L., Diamond P., Fitter S., Schultz C.G., Sims N.A., Zannettino A.C.W. The tyrosine kinase inhibitor dasatinib dysregulates bone remodelling through inhibition of osteoclasts *in vivo*. *Haematology Society of Australia and New Zealand 2009 Annual Scientific Meeting*, Adelaide, Australia, October 2009.

3. Fitter S., **Vandyke K.**, Drew J., Dewar A.L., Schultz C.G., Sims N.A., To L.B., Hughes T.P., Zannettino A.C.W. Imatinib induced bone formation in CML patients is associated with a decrease in osteoclast function and numbers. *Haematology Society of Australia and New Zealand 2009 Annual Scientific Meeting*, Adelaide, Australia, October 2009.

4. **Vandyke K.**, Dewar A.L., Menicanin D., Fitter S., Zannettino A.C.W. Imatinib causes growth plate closure *in vivo*. *Australian and New Zealand Orthopaedics Research Society 15th Annual Research Meeting*, Adelaide, Australia, October 2009.

5. **Vandyke K.**, Dewar A.L., Diamond P., Fitter S., Schultz C.G., To L.B., Hughes T.P., Zannettino A.C.W. The tyrosine kinase inhibitor dasatinib dysregulates bone remodelling *in vivo*. *8th International Meeting on Cancer Induced Bone Disease*, Sydney, Australia, March 2009.

6. **Vandyke K.**, Dewar A.L., Davis A.N., Fitter S., To L.B., Hughes T.P., Dasatinib (Sprycel™) inhibits osteoclast activity *in vitro* and *in vivo* via a c-fms-dependent and c-Src-independent mechanism. *50th American Society of Hematology Annual Meeting and Exposition*, San Francisco, USA, December 2008.

7. **Vandyke K.**, Dewar A.L., Davis A.N., Fitter S., Hughes T.P., To L.B., Zannettino A.C.W. The tyrosine kinase inhibitor dasatinib decreases osteoclast formation and activity *in vitro*. *30th Meeting of the American Society for Bone and Mineral Research*, Montreal, Canada, September 2008.

Chapter 1

Introduction

1.1 Overview

Imatinib mesylate, a rationally-designed ATP-competitive protein tyrosine kinase inhibitor, is currently the gold standard therapy for Philadelphia chromosome-positive chronic myeloid leukaemia (CML) and some gastrointestinal stromal tumours (GIST), based on its inhibition of Bcr-Abl and Kit signalling, respectively.[1] The significant incidence of acquired resistance to imatinib has led to the development of second generation tyrosine kinase inhibitors, such as nilotinib and dasatinib, that have greater affinity and/or specificity for their target kinases (reviewed in [2]).

Although the efficacy and tolerability of imatinib are a vast improvement over conventional chemotherapies, the drug exhibits off-target effects.[3,4] Unanticipated side-effects of imatinib therapy include hypophosphataemia (serum phosphate < 0.8 mM) and hypocalcaemia (serum calcium < 2.1 mM)[5-12], which in part have been attributed to drug-mediated changes to renal and gastrointestinal handling of phosphate and calcium. However, emerging data suggest that imatinib also targets cells of the skeleton[10,13-19], stimulating the retention and sequestration of calcium and phosphate to bone, leading to decreased circulating levels of these minerals. Significantly, recent studies suggest that normal skeletal remodelling is dysregulated in patients receiving imatinib therapy.[5,10,12,20]

The following introduction highlights our current understanding of the mechanisms underlying the effects of imatinib on the skeleton. In particular, it examines recent studies which suggest that imatinib has direct effects on bone-resorbing osteoclasts and bone-forming osteoblasts through inhibition of the macrophage colony stimulating factor 1 (M-CSF; also known as CSF1) receptor (Fms [McDonough feline sarcoma viral oncogene homologue]; also known as CSF1R), the stem cell factor (SCF) receptor (Kit), carbonic anhydrase II (CAII), Abelson kinase (Abl) and the platelet-derived growth factor receptor (PDGFR).

1.2 Bone structure, remodelling and growth

1.2.1 Macroscopic organisation

Bone is a specialised connective tissue which primarily acts to provide mechanical support for the organs, act as anchor sites for muscles to facilitate locomotion, protect vital organs and the bone marrow and to serve as a metabolic reserve for calcium and phosphate to maintain mineral homeostasis (reviewed in [21]).

The bones of the skeleton can be categorised into two broad groups based on gross morphology: the flat bones, comprising the ilium, mandible, scapulae and the bones of the

scull; and the long bones, including the tibia, femur and humerus. Long bones can be segmented into three broad regions: the epiphyses, which make up the extremities of the bones; the cylindrical middle portion of the bone, known as the diaphysis; and the metaphysis, which is the transitional region between the midshaft and the ends of the bone (figure 1.1). In the growing skeleton, the epiphysis and the metaphysis are separated by a layer of epiphyseal cartilage, known as the growth plate. The outer surface of the bone is made up of dense layers of calcified bone, known as the cortex, which encases the haematopoietic bone marrow in the medullary cavity. In young animals the marrow space is filled with haematopoietic stem cells and mature erythrocytes (red marrow). In contrast, the marrow of the long bones of aging animals becomes increasingly filled with adipocytes (yellow marrow) and becomes less haematopoietically active.

In the medullary cavity at the metaphysis and epiphysis of long bones, and in the axial skeleton, the marrow space is filled with a rigid sponge-like meshwork of thin, calcified bone struts, known as trabecular or cancellous bone. In general, cortical bone is less metabolically active and primarily fulfils a mechanical function, while trabecular bone is more metabolically active and also contributes to mechanical strength.

1.2.2 Bone matrix and mineral composition

Bone is a mineralised extracellular matrix which is composed of type I collagen fibrils, making up approximately 90% of the matrix proteins, and a small proportion of osteonectin, osteopontin, bone sialoprotein and serum-derived globular proteins.[22-31] Healthy mature bone is composed of tightly-packed bundles of collagen fibres that form layers (lamellae) to allow the highest possible density of collagen in the bone tissue. The inorganic mineral component of bone is predominantly calcium and phosphate in the form of hydroxyapatite crystals [$Ca_{10}(PO_4)_6(OH)_2$] (reviewed in [32]). Following rapid bone formation, for example in development or fracture healing, the collagen fibres are formed in randomly oriented bundles, termed woven bone.[33] Woven bone is progressively resorbed and replaced by lamellar bone.

1.2.3 Bone formation

1.2.3.1 Osteoblasts

Osteoblasts are mature, non-proliferative cubiodal cells with a single eccentric nucleus, an intensely basophilic cytoplasm and a prominent golgi apparatus.[33,34] These cells, which

Figure 1.1. Anatomy of long bones.

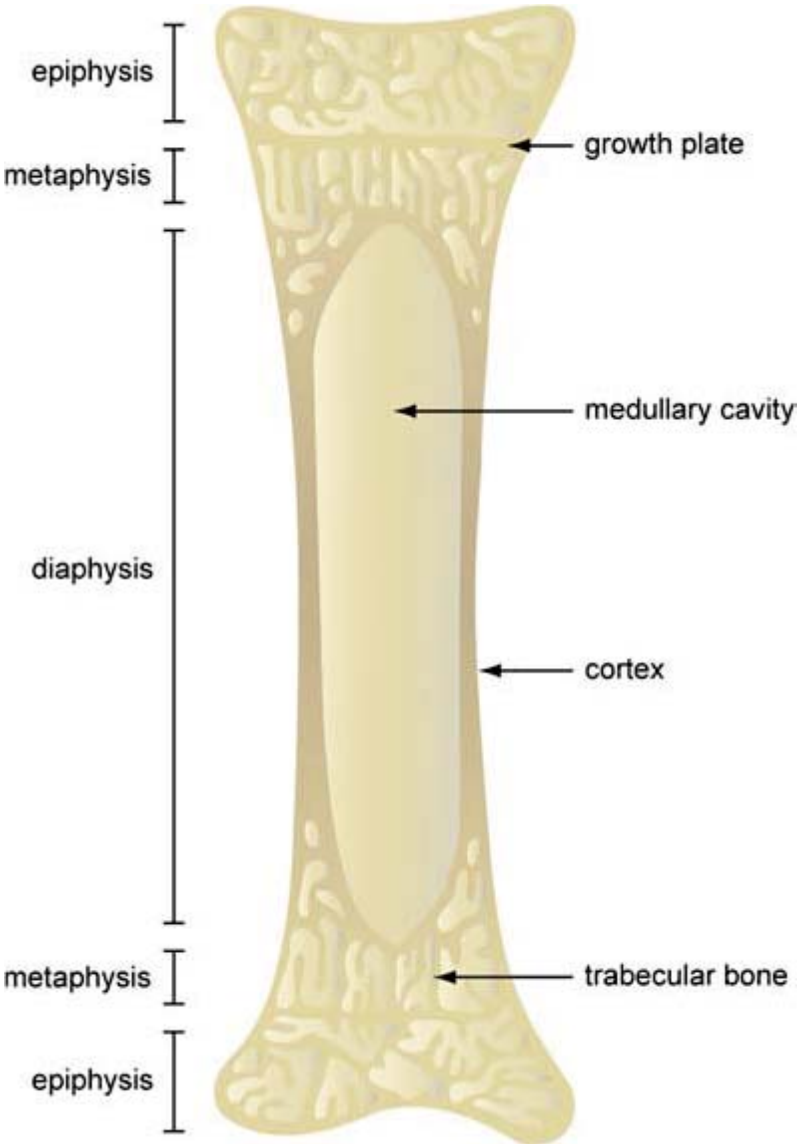
epiphysis
metaphysis
diaphysis
metaphysis
epiphysis
growth plate
medullary cavity
cortex
trabecular bone

derive from multipotent mesenchymal stem cells in the bone marrow, are responsible for the production and secretion of bone matrix, collagen and non-collagenous proteins.

During the initial phase of bone synthesis, osteoblasts rapidly deposit a layer of non-mineralised matrix, termed osteoid. Osteoblasts then release membrane-bound vesicles which allow the nucleation of hydroxyapatite crystals as a precursor to mineralisation of the matrix (reviewed in [35]). During the matrix secretion process, some osteoblasts become encapsulated in the newly-synthesised matrix and differentiate further into osteocytes. Other cells lose their synthetic capabilities and become bone-lining cells.

1.2.3.2 Osteoblast differentiation

Osteoblasts originate from multipotent mesenchymal stem cells which also give rise to chondroblasts, fibroblasts, myoblasts and adipoblasts.[36,37] The differentiation of mesenchymal progenitors into osteoblasts is associated with a defined sequence of changes in gene expression and cell activity which is controlled by a sequence of transcription factors and cytokines (figure 1.2). Bone morphogenetic proteins (BMPs), the canonical Wnt (wingless-type MMTV integration type family member) pathway and the transcription factors Runx2 (runt-related transcription factor 2) and Osterix (also known as Sp7 transcription factor) play critical roles in osteoblast differentiation.[38-43]

1.2.3.2.1 Transcriptional control of osteoblast differentiation

Runx2 is required to drive mesenchymal stem cell differentiation to the osteoblast lineage.[38,39,44] Runx2 binds to DNA as a multimeric complex with CBF-β (core-binding factor-β) and comodulators, including Smad1/5 (mothers against decapentaplegic homologues 1 and 5) and C/EBP (CCAAT/enhancer binding protein), and upregulates the expression of osteoblast genes, including those for type I collagen, osteocalcin and bone sialoprotein.[44] *Runx2* knockout mice have a complete absence of endochondral and intramembranous ossification due to defective osteoblast differentiation.[38,39] *RUNX2* expression is negatively regulated by the transcription factor Twist1, which maintains a proliferative immature mesenchymal stem cell phenotype.[45]

The transcription factor Osterix, which acts downstream of Runx2, is another key regulator of osteoblast formation, driving the final commitment of progenitors into osteoblasts. Osterix interacts with NFAT (nuclear factor for activated T cells) family members and drives expression of osteoblast-specific genes.[46] Osterix-deficient ($Osx^{-/-}$)

Figure 1.2. Osteoblast differentiation. The transcription factors Runx2 and Osterix drive mesenchymal stem cell differentiation down the osteoblast lineage. Twist1 inhibits osteoblast differentiation, maintaining mesenchymal cells in an immature phenotype. Wnt promotes osteoblastogenesis, while sclerostin, Dkk1, sFRP and Wif antagonise Wnt signalling, inhibiting commitment to the osteogenic lineage. BMP stimulation induces osteoblast differentiation, driving the expression of genes involved in osteoblast maturation.

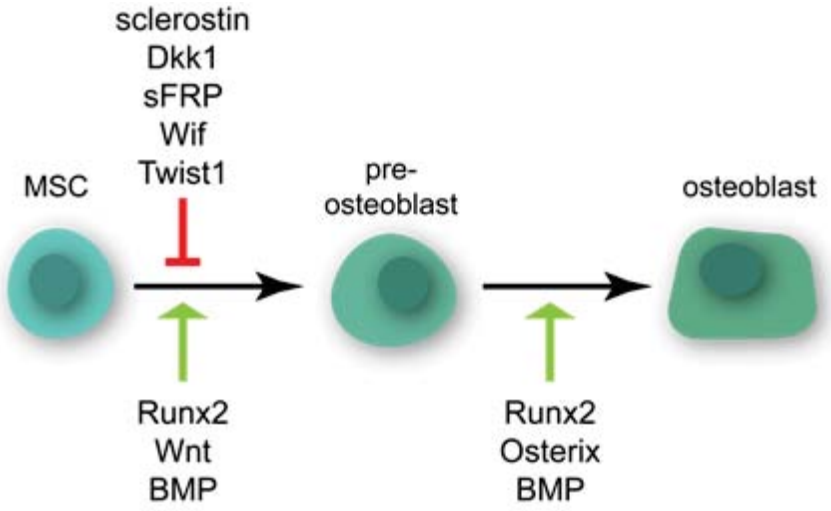
sclerostin
Dkk1
sFRP
Wif
Twist1
MSC
pre-
osteoblast
osteoblast
Runx2
Wnt
BMP
Runx2
Osterix
BMP

mice lack mature osteoblasts and, like *Runx2*$^{-/-}$ mice, have a complete absence of endochondral or intramembranous bone synthesis.[42]

1.2.3.2.2 Canonical Wnt signalling

Canonical Wnt/β-Catenin signalling is critical for bone formation, inhibiting chondrogenic differentiation and promoting osteoblastogenesis. Wnt ligands bind to a receptor complex comprising Frizzled and LRP5/6 (low density lipoprotein receptor-related protein 5 and 6), inducing a signalling cascade that directs osteoblast differentiation at the pre-osteoblast stage, enhancing Runx2 expression (figure 1.3). Wnt signalling stabilises β-Catenin, which then interacts with members of the Tcf/Lef (T-cell-specific transcription factor/lymphoid enhancer-binding factor) transcription factor family to drive the expression of genes involved in osteoblast differentiation[41] (reviewed in [47]). In the absence of Wnt ligands, glycogen synthase kinase-3β (GSK-3β) negatively regulates β-Catenin by mediating β-Catenin phosphorylation and thus targeting it for ubiquitination and proteasomal degradation.[48,49] However, the binding of Wnt ligands to the membrane Frizzled/LRP5/6 receptor complex inhibits the phosphorylation of β-Catenin by GSK-3β, thus allowing β-Catenin to translocate to the nucleus and to regulate gene transcription.[40]

A number of molecules, including secreted Frizzled-related proteins (sFRPs) and Wnt inhibitory factors (Wif), negatively regulate osteoblast differentiation by binding and sequestering Wnt ligands.[50,51] Additionally, Sclerostin and Dickkopff family members Dkk1 and Dkk2 bind the LRP5/6 receptors, precluding their binding with Wnt ligands.[52-54]

The importance of canonical Wnt signalling in osteoblastogenesis is illustrated by conditional knockout studies which show that β-Catenin is essential for osteoblast differentiation and bone formation *in vivo*.[43,55,56] Additionally, loss of function mutations in the Wnt co-receptor *LRP5* are associated with abnormal bone phenotypes in humans, including the low bone mass disease Osteoporosis Pseudo-Glioma syndrome, while gain of function mutations lead to the High Bone Mass phenotype.[57-59] In addition, deletion mutations in the *SOST* gene, encoding the Wnt inhibitor Sclerostin, also cause diseases of abnormally increased bone density (osteosclerosis), including Sclerosteosis and Van Buchem disease.[60-62]

1.2.3.2.3 BMPs

BMPs are members of the transforming growth factor-β (TGF-β) superfamily that are potent stimulators of osteoblast differentiation.[63,64] Signalling downstream of the BMP

Figure 1.3 The canonical Wnt signalling pathway. A. In the absence of Wnt signal, β-Catenin is degraded following interactions with Axin, APC and GSK-3β. **B**. Wnt ligands bind to the Frizzled/LRP5/6 receptor complex, resulting in inhibition of β-Catenin degradation. This allows the accumulation of β-Catenin in the cytoplasm and nucleus, resulting in the transcription of osteoblast-specific genes. **C**. Extracellular Wnt antagonists Sclerostin and Dkk1 inhibit Wnt signalling through the binding and sequestering of LRP5/6, while sFRP binds Wnt, preventing its binding to Frizzled.

A

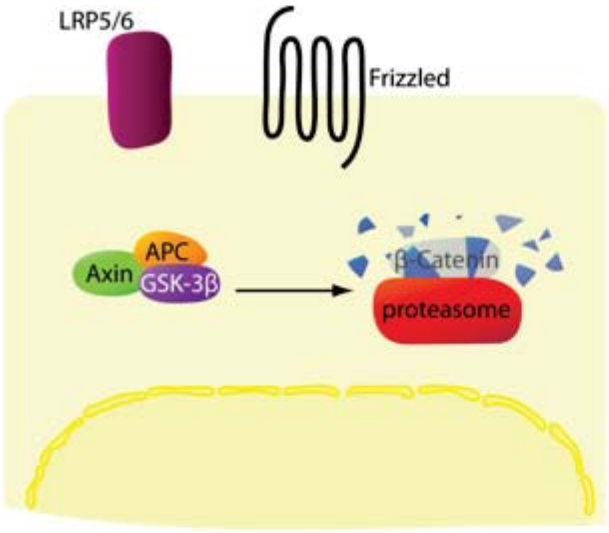
LRP5/6
Frizzled
APC
Axin
GSK-3β
β-Catenin
proteasome

B

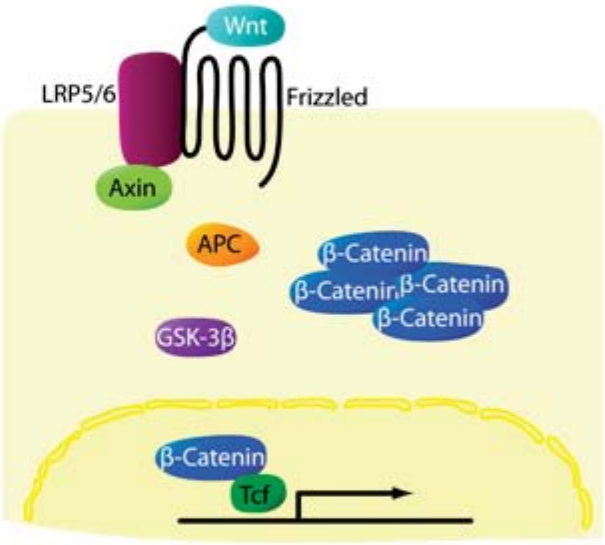
Wnt
LRP5/6
Frizzled
Axin
APC
β-Catenin
β-Catenin
β-Catenin
β-Catenin
GSK-3β
β-Catenin
Tcf

C

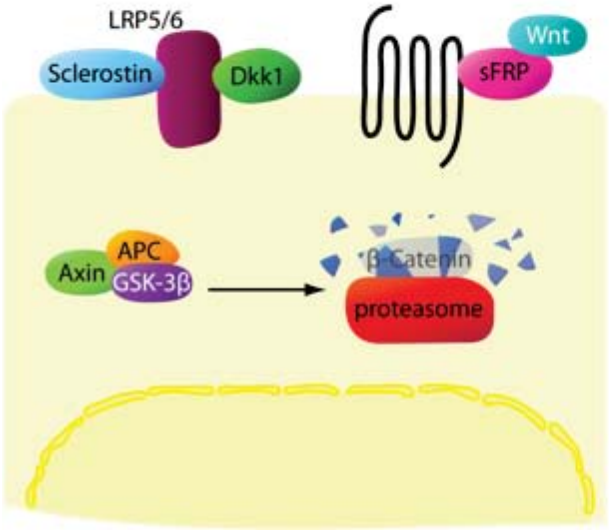
LRP5/6
Sclerostin
Dkk1
Wnt
sFRP
APC
Axin
GSK-3β
β-Catenin
proteasome

receptors is regulated by the Smad family of intracellular signalling molecules, which translocate to the nucleus following activation of BMP receptors and upregulate the expression of genes that are crucial for osteoblast formation (reviewed in [65]). BMPs also transcriptionally activate *RUNX2* and *OSX* in mesenchymal precursors *in vitro*, promoting osteoblastic differentiation.[66,67]

1.2.4 Osteocytes

The calcified bone matrix contains a network of specialised cells (osteocytes) that have important roles in monitoring skeletal integrity via a mechanosensory network. Osteocytes are terminally differentiated, non-proliferative cells that are derived from mature osteoblasts that have been embedded in the bone matrix during the process of bone formation (reviewed in [68]). Osteocytes reside in small lacunae in the bone or osteoid matrix.[33] These cells form a syncytium, connecting with other osteocytes and with osteoblasts and bone lining cells via numerous cellular processes in canaliculi (reviewed in [68]).

The osteocyte network acts as a mechanical sensor, responding to changes in extracellular fluid flow or mechanical strain by producing factors, such as insulin-like growth factor I (IGF-1) and nitric oxide, that may act as signalling molecules involved in the adaptive response to skeletal load.[69-73] It is hypothesised that osteocytes play an important role in the response to tissue strain and microfracture damage, increasing bone remodelling by stimulating osteoclast recruitment.[74,75] Studies in murine and chicken osteocyte cultures have demonstrated that osteocytes exert a constitutive inhibitory effect on osteoclast activity[76,77] and induction of osteocyte apoptosis relieves this inhibition.[77] Indeed, osteocyte apoptosis is suggested to be an essential mechanism for the induction of bone remodelling, particularly following microfracture damage.[75,78,79] In addition, osteocytes express receptors for a number of factors that are known to be important in bone function, including the parathyroid hormone (PTH)/parathyroid hormone-related peptide (PTHrP) receptor[80] and oestrogen receptor α[81], suggesting that the cells may be able to respond to systemic and locally-produced hormones and growth factors.

1.2.5 Bone resorption

1.2.5.1 Osteoclasts

Osteoclasts are motile, multinucleated monocyte/macrophage family members of haematopoietic origin that arise from mononucleated osteoclasts precursors.[82-84] They have

a highly vacuolated cytoplasm with abundant Golgi complexes and vesicles containing lysosomal enzymes.[33,34,85]

Activation of mature osteoclasts is a multi-step process that involves recognition of and binding to matrix proteins, cell polarisation and the formation of the actin ring sealing zone, which creates a enclosed microenvironment between the osteoclast and the bone surface.[33,34,86] The attachment of the cell to the bone matrix is predominantly performed via $\alpha_v\beta_3$ integrins.[87] Following adhesion, cytoskeletal reorganisation drives cell spreading and polarisation. In a process which is thought to involve microtubules, vesicles containing protons and proteases are transported to the osteoclast surface adjacent to the bone, where they fuse with the plasma membrane, forming the ruffled membrane.[33,34,85] The acidification of the extracellular compartment adjacent to the bone is achieved by the production of protons through the action of the cytoplasmic enzyme CAII.[88-91] The protons are transported across the ruffled border membrane via proton pumps (H+-ATPase), where the decreased pH solubilises the mineral component of bone.[91-93] The collagen matrix is then degraded by the activity of secreted enzymes such as cathepsin K.[94] During bone resorption, collagen type I fragments and solubilised calcium and phosphate are released into the circulation.[95,96] After resorbing bone at one site, the osteoclast disassembles the sealing zone cytoskeletal structures, migrates to a new site and restarts the bone resorption process.

1.2.5.2 Osteoclast differentiation

1.2.5.2.1 RANK-RANKL-OPG axis

Molecular interactions between osteoblasts and osteoclasts ensure the close regulation of bone turnover. These interactions are primarily under the control of two factors: receptor activator of nuclear factor-κB (RANK; also known as tumour necrosis factor [TNF] receptor superfamily member 11a), which is expressed on the surface of mature osteoclasts and osteoclast precursors, and its cognate ligand, receptor activator of nuclear factor-κB ligand (RANKL; also known as TNF ligand superfamily member 11), which is expressed primarily by stromal cells and osteoblasts.[97,98] This interaction regulates the fusion of osteoclast precursors and the subsequent activation and survival of mature osteoclasts (figure 1.4).[98,99] A soluble form of RANKL (sRANKL) is also secreted by the stromal and osteoblast cells, or can be produced by proteolytic cleavage of the membrane bound form of RANKL.[97] The importance of the interaction between RANK and RANKL has been demonstrated in mice lacking RANKL (*TNFSF11*$^{-/-}$) and RANK (*TNFRSF11A*$^{-/-}$), which

Figure 1.4. Osteoclast differentiation. Commitment of haematopoietic stem cells to the osteoclast lineage requires the expression of the transcription factor PU.1, which drives the expression of osteoclast-specific genes, including that for Fms. Activation of Fms by M-CSF promotes pre-osteoclast and osteoclast proliferation and survival and upregulates the expression of genes that are essential for commitment to the osteoclast linage, including that for RANK. Binding of RANK by RANKL drives fusion of osteoclast precursors and activation of the mature multinucleated osteoclasts thus formed. Signalling downstream of RANK activates the transcription factor NFATc1 which drives the expression of genes involved in osteoclast activity, including TRAP, cathepsin K and β_3 integrin. OPG, secreted by osteoblasts, prevents the RANK-RANKL interaction by acting as decoy receptor for RANKL, thereby preventing osteoclastogenesis.

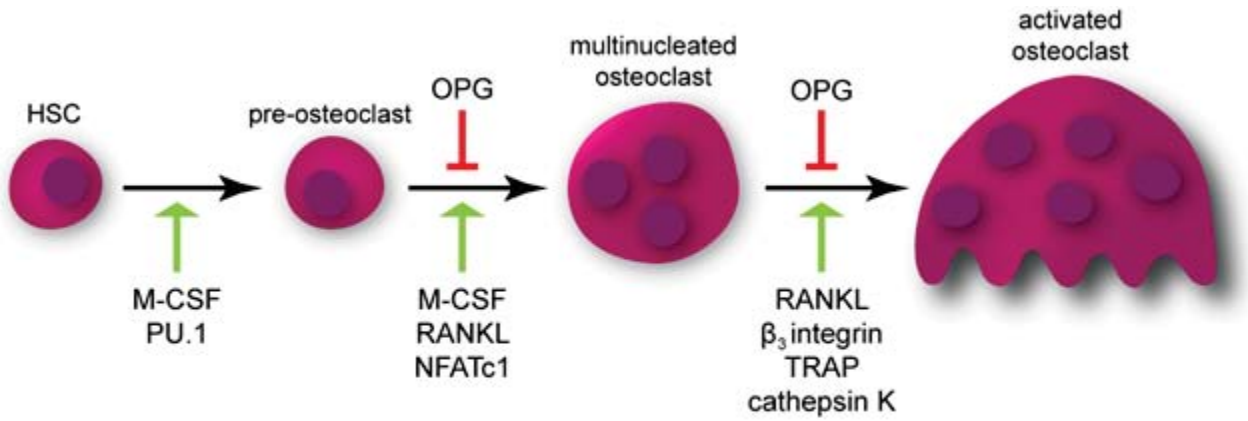
HSC
pre-osteoclast
OPG
multinucleated osteoclast
OPG
activated osteoclast
M-CSF
PU.1
M-CSF
RANKL
NFATc1
RANKL
β3 integrin
TRAP
cathepsin K

develop severe osteopetrosis (hyper-dense bones) due to the absence of mature osteoclasts.[100,101] Administration of sRANKL in mice results in reduced bone volume and high blood calcium[98]; *in vitro*, sRANKL is essential for stimulation of osteoclastogenesis in the absence of osteoblasts and stromal cells.[102]

A third protein, osteoprotegerin (OPG; also known as TNF receptor superfamily member 11b), produced by osteoblasts and other cells, acts as a soluble decoy receptor for RANKL, controlling the osteoclastogenic signal by sequestering RANKL and thus inhibiting the RANK-RANKL interaction.[97,98,103] The crucial role for OPG in bone remodelling was demonstrated in *Opg*$^{-/-}$ mice, which exhibited uncontrolled bone resorption, a severe decrease in total bone density and an accompanying high incidence of fractures.[98,104,105] It has been proposed that dysregulation of the balance between OPG and RANKL results in abnormal bone turnover and pathologically increased or decreased bone mass.[101,104] In support of this hypothesis, at the mRNA level, increasing RANKL/OPG ratio is associated with increased bone resorption in human bone and with increased osteoclastogenesis in co-cultures of the human pre-osteoclast-like cell line HL60 and the stromal cell line ST2.[106,107] Thus, the relative quantity of OPG and RANKL in the bone microenvironment, not absolute amounts of either, determines whether osteoclastogenesis and osteolytic activity occurs.

The systemic regulation of bone resorption is primarily mediated through the action of hormones on stromal cells and osteoblasts. Osteotropic factors (such as 1,25-dihydroxyvitamin D_3, PTH, PTHrP, interleukin [IL]-6, IL-1β, IL-11) stimulate osteoclastogenesis by acting on osteoblasts and bone marrow stromal cells to upregulate the production of RANKL and M-CSF (reviewed in [108]).

1.2.5.2.2 Transcriptional control of osteoclastogenesis

The early commitment to the osteoclast lineage requires the transcription factor PU.1 (also known as SPI1 [spleen focus forming virus proviral integration oncogene]) (figure 1.4). PU.1 induces the expression of a number of osteoclast-specific genes, including the Fms gene *CSF1R*, which are required to commit the precursors to the pre-osteoclast lineage.[109-111] Activation of Fms by M-CSF then drives cell proliferation and survival and upregulates the expression of *RANK*.[112-114] M-CSF also activates microphthalmia-associated transcription factor (Mitf), which is important in regulating genes involved in osteoclastogenesis, including that for cathepsin K (*CTSK*).[115] Deficiency in either PU.1 or Fms results in an complete absence of osteoclasts and causes severe osteopetrosis.[109-111]

Stimulation of osteoclasts by RANKL drives the formation of mature osteoclasts through activation of NFATc1. This involves the recruitment of TRAF6 (TNF receptor-associated factor 6) to the intracellular domain of RANK[116-118] which results in the activation of NFATc1[119,120] via NF-κB (nuclear factor of κ light polypeptide gene enhancer in B-cells 1), JNK (Jun N-terminal kinase; also known as mitogen-activated protein kinase 8), p38 (also known as AHSA1 [activator of heat shock 90 kDa protein ATPase homologue 1]) and FOS (FBJ murine osteosarcoma viral oncogene homologue) signalling pathways (reviewed in [121]). Loss of expression of TRAF6[122], Fos[123,124], NF-κB[125,126], or NFATc1[124] results in osteopetrosis due to a complete lack of multinucleated osteoclasts, despite a normal, or greater than normal, number of monocyte/macrophage cells. The activation of the NFATc1 transcription factor induces the expression of genes that are essential for osteoclast function, including the genes encoding tartrate-resistant acid phosphatase 5 (TRAP)[120,127,128], calcitonin receptor[127,128], cathepsin K[128] and β_3 integrin[129].

1.2.6 Bone remodelling

In healthy adults, bone is not static; old bone is constantly being resorbed and new bone reformed in a coordinated process known as bone remodelling. This provides the ability to alter the microarchitecture of the skeleton, to correct microfracture damage, to change bone density and to allow for management of calcium and phosphate homeostasis. The resorptive and formative components of the remodelling sequence are tightly coupled in time and space so that, in healthy adult bone, osteoclast activity is counterbalanced by equal osteoblast activity, resulting in a net balance in bone volume.

Bone remodelling is a cyclical process that is carried out by the basic multicellular unit (BMU), which is made up of a group of osteoclasts which transverse the bone undergoing resorption, followed by a group of osteoblasts that progressively synthesise bone matrix to fill the resorption lacunae (reviewed in [130]). The remodelling cycle begins on a quiescent bone surface, covered with bone lining cells. In response to signals, probably originating from osteocytes, the bone lining cells are activated and retract to expose the bone surface. A blood vessel then advances to the exposed bone surface and osteoclast precursors are recruited to the site from the marrow or the circulation. The precursors fuse to form mature osteoclasts, which adhere to the bone and undergo resorption. Once the osteoclasts have moved on from the region being resorbed, or have undergone apoptosis, osteoblasts assemble on the resorbed surface and synthesise new bone matrix.

Crosstalk between the osteoclasts and osteoblast in the BMU ensures the balanced activity of the two cell types. Osteoblasts secrete a number of proteins which are essential regulators of bone resorption, including M-CSF, RANKL and OPG.[97,98,103] The activation of osteoblasts occurs via a process that may involve osteoclast-mediated release of factors that are sequestered in the bone matrix (reviewed in [108]). In addition, cell-cell interactions between osteoclasts and osteoblasts mediated by membrane-bound receptors and ligands (for example, Ephrin B2-EphB4 binding) may be involved in the regulation of osteoblast activation in the BMU.[131]

1.2.7 Pathological bone remodelling

An uncoupling of bone resorption from bone formation can result in local or systemic bone loss or, alternatively, in an abnormal increase in bone density. Focal bone loss is symptomatic of inflammatory arthritis, multiple myeloma and skeletally metastatic breast cancer (reviewed in [132,133]). In contrast, lesions resulting from prostate cancer skeletal metastases have both osteoblastic and osteolytic components, although they usually result in an overall increase in local bone volume (reviewed in [132,133]). Irrespective of the lesion type, bone resorption is almost universally increased in patients with bone tumours (reviewed in [134]). Moreover, studies suggest that bone resorption is necessary for the establishment of tumour cells in the bone, resulting in the local release of growth factors that promote establishment of the secondary tumour.[135]

In osteolytic tumours, there is evidence to suggest that tumour cells can act directly or indirectly to increase the recruitment, maturation, activity and survival of osteoclasts, leading to an imbalance in bone remodelling and, therefore, bone loss. Additionally, factors released from the bone during osteolysis stimulate cancer cell survival, thus instigating a "vicious cycle" resulting in decreased bone density and increased tumour burden in the bone marrow microenvironment (reviewed in [133]). Thus, while direct induction of tumour cell death is the primary strategy for decreasing tumour size, anti-osteoclastogenic agents are a potential therapeutic strategy for limiting tumour progression by inhibiting tumour-associated osteolysis.

1.2.8 Bone growth

Bone formation and growth occurs through two distinct developmental mechanisms: intramembranous and endochondral bone formation. Intramembranous ossification is the primary mechanism in the development of flat bones, such as certain bones of the skull and

the lateral part of the clavicles, whereas long bones of the limbs, vertebrae and ribs are lengthened through endochondral ossification (reviewed in [136]). In intramembranous ossification, mesenchymal cells differentiate into osteoblasts which directly synthesise bone. This process is independent of prior cartilage formation. In contrast, in endochondral ossification the mesenchymal cells differentiate into chondrocytes which synthesise a cartilaginous template. This process is followed by the recruitment of osteoprogenitors which differentiate and then synthesise bone matrix.

1.2.8.1 Intramembranous ossification

In embryonic development, intramembranous bone formation begins with the proliferation of mesenchymal cells that form a connective tissue sheet of condensed mesenchymal cells (reviewed in [137]). The formation of mesenchymal condensations is driven by mesenchymal-epithelial and cell-cell matrix interactions. Within the mesenchymal condensations, cells differentiate into osteoblasts, which synthesise woven bone matrix which is gradually mineralised. Blood vessels invade through the newly-formed bone and form the haematopoietic bone marrow. The woven bone is later remodelled and replaced with mature lamellar bone.

1.2.8.2 Endochondral ossification

The embryonic development of long bones commences with the formation of a mesenchymal condensation, as is seen in the development of flat bone; however, in long bone development, cells in the mesenchymal condensation proliferate and differentiate into prechondroblasts and then into chondroblasts (figure 1.5). These chondroblasts secrete the cartilaginous matrix, predominantly composed of type II collagen[30] and chondroitin sulfate proteoglycan (aggrecan) aggregates, which consist of a core protein and keratin sulphate glycosaminoglycan (GAG) chains (reviewed in [138]). The chondroblasts become embedded within lacunae in the cartilage matrix, at which point they are termed chondrocytes. This cartilage matrix forms a template for the formation of the bony elements of the skeleton during embryonic development and in postnatal growth. Mesenchymal cells surrounding the cartilage anlage flatten and form a condensed multilayered structure known as the perichondrium and a collar of bone gradually develops around the cartilage anlage. At each end of the anlage, centres of ossification develop at specialised cartilaginous regions, known as growth plates. It is these growth plates that are responsible for the continued elongation of long bones during skeletal growth.

Figure 1.5. Endochondral ossification. **A**. During embyronic development, mesenchymal progenitors condense and differentiate into chondrocytes which produce a cartilagenous anlage that is later replaced by bone. **B**. Perichondrial mesenchymal cells differentiate into osteoblasts and synthesise a collar of bone around the cartilage anlage. **C**. Chondrocytes in the centre of the anlage proliferate and then hypertrophy, the area becomes vascularised and osteoblasts are recruited to replace the hypertrophic cartilage with mineralised bone. **D**. At the epiphyseal growth plate, the hypertrophic cartilage is progressively replaced with mineralised trabecular bone, resulting in longitudinal bone growth. At the epiphyses, secondary ossification centres are formed which undertake mineralisation of the distal ends of the bone.

A

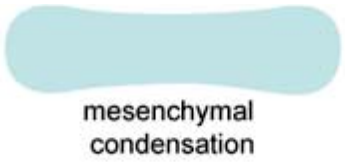
mesenchymal
condensation

B

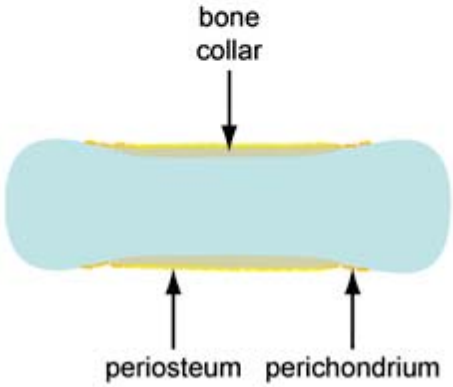
bone
collar
periosteum
perichondrium

C

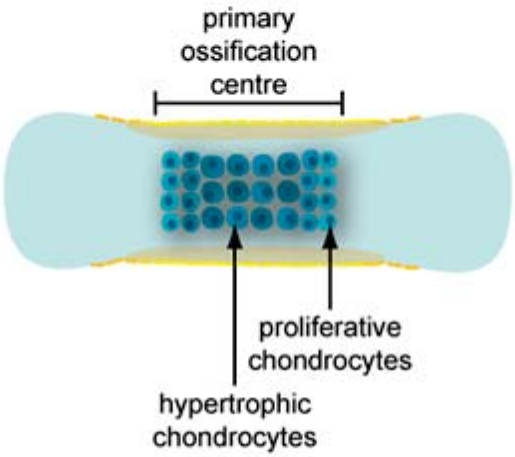
primary
ossification
centre
proliferative
chondrocytes
hypertrophic
chondrocytes

D

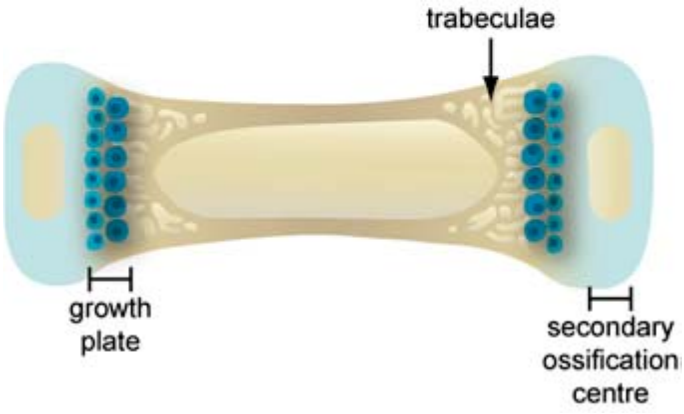
trabeculae
growth
plate
secondary
ossification
centre

Within growth plate cartilage, there are morphologically distinct zones of cellular activity (figure 1.6).[139-142] The zone furthest from the ossification front is the zone of resting (reserve) chondrocytes.[141,142] In the adjacent zone, chondroblasts proliferate, become flattened in tightly-packed isogenous clusters and synthesise cartilage matrix.[139-143] These chondrocytes then stop proliferating and undergo a maturation process to become enlarged (hypertrophic) chondrocytes.[34,141,142] The hypertrophic chondrocytes synthesise mineralised matrix through calcification of cartilage in the zone of provisional calcification and the chondrocytes then undergo apoptosis.[34,140,143] Following matrix calcification, the mineralised matrix is partially resorbed by osteoclasts and blood vessels invade to allow vascularisation of the tissue, facilitating ingress of osteoblasts and cells of the haematopoietic bone marrow.[34,140] Prehypertrophic chondrocytes then produce Indian hedgehog (Ihh), which induces the perichondrial cells to undergo osteogenic differentiation.[144] The resulting osteoblasts synthesise woven bone over the scaffold formed by the remnants of calcified cartilage to form the primary spongiosa.[34,140] This woven bone is then remodeled and replaced with lamellar bone to form mature trabecular of the secondary spongiosum.[140]

The continuing cycles of chondrocyte differentiation, cartilage mineralisation, bone matrix synthesis and remodelling at the epiphyseal growth plate allows the continued longitudinal growth of long bones and the formation of the adult bone shape. The rate of longitudinal bone growth is primarily controlled by the rate of chondrocyte proliferation, the rate of hypertrophy and the rate of matrix synthesis and degradation.[143,145] With aging, there is a progressive deceleration of chondrocyte proliferation, leading to a gradual thinning of the growth plate. The width of the growth plate correlates with the rate of longitudinal bone growth.[145] In humans, the post-natal growth rate steadily decreases until sexual maturity is reached, coinciding with the closure of the growth plate and its replacement with trabecular bone (reviewed in [146,147]).

1.2.8.3 Chondrocyte differentiation

1.2.8.3.1 Transcriptional control of chondrocyte differentiation

Chondrocytes, like osteoblasts, arise from multipotent mesenchymal stem cells.[36] A number of transcription factors play a key role in the preferential commitment of mesenchymal precursors to the chondrocyte lineage (figure 1.7). The transcription factors Runx2 and Sox9 (sex determining region Y box 9) control the commitment and differentiation to the chondrocytic lineage (reviewed in [136]). Upregulation of *Sox9*, together

Figure 1.6. The growth plate. During longitudinal bone growth, chondrocytes at the growth plates at the distal ends of the bone undergo coordinated phases of proliferation and differentiation. Chondrocytes in the growth plate are arranged into vertical columns that can be stratified into horizontal layers corresponding to different phases of chondrocyte differentiation: the resting zone, the proliferating zone and the prehypertrophic and hypertrophic zones. In the initial phase, resting zone chondrocytes are activated to proliferate and synthesise cartilagenous matrix. The cells of the proliferative zone then become quiescent and undergo hypertrophic maturation. The hypertrophic chondrocytes initiate cartilaginous matrix mineralisation and then undergo terminal differentiation and apoptosis. Following chondrocyte apoptosis, the area becomes vascularised and osteoclasts and osteoblasts are recruited to replace the hypertrophic cartilage with mineralised bone matrix, forming the primary spongiosa.

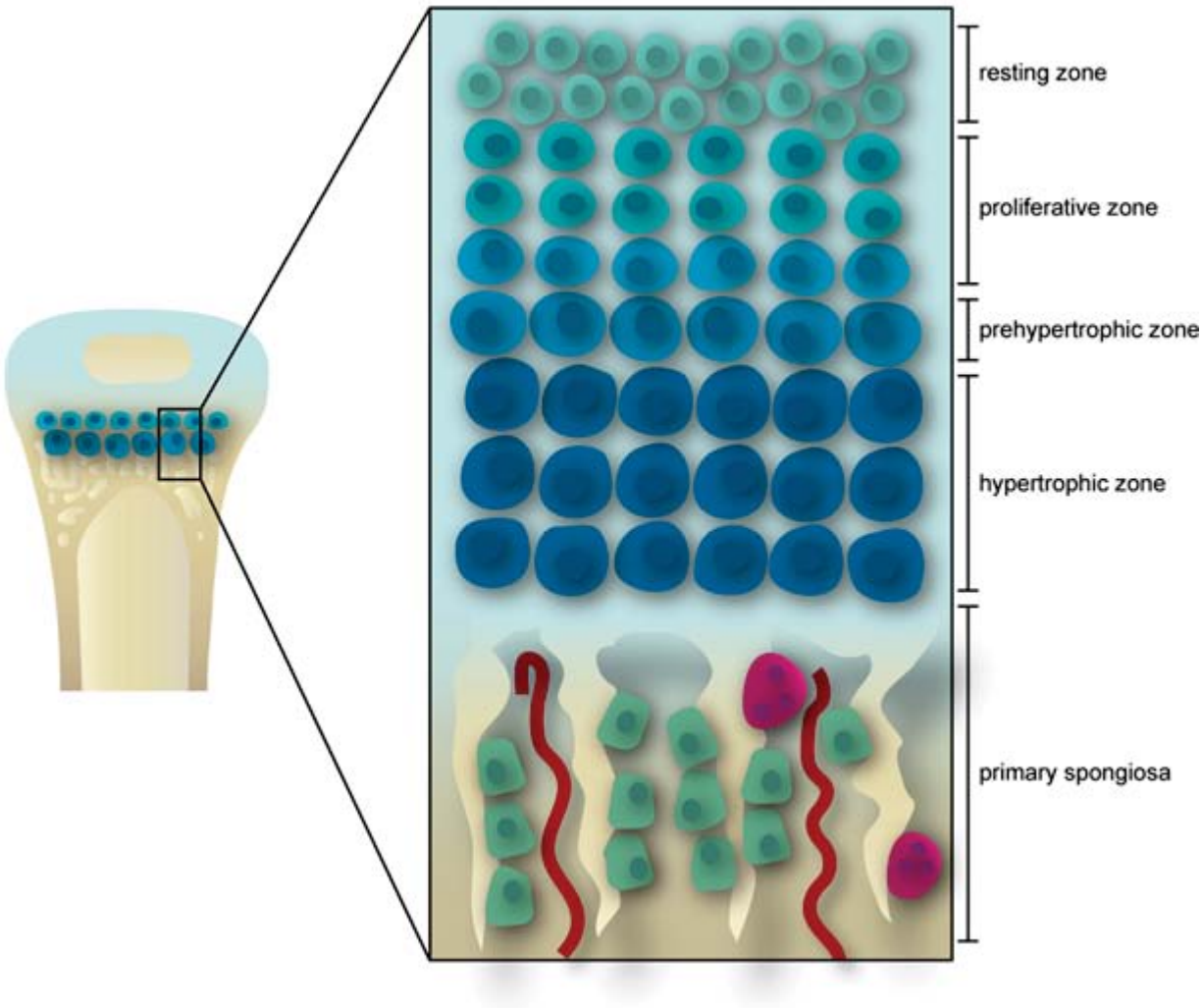
resting zone
proliferative zone
prehypertrophic zone
hypertrophic zone
primary spongiosa

Figure 1.7. Chondrocyte differentiation. The transcription factor Sox9, together with downstream targets Sox5 and Sox6, drives chondrocyte differentiation and proliferation. Chondrocyte hypertrophy is driven by the transcription factor Runx2 and is negatively regulated by Sox9. Stimulation with Ihh induces PTHrP expression which stimulates chondrocyte proliferation while inhibiting hypertrophic maturation. Conversely, FGF signaling inhibits chondrocyte proliferation whilst driving hypertrophic differentiation.

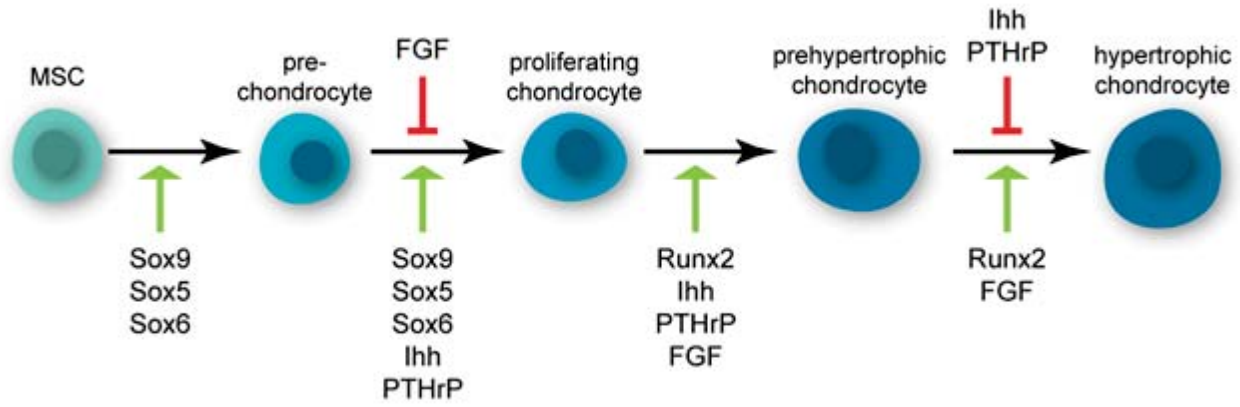
MSC
pre-
chondrocyte
FGF
proliferating
chondrocyte
prehypertrophic
chondrocyte
Ihh
PTHrP
hypertrophic
chondrocyte
Sox9
Sox5
Sox6
Sox9
Sox5
Sox6
Ihh
PTHrP
Runx2
Ihh
PTHrP
FGF
Runx2
FGF

with its targets *Sox5* and *Sox6*, is required for the differentiation of mesenchymal stem cells into chondroblasts and chondrocytes.[148-150] Sox9 stimulates the *in vitro* expression of genes encoding cartilaginous extracellular matrix proteins, including collagen II, IX and XI and aggrecan.[148,151-154] Conditional knockout of *Sox9* in mouse chondrocytes resulted in dwarfism, decreased chondrocyte proliferation and inhibited expression of cartilage matrix genes.[155] Deletion of *Sox9* in early mesenchymal precursors resulted in an absence of the bones of the limbs, resulting from a complete lack of mesenchymal condensation formation.[155]

The transcription factor Runx2 also plays an important role in growth plate development. *Runx2* is expressed by prehypertrophic and hypertrophic chondrocytes and promotes hypertrophic differentiation.[38,156-158] *Runx2*$^{-/-}$ mice, in addition to having a complete lack of osteoblasts, have decreased numbers of hypertrophic chondrocytes.[38,39,156] Conversely, over-expression of *Runx2* results in accelerated hypertrophic differentiation and aberrant mineralisation of cartilage.[158]

1.2.8.3.2 Ihh and PTHrP

A negative feedback loop involving Ihh and PTHrP regulates the rate of chondrogenic proliferation and hypertrophy at the growth plate.[159-162] Ihh, secreted by prehypertrophic and early hypertrophic chondrocytes, stimulates chondrocyte proliferation and inhibits chondrocyte hypertrophy.[144,160,163,164] Ihh binds to the membrane receptor Patched-1, resulting in activation of the membrane protein Smoothened which triggers an intracellular signalling cascade that results in the activation of target genes (reviewed in [136]). *Ihh* knockout mice exhibit severe dwarfism with a complete lack of endochondral bone formation.[144]

In vitro and *in vivo* studies have demonstrated that PTHrP mediates the effects of Ihh, with the inhibition of chondrocyte hypertrophy being dependent on the Ihh-dependent induction of PTHrP expression in perichondrial cells and early proliferating chondrocytes.[144,160,165,166] PTHrP acts on late proliferative zone and prehypertrophic chondrocytes, stimulating proliferation and delaying hypertrophy.[166,167] The inhibition of hypertrophy by PTHrP thus decreases the number of cells expressing *Ihh*, negatively regulating its expression.[167] PTHrP and PTH/PTHrP receptor deficient mice display dwarfism due to premature chondrocyte hypertrophy.[160,167-169] In humans, inactivating mutations in the PTH/PTHrP receptor gene *PTH1R* are associated with Blomstrand chondro-osteodystrophy, a condition associated with prenatal death, shortened limbs and premature ossification.[170-172]

1.2.8.3.3 Fibroblast growth factor (FGF)

Members of the FGF family play an important role in chondrogenic differentiation, negatively regulating bone growth. *In vivo* and *in vitro* studies have demonstrated that FGFs inhibit chondrocyte proliferation and increase hypertrophic differentiation. In embryonic limb explant cultures, treatment with FGF2 or FGF1 inhibits the rate of chondrocyte proliferation and accelerated hypertrophy, countering the effects of Ihh/PTHrP signalling.[173,174] Mice with activating mutations in *Fgfr3* have severely shortened limbs and decreased numbers of proliferating and hypertrophic chondrocytes.[175-179] In contrast, *Fgfr3*$^{-/-}$ mice have hyperproliferative chondrocytes and prolonged endochondral bone growth, resulting in abnormally long limbs.[180,181] In addition, in humans, constitutively activating mutations in *FGFR*3 are associated with several common forms of dwarfism, including achondroplasia[182], hypochondroplasia[183] and thanatophoric dysplasia[184].

1.2.8.3.4 IGF-I

IGFs are produced locally in the growth cartilage to mediate the effects of growth hormone on long bone growth. IGF deficiency, resulting from insensitivity to growth hormone, results in short stature in Laron syndrome in humans (reviewed in [185]). Additionally, deletion of *Igf1* or *Igfr1* in mice results in severe dwarfism.[186] *In vitro* studies have demonstrated that IGF-1 is a potent chondrocyte mitogen that promotes chondrogenic differentiation.[187-189]

1.3 Calcium and phosphate metabolism

In addition to its mechanical and protective roles, the skeleton serves as a homeostatic reservoir for calcium and phosphate storage. These minerals can be mobilised to maintain systemic mineral homeostasis in response to hormonal regulatory signals. Serum calcium and phosphate levels are primarily regulated by two hormones, PTH and 1,25-dihydroxyvitamin D_3, acting on the bone, the kidney and the gastrointestinal tract. These hormones act to maintain serum and extracellular fluid calcium and phosphate within the normal range and to maintain levels required for cellular activities, including neural and muscle function.

1.3.1 Hormonal control of calcium and phosphate metabolism

1.3.1.1 PTH

PTH is an 84-amino-acid peptide, secreted by the parathyroid gland, which mediates its effects through binding of its amino terminus to the PTH/PTHrP receptor. PTH is responsible for regulating the distribution of calcium. A decrease in serum ionised calcium levels stimulates the rapid release of PTH from the parathyroid gland and upregulates the transcription of *PTH* (reviewed in [190]). This hormone acts on bone-resorbing osteoclasts to increase dissolution of calcium and phosphate from the bone, increases renal resorption of calcium and excretion of phosphate and stimulates the production of 1,25-dihydroxyvitamin D_3 via the activation of 1α-hydroxylase enzyme (reviewed in [190]).

In the kidney, PTH increases the reabsorption of calcium, predominantly in the distal convoluted tubule. This occurs in part through upregulation of calbindin and basolateral membrane Na/Ca exchanger expression and by increasing the activity of the PMCA1 calcium pump (reviewed in [190]). In addition, PTH inhibits the reabsorption of phosphate in the kidney, in part through stimulating the internalisation of sodium-phosphate co-transporters (reviewed in [191]). Thus, hyperparathyroidism generally results in increased serum calcium and decreased serum phosphate.

There are complex regulatory effects of PTH on the bone. Continuous exposure to high levels of PTH, such as in primary and secondary hyperparathyroidism, increases osteoclastic bone resorption. This is primarily due to the stimulation osteoblasts and stromal cells to induce the production of osteoclastogenic factors, such as RANKL.[192-194] However, sporadic exposure to PTH increases osteoblast differentiation and bone matrix synthesis.[195] Some studies have also suggested that osteoclasts may directly respond to PTH as human osteoclasts express the PTH/PTHrP receptor[196], although this has not been determined conclusively.

In addition, PTH acts to stimulate the conversion of 25-hydroxyvitamin D3 to 1,25-dihydroxyvitamin D_3 in the kidney, thereby indirectly increasing the intestinal absorption of calcium and phosphate (reviewed in [190]). In turn, 1,25-dihydroxyvitamin D_3 has a negative regulatory effect on PTH production, by inhibiting *PTH* gene transcription.[197]

1.3.1.2 Vitamin D

Vitamin D is responsible for maintaining serum calcium and phosphate levels. The endogenous form of vitamin D, 1,25-dihydroxyvitamin D_3, is synthesised in a series of reactions in the skin, liver and kidney. Unhydroxylated vitamin D_3 (cholecalciferol) is

formed in the skin from the cholesterol metabolite 7-dehydrocholesterol in a reaction driven by ultraviolet (UV) radiation (reviewed in [190]). The cholecalciferol is transported in the circulation to the liver, where it is converted by a hydroxylase enzyme, CYP27B1, to 25-hydroxyvitamin D_3. In the proximal tubule of the kidney, 25-hydroxyvitamin D_3 is 1α-hydroxylated to produce 1,25-dihydroxyvitamin D_3, the most metabolically active form of the hormone. This reaction can also occur in other tissues including epidermal keratinocytes[198,199], the liver[200], monocytes/macrophages[201] and bone cells[202-204]. However, in normal circumstances, extra-renal production does not contribute to circulating levels of 1,25-dihydroxyvitamin D_3, although it may act in an autocrine and paracrine manner to regulate local cellular activity.[199,204-206] The renal synthesis of 1,25-dihydroxyvitamin D_3 is stimulated by PTH and by decreased serum phosphate and, in a positive feedback loop, by 1,25-dihydroxyvitamin D_3 itself (reviewed in [190]).

Vitamin D metabolites bind to a nuclear hormone receptor, the vitamin D receptor (VDR), which homodimerises or heterodimerises to the retinoic acid X receptor (RXR). This complex then binds to vitamin D response elements in the promoter region of target genes to regulate the transcription of genes that mediate the effects of vitamin D on calcium and phosphate metabolism.

The primary role of vitamin D is to increase intestinal absorption of calcium and phosphate (reviewed by [190]). 1,25-dihydroxyvitamin D_3 increases calcium absorption by inducing the expression of genes involved in transcellular calcium transport, including the calcium channel *TRPV6*[207], the calcium binding protein calbindin (*CALB1*)[208] and the calcium ATPase PMCA1b (*ATP2B1*)[209,210]. In addition, vitamin D may also stimulate rapid effects on transcellular calcium absorption in the intestine through directly acting on putative membrane receptors to rapidly stimulate cellular calcium flux (reviewed in [190]). 1,25-dihydroxyvitamin D_3 also increases phosphate absorption, although the mechanisms involved are less well understood. Phosphate absorption in the small intestine occurs via passive paracellular and active transcellular mechanisms. Vitamin D upregulates intestinal phosphate resorption through stimulation of the activity of the luminal Na^+/Pi transporter NPT2b or by upregulating *NPT2B* expression.[211]

In the kidney, 1,25-dihydroxyvitamin D_3 stimulates resorption of phosphate at the proximal tubule and of calcium in the distal nephron (reviewed in [190]). However, these effects are weak relative to the action of PTH on renal handling of calcium and phosphate.

1,25-dihydroxyvitamin D_3 also maintains serum phosphate and calcium levels by stimulating osteoclast activity. 1,25-dihydroxyvitamin D_3 indirectly increases the

formation and resorptive activity of mature osteoclasts through induction of RANKL expression and inhibition of OPG production by osteoblasts.[97,212] 1,25-dihydroxyvitamin D_3 also promotes mineralisation of osteoid, perhaps through increased local concentrations of calcium caused by increased osteoclast activity.[213] However, in patients with inactivating *VDR* mutations, and in vitamin D-deficient rats and *Vdr* knockout mice, normal bone formation can be restored by normalising serum calcium and phosphate levels[213-215] (reviewed in [216]). Therefore, the actions of 1,25-dihydroxyvitamin D_3 may not be necessary for regulation of osteoclast and osteoblast activity in situations where serum calcium and phosphate levels are maintained in the normal range.

1.4 Tyrosine kinase inhibitors

1.4.1 Imatinib mesylate

Imatinib mesylate (Glivec/Gleevec, STI571, CGP 57148B; Novartis, Basel, Switzerland) is a 2 phenylaminopyrimidine derivative that binds to the ATP-binding site of a select group of protein tyrosine kinases, thereby precluding ATP-binding and inhibiting kinase activity (figure 1.8).[1] Imatinib was originally discovered during a small molecule screen for specific inhibitors of tyrosine kinase activity and was subsequently found to have specificity for Bcr-Abl, Kit and PDGFR, suggesting its application for the treatment of tumours and non-malignant proliferative disorders characterised by dysregulated activity of these kinases.[1] Imatinib was the first small molecule tyrosine kinase inhibitor to be successfully used in the clinic. It is currently the gold standard treatment for Philadelphia chromosome-positive CML in chronic phase and for some forms of GIST, based on its inhibition of Bcr-Abl and Kit, respectively.

Although imatinib was designed to specifically target Bcr-Abl, many off-target kinases are affected by imatinib. At therapeutically-achievable concentrations (4.6 μM at 400 mg/day)[4], imatinib inhibits the tyrosine kinases Abl (IC_{50} = 0.22 μM)[217], Abl2 (also known as abl-related gene [ARG]; IC_{50} = 0.5 μM)[218], collagen-induced discoiddin domain receptor 1 (DDR1; IC50 = 0.34 μM)[219] and DDR2 (IC_{50} = 0.68 μM)[219], the PDGFR family members stem cell factor (SCF) receptor (Kit; IC_{50} = 0.1 μM)[220], PDGFRα and -β (IC_{50} = 0.1 μM)[220] and Fms (IC_{50} = 1.4 μM)[221]. Additionally, imatinib has recently been determined to potently inhibit the non-tyrosine kinase targets NAD(P)H:quinone oxidoreductase 2 (NQO2; IC_{50} = 0.080 μM)[222,223] and some members of the carbonic anhydrase (CA) family of metalloproteases, including CAII (IC_{50} = 0.030 μM) and CAXIV (IC_{50} = 0.47 μM)[224].

Figure 1.8. Imatinib mesylate. Imatinib binds to the ATP-binding pocket of receptor and non-receptor protein tyrosine kinases, precluding ATP binding and thus inhibiting kinase activity and downstream signalling.

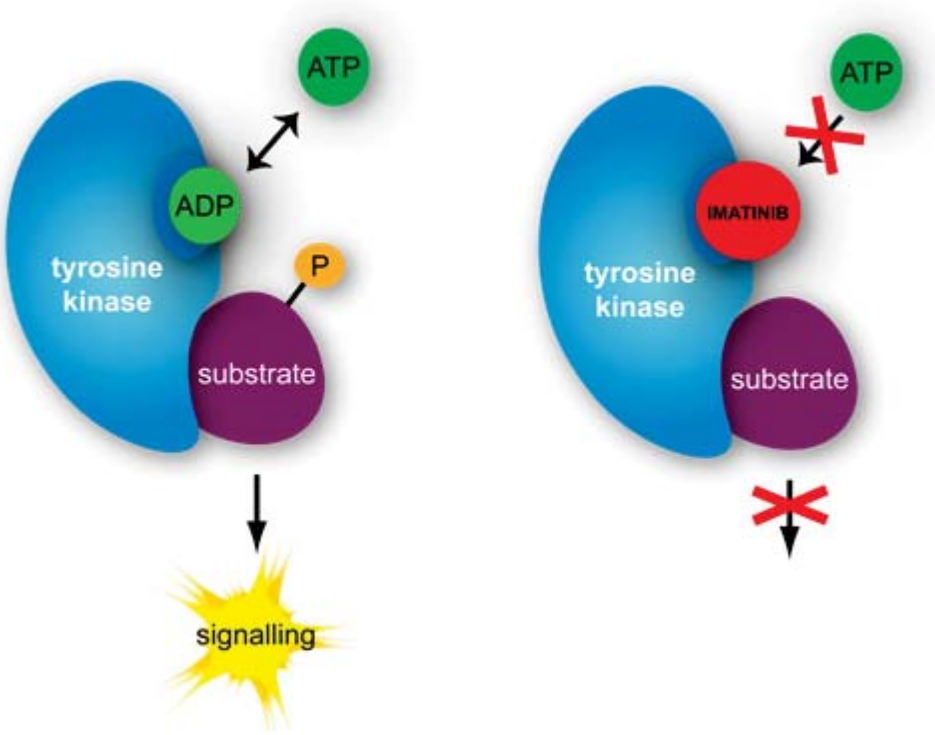
ATP
ADP
tyrosine kinase
P
substrate
signalling
ATP
IMATINIB
tyrosine kinase
substrate

1.4.1.1 Imatinib resistance and second-generation tyrosine kinase inhibitors

Imatinib is an effective treatment for CML in the proliferative chronic phase, resulting in complete haematological remission in 98% of chronic-phase, newly-diagnosed CML patients and complete cytogenetic response in 86% of patients.[4] Primary resistance to imatinib is only occasionally seen in chronic-phase CML patients, whereas patients with advanced CML or Bcr-Abl-positive acute lymphoblastic leukaemia (ALL) show substantially decreased initial response rates.[225,226] Mechanisms of resistance are complex and include high serum levels of the imatinib-binding protein α_1-acid glycoprotein[227], increased activity of the ATP-binding cassette transporter B1 (ABCB1; also known as multidrug resistance-1 [MDR1] and p-glycoprotein) drug efflux pump[228] or decreased function of the imatinib influx pump OCT-1[229-231]. In the majority of cases, however, relapse is associated with point mutations in the *BCR-ABL* or *KIT* kinase domain, resulting in a decrease in the affinity of imatinib for the kinase[232-234] (reviewed in [2]). Amino acid substitutions associated with imatinib resistance are believed to either stabilise the closed conformation of the kinase domain, or to occur at residues that come into direct contact with the drug thereby precluding drug binding.[233]

Resistance to imatinib therapy in ALL and acute/blast phase CML, and relapse in chronic CML and GIST, highlighted the need for tyrosine kinase inhibitors that show greater specificity or affinity for their target kinases to overcome imatinib-resistant mutations. This has lead to the development of second generation ATP-competitive inhibitors, such as nilotinib (Novartis), bosutinib and dasatinib (Brystol-Myers Squibb).

1.4.1.1.1 Dasatinib

Dasatinib (SPRYCEL; BMS-354825) is a thiazolecarboxamide, structurally unrelated to imatinib. Dasatinib was originally selected as a potent small molecule inhibitor of sarcoma viral oncogene homologue (Src) family kinases (including Src, Lck, Hck, Yes, Fgr, Lyn and Fyn) that was subsequently found to have activity against Abl, Kit and PDGFRα and β at concentrations of less than 10 nM.[235-237] Dasatinib has significant preclinical activity against the majority of imatinib-resistant point mutations and has been shown to be highly successful clinically in imatinib-resistant CML.[235,238] In a phase I trial of patients with chronic phase CML and imatinib-resistance, dasatinib treatment resulted in a 92% complete haematological response rate and a major cytogenetic response rate of 45%.[239] Furthermore, dasatinib showed a high activity in patients with accelerated or blast phase

CML, or Bcr-Abl-positive ALL, with a major haematological response rate of 70% in these patients.[239] In an open label, single-arm, phase II clinical trial in patients with advanced chronic-phase Bcr-Abl-positive CML, 87% of dasatinib patients achieved a complete haematological response within 8 months of treatment.[238] Based on these results, in November 2006, dasatinib was granted approval in the US and Europe for use in the treatment of imatinib resistant and intolerant Bcr-Abl-positive CML and of Bcr-Abl-positive ALL (reviewed in [240]). While dasatinib has proven to be a safe and effective treatment, it is yet to be seen whether the increased potency of dasatinib against a broader spectrum of kinase targets will result in an increase in off-target toxicities in the long term.

1.4.2 Altered calcium and phosphate metabolism in imatinib-treated patients

Considering the wide range of signalling pathways inhibited by imatinib, one might expect that imatinib therapy would be associated with severe adverse effects. However, imatinib is well tolerated, compared with traditional chemotherapies, with adverse effects that are commonly only mild to moderate, including oedema, musculoskeletal pain, nausea, diarrhoea and rash.[3,4] An additional common and unexpected side-effect of imatinib therapy is disturbed calcium and phosphate metabolism, as evidenced by decreased serum phosphate and calcium levels.

Altered phosphate metabolism was first reported in patients receiving imatinib therapy for GIST, CML and sarcoma by Berman *et al*.[5] These studies showed that a subgroup (25 of 49) of imatinib-treated patients had low serum phosphate levels, compared with healthy controls. This group was receiving significantly higher doses of imatinib than the patients with normal serum phosphate levels. Furthermore, the group of patients with low serum phosphate levels also exhibited significantly lower total calcium and, subsequently, significantly higher serum PTH levels than the group of imatinib-treated patients with normal phosphate levels. These findings were consistent with results from two clinical trials which showed that 50% of patients receiving imatinib exhibited hypophosphataemia of grade 2 or above at some stage during imatinib therapy.[6]

Subsequent to this report, several other groups have reported altered phosphate metabolism as a side-effect of imatinib treatment. A longitudinal study of GIST patients receiving imatinib for 24 months found that 10/11 patients had lower mean plasma phosphate levels during treatment than at baseline.[7] Similarly, a prospective study of 9 CML patients found that, relative to baseline, phosphate levels were significantly decreased after 3, 6 and 18 months of imatinib treatment.[8,12] In a retrospective study of 17

CML patients receiving imatinib therapy over 17 – 69 months, there was a significant decrease in serum phosphate levels, compared with baseline.[10] Osorio *et al*.[9] reported that 36 CML patients showed a significant decrease in serum phosphate levels after 3 months of imatinib treatment that was sustained until the final analysis at 12 months. In the largest study to date, Franceschino *et al*.[11] observed significantly decreased serum phosphate levels after 6 and 12 months of imatinib treatment in a cohort of 50 CML patients.

These studies strongly suggest that imatinib treatment results in decreased serum phosphate levels[7-12], resulting in hypophosphataemia in at least 50% of patients[5-7]. In addition, these patients exhibit an increase in serum levels of PTH, secondary to decreased calcium levels, and increased serum 1,25-hydroxyvitamin D_3.[5,8-10,12]

As discussed in section 1.3, homeostatic control of serum phosphate and calcium levels is achieved via three mechanisms: (1) resorption of phosphate and calcium by the kidneys, (2) absorption of dietary phosphate and calcium by the gut and (3) dissolution of phosphate and calcium from bone. Therefore, it is conceivable that reduced levels of calcium and phosphate seen in imatinib treated patients could result from one or a combination of the following mechanisms: decreased intestinal absorption of phosphate and calcium, increased urinary loss of phosphate and calcium, decreased dissolution of calcium and phosphate from bone, or sequestration of phosphate and calcium from extracellular fluid into the bone.

It is unlikely that the decreased serum calcium and phosphate levels result from gastrointestinal malabsorption. Although approximately 50% of imatinib-treated CML and GIST patients experience nausea and diarrhoea[241,242], which could result in increased loss of electrolytes, the severity of these conditions is usually mild to moderate and is unlikely to result in a sustained loss of calcium and phosphate.

Several case reports suggest that imatinib therapy may be associated with renal dysfunction. Kitiyakara & Atichartakarn[243] described a 67-year-old man with pre-existing chronic renal failure who developed acute renal failure following commencement of treatment with cytarabine and imatinib for blast phase CML. Pou *et al*. [244] reported on a 58-year-old patient who developed acute renal failure with tubular necrosis after starting imatinib therapy for CML. Another case study described a patient with haematuria who commenced treatment with imatinib and subsequently developed proximal tubular renal dysfunction (partial Fanconi Syndrome) and hypophosphataemia.[245] A fourth study described a 60-year-old woman with microalbuminuria at diagnosis who developed sub-acute renal failure during imatinib therapy, which resolved following discontinuation of

treatment.[246] In an additional 3 cases, kidney malfunction resulted from tumour lysis syndrome.[247-249] The paucity of reports describing acute renal dysfunction with imatinib therapy suggests this is a relatively rare event that may only occur as result from tumour lysis syndrome or in patients with pre-existing kidney problems.

Nonetheless, imatinib therapy is associated with decreased reabsorption of phosphate by the kidneys, suggesting that increased renal phosphate output may be causing the observed decreases in serum phosphate.[245] Berman *et al*.[5] reported increased urinary phosphate output in patients undergoing imatinib therapy compared with normal controls. Another study reported that maximal tubular resorption of phosphate (TmP/GFR) was significantly decreased, relative to baseline levels, at 3, 6 and 18 months of imatinib treatment in CML patients.[8,12]

The analysis of serum hormone levels in imatinib-treated patients suggest that the observed phosphaturia may be secondary to increased PTH. Hypophosphataemia caused by decreased tubular reabsorption of phosphate is usually associated with decreased serum levels of 1,25-dihydroxyvitamin D_3 and normal levels of PTH. However, in imatinib-treated patients, the decreased serum phosphate is associated with increased serum PTH and 1,25-dihydroxyvitamin D_3.[5,8,9,12] As PTH stimulates the proximal tubule in the kidney to decrease tubular resorption of phosphate, the increased urinary phosphate levels are likely to be secondary to increased serum PTH, rather than a direct inhibitory effect of imatinib on the kidneys. While it cannot be ruled out that kidney problems may contribute to the decreased serum phosphate levels, there has been no evidence presented thus far to demonstrate direct toxic effects of imatinib on the kidney.

Decreased serum calcium and phosphate levels could result from sequestration of these minerals to bone via a decrease in bone resorption and/or an increase in bone deposition, as has been described in patients treated with the bisphosphonate zoledronic acid.[250-252] In support of this hypothesis, there is growing evidence that patients undergoing imatinib therapy experience dysregulated bone remodelling. The next section of this chapter will discuss the possibility that these changes result from direct inhibitory effects on bone-resorbing osteoclasts and anti-proliferative and pro-differentiation effects on bone-forming osteoblasts.

1.4.3 Effects of imatinib on bone

Recent published data suggest that changes in bone parameters may occur in imatinib-treated patients. Studies from our group have shown that, relative to baseline, CML

patients receiving imatinib for periods in excess of 17 months exhibited significantly increased iliac spine trabecular bone volumes.[10] Almost half of the patients (8/17), including 4 patients that had a significant degree of osteoporosis at initial diagnosis, had an increase in trabecular bone volume of greater than 2-fold. The changes in trabecular bone volume inversely correlated with serum phosphate and total calcium levels. Conversely, no changes in trabecular bone volume were observed in a cohort of CML patients that responded to interferon-α therapy, suggesting that these changes were not related to decreased occupation of the marrow by tumour, but were due to the actions of imatinib.

In a subsequent study by Jönsson *et al*.[20], regional bone mineral density (BMD) was examined in CML patients treated with imatinib for 24 – 73 months. Imatinib-treated patients had significantly higher lumbar spine and total hip BMD compared with normal aged-matched controls, as determined by dual energy X-ray absorptiometry (DXA). Additionally, peripheral quantitative computed tomography (pQCT) analysis revealed that the radial and tibial cortical BMD, but not trabecular BMD, was significantly higher in the imatinib-treated group than in the control group. This was associated with decreased serum phosphate and calcium, as well as a decrease in serum levels of bone formation markers.

In a prospective study, O'Sullivan *et al*.[12] measured BMD in 9 CML patients receiving imatinib therapy over a 24 month period. They observed a small, but significant, increase in vertebral BMD and a trend towards an increase in total body BMD by 12 months; however, no change in proximal femur BMD was observed.

Preliminary *in vivo* studies support the hypothesis that imatinib treatment results in increased bone volume. In skeletally immature 4-week-old male C3H mice, treatment with 110 mg/kg/day or 150 mg/kg/day imatinib for 10 weeks resulted in a small, but significant, increase in tibial trabecular BMD (assessed by DXA) and bone volume (BV/TV; assessed by micro-computed tomography [μ-CT]).[253,254] This augmentation of BMD and BV/TV was associated with an increase in trabecular number and a decrease in trabecular separation.

Collectively, these data strongly suggest that imatinib alters bone remodelling in animals and patients. While the mechanism(s) remain to be fully elucidated, these changes in bone remodelling parameters may be due to a decrease in bone resorption that is not corrected by a concomitant decrease in osteoblast activity or, conversely, due to an increase in osteoblast activity that is not balanced by an increase in osteoclast activity. These effects would theoretically result in a decrease in the dissolution of calcium and phosphate from bone, or an increase in the sequestration of calcium and phosphate to bone,

resulting in decreased serum levels of phosphate and calcium (figure 1.9). In support of this hypothesis, there is growing evidence that imatinib has direct effects on the proliferation and activity of cells involved in maintaining bone homeostasis: the bone-resorbing osteoclasts and the bone-forming osteoblasts.

1.4.4 Evidence for anti-osteoclastogenic effects of imatinib

As discussed in section 1.2.5, osteoclasts are large, multinucleated haematopoietic cells of the monocyte/macrophage lineage which are capable of resorbing mineralised bone. The formation of osteoclasts from monocyte/macrophage precursor cells *in vitro* is largely dependent on two factors: RANKL, which drives osteoclast fusion, activity and survival[97-99], and M-CSF, which is essential for the proliferation and survival of the osteoclast precursor cells and for survival of the mature osteoclast.[113,114,255-257]

In vitro studies show that imatinib directly inhibits osteoclastogenesis, with treatment reducing the formation of TRAP-positive osteoclasts from human CD14+ peripheral blood mononuclear cells, primary rat bone marrow cells and primary rabbit bone marrow-derived monocytes at concentrations of 1 μM and greater.[13-15] In addition, imatinib inhibits the bone resorptive activity of human osteoclasts at concentrations lower than those required to decrease osteoclast numbers, with 0.3 μM imatinib and higher significantly decreasing their capacity to resorb a dentine substrate.[13]

There is also evidence that imatinib inhibits the survival of osteoclast precursors and mature osteoclasts *in vitro*. The proliferation, survival and activity of primary human monocyte/macrophage lineage cells were inhibited by imatinib at concentrations of 1.5 μM and greater.[258,259] In cultures of murine bone marrow cells, imatinib treatment was found to dose-dependently decrease the number of viable cells, relative to vehicle controls.[14,17] Additionally, in pure cultures of mature osteoclasts, imatinib treatment reversed the anti-apoptotic effect of M-CSF treatment, resulting in increased caspase-dependent apoptosis.[15] In contrast, imatinib treatment had no effect on apoptosis of cells cultured in IL-1α, RANKL, or without cytokines.[15]

Consistent with these *in vitro* findings, analyses of serum markers of bone turnover suggest that osteoclast activity may be decreased in imatinib-treated patients. Berman *et al*.[5] observed that patients treated with imatinib had significantly lower levels of the bone resorption marker C-terminal collagen crosslinks (CTX-1) when compared with healthy controls. This was particularly marked in patients with low serum phosphate.[5] Additionally, O'Sullivan *et al*.[12] found that serum CTX-1 levels were significantly

Figure 1.9. Proposed model for the effects of imatinib on calcium and phosphate metabolism. Decreased dissolution of calcium and phosphate from the bone, or increased deposition of calcium and phosphate in newly-formed bone, may result in decreased serum calcium and phosphate levels in imatinib-treated patients. The decrease in serum phosphate results in increased 1,25-dihydroxyvitamin D_3 production, which in turn stimulates increased phosphate and calcium resorption by the gut and decreases phosphate excretion by the kidneys. Decreased serum calcium causes increased PTH production, increasing calcium reabsorption and phosphate excretion by the kidney and stimulating a further increase in 1,25-dihydroxyvitamin D_3. PTH also stimulates bone resorption to release calcium and phosphate from bone; however, this may be inhibited by imatinib. Decreased absorption of phosphate and calcium due to gastrointestinal problems and decreased tubular resorption of phosphate may, in some cases, also contribute to the decreased levels of serum calcium and phosphate in imatinib-treated patients (not shown).

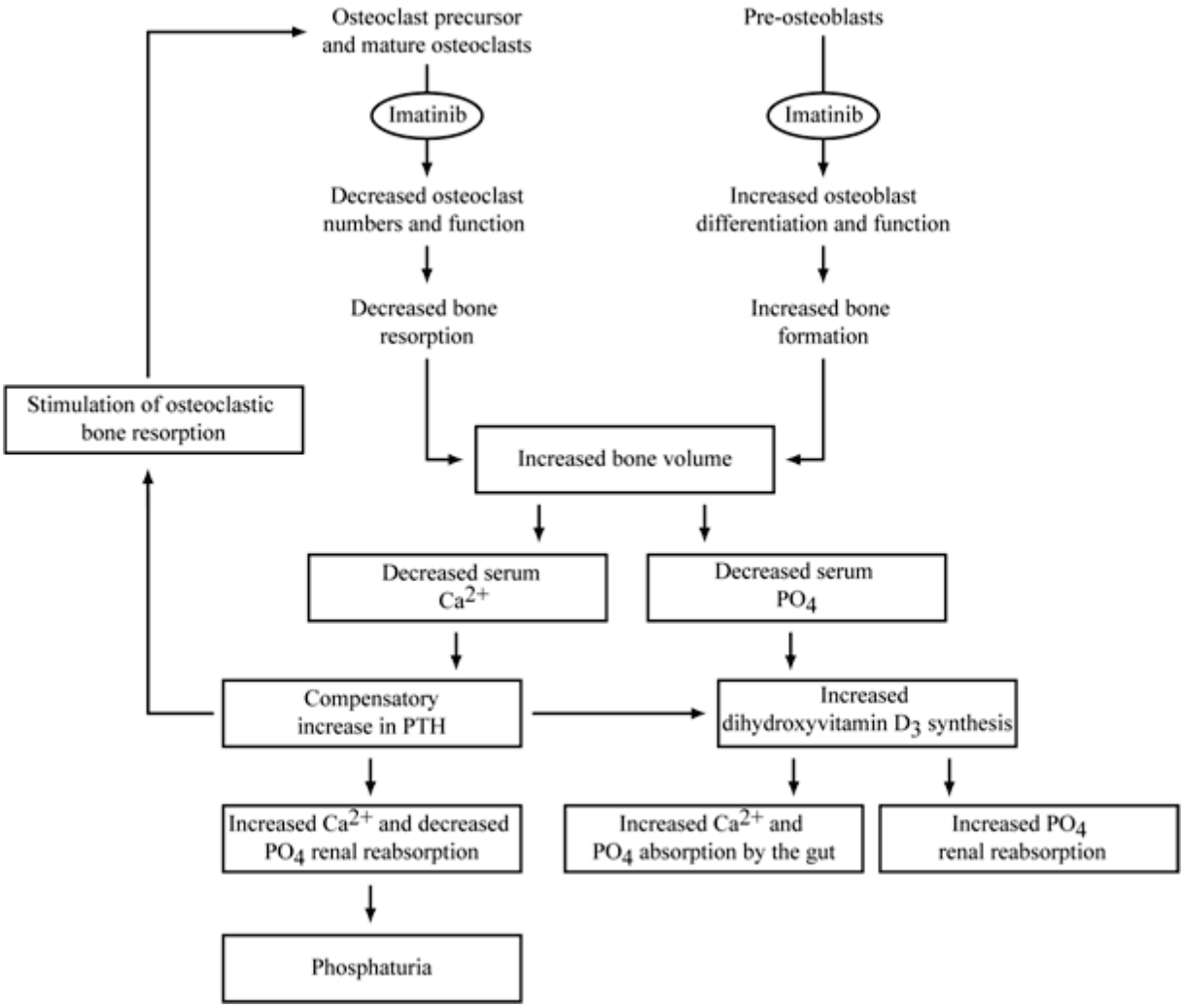
Osteoclast precursor and mature osteoclasts
Pre-osteoblasts
Imatinib
Imatinib
Decreased osteoclast numbers and function
Increased osteoblast differentiation and function
Decreased bone resorption
Increased bone formation
Stimulation of osteoclastic bone resorption
Increased bone volume
Decreased serum Ca^{2+}
Decreased serum PO_4
Compensatory increase in PTH
Increased dihydroxyvitamin D_3 synthesis
Increased Ca^{2+} and decreased PO_4 renal reabsorption
Increased Ca^{2+} and PO_4 absorption by the gut
Increased PO_4 renal reabsorption
Phosphaturia

decreased in a group of CML patients following 18 months of imatinib treatment. Decreases in serum osteoclast markers have also been observed in imatinib-treated normal mice. Preliminary results suggest that treatment of 4-week-old C3H mice with imatinib for 10 weeks resulted in a significant reduction in the serum levels of the osteoclast marker TRAP5b, compared with vehicle-treated controls[253,254], indicating that imatinib treatment mediated a decrease in osteoclast activity in these animals.

While these observed changes in bone resorption markers suggest that imatinib may be inhibiting osteoclasts, directly or indirectly, no histological studies have been carried out to determine changes in osteoclast numbers in imatinib-treated patients. In animal studies, treatment of C57BL/6 mice with 75 mg/kg imatinib resulted in a significant decrease in the number of osteoclast-occupied resorption lacunae in the tibia, relative to vehicle controls.[13] Similarly, preliminary data suggest that imatinib treatment of skeletally immature 4-week-old male C3H mice for 10 weeks resulted in a significant decrease in osteoclasts and resorption lacunae in the femorae, but not in the vertebrae.[253,254]

Taken together, these results strongly suggest that imatinib is a direct inhibitor of osteoclast survival, differentiation and activity. There are a number of known targets which may be contributing to the anti-osteoclastogenic activity of imatinib which include Fms, Kit, CAII and PDGFRα and β (figure 1.10).

1.4.4.1 The role of Fms in the inhibition of osteoclasts by imatinib

Fms is a transmembrane receptor that is a member of the type III receptor tyrosine kinase family which includes PDGFRα and β, Kit and Flt3. Fms is expressed by a variety of cell types, including primitive multipotent haematopoietic cells, mononuclear phagocyte progenitors, monocytes, tissue macrophages, osteoclasts, B-cells, smooth muscle cells, neurons and some cells of the female reproductive tract.[260] While imatinib was originally reported as having no effect on Fms phosphorylation[220], subsequent work from our laboratory[221] and those of others[261-263] showed that it potently and selectively inhibits M-CSF-induced Fms activity at therapeutically-achievable concentrations. Imatinib inhibits the phosphorylation of Fms in a murine haematopoietic cell line ectopically expressing human *CSF1R* (FDC-Fms) at an IC_{50} of 1.42 μM, without affecting total Fms protein levels.[221] Additionally, imatinib has been shown to inhibit M-CSF-dependent, but not IL-3-dependent, proliferation of FDC-Fms cells and in Rat-2 and Bac1,2F5 fibroblasts ectopically expressing human *CSF1R* at concentrations of 0.5 – 2 μM and

Figure 1.10. Hypothetical schema for the effects of imatinib on osteoclasts and osteoblasts. The proliferation and survival of osteoclast precursors (pre-OC) and the survival of mature osteoclasts (OC) is driven by M-CSF signalling through the receptor tyrosine kinase Fms. The inhibition of Fms signalling by imatinib decreases OC numbers and activity. In addition, inhibition of Kit may decrease pre-OC numbers and inhibit OC activity. Imatinib also inhibits the proton-generating activity of CAII, preventing the dissolution of mineral from bone and, hence, inhibiting bone resorption. Further, the inhibition of PDGFR signalling on osteoblasts (OB) inhibits the production of osteoclastogenic cytokines including M-CSF and RANKL. Additionally, inhibition of PDGFR by imatinib in pre-OB and OB inhibits cell proliferation but also relieves the inhibitory effects of PDGF on OB maturation, resulting in decreased cell numbers but increased OB activity. HSC: haemopoietic stem cell; MSC: mesenchymal stem cell.

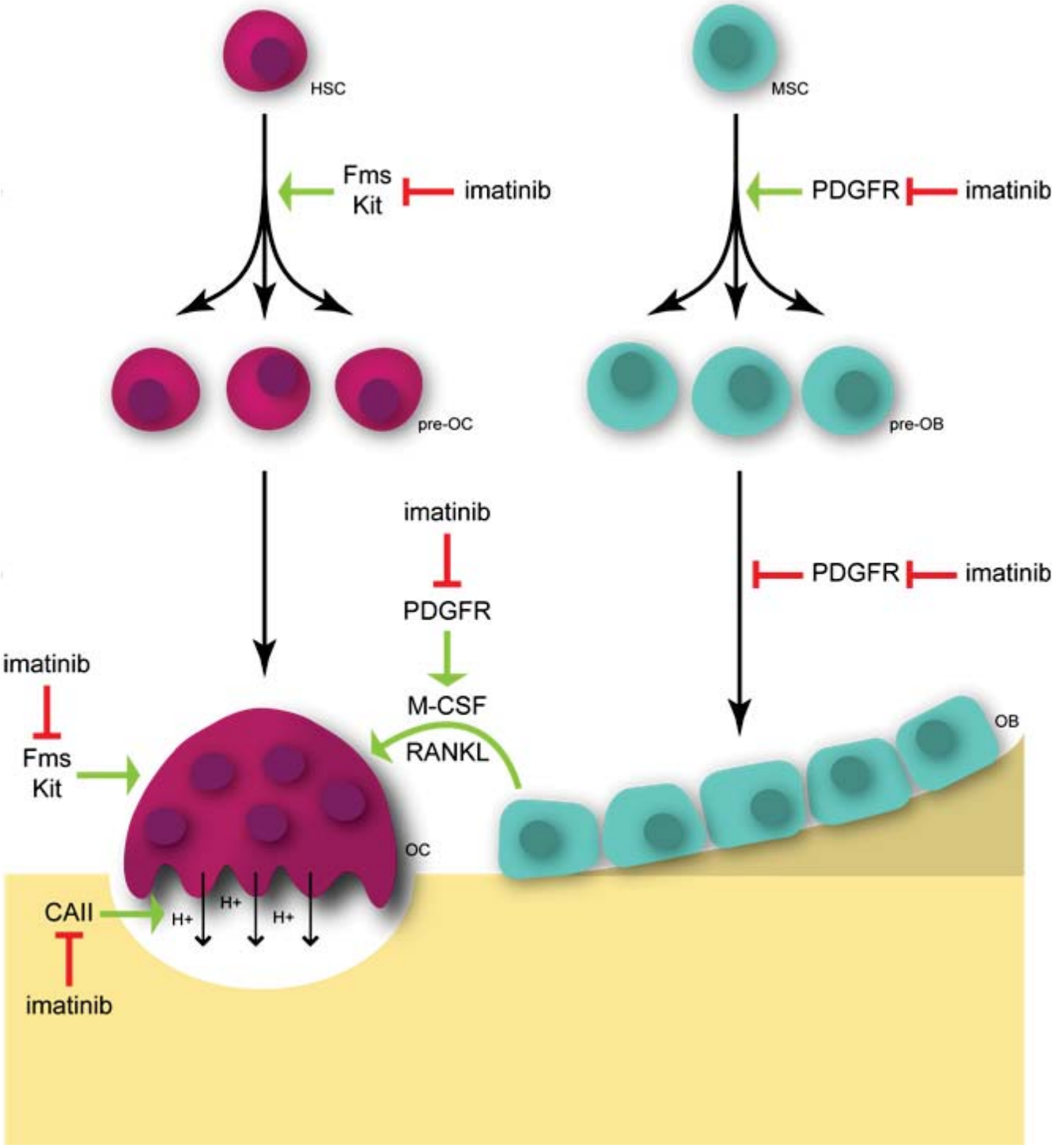
HSC
MSC
Fms
Kit
imatinib
PDGFR
imatinib
pre-OC
pre-OB
imatinib
PDGFR
imatinib
PDGFR
M-CSF
RANKL
imatinib
Fms
Kit
OB
OC
CAII
H+
H+
H+
imatinib

higher.[221,261,263,264] This specific inhibition of Fms phosphorylation/activity with imatinib treatment suggests a mechanism whereby imatinib may inhibit osteoclastogenesis.[221]

M-CSF is essential for osteoclastogenesis *in vitro* and *in vivo*. Signal transduction through Fms regulates the proliferation, differentiation, activation and survival of monocyte/macrophage lineage cells, including osteoclast precursors.[114] In osteoclasts, M-CSF inhibits apoptosis and promotes cell proliferation, migration and cytoplasmic spreading.[255-257] Although RANKL is the primary promoter of osteoclast differentiation, M-CSF also plays a role through induction of the expression of osteoclast-associated genes, including RANK.[112,113]

The importance of M-CSF in osteoclast activity is illustrated by *op/op* mice, which are M-CSF deficient.[265,266] In these animals, a profound decrease in osteoclast numbers, due to defective osteoclast proliferation and differentiation, results in severe osteopetrosis and defective tooth eruption.[265] Administering M-CSF to *op/op* animals rapidly restores osteoclast numbers.[266] Homozygous knockouts for *Csf1r* have an identical phenotype to *op/op* mice.[111]

The importance of Fms signalling in osteoclast survival and activity, together with the similarities in the IC_{50} concentrations of imatinib required to inhibit osteoclast formation and activity, suggests that inhibition of Fms is a mechanism whereby imatinib inhibits osteoclastogenesis. In addition, the second generation tyrosine kinase inhibitor nilotinib has been found to inhibit Fms and osteoclastogenesis *in vitro*.[264] Inhibition of Fms kinase activity therefore may account, in part, for the dysregulated bone remodelling observed in patients undergoing imatinib treatment.

1.4.4.2 The role of Kit in osteoclastogenesis

In addition to Fms, inhibition of signalling through Kit by imatinib may affect osteoclastogenesis. Kit is a transmembrane tyrosine kinase which binds soluble or membrane-bound isoforms of its ligand, SCF (also known as mast cell growth factor, steel factor, Kit ligand).[267] Some *in vitro* evidence suggests that Kit may play a role in osteoclastogenesis. Kit is expressed by osteoclasts[268] and SCF has been shown to be mitogenic for haematopoietic stem cells[269] and osteoclast precursors[270,271]. Soluble SCF stimulates osteoclast precursor proliferation, resulting in increased osteoclast numbers[270,271] and promotes mature osteoclast activity[272]. Kit signals via Mitf[272], which also lies downstream of Fms[115] and RANK[273]. The essential role of Mitf in osteoclast formation is demonstrated by *Mitf*$^{mi/mi}$ mice, which exhibit severe osteopetrosis due to

defective osteoclast fusion.[274,275] Inhibition of Kit signalling may therefore contribute to the anti-osteoclastogenic properties of imatinib.

1.4.4.3 The role of CAII in osteoclast activity

The recent identification of CAII as a non-kinase target of imatinib suggests another mechanism by which imatinib may inhibit bone resorption. The α-CA are a family of zinc enzymes which are responsible for catalysing the conversion of carbon dioxide and water to carbonic acid, which dissociates to form carbonate and a proton.

CAII plays an important role in the resorption of the bone matrix by the osteoclast. Bone mineral dissolution is carried out by acidification of the extracellular space formed adjacent to the resorptive surface of the osteoclast through the excretion of protons via a proton pump (H^+-ATPase).[91] CAII enables the acidification of the resorption lacunae by catalysing the reaction which provides the protons required to drive resorption of the mineralised matrix.[91]

Patients with autosomal recessive CAII deficiency exhibit osteopetrosis which is associated with cerebral calcification and renal tubular acidosis.[276] Similarly, CAII-deficient mice have a slower growth rate than their wild-type litter-mates and exhibit renal tubular acidosis[277] and mild osteopetrosis presenting as an increase in trabecular bone volume[278].

In vitro, blocking of *CA2* expression with antisense RNA or DNA inhibits osteoclast formation, intravesicular acidification and bone resorption in rat osteoclast and foetal mouse bone organ cultures.[89,90] Additionally, treatment of murine bone marrow osteoclasts and bone organ cultures with carbonic anhydrase inhibitors, such as acetazolamide, decreases osteoclast bone resorptive activity.[88,90]

The major role that CAII plays in bone resorption through resorption pit acidification suggests that inhibition of this kinase by imatinib may be another mechanism whereby imatinib inhibits osteoclast activity.

1.4.4.4 The role of PDGFR in osteoclastogenesis

PDGF is a potent mitogen and chemotactic agent for cells of mesenchymal origin. The PDGF isoforms A and B can form either homodimers or heterodimers which bind to the receptors PDGFRα (PDGF-AA, PDGF-BB and PDGF-AB) and PDGFRβ (PDGF-BB only). Treatment with PDGF-BB and, to a lesser extent, PDGF-AA increases osteoclast number and bone resorption surface in cultured foetal mouse calvaria.[279,280] In cultures of

iliac crest-derived primary human bone cells, PDGF-BB treatment significantly increased osteoclastic bone resorption *in vitro*.[281] The observed increase in osteoclast activity is likely to be due to PDGF-BB stimulating osteoblasts and stromal cells to release cytokines which have stimulatory effects on osteoclasts. For example, in cultures of murine cell lines and primary osteoblasts, PDGF-BB treatment has been shown to upregulate the expression of M-CSF and of a number of cytokines, including IL-6[282], which stimulates the production of RANKL by osteoblasts[283]. Thus, inhibition of PDGFR signalling by imatinib *in vivo* could indirectly have effects on osteoclastogenesis via inhibition of cytokine secretion by stromal cells and osteoblasts.

1.4.5 Effects of imatinib on osteoblasts

In addition to having inhibitory effects on osteoclasts, there is emerging evidence that imatinib can affect osteoblasts. As described in section 1.2.3, osteoblasts are bone marrow cells of mesenchymal origin that are responsible for synthesis of new bone matrix.

Studies from our laboratory[10] and those of others[16-19], suggest that imatinib decreases *in vitro* osteoblast proliferation, while increasing their activity. In *in vitro* mineralisation assays using stromal cells isolated from human bone explants, treatment with therapeutically-achievable concentrations of imatinib significantly increased mineral deposition[10,19], decreased proliferation of stromal cells[10,16] and suppressed stromal cell clonogenicity[16]. Similarly, imatinib increases mineralisation by primary rat osteoblast cells and by the mouse osteoblast-like cell line MC3T3-E1.[17] Treatment with therapeutically-relevant concentrations of imatinib partially inhibited proliferation of primary rat osteoblasts, the human osteoblast-like cell line SaOS2, the murine stromal cell line ST2[17] and the mouse osteoblast-like cell line MC3T3-E1[18] and increased apoptosis in primary rat osteoblasts[17].

There is some suggestion that patients under going imatinib therapy have altered serum levels of osteoblast markers. In CML patients, serum levels of the osteoblast markers osteocalcin and pro-collagen type I amino-terminal propeptides (P1NP) have been shown to be significantly increased after 3 months of imatinib treatment[8,12], with elevated levels returning to baseline by 24 months[12]. Studies by Tibullo *et al*.[19] found that increased serum osteocalcin levels in patients undergoing imatinib therapy were sustained until 24 months of treatment. These studies contrast those of Berman *et al*.[5], who reported that patients treated with imatinib for an unspecified amount of time did not have significantly altered levels of bone-specific alkaline phosphatase, relative to normal controls. Moreover,

the imatinib treated patients had significantly lower levels of osteocalcin compared with aged-matched normal controls.[5]

Taken together, these results suggest that osteoblast activity may be transiently increased by imatinib treatment, but subsequently decreases to levels at, or lower than, those at baseline over time. This is consistent with *in vitro* data showing that imatinib increases osteoblast activity while inhibiting osteoblast proliferation.[10] One could hypothesise that, at the commencement of treatment, imatinib may increase the differentiation of the existing pool of osteoblast precursors, thereby increasing the number of committed osteoblasts. However, as imatinib inhibits mesenchymal cell proliferation, the number of osteoblast precursors, and thus the number of osteoblasts, would decrease over time. Histomorphometric analysis is therefore required to determine the temporal changes in osteoblasts and bone deposition rates occurring in patients undergoing imatinib therapy.

The proliferation and differentiation of osteoblasts is regulated through a number of signalling pathways, including known imatinib targets Abl and PDGFR. While loss of signalling through Abl is thought to inhibit osteoblast activity[284], PDGFR signalling is known to be mitogenic to mesenchymal cells and to have a negative regulatory effect on osteoblastogenesis and thus represents the best candidate to explain the mechanism whereby imatinib activates osteoblast differentiation whilst inhibiting mesenchymal cell proliferation.

1.4.5.1 The role of PDGFR in osteoblast formation and activity

In addition to inducing expression of osteoclastogenic cytokines by osteoblasts and stromal cells, PDGF is known to have direct effects on osteoblast proliferation and differentiation. Osteoblasts express PDGF receptors[285] and PDGF-AA[286,287]. PDGF-BB and, to a lesser extent, PDGF-AA are mitogenic for mesenchymal cells and inhibit osteoblast differentiation *in vitro*. Recombinant PDGF enhances proliferation of osteoblasts in rat calvarial cultures, isolated foetal rat calvarial osteoblasts and mouse osteoblast-like MC3T3-E1 cells *in vitro*.[280,288] Additionally, inhibition of osteoblast differentiation by PDGF-BB has been observed in human osteoblast cultures, MC3T3-E1 cells and foetal rat calvarial cultures[288-290] resulting in decreased mineralised nodule formation[288]. Furthermore, PDGF-AA and -BB were found to decrease mineral apposition rate and bone formation rate in foetal rat calvarial organ cultures, suggesting an inhibition of

mineralisation activity.[280] In support of these findings, targeted deletion of PDGFRβ in murine mesenchymal cells promotes osteoblast differentiation and function.[291]

As expected, imatinib is able to reverse the effects of PDGF on osteoblasts *in vitro.* Treatment of human bone explant cultures and MC3T3-E1 cells with PDGF-BB inhibited mineralised matrix formation; this was prevented by pre-treatment with imatinib.[10,17] In rat primary osteoblasts, proliferation is activated by PDGF-BB.[17] This is reversed by imatinib, resulting in enhanced mineralisation on a per cell basis.[17] These results suggest that inhibition of PDGFR signalling may be one mechanism whereby imatinib inhibits osteoblast proliferation and activates differentiation *in vitro*.

1.4.5.2 The role of Abl in osteoblast activity

Abl knockout mouse studies have suggested a role for Abl in osteoblast activity. Abl-deficient mice have decreased cortical and trabecular bone volume resulting from a decrease in mineral apposition rates.[284] Isolated *Abl*$^{-/-}$ stromal cells show defective mineralised nodule formation *in vitro*, with no effect on osteoblast progenitor numbers.[284] It is unclear whether these effects are dependent on Abl kinase activity or are a result of Abl functioning as a coupling molecule. However, if Abl kinase activity is required for the apparent pro-osteoblastic activity of Abl, inhibition of this kinase by imatinib would be expected to inhibit osteoblast activity.

1.5 Summary and project aims

In summary, there is a mounting body of evidence which suggests that dysregulated bone remodelling may be a side-effect of imatinib treatment. This is likely to result from inhibition of osteoclasts, by blocking Fms, Kit, CAII and PDGFR signalling, and alteration of osteoblast formation and activity through inhibition of PDGFR and Abl. Clearly, the suggestion that imatinib may increase bone strength, through positive effects on BMD and trabecular bone volume, warrants further investigation.

In patients, imatinib treatment decreases serum calcium and phosphate levels and increases trabecular bone volume suggesting that imatinib may increase osteoblast activity and/or inhibit osteoclast activity, dysregulating the normal cycles of bone remodelling. While some insights into the effects of imatinib on osteoclasts and osteoblasts have been gained, there is no direct evidence for the effects of imatinib on osteoblasts and osteoclasts in patients. Longitudinal histological assessment of the effects of imatinib on osteoclasts and osteoblasts in patients or animal models has not been undertaken.

The significant incidence of acquired resistance to imatinib has led to the development of second generation tyrosine kinase inhibitors, such as dasatinib, which have greater affinity for their target kinases. As the target profile of these second generation inhibitors overlaps with that of imatinib, there is a potential for off-target skeletal effects of these compounds which should be investigated. Furthermore, it has not been investigated whether dasatinib, like imatinib, is an inhibitor of Fms. Additionally, dasatinib, unlike imatinib, has also been shown to inhibit the activity of Src, a non-receptor tyrosine kinase which is essential in osteoclast activity.[255,292-296] As such, further studies are required to determine whether dasatinib has inhibitory effects on osteoclasts.

In order to investigate these issues, the studies presented in this thesis addressed the following aims:

1. To investigate the dysregulation of bone remodelling by imatinib in a longitudinal study of imatinib-treated CML patients
2. To determine the effects of dasatinib on osteoclast and osteoblast activity *in vitro* and *in vivo*

Chapter 2

Materials and Methods

2.1 Reagents

Imatinib and zoledronic acid were provided by Novartis (Basel, Switzerland). Dasatinib was provided by Bristol-Myers Squibb (New York, USA). PP2 was purchased from Calbiochem (catalogue number 529573; San Diego, USA). PD098059 was purchased from Sigma-Aldrich (catalogue number P215; Castle Hill, NSW). All other reagents are detailed in table 2.1.

Table 2.1: Reagents and suppliers

Reagent	Supplier	Catalogue number
2-Ethylene glycol monoethyl ether	Merck, Kilsyth, VIC	8.00857.2500
α-Modified Eagle's medium (α-MEM)	SAFC Biosciences, Lenexa, USA	51451C
β-glycerophosphate	Sigma-Aldrich	G9891
β-mercaptoethanol	Sigma-Aldrich	M6250
Acetate solution	Sigma-Aldrich	386-3
Acetic acid	Merck	6.10001.2500
Acetone	Ajax Finechem, Taren Point, NSW	6-2.5L
Acrylamide (30% bis solution)	BioRad, Gladesville, NSW	161-0148
Alizarin red	Sigma-Aldrich	A5533
Aluminium ammonium sulphate	Merck	100073A
Ammonium persulphate (APS)	BioRad	161-0700
Bovine serum albumin (BSA) powder (Fraction V)	JRH Bioscience, Lenexa, USA	85040-1K
Bromophenol blue	M & B Chemicals, Dagenham, England	B971861
Butanol	Sigma-Aldrich	B1417
Calcein	Sigma-Aldrich	C0875
Calcium chloride	Sigma-Aldrich	C1016
Cetyl pyridinyl chloride (CPC) monohydrate	Sigma-Aldrich	C032
Chondroitin sulphate A (CSA)	Sigma-Aldrich	C4382

Table 2.1, continued: Reagents and suppliers

Reagent	Supplier	Catalogue number
Chromium (III) potassium sulphate dodecahydrate	Sigma-Aldrich	243361
Citric acid, powder	Sigma-Aldrich	C1909
Citric acid solution	Sigma-Aldrich	91-S
DePeX mounting medium	Merck	361254A
Dimethyl sulphoxide (DMSO)	Ajax Finechem	225-2.5L
Dithiothreitol (DTT)	Invitrogen, Mulgrave, VIC	D1532
Dulbecco's modified Eagle's medium (DMEM)	SAFC	51441C
Eosin Y	Merck	1.15935.0025
Ethylenediaminetetraacetic acid (EDTA)	Chem Supply, Gilman, SA	EA023
Ethanol (analytical grade)	Merck	6.10107.2511
Ethanol, denatured	Ace Chemical Company, Camden Park, SA	F386
Fast garnet GBC salt	Sigma-Aldrich	387-2
Fast green	Sigma-Aldrich	F7252
Foetal calf serum (FCS)	SAFC	12003C
Formaldehyde, 40% (w/v)	Merck	10113
Gelatine	Sigma-Aldrich	G9391
Glycerol	Ajax Finechem	242-25L
Glycine	Chem Supply	GA007
Haematoxylin	ProSciTech, Thuringowa Central, QLD	C1071
Hanks' buffered saline solution (HBSS)	SAFC	55021C
L-ascorbate-2-phosphate	Wako Pure Chemical Industries, Osaka, Japan	013-12061
L-glutamine, 200 mM	SAFC	59202C

Table 2.1, continued: Reagents and suppliers

Reagent	Supplier	Catalogue number
Hoescht 33258	Sigma-Aldrich	B61405
Hydrochloric acid (HCl), 35%	Merck	6.10307.2511
Membrane blocking agent	GE Healthcare, Little Chalfont, UK	RPN2125V
Methanol	Chem Supply	MA004-P
Methyl green	Sigma-Aldrich	M8884
Methylmethacrylate	Merck	8.00590.1000
Microscint™ 20	Perkin Elmer, Boston, USA	6043621
N-2-hydroxyethylpiperazine-N'-2-ethanesulfonic acid (HEPES; 1M)	SAFC	59202C
N-acetyl-L-cysteine	Sigma-Aldrich	A7250
Naphthol AS-BI phosphoric acid solution	Sigma-Aldrich	387-1
Naphthol AS-BI phosphate	Sigma-Aldrich	N1225
Neutral buffered formalin (NBF, 10%)	Fronine Laboratory Supplies, Riverstone, NSW	JJ01810
N,N-dimethylformamide	Sigma-Aldrich	D8654
N,N,N,N-tetramethylethylenediamine (TEMED)	MP Biomedicals, Seven Hills, NSW	194019
Nonidet® P40 substitute	Sigma-Aldrich	74385
Papain (3.1 U/mg)	Sigma-Aldrich	76220
Paraformaldehyde	Merck	296474L
Pararosaniline hydrochloride	Sigma-Aldrich	P3750
Penicillin 5000 U/mL, streptomycin 5 mg/mL	Sigma-Aldrich	P4458
Perkadox 16	AkzoNobel, Tullamarine, VIC	1552-11-3
Phenol red-free DMEM	SAFC	51449C
Phenylmethylsulphonyl fluoride (PMSF)	Sigma-Aldrich	P7626

Table 2.1, continued: Reagents and suppliers

Reagent	Supplier	Catalogue number
Phloxine B	Sigma-Aldrich	P2759
Phosphate buffered saline (PBS), 20x	Media Production Unit, IMVS	N/A
PBS, calcium and magnesium-free	Sigma-Aldrich	D5652
Polyethylene glycol 300 (PEG 300)	Sigma-Aldrich	81162
Polyethylene glycol 400 (PEG 400)	Sigma-Aldrich	202398
Protease inhibitor tablets, EDTA-free	Roche, Basel, Switzerland	04693159001
Proteinase K	Invitrogen	25530-015
Recombinant human M-CSF (rhM-CSF)	PeproTech (Rocky Hill, USA)	PT300-25-100
Recombinant human PDGF-BB (rhPDGF-BB)	PeproTech	PT100-14B-10
Recombinant human RANKL (rhRANKL)	PeproTech	PT310-10-100
Recombinant human TGF-β1 (rhTGF-β1)	PeproTech	PT100-21-10
Safranin O	Sigma-Aldrich	S8884
Salmon sperm DNA	Sigma-Aldrich	31149
Silver nitrate	Rhone Poulenc Chemicals, Clayton South, VIC	SL810
Sodium acetate trihydrate	Sigma-Aldrich	236500
Sodium bicarbonate	McKenzie's, Altona, VIC	N/A
Sodium carbonate	Merck	010240
Sodium chloride	Sigma-Aldrich	S9625
Sodium dodecyl sulphate (SDS)	Merck	444464T
Sodium fluoride	Sigma-Aldrich	S7920
Sodium hydroxide, pellets	Merck	567530
Sodium hypochlorite (12.5% w/v)	ACE Chemical Company	F386

Table 2.1, continued: Reagents and suppliers

Reagent	Supplier	Catalogue number
Sodium iodate	Sigma-Aldrich	S4007
Sodium-L-tartrate	Sigma-Aldrich	228729
Sodium nitrite solution	Sigma-Aldrich	91-4
Sodium phosphate	Sigma-Aldrich	S342483
Sodium pyrophosphate	Sigma-Aldrich	S9515
Sodium pyruvate	Sigma-Aldrich	P5280
Sodium thiosulfate	Sigma-Aldrich	S7143
Sodium vanadate	Sigma-Aldrich	450243
Sulfur-35 radionuclide ($^{35}SO_4^{2-}$; 5 mCi/mL)	Perkin Elmer	NEX042
Tartrate solution	Sigma-Aldrich	387-3
Toluidine blue	Sigma-Aldrich	T3260
Tris (Sigma-7-9®)	Sigma-Aldrich	T1378
Trypan blue (0.4%)	Sigma-Aldrich	T8154
Trypsin-EDTA (0.5%)	Gibco	15400-054
Tween-20	Sigma-Aldrich	P9416
WST-1	Tanaka, Madison, USA	11644807601
Xylene	Ajax Finechem	577-102

2.2 Solutions, buffers and media for cell culture

2.2.1 β-glycerophosphate, 1 M solution

β-glycerophosphate (2.16 g) was dissolved in 10 mL HBSS and the solution was sterilised using a 0.2 µm syringe filter (Nalgene, Rochester, USA). 1 mL aliquots were stored at -20°C until use. Thawed aliquots were stored at 4°C.

2.2.2 Additives for tissue culture medium

L-glutamine (200 mM; 100 mL), sodium pyruvate (100 mM; 100 mL), penicillin/streptomycin (5000 U/mL and 5 mg/mL, respectively; 100 mL) and HEPES

(1 M; 150 mL) were thawed at 4°C, mixed thoroughly and 22.5 mL aliquots were stored at -20°C until use.

2.2.3 Ascorbate-2-phosphate, 10 mM

L-ascorbate-2-phosphate (289 mg) was dissolved in 100 mL HBSS, filter-sterilised using a 0.2 µm syringe filter and 5 mL aliquots were stored at -20°C until use.

2.2.4 Calcium standards

Calcium chloride (11.098 g) was dissolved in RO water (100 mL) and this 1 M stock solution was stored at room temperature until use. A standard curve for the cresolphthalein complexone assay was prepared by diluting the stock solution from 2.5 – 0.25 mM in RO water. Diluted standards were stored at 4°C until use.

2.2.5 Collagenase

Collagenase type I (500 mg) was dissolved in 250 mL HBSS, filter-sterilised using a 0.2 µm syringe filter and 5 mL aliquots stored at -20°C until use.

2.2.6 Complete α-MEM (c-α-MEM)

To prepare c-α-MEM (containing 10% FCS, 2 mM L-glutamine, 1 mM sodium pyruvate, 15 mM HEPES, 50 U/ml penicillin and 50 µg/ml streptomycin), additives and FCS were thawed at 37°C. Additives were filtered using a 0.2 µm syringe filter. α-MEM (425.5 mL) was supplemented with 50 mL FCS and 22.5 mL additives and was stored at 4°C. Every 2 weeks, if required, media were supplemented with an additional 5 mL of L-glutamine solution to achieve a final concentration of 2 mM L-glutamine.

2.2.7 Complete DMEM (c-DMEM)

To prepare c-DMEM (containing 10% FCS, 2 mM L-glutamine, 1 mM sodium pyruvate, 15 mM HEPES, 50 U/ml penicillin and 50 µg/ml streptomycin), additives and FCS were thawed at 37°C. Additives were filtered using a 0.2 µm syringe filter. DMEM (425.5 mL; with or without phenol red) was supplemented with 50 mL FCS and 22.5 mL additives and was stored at 4°C. Every 2 weeks, if required, media were supplemented with an additional 5 mL of L-glutamine solution for a final concentration of 2 mM L-glutamine.

2.2.8 CPC solution, 2.5% (w/v)

CPC (1 g) was dissolved in 16 mL ethanol and was then mixed with 24 mL RO water for a final solution of 2.5% (w/v) CPC and 40% (v/v) ethanol. Prepared solution was stored at room temperature until use.

2.2.9 CSA solution, 5 mg/mL

CSA (50 mg) was dissolved in 10 mL RO water and 1 mL aliquots were stored at -20°C. Solution was diluted 1:4 in RO water prior to use.

2.2.10 Dasatinib, 1 mM, for tissue culture

Dasatinib (48.801 mg) was dissolved in 10 mL sterile DMSO and then stored as 20 µL aliquots at -80°C. Thawed aliquots were stored at 4°C, in the dark, for up to 1 month.

2.2.11 Dispase, 2 mg/mL

Dispase (500 mg) was dissolved in 250 mL HBSS, filter-sterilised using a 0.2 µm syringe filter and 5 mL aliquots were stored at -20°C until use.

2.2.12 DNA standards

Salmon sperm DNA (10 mg) was dissolved in 10 mL RO water at 4°C overnight, for a 1 mg/mL stock solution. One hundred microlitre aliquots were stored at -20°C. To prepare standards, 4 mL sodium chloride (4 M solution) and 4 mL sodium phosphate (0.1 M solution) were mixed and salmon sperm DNA was diluted in the sodium chloride/sodium phosphate solution for final concentrations of 1.56 – 100 µg/mL DNA. Diluted standards were stored at 4°C until use.

2.2.13 EDTA, 0.5 M

EDTA (93.05 g) was dissolved in 500 mL RO water and the pH was adjusted to 8.0 with sodium hydroxide pellets. The solution was stored at room temperature until use.

2.2.14 Hoescht DNA assay buffer

Hoescht 33258 (20 mg) was dissolved in 20 mL RO water and this 1 mg/mL stock solution was stored at 4°C in the dark until use. On the day of use, 7.5 mL sodium chloride (4 M) was mixed with 7.5 mL sodium phosphate (0.1 M) and 20 µL Hoescht stock solution was

added for a final solution of 1.33 µg/mL Hoescht, 2 M sodium chloride and 0.05 M sodium phosphate.

2.2.15 HHF (HBSS; 10 mM HEPES; 5% FCS)

FCS was thawed at 37°C. HBSS (470 mL) was supplemented with 25 mL FCS and 5 mL HEPES (1 M) and the solution was stored at 4°C.

2.2.16 Imatinib, 10 mM, for tissue culture

Imatinib (58.97 mg) was dissolved in 10 mL Milli-Q water (18.2 mΩ/cm) and the solution was sterilised using a 0.2 µM syringe filter. The solution was aliquotted at 500 µL and stored at -80°C until use. Thawed aliquots were stored at 4°C, in the dark, for up to 3 months.

2.2.17 N-acetyl-L-cysteine, 200 mM

N-acetyl-L-cysteine (653 mg) was dissolved in 20 mL RO water and 1 mL aliquots were stored at -20°C until use.

2.2.18 Papain digest solutions, 20 U/mL and 100 U/mL

To prepare 20 U/mL and 100 U/mL papain digest solutions, 62.1 mg or 320 mg papain were dissolved in 333 µL sodium acetate (3 M) and were mixed with 48 µL EDTA (0.5 M), 1 mL N-acetyl-L-cysteine (200 mM) and 8.619 mL RO water for a final concentration of 0.1M sodium acetate, 2.4 mM EDTA, 20 mM N-acetyl-L-cysteine and 20 U/mL or 100 U/mL papain, respectively. Papain digest solution was used on the day of preparation.

2.2.19 Proteinase K, 10 mg/mL stock solution

Proteinase K (100 mg) was dissolved in 10 mL RO water and 1 mL aliquots were stored at -20°C until use. Thawed aliquots were stored at 4°C for up to 1 week.

2.2.20 PD098059, 10 mM stock solution

PD098059 (100 mg) was dissolved in DMSO (371.14 µL) and 10 µL aliquots were stored at -20°C until use. Thawed aliquots were stored at 4°C for up to 1 week.

2.2.21 PP2, 10 mM stock solution

PP2 (100 mg) was dissolved in DMSO (331.45 µL) and 50 µL aliquots were stored at 4°C in the dark until use.

2.2.22 rhM-CSF, 25 µg/mL stock solution

Milli-Q water (1 mL) was added to 100 µg rhM-CSF and was incubated at room temperature for 30 minutes to dissolve. The solution was quickly centrifuged and was mixed with 3 mL HBSS. The solution was filtered through a 0.2 µm syringe filter and 20 µL aliquots were stored at -80°C until use. Thawed aliquots were stored at 4°C for up to 1 week.

2.2.23 rhPDGF-BB, 10 µg/mL stock solution

Milli-Q water (1 mL) was added to 10 µg rhPDGF-BB and was incubated at room temperature for 30 minutes to dissolve. The solution was mixed, quickly centrifuged and was filtered through a 0.2 µm syringe filter. Aliquots (10 µL) were stored at -80°C until use. Thawed aliquots were stored at 4°C for up to 1 week.

2.2.24 rhRANKL, 500 µg/mL stock solution

Milli-Q water (200 µL) was added to 100 µg rhRANKL and was incubated at room temperature for 30 minutes to dissolve. The solution was quickly centrifuged and was then filtered through a 0.2 µm syringe filter. Aliquots (5 µL) were stored at -80°C until use. Thawed aliquots were stored at 4°C for up to 1 week.

2.2.25 rhTGF-β1, 10 µg/mL stock solution

Milli-Q water (1 mL) was added to 10 µg rhTGF-β1 and was incubated at room temperature for 30 minutes to dissolve. The solution was mixed, quickly centrifuged and was then filtered through a 0.2 µm syringe filter. Aliquots (10 µL) were stored at -80°C until use. Thawed aliquots were stored at 4°C for up to 1 week.

2.2.26 Serum-free α-MEM (sf-α-MEM)

Tissue culture additives were thawed at 37°C and were filtered using a 0.2 µm syringe filter. α-MEM (477.5 mL) was supplemented with 22.5 mL additives for a final concentration of 2 mM L-glutamine, 1 mM sodium pyruvate, 15 mM HEPES, 50 IU/ml penicillin and 50 µg/ml streptomycin and was stored at 4°C. Every 2 weeks, if required,

media were supplemented with an additional 5 mL of L-glutamine solution for a final concentration of 2 mM L-glutamine.

2.2.27 Serum-free DMEM (sf-DMEM)

Tissue culture additives were thawed at 37°C and were filtered using a 0.2 µm syringe filter. DMEM (477.5 mL) was supplemented with 22.5 mL additives for a final concentration of 2 mM L-glutamine, 1 mM sodium pyruvate, 15 mM HEPES, 50 IU/ml penicillin and 50 µg/ml streptomycin and was stored at 4°C. Every 2 weeks, if required, media were supplemented with an additional 5 mL of L-glutamine solution for a final concentration of 2 mM L-glutamine.

2.2.28 Sodium acetate, 3 M

Sodium acetate (123.05 g) was dissolved in 500 mL RO water and the solution was stored at room temperature until use.

2.2.29 Sodium chloride, 4 M

Sodium chloride (116.9 g) was dissolved in 500 mL RO water and the solution was stored at room temperature until use.

2.2.30 Sodium phosphate, 0.1 M, pH 7.4

Sodium phosphate (1.64 g) was dissolved in 100 mL RO water, the pH was adjusted to 7.4 and the solution was stored at room temperature until use.

2.2.31 Trypsin, 0.05%

Tryspin-EDTA (1 mL; 0.5%) was thawed at 37°C, mixed with 9 mL HBSS and was stored at 4°C for up to 1 week.

2.3 Stains, buffers and solutions for histology

2.3.1 Acetate-tartrate buffer

On the day of use, 2.72 g sodium acetate and 2.3 g sodium tartrate were dissolved in 80 mL RO water and the pH was adjusted to 5.2 with 1.2% acetic acid. RO water was added for a final volume of 100 mL for a final concentration of 200 mM sodium acetate and 100 mM sodium tartrate.

2.3.2 Acid alcohol

Water (297 mL), ethanol (700 mL) and hydrochloric acid (3 mL) were mixed for a final solution of 70 % (v/v) ethanol and 0.3% (v/v) hydrochloric acid. The solution was stored at room temperature and was used to differentiate Haematoxylin staining.

2.3.3 Citrate/acetone/formaldehyde fixative

Citric acid solution (5 mL), acetone (13 mL) and formaldehyde (1.6 mL) were mixed thoroughly for a final concentration of 4.6 mM citric acid, 66.3% (v/v) acetone and 3.3% (v/v) formaldehyde. The fixative was used on the day of preparation.

2.3.4 Decalcification buffer

PBS (200 mL; 20 x solution) was added to 3 L RO water and approximately 50 g NaOH pellets were dissolved. EDTA (744.2 g) was then dissolved at room temperature and pH was adjusted to 8.0 with additional NaOH pellets, as required. Paraformaldehyde (20 g) was added to the EDTA solution and was dissolved with heating in a fume cupboard. The final volume was made up to 4 L for a final concentration of 0.5 M EDTA and 0.5% (w/v) paraformaldehyde in PBS. Decalcification solution was stored at 4°C for up to 1 month.

2.3.5 Eosin

RO water (22 mL), ethanol (420.5 mL), eosin Y (57 mL; 1% solution), phloxine (5.7 mL; 1% solution) and acetic acid (2.3 mL) were combined and mixed well for a final concentration of 11% (w/v) eosin, 1.1% (w/v) phloxine and 83% (v/v) ethanol. The prepared stain was stored at 4°C until use.

2.3.6 Fast garnet TRAP stain

Just prior to use, 150 µL fast garnet GBC base solution was combined with 150 µL sodium nitrite solution in a 1.5 mL microfuge tube. The solutions were mixed by inversion and left to stand for 2 minutes. The freshly diazotised fast garnet GBC salt thus formed was mixed with 15 mL RO water, 150 µL naphthol AS-BI phosphoric acid solution, 300 µL sodium-L-tartrate solution and 600 µL sodium acetate solution for a final solution containing fast garnet GBC salt (0.09 mg/mL), sodium L-tartrate (6.77 mM), sodium acetate (101 µg/mL) and naphthol AS-BI phosphoric acid (126 µg/mL).

2.3.7 Fast green stain, 0.2% (w/v)

Fast green (100 mg) was dissolved in 50 mL RO water and was stored at room temperature until use.

2.3.8 Gelatin/chromic potassium sulphate solution

Gelatine (10 g) was dissolved in 1000 mL RO water and was heated, with stirring, until dissolved. The solution was allowed to cool and 500 mg chromium (III) potassium sulphate dodecahydrate was added. The solution was mixed thoroughly for a final concentration of 1% gelatine and 0.05% chromic potassium sulphate and was stored at room temperature until use.

2.3.9 Mayer's haematoloxylin

Aluminium ammonium sulphate (100 g) was dissolved in 1400 mL RO water by heating. The solution was cooled and 10 g haematoxylin, 20 mL ethanol, 2.0 g sodium iodate, 40 mL acetic acid and 600 mL glycerol were added for a final concentration of 5% (w/v) aluminium ammonium sulphate, 0.5% (w/v) haemotoxylin, 1% (v/v) ethanol, 0.1% (w/v) sodium iodate, 2% (v/v) acetic acid and 30% (v/v) glycerol. The solution was stored at room temperature until use.

2.3.10 Methyl green, 0.5 mg/mL

Methyl green (25 mg) was dissolved in 50 mL RO water and was stored at room temperature until use.

2.3.11 Naphthol AS-BI phosphate, 0.39 mg/mL

Immediately prior to use, 20 mg naphthol AS-BI phosphate was dissolved in 1 mL N,N-dimethylformamide and was diluted in 50 mL acetate-tartrate buffer.

2.3.12 Pararosaniline, 40 mg/mL stock solution

Pararosaniline (1 g) was heated in 20 mL RO water in a fume cupboard until almost completely dissolved. Hydrochloric acid (5 mL) was added and the solution was filtered with a 0.45 μm syringe filter and then stored at 4°C in the dark for up to 1 month.

2.3.13 Pararosaniline TRAP stain

Sodium nitrite (80 mg) was mixed with 2 mL RO water until dissolved. Immediately before use, pararosaniline was hexaazotised by mixing 2 mL pararosaline stock solution with 2 mL sodium nitrite solution and incubating at room temperature for 5 minutes. Hexaazotised pararosaniline solution (2.5 mL) was added to 50 mL acetate-tartrate buffer, heated to 37°C, for a final concentration of 1 mg/mL pararosaniline.

2.3.14 Safranin O stain, 0.1% (w/v)

Safranin O (50 mg) was dissolved in 50 mL RO water and was stored at room temperature until use.

2.3.15 Silver nitrate, 5% (w/v)

Silver nitrate (25 g) was dissolved in 500 mL RO water and the solution was stored at 4°C in the dark. The solution was used neat or was diluted 1:4 in RO water prior to use.

2.3.16 Sodium carbonate, 5% (w/v)

Sodium carbonate (12.5 g) was dissolved in 250 RO water and the solution was stored at room temperature until use.

2.3.17 Sodium thiosulphate, 5% (w/v)

Sodium thiosulfate (12.5 g) was dissolved in 250 mL RO water and the solution was stored at room temperature until use. The solution was used neat or was diluted 1:1 in RO water prior to use.

2.3.18 Spreading solution

2-ethylene glycol monoethyl ether (300 mL) was combined with 490 mL ethanol and 210 mL RO water final solution of 30% 2-ethylene glycol monoethyl ether in 49% ethanol. Spreading solution was stored at room temperature until use.

2.3.19 Sodium bicarbonate, 0.1% (w/v)

Sodium bicarbonate (500 mg) was dissolved in 500 mL RO water on the day of use. Solution was used as a blueing agent for haematoxylin staining.

2.3.20 Sodium phosphate/citrate buffer

Citric acid (1.58 g) and sodium phosphate (0.75 g) were dissolved in 800 mL RO water for a final concentration of 8.22 mM citric acid and 4.575 mM sodium phosphate. The pH was adjusted to 3.7, the volume made up to 1 L and the solution stored at room temperature until use.

2.3.21 Toluidine blue stain, 2% (w/v)

Toluidine blue (2 g) was dissolved in 80 mL sodium phosphate/citrate buffer. The pH was adjusted to 3.7, the volume was made up to 100 mL with sodium phosphate/citrate buffer and the solution was filtered through a 0.45 μm syringe filter. The solution was stored at room temperature until use.

2.4 Cell culture techniques

2.4.1 Cell lines and standard culture conditions

All appropriate tissue culture techniques were performed in a Class II laminar flow hood (Top Safe 1.2, Bio Air, Siziano, Italy). Cell lines were maintained in a humidified environment at 37°C in 5% carbon dioxide. All media were warmed to 37°C before use. All tissue culture plates were obtained from BD Biosciences (North Ryde, NSW).

2.4.1.1 RAW 264.7 cell culture

The murine monocyte/macrophage-like cell line RAW 264.7[297] was kindly provided by Gerald Atkins (Orthopaedics and Trauma, IMVS, Adelaide, SA). These cells were routinely maintained at less than 80% confluence in c-DMEM and were subcultured 1:15 once per week by cell scraping.

2.4.1.2 ATDC5 cell culture

The pre-chondrocyte cell line ATDC5, derived from a mouse teratocarcinoma cell line[298], was obtained from the American Type Culture Collection (ATCC; Manassas, USA). These cells were routinely maintained in c-α-MEM containing ascorbate-2-phosphate (100 μM) and were subcultured by trypsinisation.

2.4.2 Trypsinisation of adherent cell lines

Briefly, cells were washed with prewarmed HBSS and then detached from the flasks by treatment with 5 mL 0.05% trypsin-EDTA for 3 – 5 minutes at 37ºC. Cells were dislodged by firmly tapping the flask and the trypsin activity was inhibited by the addition of 5 mL HHF. The cells were centrifuged at 800 g for 5 minutes at 4°C in an Eppendorf 5810 centrifuge (Eppendorf South Pacific, North Ryde, NSW). The supernatant was aspirated, the cell pellet resuspended in an appropriate volume of culture medium and the cell suspension was triturated to produce a single cell suspension. A fraction of this cell suspension was then transferred into a new culture flask containing medium at 37ºC.

2.4.3 Cell counts and viability staining

Counts of viable cells were obtained by trypan blue staining. Twenty microlitres of cell suspension were added to an equal volume of 0.4% (w/v) trypan blue and the cells were incubated at room temperature for 3 – 10 minutes. The cells were then loaded onto a haemocytometer (Weber Scientific International, Teddington, England) in duplicate. The cells were counted using a light microscope (Olympus BX40, Tokyo, Japan) and cell concentration and viability were calculated.

2.4.4 Cryopreservation and storage of cells

Cells were preserved by storing at -196°C in liquid nitrogen in medium containing 20% FCS and 10% DMSO. A cell suspension was centrifuged at 800 g for 5 minutes in an Eppendorf 5810R centrifuge and the supernatant was aspirated. The cell pellet was resuspended in ice-cold 40% FCS in the appropriate serum-free medium. Ice-cold 20% DMSO in serum-free medium was added drop-wise to the cell suspension for a final concentration of 1 – 2 x 10^6 cells/mL (20% FCS, 10% DMSO in media). One millilitre volumes were then aliquotted into cryovials (Greiner, Kremsmuester, Germany) which were transferred to a 4°C cryo freezing container (Mr Frosty; catalogue number 5100-0001; Nalgene) and were cooled to -80ºC overnight before transfer to liquid nitrogen storage tanks.

2.4.5 Thawing of cryopreserved cells

Ampoules of cells were warmed quickly by placing the cryovials from liquid nitrogen storage directly into a 37ºC waterbath. As soon as the ice crystals had melted, the cells were triturated gently to form a cell suspension and transferred to 9 mL pre-warmed

culture medium. Cells were centrifuged at 800 g in an Eppendorf 5810R centrifuge for 5 minutes, the supernatant was aspirated, the cell pellet resuspended in 15 mL culture medium and the cells were seeded in a 75 cm^2 flask and placed in the 37ºC incubator. After thawing, cells were passaged at least once before use in experiments.

2.4.6 Establishment of murine bone marrow monocyte (mBM and rBM) cultures

Murine bone marrow monocyte cultures were established as previously described.[299] Briefly, 10-week-old female Sprague-Dawley rats or 6 – 13-week-old male C57 BL/6 mice (Veterinary Services Division, IMVS) were humanely killed by carbon dioxide overdose. Under sterile conditions, the femurs and tibiae were dissected free of tissue and a scalpel blade was used to remove the ends of the bones. Using a 21 gauge needle (rats) or a 23 gauge needle (mice), bone marrow was flushed from femurs using ice-cold c-α-MEM.

Cells were washed once in HBSS, resuspended in c-α-MEM and triturated thoroughly to obtain a single-cell suspension. The bone marrow cells were then seeded at 9 x 10^5 cells/cm^2 in 175 cm^2 flasks. Cells were incubated overnight at 37°C in 5% carbon dioxide to allow stromal cells to adhere. The non-adherent rat and mouse bone marrow cells (rBM and mBM, respectively) were aspirated, pelleted at 800 g in an Eppendorf 5810R centrifuge at 4°C for 5 minutes and then were used as monocyte/macrophage osteoclast precursor cells in Western blot experiments, WST-1 assays and osteoclast formation and activity assays.

2.4.7 Establishment of rat bone marrow stromal cell (rBMSC) cultures

rBMSC cultures were established as previously described.[69] Briefly, 10-week-old female Sprague-Dawley rats (Veterinary Services Division, IMVS) were humanely killed by carbon dioxide overdose. The bone marrow was flushed from femurs and tibiae, as described in section 2.4.6, and the bones were crushed into 1 – 2 mm pieces with sterile scissors. The bone chips were then suspended in 12.5 mL c-α-MEM supplemented with 100 μM ascorbate, seeded into a 75 cm^2 flask and were incubated at 37°C and 5% carbon dioxide for 2 weeks to allow rBMSC to proliferate. rBMSC were passaged twice before use in mineralisation, proliferation and Western blot experiments. For routine culture, rBMSC were seeded at 8 x 10^3 cells/cm^2 and media were replaced twice weekly. Cells were sub-cultured by trypsinisation.

2.5 Osteoclastogenesis assays

2.5.1 mBM and rBM osteoclast formation and activity assays

For TRAP staining or calcium phosphate resorption assays, rBM or mBM cells were cultured as previously described[299] in 96-well plates, in 16-well calcium phosphate-coated quartz slides (BioCoat™ Osteologic™ MultiTest slides) or on slices of elephant tusk dentine in 96-well plates. Briefly, rBM and mBM cells were cultured at 3.1 x 10^5 cells/cm^2 in 200 µL c-α-MEM supplemented with 75 ng/mL rhM-CSF. Following overnight incubation, to allow the cells to adhere, the media were aspirated and replaced with 200 µL c-α-MEM containing 75 ng/ml rhM-CSF and 75 ng/mL rhRANKL (day 0). Treatment media were replaced on days 3 and 6. Where indicated, inhibitors were added on day 0 and included for the duration of the experiment. The formation of TRAP-positive bone-resorbing osteoclasts was assessed after 6 days. The resorption of calcium phosphate or dentine was assessed after a period of 9 days.

2.5.2 RAW 264.7 osteoclastogenesis assays

The effects of inhibitors on Fms-independent osteoclast formation or activity were determined in RAW 264.7 cell cultures. Briefly, cells were cultured at 5 x 10^2 cells/cm^2 in 96-well plates or on calcium phosphate-coated (Osteologic™) slides in 200 µL c-DMEM supplemented with 100 ng/mL rhRANKL. Following overnight incubation, the media were replaced with c-DMEM containing 100 ng/ml rhRANKL and, where indicated, imatinib, dasatinib, PP2, PD098059 or vehicle (day 0). For resorption assays, the treatment media were replaced on day 3. The formation of TRAP-positive bone-resorbing osteoclasts and the resorption of calcium phosphate were assessed after a period of 4 and 6 days, respectively.

2.5.3 TRAP stain

Cells were stained for TRAP activity with the Leukocyte Acid Phosphatase (TRAP) kit (catalogue number 387-1KT; Sigma-Aldrich) as per the manufacturer's recommendations. Briefly, cells were fixed in 100 µL/well freshly-prepared citric acid/acetone/formaldehyde solution for 3 – 5 minutes. Cells were carefully washed 3 times in 250 µL/well RO water and were then incubated with freshly-prepared fast garnet TRAP stain for 15 – 20 minutes at 37°C in the dark. Wells were washed 4 times with 250 µL/well RO water and the plates were left to dry by evaporation. The number of osteoclasts (defined as TRAP-positive cells

with 3 or more nuclei) per well were enumerated in quadruplicate wells. Cells were visualised and photographed with an Olympus CKX41 inverted microscope and an Olympus DP11 digital camera (Olympus Japan) at 200 x magnification.

2.5.4 von Kossa silver stain

Calcium phosphate-coated slides were stained for mineral using von Kossa silver stain. The slides were washed once in 250 μL/well RO water and were subsequently bleached in 12.5% (w/v) sodium hypochlorite for 5 minutes. The wells were then washed 3 times with 250 μL RO water to remove cell debris. The calcium phosphate layer was then stained with 100 μL/well 5% silver nitrate solution for 30 minutes at room temperature. Developer was prepared fresh by diluting formaldehyde 1:4 in sodium carbonate for a final concentration of 4% (w/v) sodium carbonate and 9.25% (w/v) formaldehyde. The slides were washed 3 times in 250 μL/well RO water and were then incubated with 100 μL/well developer for 30 to 60 seconds. Following a further 3 washes with 250 μL/well RO water, the stain was fixed with 100 μL/well 5% sodium thiosulphate for 2 minutes followed by a final wash in RO water.

Slides were photographed with Olympus CKX41 inverted microscope with an Olympus DP11 digital camera at 40 x final magnification. Resorption area (cleared, unstained foci in the mineral layer) was quantitated with Adobe Photoshop CS3 following the protocol recommended by BD Biosciences.

2.5.5 Toluidine blue stain

Cells were removed from dentine slices with 6 M ammonia hydroxide (100 μL/well) at room temperature for 2 – 6 hours and were cleaned and stained immediately or were stored at room temperature in PBS until use. Cell debris was cleaned from the dentine slices using a bench-top ultrasonic cleaner (model number FXP12P, Ultrasonics Australia, Manly Vale, NSW) followed by scrubbing with a stiff paintbrush. Dentine slices were incubated for 10 minutes in 0.5% (w/v) toluidine blue (100 μl/well) and the slices were then washed four or more times with RO water.

For visualisation and photography of resorption pits, the dentine slices were placed on a 24-well tissue culture dish lid and the slices were examined and photographed with an Olympus CZ-60 stereomicroscope (dissecting microscope) and an Olympus DP11 digital camera at approximately 30 x final magnification. The area of the resorption pits was

quantitated with Olysia Bioreport software (version 3.2, Olympus) by manually tracing the resorption pits and calculating the area of the pits relative to the total area of the slice.

2.6 Osteoblastogenesis assay

2.6.1 Mineralisation assay

For mineralisation assays, rBMSC cells were cultured in 96-well plates in 200 µL c-α-MEM with 100 µM ascorbate. Cells were cultured overnight, to adhere, and then the media were replaced with 100 µL StemXVivo™ base media (catalogue number CCM007; R&D Systems, Mineapolis, USA) supplemented with StemXVivo™ osteogenic supplement (5% v/v; catalogue number CCM009; R&D Systems) and dasatinib or imatinib (containing 0.5% DMSO vehicle) or vehicle alone. Where indicated, 10 ng/mL rhPDGF-BB was included for the duration of the experiment. Treatment media were changed twice weekly.

2.6.2 Mineral quantitation

After 6 weeks, the wells were washed 3 times in 250 µL calcium- and magnesium-free PBS and the mineralised matrix was dissolved in 100 µL 0.6 M hydrochloric acid for 1 hour at room temperature. The supernatant was then transferred to a 96-well microtitre plate and calcium levels were quantitated by the cresolphthalein complexone assay (catalogue number TR29025; Thermo Electron Corporation, Melbourne, VIC). Briefly, supernatants were diluted 1:3 in water and 4 µL volumes were transferred to single wells of a fresh microtitre plate. A calcium chloride standard curve was also established in triplicate. Equal volumes of reagent A and reagent B were mixed and 200 µL were added per well. The plate was incubated at room temperature for 2 minutes and the absorbance was read at 540 nm on a microplate reader (EL808 Ultra, BIO-TEK Instruments) after a 10 second shake step.

Following dissolution of the mineral with hydrochloric acid, the wells were washed 3 times with 250 µL PBS and the cells were digested with 100 µL proteinase K (100 µg/mL) for 1 – 2 hours at room temperature or overnight at 4°C. The cells were then triturated thoroughly to ensure complete disruption of the cells and 50 µL volumes were transferred to a white 96-well microtitre plate (catalogue number 3912; Corning, New York, USA). DNA content per well was then determined using the Hoescht DNA assay.

2.6.3 Hoescht DNA assay

DNA content was measured using Hoecht 33258 dye, as described previously[300], as a surrogate marker of cell number. Hoescht solution (13.3 μg/mL; 150 μL) was added to samples and DNA standards in a white microtitre plate and the plate was gently agitated to mix. Fluorescence was then measured using a fluorescence spectrometer (LS 55, PerkinElmer Instruments) with an excitation wavelength of 350 nm, an emission wavelength of 450 nm and a slit width of 2.5 nm.

2.7 Chondrocyte activity assay

2.7.1 GAG production

ATDC5 cells (1.56 x 10^5 cells/cm^2) were cultured in 96-well plates in 200 μL c-α-MEM containing ascorbate-2-phosphate (100 μM). Following overnight adhesion, the cultures were treated with the indicated doses of imatinib, dasatinib (containing 0.05% DMSO vehicle) or vehicle alone with or without 10 ng/mL rhTGF-β1 or 100 ng/mL rhPDGF-BB. After 48 hours, treatment media were replaced with 100 μL media containing 1 μCi $^{35}SO_4$ and the plates were incubated at 37°C in 5% carbon dioxide, overnight. The matrix was then digested at 65°C for 2 hours with 100 μL papain digest solution (20 U/mL). GAG were precipitated by the addition of 40 μL of cetylpyridinium chloride solution with mixing for 5 minutes.[301] Chondroitin sulfate A solution (10 μL) was then added, as a carrier, and the plate was mixed for a further 5 minutes. The precipitated proteins were then transferred to a glass fibre filter (catalogue number 6005422; Packard Bioscience Company, Meriden, USA) using a cell harvester (Packard Filtermate Harvester). The membranes were dried for at least 2 h, 25 μL Microscint™ was added per well and the amount of $^{35}SO_4$-labelled GAG per well was measured using a scintillation counter (Top Count NXT, Perkin Elmer).

In replicate cultures, cells were digested in 100 μL papain digest solution (100 U/mL) at 65°C for 6 hours. Cell lysates (50 μL) were then transferred to a white microtitre plate and DNA content was measured using Hoecht 33258 dye, as described in section 2.6.3. GAG levels were then normalised to DNA content to determine relative GAG production per cell.

2.8 WST-1 assay

To determine the effects of dasatinib and imatinib on cell survival/proliferation, mBM and rBM (3.13 x 10^5 cells/cm^2, in c-α-MEM supplemented with 75 ng/mL rhM-CSF), rBMSC (8 x 10^3 cells/cm^2, in c-α-MEM supplemented with 100 μM ascorbate), ATDC5 (1.56 x 10^4 cells/cm^2, in c-α-MEM supplemented with 100 μM ascorbate) or RAW 264.7 cells (9.38 x 10^3 cells/cm^2, in c-DMEM) were plated in 96-well plates and were allowed to adhere overnight. Cells were then treated with inhibitors or vehicle in 200 μL media. Following the indicated incubation period, the relative number of viable, metabolically active cells per well was detected by the quantification of mitochondrial dehydrogenase activity via the formation of formazan from WST-1 (4-[3-(4-Iodophenyl)-2-(4-nitrophenyl)-2H-5-tetrazolio)-1,3-benzene disulphonate) following the manufacturer's instructions (Tanaka). Briefly, media were aspirated and 110 μL volumes of 9.1% WST-1 solution in phenol red-free c-DMEM (v/v) was added to each test well and to empty wells (for background determination). The cells were incubated at 37°C in humidified carbon dioxide for 30 minutes (RAW 264.7) or 120 minutes (rBM, mBM, rBMSC, ATDC5) to allow colour to develop. The optical density of the medium was then read at 540 nm using a microtitre plate reader (BioTek Instruments, Winooski, USA).

2.9 Patient study

2.9.1 Patients

Patients included in this study were enrolled in the Australasian Leukaemia and Lymphoma Group Therapeutic Intensification in *de Novo* Leukaemia (TIDEL) II (CML9) trial (clinical trial number ACTRN12607000325404), an open label phase 2 dose escalation study in adult patients with newly-diagnosed chronic-phase CML. All patients were within 6 months of diagnosis and had not received prior therapy for CML, other than treatment with hydroxyurea or anagrelide.

All procedures were approved by the Research Ethics Committee of the Royal Adelaide Hospital and all patients provided written informed consent.

2.9.2 Study protocol

Patients commenced imatinib therapy at 600 mg/day. If the serum imatinib trough level was sub-therapeutic (less than 1000 ng/mL) at day 22, or the patient failed to achieve ≥ 1 log, ≥ 2 log, or ≥ 3 log reduction in *BCR-ABL* transcripts by 3, 6 or 12 months,

respectively, the dose was increased to 400 mg *bis in die* (BID; 800 mg/day). If, following dose escalation, the expected level of response was not achieved after a further 3 months of 800 mg/day imatinib, or if ≥ 2 log reduction in *BCR-ABL* transcripts was not achieved by 9 months, the patient was switched to nilotinib 400 mg BID (800 mg/day). Patients receiving 600 mg/day switched directly to nilotinib 400 mg BID if the patient was intolerant to imatinib, or the patient displayed evidence of acquired imatinib resistance by pre-defined parameters.

At baseline and after 6 and 12 months of treatment, blood was collected, a posterior-superior iliac spine bone biopsy was carried out and DXA analysis of body composition was carried out.

Blood samples were collected into vacuum blood collection tubes (Greiner Bio-One) with no additives (sera) or with lithium heparin (plasma) between 9 am and noon after fasting overnight and before the patient took their morning dose of imatinib. Blood sera or plasma was collected by centrifugation at 2000 g for 10 minutes and was used immediately or was stored at -80°C.

Following collection, trephines were immediately placed in normal saline and were then transferred to 10% neutral buffered formalin at 4°C for up to 3 hours before scanning by μ-CT. Samples were then fixed in 10% neutral buffered formalin at 4°C overnight and then embedded in methyl methacrylate.

2.10 Normal bone remodelling *in vivo* study

2.10.1 Animals

Female Sprague-Dawley rats (n = 51) were obtained from the Veterinary Services Division, IMVS. As imatinib and dasatinib are predominantly used in adult CML patients, with a median age of 53 years at presentation[302], 9-month-old rats were chosen to examine the effects of this compound on mature, non-modelling skeletons[303]. Rats were provided standard commercial rat chow and tap water *ad libitum*. All procedures were approved by the Animal Ethics Committees of the University of Adelaide and of the IMVS.

2.10.2 Experimental design

Prior to treatment, the proximal tibia of all animals were scanned using μ-CT whilst anaesthetised with ketamine (45 mg/kg; Ilium Veterinary Products, Smithfield, NSW) and xylazine (5.6 mg/kg; Ilium), injected intraperitoneally (IP). Animals were randomly

assigned to 4 groups: group 1 received treatment by daily gavage with 32 mg imatinib (equivalent to approximately 100 mg/kg; n = 15) in 10% DMSO/90% PEG 300 vehicle; group 2 received 1.6 mg dasatinib by daily gavage (equivalent to approximately 5 mg/kg; n = 15); group 3 received vehicle alone by daily gavage (n = 17); group 4 received a sub-cutaneous injection with zoledronic acid (100 μg/kg, in 100 μL PBS)[304] at day 0 and at 6 weeks (n = 4). These doses of imatinib and dasatinib have been previously shown to achieve serum concentrations in rodents similar to those achieved in patients.[4,305-309] Imatinib (3200 mg) was dissolved in sterile DMSO (20 mL) at 37°C for 30 – 60 minutes and the solution was stored at room temperature in the dark for up to 2 weeks. Dasatinib (160 mg) was dissolved in sterile DMSO (20 mL) and was stored at room temperature in the dark for up to 2 weeks. Imatinib, dasatinib or DMSO was diluted 1:9 in PEG 300 immediately prior to gavage. Gavage (2 mL volume) was performed using 15 gauge, 78 mm polypropylene gavage needles (catalogue number FTP-15-78; Solomon Scientific, San Antonio, USA).

After 4, 8 and 12 weeks of treatment, 6 animals each from the vehicle, imatinib and dasatinib groups were humanely killed for sera, μ-CT and histological analysis. The zoledronic acid-treated group were humanely killed after 12 weeks of treatment. At 2 weeks and at 3 days prior to cull, the rats were injected intraperitoneally with calcein (30 mg/kg) and alizarin (30 mg/kg), respectively, in sodium carbonate buffer (pH 7.4).

Animals were anaesthetised with isoflurane and blood was collected by cardiac puncture prior to sacrifice by carbon dioxide overdose. Cardiac blood samples were spun at 800 g for 10 minutes and the collected sera were stored at -20°C until analysis. The left tibiae were fixed in 10% NBF at 4°C for 3 to 5 days prior to scanning by μ-CT. Following scanning, the cortex was shaved from the medial facet of the tibiae using a Buehler Isomet Low-Speed saw and the undecalcified bones were embedded in methyl methacrylate as described below. Right tibiae were fixed in 10% NBF for 48 hours before decalcification and embedding in paraffin.

2.11 Pharmacokinetics study

2.11.1 Animals

Female 7-month-old Sprague-Dawley rats (n = 21) were obtained from the Veterinary Services Division, IMVS. Rats were provided standard commercial rat chow and tap water

ad libitum. All procedures were approved by the Animal Ethics Committees of the University of Adelaide and of the IMVS.

2.11.2 Experimental design

All animals were administered with 27.4 mg imatinib (equivalent to approximately 100 mg/kg) in 10% DMSO/90% polyethylene glycol [PEG]300 vehicle; n = 18) by gavage.

At pre-determined time-points, 3 animals were anaesthetised with isoflurane and blood was collected by cardiac puncture, prior to sacrifice by carbon dioxide overdose. Cardiac blood samples were collected, spun at 800 g for 15 minutes and the collected sera were stored at -20°C until analysis. Collected blood was analysed for achieved levels of serum imatinib by high performance liquid chromatography (HPLC), as described in section 2.15.2.

2.12 DXA

DXA measurements were performed using a total body DXA scanner (GE-Lunar Prodigy™ with Encore software version 10.50; GE Healthcare). Scan analysis was performed using standard software and protocols to determine BMD and bone mineral content (BMC).

For the patient study, scans of the lumbar spine (L2-L4 vertebrae), femoral neck, forearm (33% radius), lower leg (tibia and fibula) and total body regions were analysed.

Animals were anaesthetised with ketamine/xylazine, injected IP, and whole-body BMD was determined. The inter-animal variation for measured BMD was 2.75%; the intra-animal variation was 1.70%.

2.13 μ-CT

The 3-dimensional microarchitecture of patient bone biopsies and rat proximal tibiae were evaluated using μ-CT (Skyscan 1076 X-ray Microtomograph, Skyscan). Bone samples were scanned at 74 kV/100 *m*A, with an isometric resolution of 8.7 μm/pixel using a 1 mm aluminium filter and 2 frame averaging. Reconstruction of the original scan data was performed using NRecon (SkyScan).

Analysis of microarchitectural parameters was performed using CTAn (SkyScan). For patient trephines, a circular region of interest was defined to exclude bone immediately

adjacent to the edge of the trephine. A total of 500 slices (4.351 mm) were analysed for each trephine, excluding any region of cortical bone. For the rat proximal tibiae, a trabecular polygonal region of interest was manually defined to exclude the cortex. A total of 500 slices (4.351 mm) were analysed for each tibia, commencing 250 slices (2.351 mm) distal to the growth plate. For analysis of rat cortices, a 1.3 mm long diaphyseal region was selected, extending 13.05 mm (1500 slices) distal to the growth plate.

Digital segmentation of the bone from air/tissues was performed by adaptive (median-C) thresholding. For rat bones, despeckling and smoothing protocols were run to minimise background noise.

For trabecular bone regions, bone volume fraction (BV/TV), bone surface fraction (BS/BV), trabecular thickness (Tb.Th.), trabecular number (Tb.N), trabecular spacing (Tb.Sp), structure model index (SMI) and trabecular pattern factor (Tb.Pf) were calculated using CTAn. Tb.Th measurements were calibrated by scanning and analysing 4 aluminum foils with thicknesses of 20, 50, 125 and 250 μm (SkyScan).[310] Cortical thickness (Ct.Th) and cortical bone volume fraction (Ct.BV/TV) were calculated for the diaphyseal region.

Bone mineral density was calculated using CTAn, using phantoms of known density (0.25 g/cm^3 and 0.75 g/cm^2) and a region corresponding to water as a reference.

The volumes of interest were reconstructed in 3 dimensions using adaptive 3-dimensional modelling and were visualised using ANT software (SkyScan).

2.14 Histology

2.14.1 Methacrylate embedding

Trephines and rat tibiae were embedded in methylmethacrylate as described previously.[311] The fixed samples were dehydrated in sequential changes of graded acetone (70% acetone for 1 hour; 90% acetone, 1 hour; 100% acetone, 1 hour; 100% acetone, 1 hour) at 4°C and subsequently infiltrated in 91% methylmethacrylate/9% PEG 400 under a vacuum for 1 week at room temperature in polypropylene specimen containers. After infiltration, the samples were embedded in 10 mL methylmethacrylate/PEG 400 (10:1) with Perkadox 16 (0.4% w/v) at 37°C for 48 hours. Blocks were attached to aluminium block holders with Araldite epoxy resin (Selleys, Padstow, NSW) prior to sectioning.

Using a D-profile blade, 5 μm thick sections were taken from each block using a Leica SM2500 motorised sledge microtome (Leica Microsystems). Gelatine-coated slides were prepared by dipping clean, dust-free slides (SuperFrost, Menzel-Gläser) in

gelatine/chromic potassium sulphate solution and allowing the slides to dry overnight prior to use. Sections were attached to gelatine-coated slides using spreading solution heated to 60 – 70°C and the sections were covered with a polyethylene sheet which was pre-soaked in spreading solution for 10 seconds. The slides were interleaved with blotting paper, clamped together using a bulldog clip and were incubated at 42°C for 18 – 48 hours to dry.

Sections were deplasticised by submersion in 100% acetone for 15 minutes prior to staining.

2.14.2 Paraffin embedding

Fixed tibiae were decalcified in 0.5 M EDTA/0.5% parafomaldehyde decalcification solution, changed thrice weekly, for 5 months. Complete decalcification of the samples was confirmed by X-ray. The cortex was cut from the medial facet of the tibia and the samples were processed through sequential changes of ethanol, xylene and paraffin and then embedded in paraffin. Longitudinal sections (5 μm) were cut and were mounted on Snowcoat X-tra slides (Surgipath, Richmond, USA) and were stained with safranin O/fast green or TRAP.

2.14.3 Histomorphometric analysis

Histomorphometric analyses were conducted on blind-coded slides using OsteoMeasure XP (OsteoMetrics, Decatur, USA).

Unstained, deplasticised sections of rat tibiae were cover-slipped and used for dynamic measurements of bone formation. Due to the slow rate of bone formation in these aged rats the alizarin label, administered 3 days prior to cull, was not visible. Mineral apposition rate (MAR) was therefore evaluated as the mean distance between the calcein-labelled mineralised surface (MS) and the edge the bone (BS), divided by 14 days (the interval between labelling and the death of the animals). Bone formation rate (BFR) was derived using the formula: BFR = MAR × MS/BS × 365/100.

Histomorphometric analyses of osteoclast numbers (N.Oc/B.Pm) and osteoclast-occupied bone surface (Oc.S/BS) in the proximal rat tibiae were performed on TRAP-stained slides in a 2.85 mm^2 region of secondary spongiosa distanced 0.78 mm from the growth plate.

Histomorphometric analysis of patient trephines was performed on toluidine blue-stained slides on the trabecular region of the biopsy excluding cortical bone and the tissue immediately adjacent to the edge of the trephines.

Additionally, analysis of rat growth plate thickness was performed on safranin O/fast green-stained paraffin sections at 5 x magnification at 5 equidistant points along a 2.32 mm region of the proximal tibial growth plate.

2.14.4 TRAP

Sections were stained for TRAP using naphthol AS-BI as a substrate and pararosaniline as a coupler.[312] Briefly, slides were incubated at 37°C for 30 minutes in acetate-tartate buffer (200 mM sodium acetate, 100 mM sodium tartrate, pH 5.2) containing 0.4 mg/mL naphthol AS-BI phosphate. The slides were then transferred to pararosaniline TRAP stain solution and were incubated at 37°C for a further 30 minutes. Slides were rinsed in water and were counter-stained in methyl green (0.5 mg/mL) for 5 – 60 seconds. Slides were rinsed in water and were then dehydrated through ethanol and cleared in xylene before coverslipping using DePeX mounting medium.

2.14.5 von Kossa stain

Mineralised bone was stained using von Kossa silver stain. Briefly, the slides were stained with 1% silver nitrate for 60 minutes under ultraviolet light at room temperature. The brown stain was developed in 4% sodium carbonate and 10% formaldehyde for 60 seconds. The slides were washed with RO water and then fixed in 2.5% sodium thiosulphate for 2 minutes. The slides were then rinsed in RO water and the sections were stained with haematoxylin and eosin using standard protocols[313] before being dehydrated through ethanol, cleared in xylene and coverslipped using DePeX.

2.14.6 Toluidine blue stain

For toluidine blue staining, deplasticised slides were incubated for 5 minutes in 2% toluidine blue stain. The slides were then washed in 2 changes of sodium phosphate-citrate buffer, dehydrated through ethanol, cleared in xylene and were coverslipped using DePeX.

2.14.7 Safranin O stain

Deplasticised sections were incubated for 5 minutes in fast green stain and were then rinsed in 1% acetic acid. The slides were then incubated in safranin O stain for a further 5 minutes. The slides were rinsed in 1% acetic acid and then dehydrated through ethanol and cleared in xylene before coverslipping with DePeX.

2.15 Serum analysis

2.15.1 Serum biochemistry

Levels of phosphate, total calcium, urea and creatinine were measured in human and murine sera by the Division of Clinical Pathology, IMVS, using an Olympus AU5400 Chemistry Analyser. Ionised Calcium is calculated from total calcium, albumin, globulins, bicarbonate, anion gap as described by Nordin *et al*.[314] This calculation correlates extremely well with measured ionised calcium levels.

Serum levels of intact PTH in human sera were measured by IMMULITE® 2000 Analyzer (Siemens Medical Solutions Diagnostics, Los Angeles, USA). The intra-assay variation was 4.0 – 5.7%; the inter-assay variation was 6.3 – 8.8%.

Levels of 25-hydroxyvitamin D_3 and 1,25-dihydroxyvitamin D_3 were measured by radioimmunoassay (IDS, Bolden, England) by the IMVS. The inter-assay variation for 25-hydroxyvitamin D_3 and 1,25-dihydroxyvitamin D_3 were 5.0% and 7.3%, respectively. The intra-assay coefficients of variance were 3.3% (25-hydoxyvitamin D_3) and 8.8% (1,25-hydroxyvitamin D_3).

Human serum levels of β-CrossLaps (CTX-1) were measured by the IMVS with a Cobas® kit using a Roche modular E170 analyser. The intra-assay variation was 1.0 – 4.6%; the intra-assay variation was 1.6 – 4.7%.

Levels of rat CTX-1 were measured in cleared sera by enzyme-linked immunosorbent assay (ELISA), as described by the manufacturer (Nordic Biosciences). The inter- and intra-assay variations of this ELISA were both 6%.

The serum levels of human osteocalcin were measured using an IMMULITE® 2000 Analyzer (Siemens Medical Solutions Diagnostics, Los Angeles, USA) by the IMVS. Intra-assay variation was 4.8%; inter-assay variation was 7.0%.

The serum levels of rat osteocalcin were measured by ELISA in accordance with the manufacturer's instructions (Biomedical Technologies). The inter- and intra-assay variations were 7% and 4%, respectively.

Serum levels of bone-specific alkaline phosphatase (bALP) in patient plasma were analysed using a commercial ELISA (catalogue number 8021; Quidel corporation, San Diego, USA). The intra- and inter-assay variances for this assay were 5% and 5.9%, respectively.

P1NP levels in rat sera were assessed using a commercial ELISA (catalogue number AC33F1; IDS) with intra- and inter-assay coefficients of variance of 8% and 12%, respectively.

2.15.2 Serum imatinib HPLC

Concentrations of imatinib mesylate in human plasma or rat sera were determined by the Veterinary Services Division, IMVS using high-performance liquid chromatography (HPLC) with UV detection. Proteins were precipitated with methanol (100 µL plasma:150 µL methanol) and were pelleted by centrifugation. The supernatant was then injected onto a reverse phase HPLC column (Kromasil C8, 250 x 4.6 mm, Eka Chemicals AB, Sweden) running a mobile phase of acetonitrile:20 mM KH_2PO_4 (3:7, v/v) at 1.0 ml/minute. A UV detector, set at 267 nm, monitored the eluate. The extracts were assayed against a calibration curve with a concentration range of 0.1 – 25 µg/ml (0.17 µM – 42.4 µM) imatinib mesylate.

2.16 Western blotting reagents

2.16.1 Blocking solution

On the day of use, 1 g membrane blocking agent was dissolved in 40 mL TBS-Tween at room temperature with agitation.

2.16.2 Non-reducing lysis buffer

One protease inhibitor tablet was dissolved in 5.6 mL RO water with agitation. Tris (200 µL; 1 M; pH 7.5), 20 µL EDTA (0.5 M), 750 µL sodium chloride (2 M), 100 µL Nonidet P40, 200 µL sodium vanadate (100 mM), 500 µL sodium fluoride (0.5 M), 100 µL SDS (10% w/v), 400 µL sodium pyrophosphate (250 mM), 1250 µL glycerol (80% v/v), 200 µL sodium vanadate (0.5 M) and 50 µL phenylmethylsulfonyl fluoride (100 mM) were then added and mixed thoroughly. The resulting solution of 1% Nonidet P40, 20 mM Tris, 150 mM sodium chloride, 1 mM ethylenediaminetetraacetic acid, 25 mM sodium fluoride, 10 mM sodium phosphate, 2 mM sodium vanadate and 0.5 mM phenylmethylsulfonyl fluoride, supplemented with complete protease inhibitors, was stored in 1 mL aliquots at -20°C for up to 3 months.

2.16.3 5% polyacrylamide gel (stacking gel)

RO water (6.8 mL), 1.7 mL bis-acrylamide, 1.25 mL Tris (1.0 M; pH 6.8), 100 µL SDS (10% w/v) and 100 µL APS (10% w/v) were combined and were mixed by inversion. Immediately before use, 10 µL TEMED was added and the solution was mixed carefully to avoid creating bubbles.

2.16.4 8% polyacrylamide gel (separating gel)

RO water (9.3 mL), 5.3 mL bis-acrylamide, 5 mL Tris (1.5 M; pH 8.8), 200 µL SDS (10% w/v) and 200 µL APS (10% w/v) were combined and were mixed by inversion. Immediately before use, 12 µL TEMED was added and the solution was mixed carefully to avoid creating bubbles.

2.16.5 10% polyacrylamide gel (separating gel)

RO water (7.9 mL), 6.7 mL bis-acrylamide, 5 mL Tris (1.5 M; pH 8.8), 200 µL SDS (10% w/v) and 200 µL APS (10% w/v) were combined and were mixed by inversion. Immediately before use, 8 µL TEMED was added and the solution was mixed carefully to avoid creating bubbles.

2.16.6 Reducing loading buffer, 5 x

Glycerol (25 mL), 25 mL Tris (1.0 M, pH 6.8), 8 g SDS, 400 mg bromophenol blue, 8 mL β-mercaptoethanol and 25 mL RO water were mixed, the solution was filtered using a 0.45 µm syringe filter and 2.5 mL aliquots were stored at -20°C. Thawed aliquots were stored at 4°C until use. Cell lysates for Western blotting were diluted 1:4 in loading buffer for a final concentration of 50 mM Tris, 1.6% SDS, 0.08% (w/v) bromophenol blue and 1.6% β-mercaptoethanol.

2.16.7 Running buffer, 10 x

Tris (30.3 g), 144 g glycine and 10 g SDS were dissolved in RO water, the pH was adjusted to 8.3 and the volume was made up to 1 L. The solution was stored at room temperature and was diluted 1:9 in RO water prior to use for a final concentration of 0.3% (w/v) Tris-HCl, 1.44% (w/v) glycine and 0.1% (w/v) SDS.

2.16.8 Tris-buffered saline (TBS), 10 x

Tris (24.2 g) and 80 g sodium chloride were dissolved in RO water, the pH was adjusted to 7.6 and the volume was made up to 1 L. The solution was stored at room temperature and was diluted 1:9 in RO water before use.

2.16.9 1% Tween/TBS (TBS-Tween)

Tween 20 (1 mL) was added to 100 mL TBS (10 x) and 899 mL RO water and was carefully mixed to avoid bubbles. Solution was stored at room temperature until use.

2.16.10 TBS-Tween with 10% BSA

BSA (0.5 g) was dissolved in 50 mL TBS-Tween, with agitation. The solution was filtered using a 0.45 μM syringe filter and was stored at 4°C. The solution was diluted 1:9 in TBS-Tween prior to use.

2.16.11 Transfer buffer (1 x)

Tris (12.104 g) and 57.66 g glycine were dissolved in 3.0 L RO water, 0.6 L methanol was added and the volume was made up to 4.0 L. The solution was stored at 4°C and was used up to 2 times before discarding.

2.17 Western blotting

2.17.1 Preparation of cell lysates

For Western blotting experiments, mBM and rBM cells were cultured at 3.13 x 10^5 cells/cm^2 in 60 mm dishes in 3 mL c-α-MEM with 75 ng/mL rhM-CSF for 1 week to form committed osteoclast precursors. Cells were washed in 5 mL HBSS and were then starved for 120 minutes in 2 mL sf-α-MEM with imatinib, dasatinib or vehicle. In some cases, prior to being harvested, the cells were stimulated with 75 ng/mL rhM-CSF for 5 minutes at 37°C.

RAW 264.7 cells were seeded in a 6-well plate in 2 mL in c-DMEM at 9.38 x 10^3 cells/cm^2. After 24 h, the wells were washed with 3 mL HBSS and the cells were starved with sf-DMEM overnight. The cells were then treated with imatinib, dasatinib or vehicle for 120 minutes in 2 mL sf-DMEM prior to being harvested. In some experiments, cells were stimulated with 75 ng/mL rhM-CSF for 5 minutes at 37°C prior to being harvested.

rBMSC (8 x 10^3 cells/cm^2) or ATDC5 cells (1.56 x 10^5 cells/cm^2) were cultured in 6 well plates for 24 hours in 2 mL c-α-MEM supplemented with ascorbate (100 μM). Cells were washed in 3 mL HBSS and were then starved in sf-α-MEM overnight before being treated with imatinib, dasatinib or vehicle for 120 minutes in 2 mL sf-α-MEM. Where indicated, the cells were stimulated with 10 ng/mL rhPDGF-BB for 5 minutes at 37°C prior to being harvested.

Following treatment, the cells were scraped into 100 μL ice-cold non-reducing lysis buffer, the lysates were transferred to 1.5 mL microfuge tubes (Eppendorf, North Ryde, NSW) and the cells were lysed by sonication at 3 watts for 10 seconds using a probe sonicator (model number XL2007; MiSonix, Farmindale, USA). The lysates were cleared by centrifugation at 13000 g for 10 minutes at 4°C and the supernatants were transferred to 1.5 mL microfuge tubes. The protein concentration of the supernatant was determined using a RC/DC protein assay kit (catalogue number 500-0120; BioRad), following the protocol of the manufacturer. The lysates were then stored at -20°C until being used for SDS-polyacrylamide gel electrophoresis (SDS-PAGE).

2.17.2 Preparation of samples for SDS-PAGE

Cell lysates were thawed on ice and equivalent amounts of protein, as determined by RC/DC assay, were transferred to 1.5 mL microfuge tubes. Appropriate volumes of 5 x reducing loading buffer were added and the samples were incubated for 5 minutes at 95°C on a heat block. The samples were cooled on ice, quickly centrifuged and the samples were loaded onto SDS-PAGE gels with a pre-stained protein marker (Bench-mark; catalogue number 10748-010; Invitrogen).

2.17.3 SDS-PAGE gel preparation

Spacer plates (1.5 mm; catalogue number 1653312; Bio-Rad) and short plates (catalogue number 1653308; Bio-Rad) were assembled in a gel casting frame. Immediately following addition of TEMED, separating gel was poured until it was 2 cm below the top of the short plate. The gel was then covered with water-saturated butanol to remove bubbles and was left for 15 minutes to set.

When the gel was set, the butanol was poured off, the stacking gel was poured, a 10-well comb (catalogue number 1653365; Bio-Rad) was inserted and the gel was left to set for 15 minutes.

2.17.4 Loading and running of SDS-PAGE gels

The gels were assembled with the Mini-Protean® 3 (Bio-Rad) electrode assembly and clamping frame, the assembly was placed in a tank and the combs were removed. The inner chamber was filled with running buffer, ensuring the wells were well-rinsed with buffer. The tank was then half-filled with running buffer and the prepared samples and protein markers were loaded in appropriate wells. The lysates were run through the stacking gel at 20 mA and were then resolved through the separating gel at 40 mA.

2.17.5 Transfer of protein to polyvinylidene difluoride (PVDF) membranes

PVDF membrane (Hybond-P membrane, Amersham Biosciences, GE Healthcare, Little Chalfont, UK) was cut to size (7 x 9 cm) and was pre-equilibrated in methanol for 5 minutes. The membrane, blotting paper and fibre pads were then soaked in transfer buffer until use. Following electrophoresis, the gel assembly was dismantled and the electrophoretic transfer cell (Mini Trans-Blot, Bio-Rad) was assembled, following the instructions of the manufacturer. Briefly, 2 sheets of blotting paper were placed on a fibre pad on the black side of the gel cassette holder and the gel was carefully placed on top. The pre-equilibrated membrane was laid over the gel, followed by 2 sheets of blotting paper, any air bubbles were expelled by rolling over the filter paper with a pipette and a final fibre pad was placed on top. The assembly was then placed in a tank with a cooling unit (cooled to -20°C), the tank was filled with transfer buffer and the protein transfer was carried out overnight at 30 mA or for 2 hours at 200 mA.

2.17.6 Protein detection

Following Western blotting, the PVDF membrane was rinsed in TBS-Tween before being incubated for 2 hours in blocking buffer with agitation. The membrane was rinsed briefly in TBS-Tween and was then probed with primary antibody (detailed in table 2.2) diluted in 1% BSA in TBS-Tween either overnight at 4°C or for 2 hours at room temperature with agitation. The membranes were then washed 3 times for 5 minutes in TBS-Tween and the immunoreactive proteins were subsequently detected by incubation with alkaline-phosphatase-conjugated antibodies against rabbit immunoglobulin (Ig) (catalogue number AP182A; Chemicon, Melbourne, VIC) or mouse Ig (catalogue number AP322A; Chemicon), diluted 1:2000 in 1% BSA/TBS-Tween, for 1 hour at room temperature with agitation. The membranes were then washed 3 times for 5 minutes at room temperature with agitation, followed by a final rinse in TBS.

Table 2.2: Antibodies for Western blotting

Antibody	Supplier	Catalogue number	Dilution	Isotype
Phosphorylated Akt	Cell Signaling, Danvers, USA	4051	1:1000	Mouse IgG2b
Fms	Cell Signaling	3152	1:1000	Rabbit IgG
Phosphorylated Fms	Cell Signaling	3151	1:1000	Rabbit IgG
Phosphorylated ERK1/2	Cell Signaling	9101	1:2000	Rabbit IgG
Phosphorylated Src	Millipore, Billerica, USA	07-909	1:1000	Rabbit IgG
Heat shock protein 90 kDa (HSP90)	Santa Cruz, Santa Cruz, USA	sc-7947	1:5000	Rabbit IgG

The protein was then detected by incubation with 1 mL enhanced chemifluorescence (ECF™) substrate (catalogue number RPN5785; Amersham) prior to imaging using a Typhoon 9410 fluorimager (Amersham) at 488 nm excitation. Quantitation was performed using ImageQuant software (version 7.0, GE Healthcare).

Where required, membranes were stripped of antibodies using a commercial stripping buffer (Western blot recycling kit; catalogue number 90100; Alpha Diagnostics, San Antonio, USA), following the instructions of the manufacturer. The blots were then rinsed in TBS and incubated for 1 hour in blocking buffer before reprobing with primary antibody.

2.18 Statistical analyses

Analysis of patient data was carried out using SAS (version 9.2; SAS Institute Incorporated, Cary, USA). To account for serially collected data, longitudinal data from each patient were compared with baseline values using a linear mixed effects model.

Analysis of all other data was performed using GraphPad PRISM (version 5.02; GraphPad Software, La Jolla, USA). For *in vitro* dose-response experiments, treatments were compared using one-way analysis of variance (ANOVA) with Dunnett's post-tests. In *in vivo* experiments, for serum CTX-1 analysis, as some values were below the detection limit of the ELISA used, the non-parametric Kruskal-Wallis test with Dunn's post-tests was used. Changes in the body weights of the animals over time were assessed using

repeated measures ANOVA with Dunnett's post-tests. For all other *in vivo* experiments, treated groups were compared with vehicle controls at each time-point using one-way ANOVA with Dunnett's post-tests.

Correlations between serum imatinib concentrations and other indices were assessed using the Pearson test.

Differences were considered to be statistically significant when the *P* value was less than 0.05.

The calculation of 50% inhibitory concentration (IC_{50}) values was performed using the Hill equation: $y = 100/(1 + 10_{50}^{(logIC-x)*Hillslope})$, where y is the level of inhibition and x is the logarithmic drug concentration.

Chapter 3

The effects of imatinib on bone remodelling in CML patients

3.1 Introduction

Prior to the introduction of imatinib mesylate therapy, the primary front-line treatment for chronic phase CML was interferon-α therapy or allogeneic bone marrow transplant (reviewed in [315]). While allogeneic stem cell therapy has an impressive long-term survival rate, particularly in young patients where human leukocyte antigen (HLA)-matched donors are available, it is associated with significant treatment-related mortality (reviewed in [315]). Interferon-α was the therapy of choice for patients for whom transplant was not an option and was relatively effective, with a complete cytogenetic response rate of 6% to 9% and a 5-year survival rate of approximately 55% in randomised controlled trials.[316-318] However, interferon-α treatment is associated with a high level of grade 3 and 4 toxicity resulting in dose reduction or discontinuation in a large proportion of patients[3,316,319] (reviewed in [315]).

Imatinib represents a vast improvement over these therapeutic strategies for CML in regard to both therapeutic efficacy and toxicity. A phase 3 study (International Randomized Study of Interferon and STI571 [IRIS] study) comparing imatinib with interferon-α and cytarabine in chronic phase CML patients found that the complete cytogenic response rate in the imatinib treatment arm was 87%, with an estimated 5-year survival rate of 89%.[3,241] Side-effects of imatinib treatment, while common, are generally mild to moderate in severity.[3,241,320] Myelosuppression is the most common haematological adverse event following imatinib therapy and is more severe in advanced phase disease.[3,241,320] Haematological suppression following imatinib therapy may result from decreased numbers of residual normal stem cells in patients with advanced disease (reviewed in [321]). Additional effects may be due to the off-target inhibition of kinases other than Bcr-Abl, including Kit (reviewed in [321]). Common non-haematological toxicities with imatinib therapy include nausea, diarrhoea, rash and oedema.[3,241,320] Additionally, muscle cramps affect approximately 50% of imatinib-treated CML patients, but are usually manageable with increased fluid intake and calcium supplements[3,241] (reviewed in [321]). Bone and joint pain also occur in more than 30% of patients.[3,241]

These musculoskeletal side-effects may in part relate to the effects of imatinib on calcium and phosphate metabolism. Hypophosphataemia was first identified as a common side-effect of imatinib therapy in a retrospective analysis of patients undergoing imatinib treatment for CML or GIST.[5] This observation was subsequently confirmed by longitudinal studies, showing that decreased levels of serum phosphate occur as early as 3 months following initiation of imatinib treatment in CML and GIST patients.[7-9,11,12] Decreased serum phosphate levels in imatinib-treated patients are associated with

increased serum PTH levels and, in at least some cases, a decrease in serum calcium levels.[5,8-10,12,20] Recent evidence suggests that these changes in serum biochemistry may result from increased sequestration of calcium and phosphate to bone, due to altered skeletal metabolism. In a cohort of CML patients treated with imatinib for 17 – 62 months, trabecular bone volume in iliac spine trephines was significantly increased following treatment, relative to at baseline[10] Additionally, 2 subsequent studies showed that CML patients undergoing long-term imatinib therapy exhibited small increases in regional BMD at some, but not all, sites.[12,20]

While the aetiology of these changes in mineral metabolism remains to be determined, decreased osteoclast activity has been associated with these phenomena. Berman *et al*. were the first to demonstrate that serum levels of the osteoclast marker N-telopeptide of collagen crosslinks (NTX) were decreased in imatinib-treated CML and GIST patients, relative to healthy controls.[5] The authors posited that decreased osteoclast activity may decrease dissolution of calcium and phosphate from the bone, thus resulting in hypophosphataemia. A longitudinal study has subsequently confirmed that serum osteoclast markers are decreased following imatinib therapy.[8,12] This is associated with decreased serum calcium and phosphate and an increase in PTH levels. Serum PTH levels are increased in response to decreased serum calcium levels and sustained increases in PTH usually result in increased osteoclast activity, secondary to stimulation of RANKL production by osteoblasts.[192-194] Thus, the observed decrease in osteoclast activity in imatinib-treated patients is unexpected in the presence of increased PTH and suggests that imatinib may have direct inhibitory effects on osteoclasts. While there is substantiative evidence that imatinib inhibits osteoclast survival and activity *in vitro*[13-15] no direct evidence of effects on osteoclast numbers or activity has been demonstrated histologically in patients.

Inhibition of osteoclast activity, if not corrected by a decrease in osteoblast activity, could explain the increase in bone volume observed in imatinib-treated patients. The effects of imatinib on osteoblasts in patients are unclear as there are conflicting data regarding the effects of imatinib on serum markers of osteoblast activity. Berman *et al*. found that serum osteocalcin levels were significantly decreased in imatinib-treated patients, relative to healthy controls, while serum bone-specific alkaline phosphatase levels were not different between these groups.[5] Similarly, Jönsson *et al*. found that serum osteocalcin levels were significantly decreased in patients treated with imatinib for 24 – 73 months, relative to aged-matched normal controls. Longitudinal studies have observed

increases in serum osteocalcin and P1NP levels early in treatment which either return to baseline levels by 18 months of therapy[8,12] or are sustained until at least 24 months of treatment[19]. Some of the apparent differences in effects of imatinib on serum osteoblast markers may relate to the divergent effects of imatinib on osteoblast proliferation and activity. *In vitro*, imatinib inhibits mesenchymal cell proliferation while increasing mineralised matrix production by osteoblasts.[10,16-19] Thus, while imatinib may induce early increases in osteoblast activity, osteoblast numbers may decrease over time. Longitudinal histological assessment would be useful to directly examine osteoblast numbers and activity in patients undergoing imatinib therapy.

The aim of this study was to determine the mechanisms by which imatinib therapy augments bone volume and density in CML patients. The effects of imatinib therapy on bone remodelling were determined by undertaking prospective histological and μ-CT analysis of bone trephine specimens collected prior to and following commencement of imatinib therapy for CML.

3.2 Results

3.2.1 Patients

Fourteen South Australian CML patients were recruited to this study from the Australasian Leukaemia and Lymphoma Group CML9 (TIDEL II) trial. Two patients were excluded from the study at diagnosis due to pre-existing medical conditions (elevated amylase levels or distal metastases). An additional patient was transferred to the nilotinib treatment arm prior to the 6 month time-point and was excluded from further analysis. Of the 11 patients in the cohort used in this study (8 men, 3 women; mean age at diagnosis, 52 years; range, 32 – 76 years), 2 patients had a dose increase to 800 mg/day, and 1 patient had a dose reduction to 400 mg/day, during the 12 months of treatment. The remaining patients received 600 mg/day imatinib. All patients achieved complete cytogenetic remission during the course of the study.

3.2.2 Plasma imatinib concentrations

The average steady-state plasma concentration of imatinib achieved in these patients was 2.21 μM (range: 0.44 – 3.80; 6 months) and 2.51 μM (range: 0.37 – 4.19; 12 months) (figure 3.1). This is consistent with previous data from CML patients receiving 600 mg/day imatinib (trough concentration: 2.065 ± 1.39 μM [mean ± SD]).[322]

3.2.3 Effects of imatinib on calcium and phosphate metabolism

3.2.3.1 Serum biochemistry

Serum samples, collected after 0, 6 and 12 months of imatinib therapy, were analysed to determine the effects of treatment on serum biochemistry. Decreased serum phosphate levels were observed in 11/11 patients, including 2 patients who were hyperphosphataemic prior to treatment. Mean phosphate concentrations were decreased from 1.25 ± 0.07 mM (mean ± SEM) at baseline to 0.86 ± 0.06 mM ($p < 0.05$) and 0.87 ± 0.05 mM ($p < 0.05$) following 6 and 12 months of treatment, respectively (figure 3.2A). Additionally, total calcium levels were significantly lower after imatinib therapy, compared with baseline levels (figure 3.2B). Serum calcium concentrations were reduced from 2.29 ± 0.03 mM (mean ± SEM) to 2.18 ± 0.03 ($p < 0.05$) and 2.18 ± 0.02 ($p < 0.05$) after 6 and 12 months, respectively (figure 3.2B). Ionised calcium levels were not significantly altered after 6 or 12 months of imatinib therapy ($p = 0.27$; figure 3.2C). Mild hypophosphataemia (< 0.8 mM phosphate) was observed in 5/11 patients, and hypocalcaemia (< 2.1 mM total calcium) in 1/11 patients, at 6 or 12 months of treatment.

Figure 3.1. Plasma concentrations of imatinib in CML patients. Peripheral blood was collected following 6 or 12 months of imatinib treatment and plasma levels of imatinib were analysed by HPLC. Graph depicts mean ± SEM.

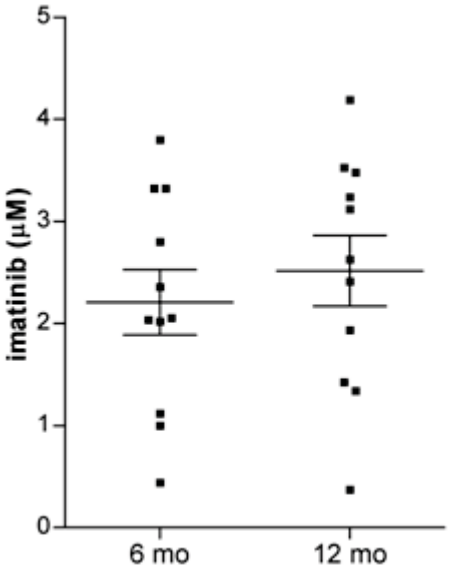
imatinib (μM)
5
4
3
2
1
0
6 mo
12 mo

Figure 3.2. The effects of imatinib treatment on serum biochemistry in CML patients. Peripheral blood was collected at diagnosis and after 6 and 12 months of imatinib treatment. Plasma levels of phosphate (**A**), calcium (**B**), ionised calcium (**C**), urea (**D**), creatinine (**E**), PTH (**F**), 25-hydroxyvitamin D_3 (**G**) and 1,25-dihydroxyvitamin D_3 (**H**) were determined. Graphs depict mean ± SEM (n = 10 – 11). * $p < 0.05$, relative to baseline (linear mixed effects model).

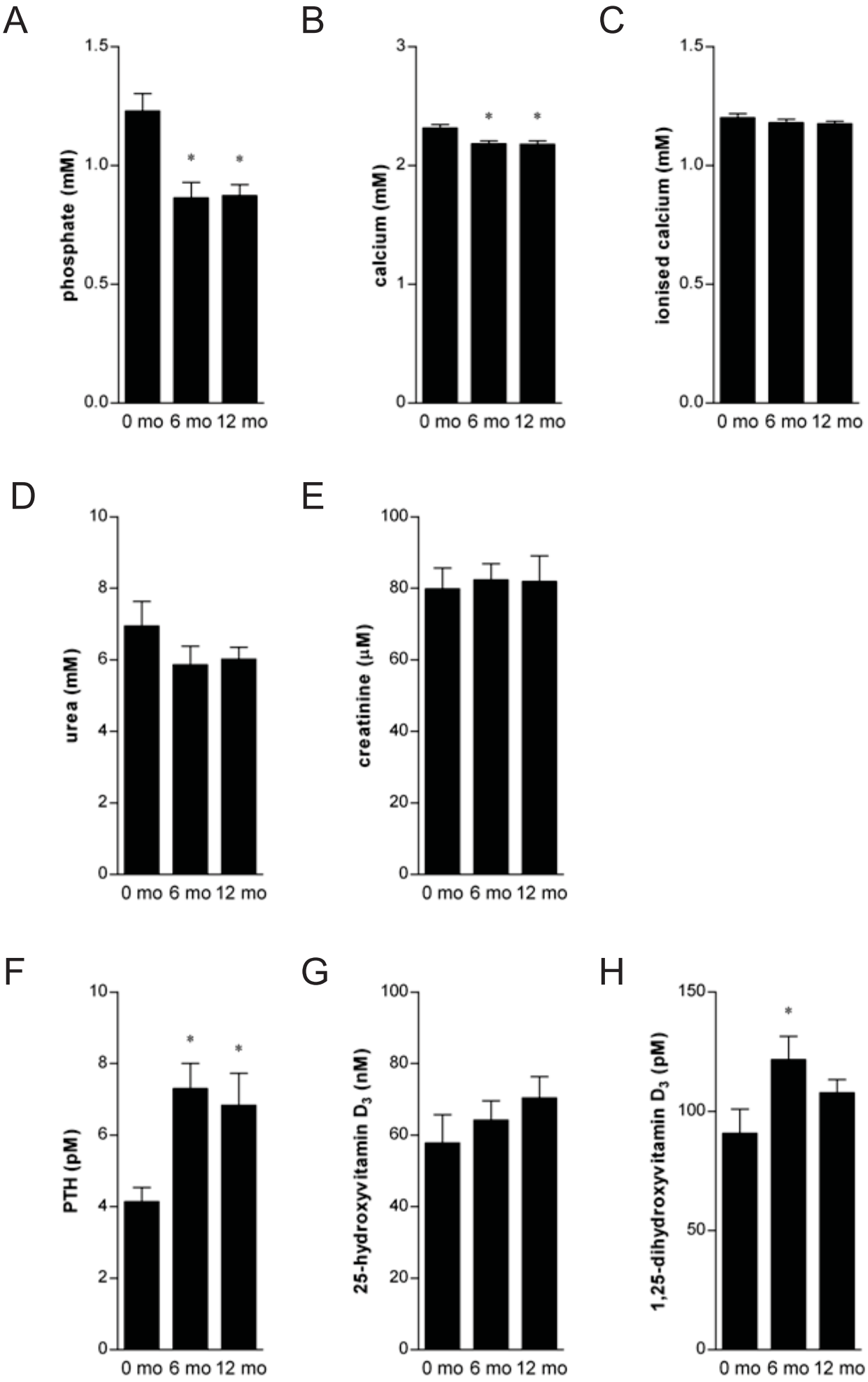
A
phosphate (mM)
1.5
1.0
0.5
0.0
*
*
0 mo 6 mo 12 mo
B
calcium (mM)
3
2
1
0
*
*
0 mo 6 mo 12 mo
C
ionised calcium (mM)
1.5
1.0
0.5
0.0
0 mo 6 mo 12 mo
D
urea (mM)
10
8
6
4
2
0
0 mo 6 mo 12 mo
E
creatinine (µM)
100
80
60
40
20
0
0 mo 6 mo 12 mo
F
PTH (pM)
10
8
6
4
2
0
*
*
0 mo 6 mo 12 mo
G
25-hydroxyvitamin D3 (nM)
100
80
60
40
20
0
0 mo 6 mo 12 mo
H
1,25-dihydroxyvitamin D3 (pM)
150
100
50
0
*
0 mo 6 mo 12 mo

There were no detectable effects of imatinib on serum urea or creatinine levels ($p = 0.17$ and 0.51, respectively; figure 3.2D,E), suggesting that imatinib treatment had no negative effects on renal function.

3.2.3.2 Serum hormone levels

Mean concentrations of PTH were significantly increased after 6 months (85% ± 29% SEM, $p < 0.05$) and 12 months (74% ± 28% SEM, $p < 0.05$) of imatinib therapy, relative to at baseline (figure 3.2F). The majority of patients (10/11) exhibited increases in serum PTH above the normal range (> 5.5 pM PTH) following 6 or 12 months of treatment. This included 2 patients with higher than normal PTH levels at baseline, who exhibited further increases in serum PTH while receiving imatinib therapy.

While 25-hydroxyvitamin D_3 levels were unchanged by imatinib therapy ($p = 0.25$), there was a significant increase in mean 1,25-hydroxyvitamin D_3 levels after 6 months (52% ± 16% SEM; $p < 0.05$; figure 3.2G) of imatinib treatment (figure 3.2H). Serum 1,25-dihydroxyvitamin D_3 levels returned to baseline levels by 12 months ($p = 0.15$).

3.2.4 DXA

In order to determine the effects of imatinib therapy on BMD and BMC, patients were DXA scanned prior to commencement of imatinib therapy and then after 6 and 12 months of treatment. Ten patients, who had scans conducted at 2 or more time-points, were included in this analysis. One patient showed evidence of degenerative changes to the spine prior to treatment and was excluded from analysis of vertebral BMD and BMC. Three patients displayed evidence of osteopoenia or osteoporosis at baseline.

Site-specific differences in BMD and BMC were observed during imatinib treatment (table 3.1 and 3.2). In 8/10 patients, an increase in BMD at the 33% radius was measured, including 1 patient who had low BMD (z-score < -1.0) at this site at diagnosis. BMD was increased by 1.3% ± 0.007% (mean ± SEM) at the 33% radius site at 12 months, relative to at baseline ($p < 0.05$; figure 3.3A). Similarly, there was a statistically-significant 2.5% ± 0.007% increase in BMC at this site after 12 months of imatinib treatment ($p < 0.05$; figure 3.3B). Tibia and fibula BMC ($p < 0.05$), but not BMD ($p = 0.54$), was increased by 2.3% ± 0.8% after 12 months of imatinib therapy, when compared with at baseline (figure 3.3C,D). Neither total body BMD nor total body BMC were significantly change during the course of treatment ($p = 0.82$ and 0.23, respectively; figure 3.3E,F).

Table 3.1: Effects of imatinib mesylate on bone mineral density (BMD) in CML patients

	BMD (g/cm^2)[1]				
	baseline	6 months	12 months	p-value[2]	p-value[3]
33% radius	0.93 ± 0.03 (0.81 – 1.05)	0.92 ± 0.03 (0.80 – 1.05)	0.94 ± 0.03 (0.81 – 1.08)	NS	0.037
Total body	1.25 ± 0.04 (0.99 – 1.39)	1.23 ± 0.04 (0.99 – 1.37)	1.24 ± 0.04 (0.97 – 1.36)	NS	NS
Tibia and fibula	1.35 ± 0.05 (1.06 – 1.52)	1.31 ± 0.06 (0.98 – 1.55)	1.33 ± 0.05 (0.98 – 1.51)	NS	NS
Vertebrae L2-L4[4]	1.29 ± 0.07 (0.93 – 1.56)	1.25 ± 0.07 (0.94 – 1.46)	1.29 ± 0.07 (0.91 – 1.58)	NS	NS
Femoral neck	1.03 ± 0.05 (0.82 – 1.31)	0.97 ± 0.05 (0.80 – 1.20)	0.98 ± 0.04 (0.82 – 1.23)	0.0010	0.0004

[1] data represent mean ± SEM (range); n = 9 (6 months) and n = 10 (baseline and 12 months)

[2] 6 months v baseline

[3] 12 months v baseline

[4] One patient showed evidence of degenerative changes in the spine at baseline and was excluded from the analysis of vertebral BMD and BMC

NS: not significant

Table 3.2: Effects of imatinib mesylate on bone mineral content (BMC) in CML patients

	BMC (g)[1]				
	baseline	6 months	12 months	p-value[2]	p-value[3]
33% radius	2.71 ± 0.19 (1.99 – 3.61)	2.69 ± 0.20 (1.95 – 3.68)	2.77 ± 0.19 (1.98 – 3.76)	NS	0.034
Total body	3184 ± 249 (2079 – 4123)	3164 ± 268 (2145 – 4157)	3243 ± 248 (2089 – 4156)	NS	NS
Tibia and fibula	228.9 ± 13.2 (159.4 – 287.2)	225.7 ± 14.4 (157.6 – 292.6)	234.1 ± 13.6 (159.9 – 298.2)	NS	0.0085
Vertebrae L2-L4[4]	61.8 ± 5.2 (36.0 – 75.4)	60.1 ± 5.3 (36.3 – 74.7)	62.1 ± 5.3 (35.1 – 79.4)	NS	NS
Femoral neck	5.37 ± 0.36 (4.01 – 7.24)	5.12 ± 0.36 (3.86 – 6.92)	5.20 ± 0.32 (3.98 – 7.05)	0.0079	0.0021

[1] data represent mean ± SEM (range); n = 9 (6 months) and n = 10 (baseline and 12 months)

[2] 6 months v baseline

[3] 12 months v baseline

[4] One patient showed evidence of degenerative changes in the spine at baseline and was excluded from the analysis of vertebral BMD and BMC

NS: not significant

Figure 3.3. The effects of imatinib therapy on radius, tibia and fibula and total body BMD and BMC. After 0, 6 and 12 months of imatinib treatment, patient BMD and BMC were analysed by DXA. 33% radius BMD (**A**), 33% radius BMC (**B**), tibia and fibula BMD (**C**), tibia and fibula BMC (**D**), total body BMD (**E**), total body BMC (**F**). Graphs depict mean ± SEM, expressed relative to baseline values (n = 8 – 10). * $p < 0.05$, relative to baseline (linear mixed effects model).

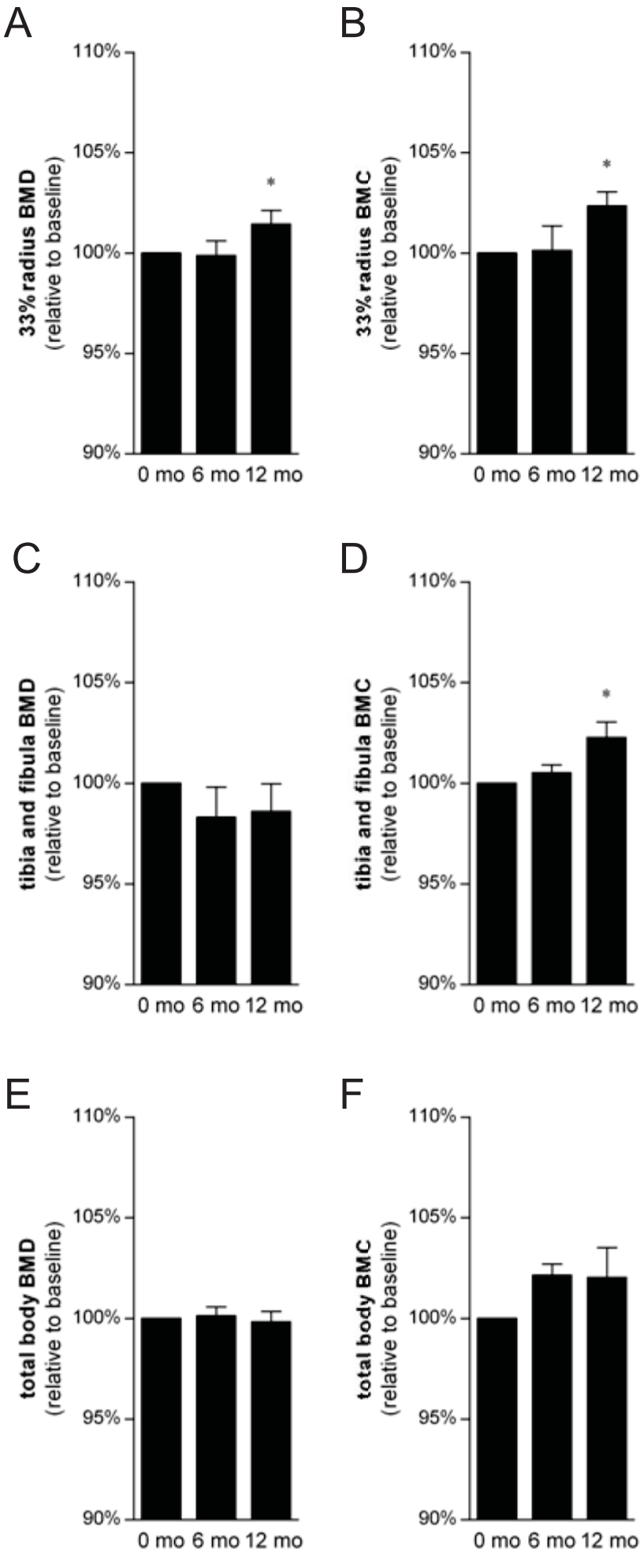
A
B
C
D
E
F
33% radius BMD
(relative to baseline)
33% radius BMC
(relative to baseline)
tibia and fibula BMD
(relative to baseline)
tibia and fibula BMC
(relative to baseline)
total body BMD
(relative to baseline)
total body BMC
(relative to baseline)
110%
105%
100%
95%
90%
0 mo 6 mo 12 mo
*

DXA analysis revealed no significant changes in BMD ($p = 0.93$) or BMC ($p = 0.94$) in the L2-L4 vertebrae at 6 or 12 months of treatment (figure 3.4A,B).

In contrast, BMD at the femoral neck was decreased by 4.1% ± 0.009% (mean ± SEM) after 6 months ($p < 0.05$) and 12 months ($p < 0.05$), when compared with prior to treatment (figure 3.4C). Femoral neck BMC was similarly decreased at 6 and 12 months of treatment ($p < 0.05$; figure 3.4D).

3.2.5 Trabecular bone morphometry

3.2.5.1 μ-CT

To determine the effects of imatinib treatment on trabecular bone morphometry, trephines were collected from the posterior iliac spine of CML patients prior to commencement of treatment and after 6 and 12 months of imatinib therapy. Trephines were fixed in neutral buffered formalin and biopsies were scanned by μ-CT.

Suitable trephines for μ-CT analysis were obtained from 9/11 patients at baseline, 9/11 patients at 6 months and 11/11 patients at 12 months. μ-CT analysis revealed an increase in trabecular thickness in trephines collected following imatinib treatment, when compared with baseline (table 3.3; figure 3.5). Although there was an increase in trabecular BV/TV following 6 and 12 months of treatment in 6/9 patients for which there were biopsies available at baseline (mean increase at 12 months: 30% ± 12% SEM; range: -18% – 77%), this did not reach statistical significance ($p = 0.14$; figure 3.6A). Following 12 months of imatinib therapy, Tb.Th was increased by 30% ± 12% (mean ± SEM), relative to at baseline ($p < 0.05$; figure 3.6B). This was reflected by a significant decrease in bone surface to volume ratio (BS/BV) after 12 months of imatinib therapy ($p < 0.05$; figure 3.6D). Tb.N, Tb.Sp and bone surface density (BS/TV) were not significantly altered by imatinib treatment ($p = 0.75$, 0.83 and 0.91, respectively; figure 3.6C,E,F). SMI was unchanged by imatinib treatment ($p = 0.80$; figure 3.6G). Tb.Pf was significantly decreased at the 12 month time-point ($p < 0.05$), relative to baseline, suggesting an increase in trabecular connectivity (figure 3.6H).

3.2.5.2 Histomorphometry

Following μ-CT scanning, trephines were embedded in methyl methacrylate, sectioned and stained with toluidine blue for histomorphometric assessment (figure 3.7). Suitable biopsies were obtained from all patients at 2 or more time-points. Histological assessment of the marrow tissue showed marked myeloid hyperplasia prior to treatment. After 6 and

Figure 3.4. The effects of imatinib therapy on lumbar vertebrae and femoral BMD and BMC. After 0, 6 and 12 months of imatinib treatment, patient BMD and BMC were analysed by DXA. L2-L4 lumbar vertebrae BMD (**A**), L2-L4 lumbar vertebrae BMC (**B**), femoral neck BMD (**C**), femoral neck BMC (**D**). Graphs depict mean ± SEM, expressed relative to baseline values (n = 9 – 10). * $p < 0.05$, relative to baseline (linear mixed effects model).

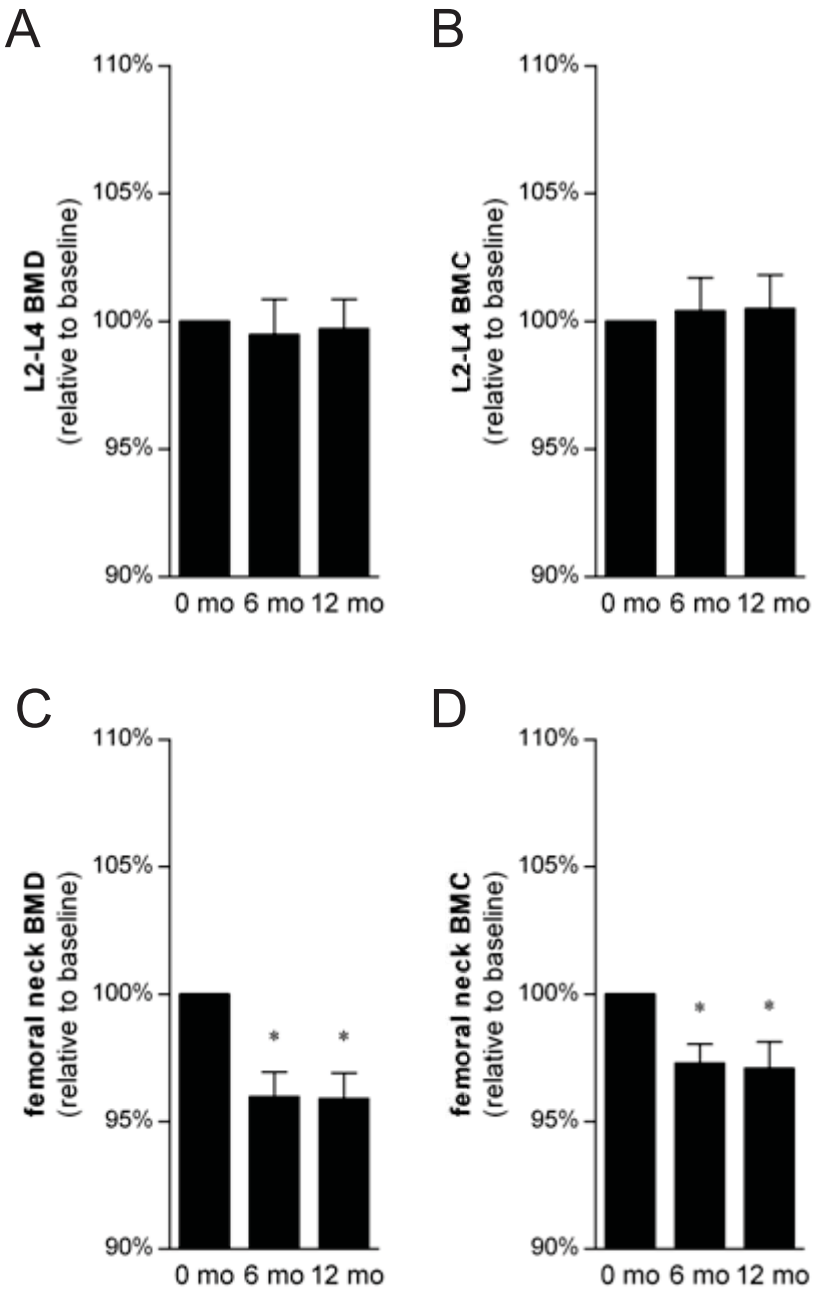
A
B
C
D
L2-L4 BMD
(relative to baseline)
L2-L4 BMC
(relative to baseline)
femoral neck BMD
(relative to baseline)
femoral neck BMC
(relative to baseline)
110%
105%
100%
95%
90%
0 mo 6 mo 12 mo
*

Table 3.3: Effects of imatinib on trabecular morphometry, assessed by µ-CT

	baseline[1]	6 months[1]	12 months[1]	p-value[2]	p-value[3]
BV/TV (%)	6.38 ± 0.43 (5.01 – 8.71)	7.36 ± 0.47 (5.75 – 10.4)	7.69 ± 0.52 (5.43 – 9.89)	NS	NS
Tb.Th (µm)	120.0 ± 5.0 (99.6 – 146.6)	136.7 ± 7.8 (116.1 – 185.5)	154.1 ± 9.1 (106.4 – 202.8)	NS	0.0056
Tb.N (mm^{-1})	0.54 ± 0.05 (0.39 – 0.77)	0.56 ± 0.06 (0.35 – 0.89)	0.51 ± 0.04 (0.37 – 0.80)	NS	NS
Tb.Sp (µm)	687 ± 27 (572 – 805)	682 ± 21 (571 – 761)	702 ± 27 (509 – 836)	NS	NS
BS/BV (mm^{-1})	30.0 ± 0.9 (26.8 – 33.8)	27.1 ± 1.0 (21.1 – 30.8)	25.7 ± 1.2 (19.5 – 32.2)	NS	0.0094
BS/TV (mm^{-1})	1.92 ± 0.14 (1.35 – 2.48)	2.01 ± 0.17 (1.38 – 2.84)	1.96 ± 0.14 (1.40 – 3.10)	NS	NS
Tb.Pf (mm^{-1})	6.48 ± 0.68 (3.31 – 9.59)	6.36 ± 0.45 (3.93 – 8.93)	4.37 ± 0.33 (2.72 – 4.95)	NS	0.0070
SMI	1.55 ± 0.10 (1.01 – 1.94)	1.64 ± 0.14 1.05 – 2.35)	1.66 ± 0.10 (1.00 – 2.02)	NS	NS

[1] mean ± SEM (range)

[2] 6 months v baseline

[3] 12 months v baseline

NS: not significant

Figure 3.5. Trabecular bone volume is increased by imatinib treatment. CML patients (n = 11) were treated with imatinib (400 – 800 mg/day) for 12 months. At baseline and after 6 or 12 months of treatment, posterior iliac crest trephines were collected for μ-CT analysis of a 4.351 mm long region of trabecular bone. Three-dimensional images of biopsies from a representative patient are shown.

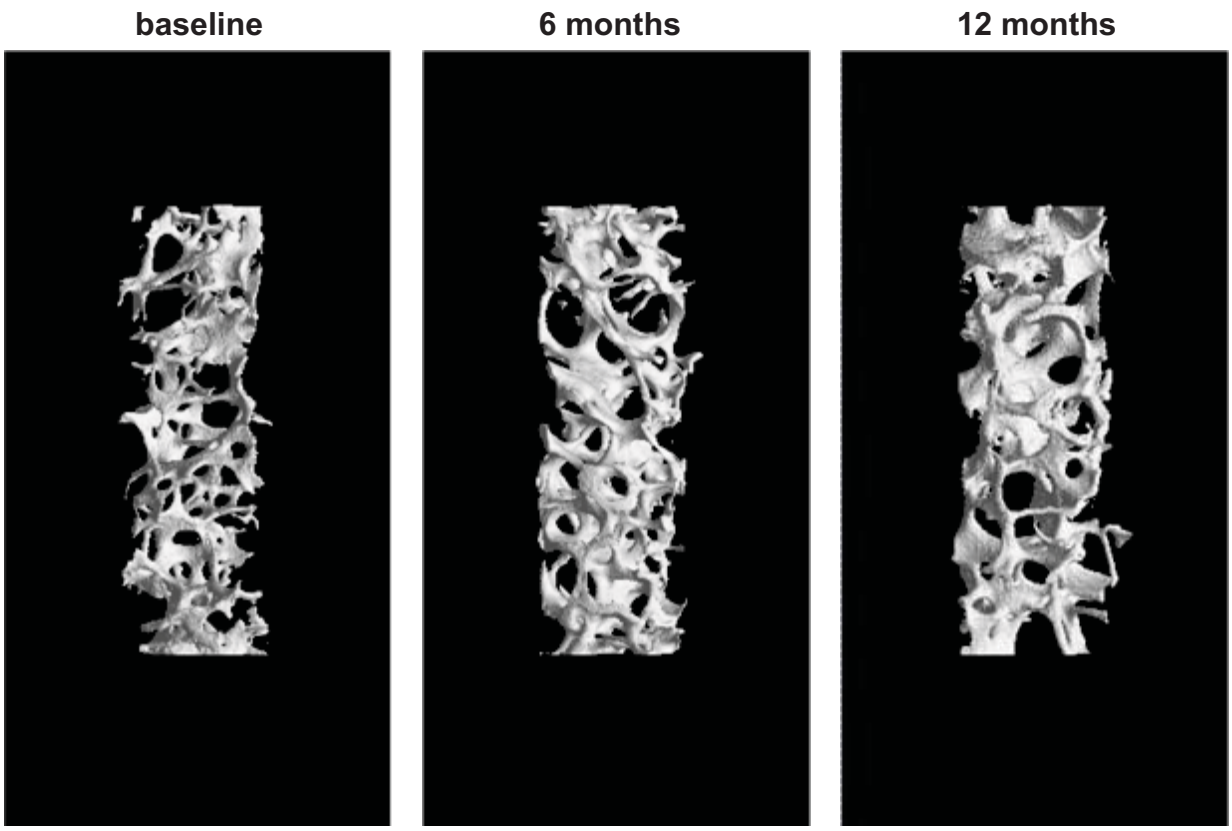
baseline
6 months
12 months

Figure 3.6. Trabecular morphology in iliac crest biopsies is altered by imatinib treatment. At baseline and after 6 and 12 months of imatinib treatment iliac crest biopsies were collected for μ-CT analysis of a 4.351 mm long region of trabecular bone. BV/TV (**A**), Tb.Th (**B**), Tb.N (**C**), BS/BV (**D**), BS/TV (**E**), Tb.Sp (**F**), SMI (**G**), Tb.Pf (**H**). Graphs depict mean ± SEM, expressed relative to baseline values (n = 9 – 11). * $p < 0.05$, relative to baseline (linear mixed effects model).

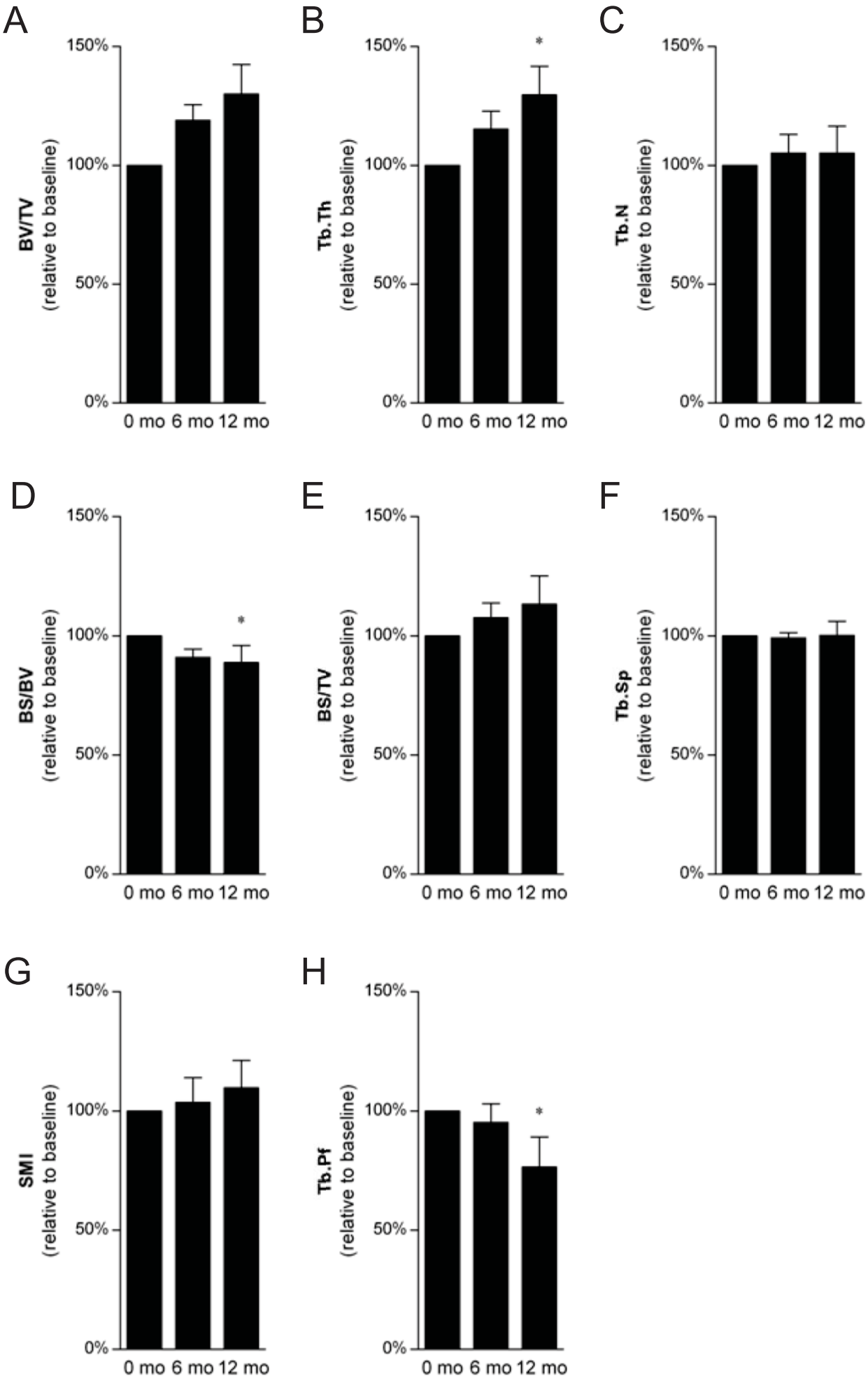
A
BV/TV
(relative to baseline)
150%
100%
50%
0%
0 mo 6 mo 12 mo
B
Tb.Th
(relative to baseline)
*
C
Tb.N
(relative to baseline)
D
BS/BV
(relative to baseline)
E
BS/TV
(relative to baseline)
F
Tb.Sp
(relative to baseline)
G
SMI
(relative to baseline)
H
Tb.Pf
(relative to baseline)

Figure 3.7. Histological examination of trabecular bone biopsies in imatinib-treated CML patients. At baseline and following 6 and 12 months of treatment with imatinib, trephines were collected, embedded in methyl methacrylate and 5 μm sections were stained with von Kossa (**A**) or toluidine blue (**B**). Images from 2 representative patients are shown. Scale bar: 300 μm.

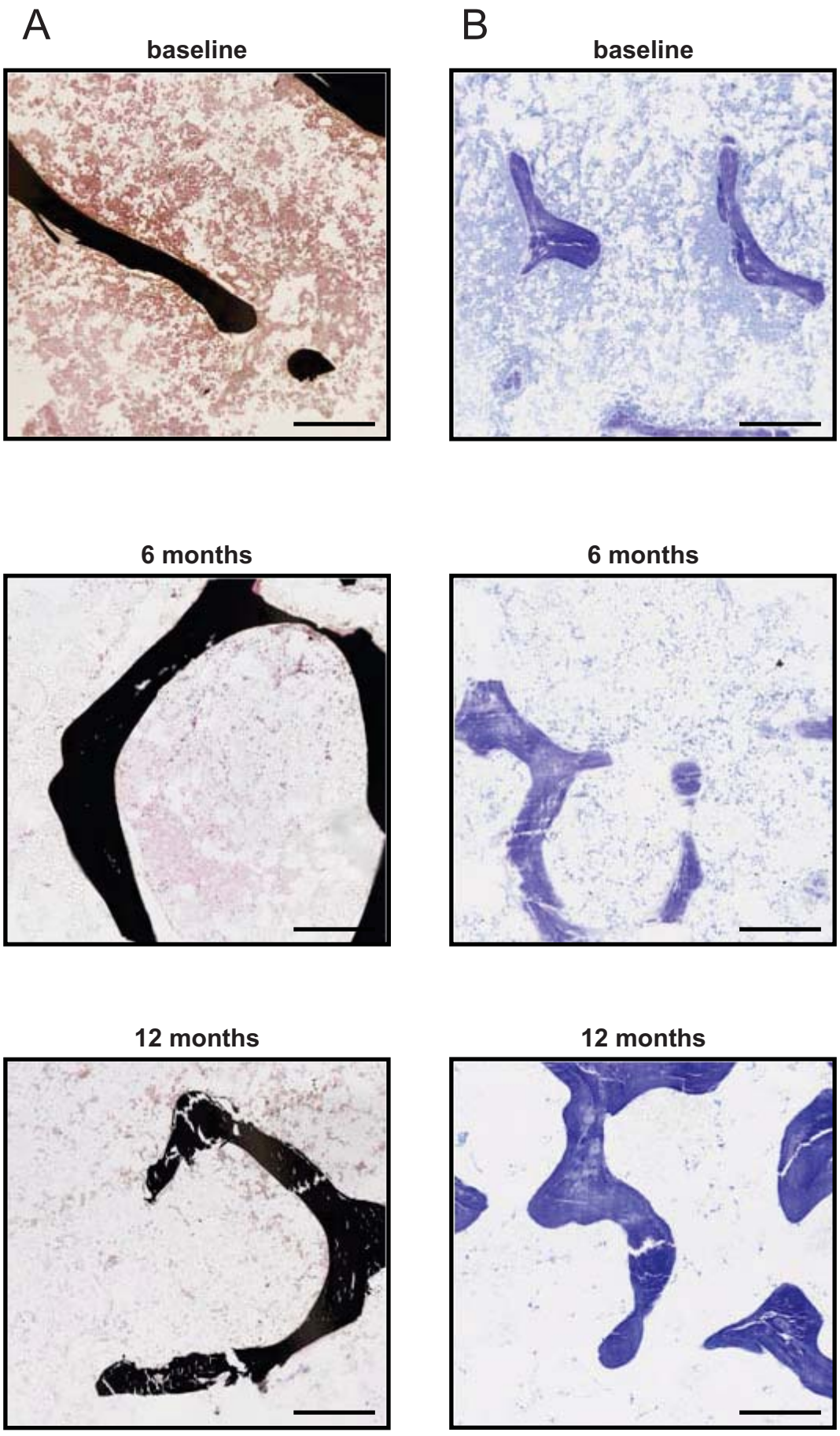
A
baseline
B
baseline
6 months
6 months
12 months
12 months

12 months of imatinib treatment, the marrow space showed hypocellularity or normal cellularity, with normal myelopoiesis and an increase in adipocyte numbers (figure 3.7).

Histomorphometric analysis of trabecular architecture revealed similar increases in bone volume to those detected by μ-CT (table 3.4). Neither total BV/TV nor mineralised bone volume (min.BV/TV) were significantly increased by imatinib therapy ($p = 0.14$ and 0.23, respectively; figure 3.8A,B). Tb.Th was 42 ± 18% (mean ± SEM) higher in patients treated with imatinib for 12 months, when compared with at baseline ($p < 0.05$; figure 3.8C). This was reflected by a significant decrease in bone surface to volume ratio (BS/BV) at 12 months after commencement of therapy ($p < 0.05$; figure 3.8F). Histomorphometry revealed no statistically significant changes in Tb.N, Tb.Sp or BS/TV ($p = 0.74$, 0.66 and 0.74, respectively; figure 3.8D,E,G), confirming the results obtained by μ-CT.

3.2.6 Effects of imatinib on osteoclasts

3.2.6.1 Osteoclast numbers

We next examined whether imatinib treatment affected bone resorption in CML patients. Trephines were embedded in methyl methacrylate, sectioned and osteoclasts were stained positive based on tartrate-resistant alkaline phosphatase (TRAP) activity (figure 3.9A). Histomorphometric assessment of bone biopsies revealed a significant decrease in osteoclast numbers (N.Oc/B.Pm) following 6 and 12 months of imatinib treatment ($p < 0.05$; figure 3.9B). All patients displayed a decrease in osteoclast numbers below baseline levels at final follow-up. Osteoclast surface (Oc.S/BS) was also significantly decreased after 6 and 12 months of treatment, relative to baseline levels ($p < 0.05$; figure 3.9C).

3.2.6.2 Serum markers of osteoclast activity

Concomitant with the decrease in osteoclast numbers, osteoclast activity, as assessed by the serum marker CTX-1, was significantly lower following imatinib treatment (figure 3.9D). A significant decrease in mean CTX-1 levels was observed after 6 and 12 months (47% ± 9% SEM at both time-points; $p < 0.05$) of imatinib treatment, compared with baseline values (figure 3.9D).

Table 3.4: Effects of imatinib on trabecular histomorphometry

	baseline[1]	6 months[1]	12 months[1]	p-value[2]	p-value[3]
BV/TV (%)	11.1 ± 1.1 (5.2 – 16.3)	14.4 ± 2.4 (6.2 – 31.7)	15.9 ± 1.6 (9.9 – 24.5)	NS	NS
Min.BV/TV (%)	11.0 ± 1.1 (5.03 – 16.0)	14.2 ± 2.6 (6.04 – 30.7)	15.5 ± 1.6 (9.70 – 24.3)	NS	NS
Tb.Th (μm)	81.3 ± 4.8 (51.1 – 103.1)	94.8 ± 9.5 (66.6 – 156.7)	108.2 ± 8.2 (67.3 – 150.7)	NS	0.0093
Tb.N (mm^{-1})	1.36 ± 0.11 (1.01 – 2.14)	1.48 ± 0.15 (0.77 – 2.25)	1.48 ± 0.10 (0.96 – 1.85)	NS	NS
Tb.Sp (μm)	690 ± 54 (3945 – 936)	662 ± 88 (338 – 1218)	601 ± 54 (410 – 936)	NS	NS
BS/BV (mm^{-1})	25.5 ± 1.8 (19.4 – 36.1)	22.9 ± 1.8 (12.8 – 30.0)	19.5 ± 1.6 (13.3 – 29.7)	NS	0.010
BS/TV (mm^{-1})	2.72 ± 0.22 (2.03 – 4.28)	2.96 ± 0.30 (1.54 – 4.51)	2.96 ± 0.21 (1.93 – 3.70)	NS	NS

[1] mean ± SEM (range)

[2] 6 months v baseline

[3] 12 months v baseline

NS: not significant

Figure 3.8. Trabecular histomorphology in iliac crest bone biopsies is altered by imatinib treatment. Iliac crest trephines were collected prior to the commencement of treatment and after 6 and 12 months of imatinib therapy. Trephines were embedded in methyl methacrylate and 5 μm toluidine blue-stained sections were histomorphometrically examined. BV/TV (**A**), Min.BV/TV (**B**), Tb.Th (**C**), Tb.N (**D**), Tb.Sp (**E**), BS/BV (**F**), BS/TV (**G**). Graphs depict mean ± SEM, expressed relative to baseline values (n = 9 – 11). * $p < 0.05$, relative to baseline (linear mixed effects model).

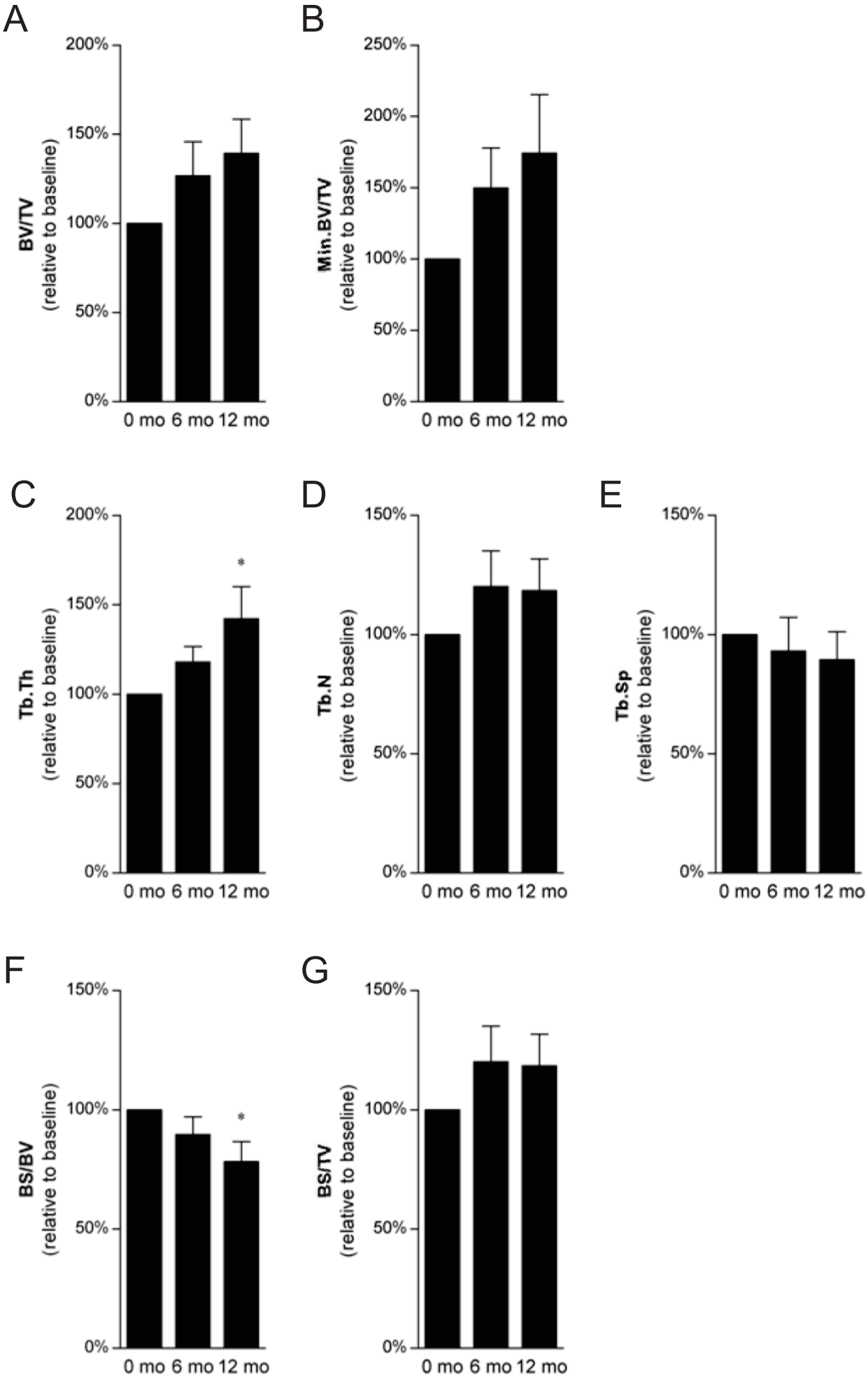
A
BV/TV
(relative to baseline)
200%
150%
100%
50%
0%
0 mo 6 mo 12 mo
B
Min.BV/TV
(relative to baseline)
250%
200%
150%
100%
50%
0%
0 mo 6 mo 12 mo
C
Tb.Th
(relative to baseline)
200%
150%
100%
50%
0%
*
0 mo 6 mo 12 mo
D
Tb.N
(relative to baseline)
150%
100%
50%
0%
0 mo 6 mo 12 mo
E
Tb.Sp
(relative to baseline)
150%
100%
50%
0%
0 mo 6 mo 12 mo
F
BS/BV
(relative to baseline)
150%
100%
50%
0%
*
0 mo 6 mo 12 mo
G
BS/TV
(relative to baseline)
150%
100%
50%
0%
0 mo 6 mo 12 mo

Figure 3.9. Imatinib treatment decreases osteoclast numbers in CML patients. Trephines were collected, embedded in methyl methacrylate and 5 μm sections were stained for TRAP and counterstained with methyl green. Images from 2 representative patients are shown (**A**). Scale bar: 100 μm. Arrows indicate osteoclasts. N.Oc/B.Pm (**B**), Oc.S/BS (**C**). Peripheral blood was collected after 0, 6 and 12 months of imatinib therapy and plasma levels of CTX-1 were analysed (**D**). Graphs depict mean ± SEM (n = 9 – 11). * $p < 0.05$, relative to baseline (linear mixed effects model).

A

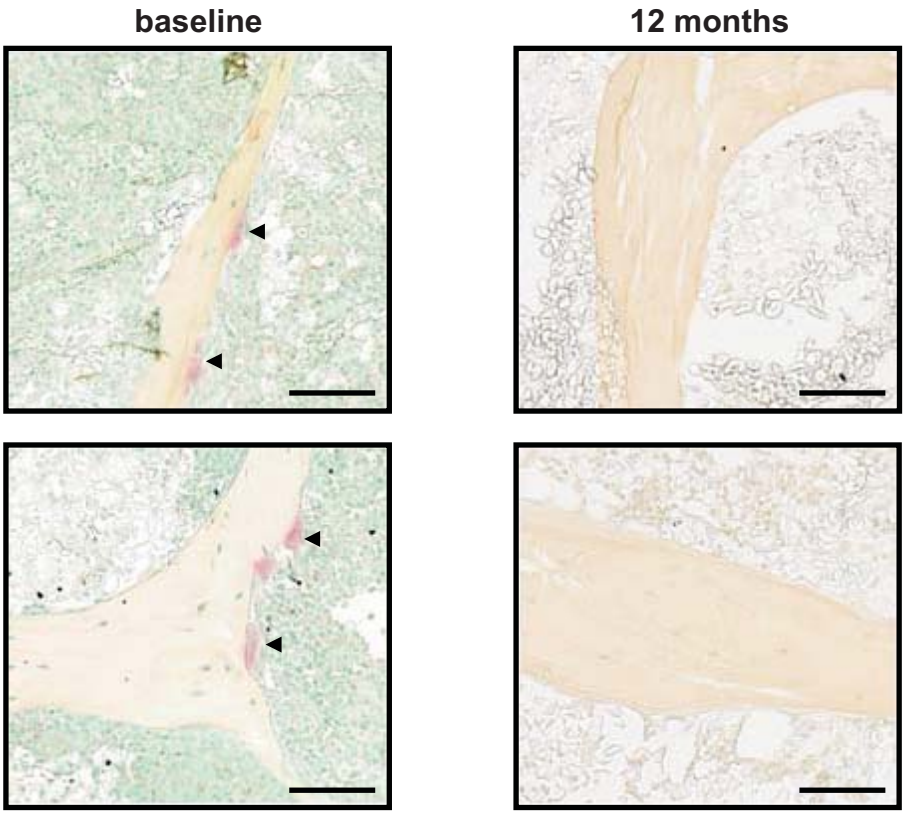
baseline
12 months

B

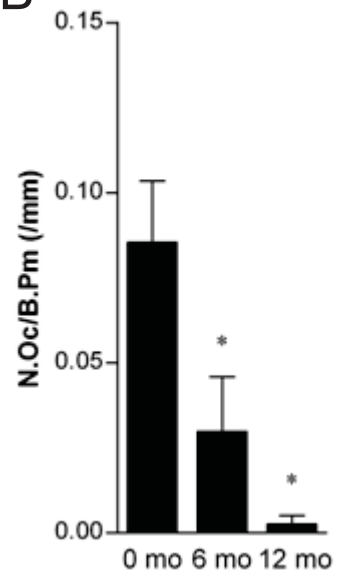
N.Oc/B.Pm (/mm)
0.15
0.10
0.05
0.00
*
*
0 mo 6 mo 12 mo

C

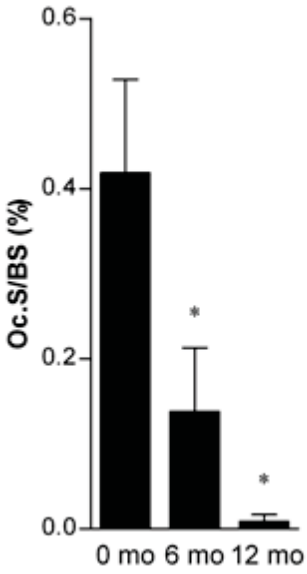
Oc.S/BS (%)
0.6
0.4
0.2
0.0
*
*
0 mo 6 mo 12 mo

D

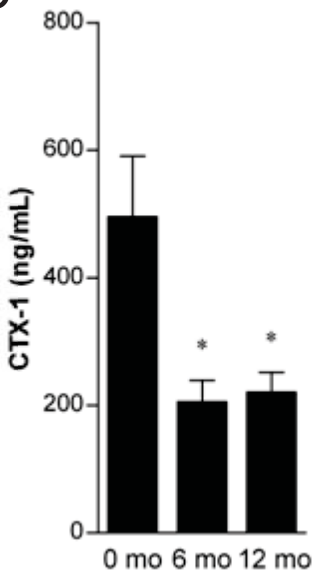
CTX-1 (ng/mL)
800
600
400
200
0
*
*
0 mo 6 mo 12 mo

3.2.7 Effects of imatinib on osteoblasts

3.2.7.1 Osteoblast numbers and osteoid

To determine whether imatinib therapy also affected osteoblast numbers and activity, osteoblast numbers (N.Ob/B.Pm) and osteoblast surface (Ob.S/BS) were quantitated (figure 3.10A). In contrast to the effects of imatinib on osteoclasts, treatment for up to 12 months had no statistically-significant effects on N.Ob/B.Pm ($p = 0.17$; figure 3.10B) or Ob.S/BS ($p = 0.060$; figure 3.10C).

Osteoid surface (OS/BS), osteoid volume (OV/BV) and osteoid thickness (O.Th) were quantitated on undecalcified, toluidine blue-stained sections, to assess the effects of imatinib treatment on bone synthesis (figure 3.11). While OS/BS was significantly increased following 12 months of imatinib treatment, relative to baseline levels ($p < 0.05$; figure 3.11A), OV/BV was not significantly altered by up to 12 months of imatinib therapy ($p = 0.16$; figure 3.11B). There was a trend towards an increase in osteoid thickness after 6 months of therapy ($p = 0.051$) which returned to baseline levels by 12 months (figure 3.11C).

3.2.7.2 Serum markers of osteoblast activity

Serum markers of osteoblast activity, osteocalcin and bALP, were next examined in imatinib-treated patients. Serum concentrations of bALP were not significantly altered by imatinib treatment for up to 12 months ($p = 0.17$; figure 3.10D).

Consistent with previous reports suggesting that osteocalcin levels are decreased in CML patients[19], serum osteocalcin levels were below the level of detection (< 2 μg/L) in the majority (7/11) of patients prior to imatinib therapy (2.62 ± 0.28 [mean ± SEM]). However, after 6 months of imatinib therapy, serum osteocalcin levels were detectable in 7/11 patients, suggesting an increase in serum osteocalcin levels (3.69 ± 0.49 [mean ± SEM]; $p < 0.05$). At 12 months, serum osteocalcin was detectable in only 2/11 patients (2.56 ± 0.34 [mean ± SEM]).

Figure 3.10. Imatinib in does not affect osteoblast numbers. At baseline and following 6 and 12 months of treatment with imatinib, trephines were collected, embedded in methyl methacrylate and 5 μm sections were stained with toluidine blue for histomorphometric measurements. Representative images from 2 patients are shown (**A**). Scale bar: 100 μm. Arrows indicate osteoblasts lining the osteoid surface. N.Ob/B.Pm (**B**), Ob.S/BS (**C**). Peripheral blood was collected after 0, 6 and 12 months of imatinib therapy and plasma levels of bALP (**D**) were analysed. Graphs depict mean ± SEM (n = 9 – 11).

A

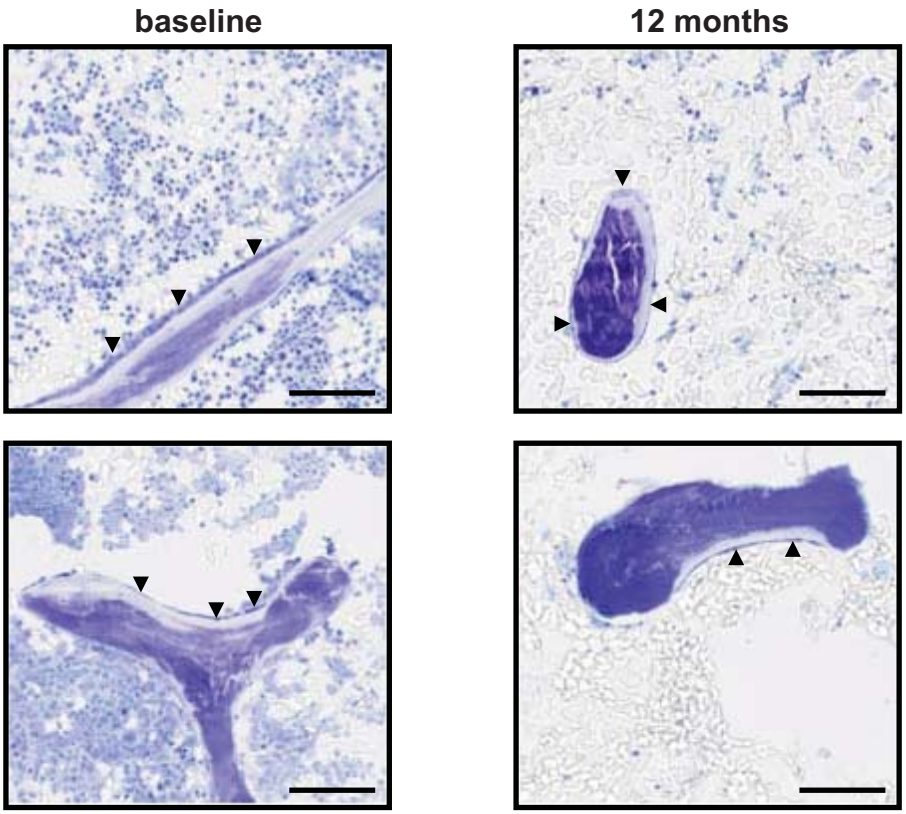
baseline
12 months

B

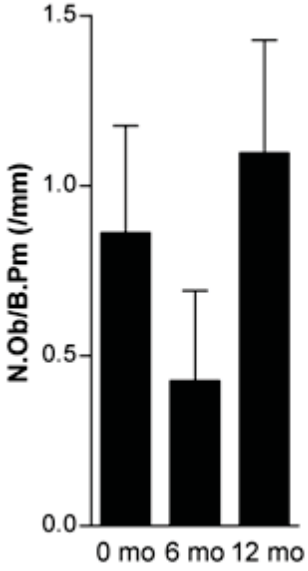
N.Ob/B.Pm (/mm)
1.5
1.0
0.5
0.0
0 mo 6 mo 12 mo

C

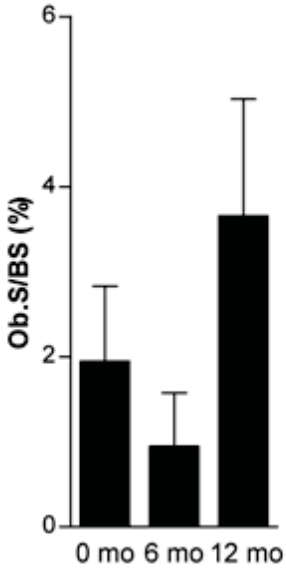
Ob.S/BS (%)
6
4
2
0
0 mo 6 mo 12 mo

D

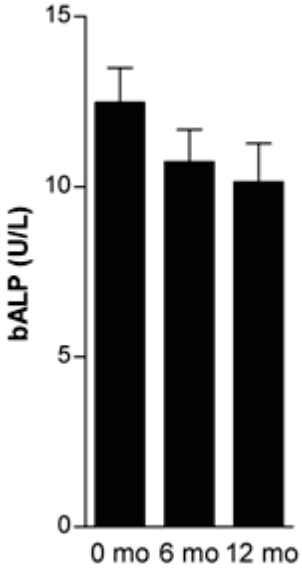
bALP (U/L)
15
10
5
0
0 mo 6 mo 12 mo

Figure 3.11. Osteoid surface is increased in imatinib-treated CML patients. After 0, 6 and 12 months of imatinib treatment, trephines were collected, embedded in methyl methacrylate and 5 μm sections were stained with toluidine blue for histomorphometric measurements of OS/BS (**A**), OV/BV (**B**) and O.Th (**C**). Graphs depict mean ± SEM (n = 9 – 11). * < 0.05, relative to baseline (linear mixed effects model).

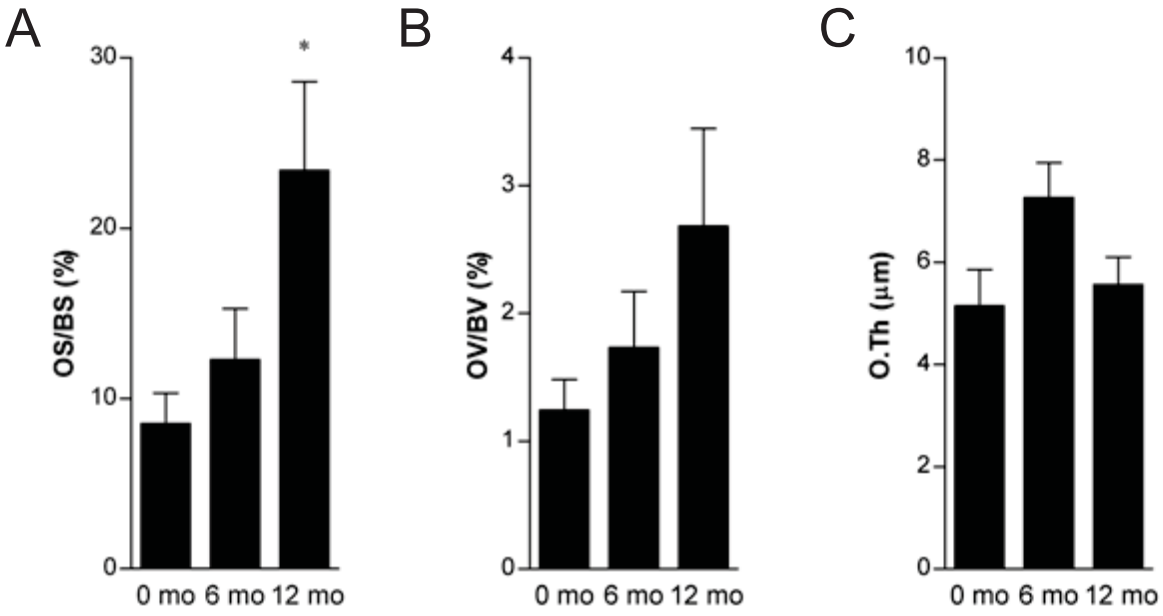
A
B
C
OS/BS (%)
OV/BV (%)
O.Th (μm)
*
0 mo 6 mo 12 mo
0 mo 6 mo 12 mo
0 mo 6 mo 12 mo

3.3 Discussion

Altered serum levels of bone remodelling markers have previously been associated with imatinib treatment for CML and GIST.[5,8,9,11,12] Consistent with these studies, the data presented here indicate that imatinib therapy is associated with a decrease in serum phosphate and total calcium and an increase in PTH and 1,25-dihydroxyvitamin D_3. We investigated if these serum changes were in response to alterations in osteoclast and osteoblast numbers in bone biopsies collected prior to and up to 12 months after the commencement of imatinib therapy. In addition, trabecular bone morphometry was assessed by μ-CT and histomorphometry. Supporting previous reports[10], these studies showed that imatinib treatment resulted in an increase in trabecular thickness in iliac crest biopsies. This was associated with an increase in BS/BV and trabecular connectivity. Increased cancellous bone strength is strongly associated with increased bone volume and trabecular thickness and with decreased Tb.Pf.[323-325] Our results suggest that imatinib induces changes to the trabecular architecture that may convey an increase in bone strength, at least at some skeletal sites.

While the mechanism(s) remain to be elucidated, the decrease in osteoclast activity, as evidenced by a decrease in osteoclast numbers (N.Oc/B.Pm) and serum CTX-1 levels, in imatinib-treated patients suggests inhibition of osteoclasts as a likely mechanism for the observed changes in trabecular bone morphology. These results are consistent with previous studies which have demonstrated that serum CTX-1 levels are decreased in imatinib-treated CML and GIST patients, relative to pre-treatment levels[8,12] or to healthy controls[5]. Additionally, previous reports suggest that osteoclast numbers are decreased in normal mice treated with imatinib[13,253,254], suggesting that imatinib-induced decreases in osteoclast numbers also can occur in a CML-free setting.

In contrast to the observed anti-osteoclastogenic activity of imatinib, we observed no significant changes in osteoblast numbers, osteoblast-occupied bone surface or serum levels of the osteoblast marker bALP following imatinib treatment. These results contrast with *in vitro* studies which show that imatinib inhibits mesenchymal cell proliferation while increasing mineralised matrix deposition.[10,16-19] However, the lack of statistically significant differences in osteoblast indices in this study may be attributable to a lack of sufficient statistical power rather than a lack of biological response. The small number of patients used in this study, and the relatively large intra-individual variation in histomorphometric assessment of osteoblast parameters[326-328], may confound detection of small variations in osteoblast numbers. Additionally, potential imatinib-induced changes in

osteoblast numbers may not occur during the 12 month time-frame of this study. Previous longitudinal studies have reported significant increases in the osteoblast markers osteocalcin and bALP after 3 months of treatment that were no longer detectable after 6 or 18 months of treatment.[8,12] Furthermore, long-term (≥ 24 months) imatinib treatment has previously been reported to increase serum osteocalcin levels, relative to imatinib-naïve CML controls[19], and to decrease bALP levels, relative to aged-matched normal controls[20]. As such, it is conceivable that effects of imatinib on osteoblasts were not detected due to the time-frame of this study. However, despite the lack of detectable change in osteoblast numbers during the course of the experiment, the increase in osteoid surface detected after 12 months of imatinib therapy may be suggestive of an increase in osteoblast activity. In normal healthy individuals, the activity of bone resorptive osteoclasts is closely coupled to bone formation by osteoblasts, with any decrease in osteoclast activity being corrected by a concomitant decrease in osteoblast activity. In this study, imatinib treatment for 6 or 12 months strongly inhibited osteoclast activity in CML patients without having a compensatory inhibitory effect on osteoblasts, suggesting that imatinib may have an uncoupling effect on bone turnover. Further investigation is required to definitively determine the contribution of osteoblasts to the anabolic effects of imatinib treatment.

Increased osteoid volume/thickness can result from either rapid bone formation or disturbed mineralisation and is symptomatic of a number of skeletal diseases. Severe decreases in serum phosphate, for example resulting from inadequate gastrointestinal absorption or decreased renal resorption, can result in accumulation of osteoid (osteomalacia) due to a lack of phosphate availability for bone mineralisation[329] (reviewed in [330]). In addition, hyperparathyroidism can cause an increase in trabecular osteoid, resulting from increased osteoblast numbers secondary to increased osteoclast activity.[331-333] However, in this study, imatinib treatment was associated with a decrease in osteoclast numbers and no change in osteoblast numbers, which persisted despite the secondary hyperparathyroidism. Thus, the increase in bone turnover induced by PTH may be blocked by the anti-osteoclastogenic effects of imatinib, at least in the ilium. The relatively small increase in osteoid surface and osteoid thickness suggest that increased bone synthesis, rather than defective mineralisation, is the cause of the osteoid accumulation. However, measurement of dynamic bone formation rates in future studies would be required to definitively differentiate osteomalacia from increased bone formation.

It has been suggested that decreased gastrointestinal or renal resorption of calcium and phosphate could promote the alterations in serum biochemistry observed following

imatinib therapy. While these factors may contribute, our results support the hypothesis that changes in skeletal metabolism are largely driven by imatinib-mediated inhibition of osteoclasts. In this model, inhibition of osteoclast numbers and activity results in decreased dissolution of calcium and phosphate from the bone, leading to decreased serum calcium and phosphate. Decreased ionised calcium stimulates PTH secretion, which increases renal resorption of calcium and stimulates 1,25-dihydroxyvitamin D_3 synthesis. In addition, PTH decreases renal phosphate resorption, resulting in phosphaturia, thereby compounding the decrease in serum phosphate. 1,25-dihydroxyvitamin D_3 stimulates the intestinal and renal absorption of calcium and phosphate, which, in concert with the effects of PTH, results in a correction of serum ionised calcium levels. In support of this theoretical model, treatment with the osteoclast inhibitory drugs bisphosphonates causes similar changes in serum biochemistry to those observed following imatinib treatment. Hypophosphataemia is a commonly-reported side-effect of bisphosphonate treatment (reviewed in [250,252]). In addition, there is evidence to suggest that most patients treated with bisphosphonates, such as intravenous zoledronic acid, exhibit hypocalcaemia, although in most cases this is reversed by secondary hyperparathyroidism[251] (reviewed in [250]). This is consistent with published findings suggesting that although the majority of imatinib-treated patients exhibit elevated serum PTH, only some patients experience hypocalcaemia.[5,8-10,12]

Previously published results have indicated that long-term (≥ 24 months) imatinib treatment is associated with significant increases in radial cortical BMD and lumbar spine BMD, relative to age and sex-matched healthy controls.[20] O'Sullivan *et al*. demonstrated that lumbar spine BMD was significantly increased in a group of 9 patients following 12 and 24 months of imatinib treatment, relative to baseline, while no statistically significant changes in total femur or total body BMD were observed over the 24 months of treatment.[12] Similarly, DXA analysis in this present study showed that BMD and BMC were increased at the radius and the tibia and fibula following imatinib therapy, while there was no significant change in lumbar vertebrae or total body BMD or BMC. In contrast, femoral neck BMD and BMC was lower in patients following imatinib treatment, compared with baseline measurements. This observation is potentially a cause for concern, as BMD strongly correlates with mechanical strength in cortically-rich bone and this indice is a primary determinant of risk of fracture (reviewed in [334]). However, our evidence suggests that imatinib does not cause generalised bone loss, as decreased BMD or BMC was not observed in any site other than the femur.

The mechanism involved in the site-specific loss of bone at the proximal femur observed in this present study is unclear. However, differences in osteoclast activity at different sites, prior to imatinib therapy, may play a role. There are large variations in the amount of mechanical strain, and therefore the rate of remodelling, occurring in different skeletal sites[335,336] (reviewed in [337]). The femoral neck is a highly loaded site which is subjected to repetitive cyclical mechanical strain, and thus has a high remodelling rate, relative to non-loaded site such as the radius. Iliac crest osteoclast quantitation and serum CTX-1 levels suggest that imatinib treatment does not completely ablate osteoclasts during the first 12 months of treatment. Therefore, there may be sufficient residual osteoclastic activity in highly metabolically-active skeletal sites to be sensitive to the pro-osteoclastogenic effects of PTH. Sustained elevations in PTH are associated with increased osteoclast activity, resulting in cortical bone loss and decreased BMD[192-194,338,339] (reviewed in [330,340]). Thus, increased PTH in imatinib-treated patients may result in local cortical bone loss and decreased BMD at high-turnover sites. The long-term consequences of this bone loss remain to be determined. However, Jönsson *et al*. found that imatinib treatment for ≥ 24 months significantly increased hip BMD, suggesting that the loss of bone mass at the proximal femur may reverse over time.[20]

CML is associated with myeloid hyperplasia which results in hypercellularity in the marrow space. Despite these increases in marrow cellularity, skeletal metabolism in CML patients is generally normal[341,342] although lytic lesions are observed in rare cases[343-345] and are usually associated with acute blastic transformation[344,346]. While CML is not generally associated with a skeletal phenotype, the possibility that the return to normal marrow cellularity or hypocellularity following imatinib therapy may indirectly affect bone metabolism should be addressed. As ethical considerations prevented this study from being placebo-controlled, it cannot be concluded whether the observed effects of imatinib on the skeleton were due to disease remission or were due to direct actions of imatinib on osteoclasts and osteoblasts. However, previous data from CML patients treated with interferon-α suggest that dysregulated bone remodelling is not a general consequence of disease remission. Analysis of a cohort of patients responding to interferon-α therapy revealed that decreased marrow cellularity was not associated with any change in iliac crest trabecular bone volume.[10] Additionally, interferon-α therapy was not associated with decreased serum phosphate or calcium levels.[10] Furthermore, comparison of our data with previous findings in GIST patients suggests that dysregulated bone remodelling is consistently seen in imatinib-treated patients, regardless of whether there is marrow tumour

involvement. A study of 16 GIST patients and 8 CML patients undergoing imatinib therapy found that imatinib-treated patients had increased serum levels of the osteoclast marker NTX and increased PTH, relative to normal controls, regardless of the underlying disease.[5] Therefore, although it cannot be definitively determined whether the changes in bone morphometry observed in this present study are due to direct effects of imatinib, it is unlikely that it is secondary to disease remission.

In summary, these data suggest that imatinib therapy dysregulates bone remodelling, causing a general decrease in osteoclast activity which is not counteracted by a concomitant decrease in osteoblast activity. This osteoclast inhibition results in increased trabecular thickness and, in at least some patients, increased bone volume in iliac crest biopsies. Decreased osteoclast activity and increased bone volume were observed in 2 patients who exhibited osteoporosis prior to treatment, suggesting that imatinib may be affective as an anti-osteolytic agent in conditions involving pathological bone loss. However, the significant decrease in femoral neck BMD observed after 6 months of treatment is a cause for concern and long-term investigations are required to determine the mechanisms underlying the site-specific differences in the skeletal effects of imatinib.

Chapter 4

The effects of tyrosine kinase inhibition on bone remodelling *in vivo*

4.1 Introduction

While there is substantial evidence to suggest that imatinib can affect osteoclast and osteoblast activity[5,7,8,10], the potential that second generation tyrosine kinase inhibitors, such as dasatinib, could also affect bone remodelling in CML patients has not been explored. Dasatinib is clinically active against CML in patients who are resistant to imatinib[235,238] due to its enhanced affinity for the CML oncoprotein Bcr-Abl and its insensitivity to mutations in the Bcr-Abl kinase domain[347]. In addition to inhibiting the imatinib targets Abl (IC_{50} = 0.8 nM)[236], Kit (IC_{50} = 5 nM)[348], PDGFRα (IC_{50} = 63 nM)[222] and PDGFRβ (IC_{50} = 28 nM)[348], dasatinib also inhibits Flt3 (IC_{50} = 100 nM)[237], the Tec family members Btk (IC_{50} = 1.1 nM)[349] and Bmx (IC_{50} = 10 nM)[237], the Src family kinase members Src (IC_{50} = 0.5 nM)[348], Lck (IC_{50} = 0.4 nM)[348], Fyn (IC_{50} = 0.2 nM)[349], Blk (IC_{50} = 8 nM)[222], Lyn (IC_{50} = 8.5 nM)[350], Fgr (IC_{50} = 10 nM)[237] and Yes (IC_{50} = 0.5 nM)[348] and the Eph receptor family members EphB1, EphB2 and EphB4 (IC_{50} = 10 nM)[237].

Furthermore, in cultures of M-CSF-dependent Ba/F3 cells which ectopically express human Fms, treatment with dasatinib decreased cell numbers indicating that dasatinib may inhibit Fms.[237] M-CSF activation of Fms is essential for the survival and activity of osteoclast-lineage cells.[109-111,255-257] M-CSF- or Fms-deficient mice and rats have severe osteopetrosis and an absence of tooth eruption due to a profound decrease in osteoclast numbers.[111,265,351,352] Thus dasatinib, like imatinib, could potentially inhibit osteoclastogenesis through inhibition of Fms.

Dasatinib may have further anti-osteoclastogenic effects through the inhibition of Src. Src is a cytoplasmic tyrosine kinase that is essential for normal osteoclast activity due to its role in pathways regulating vesicle transport, adhesion, migration and resistance to apoptosis.[292-296] *Src*$^{-/-}$ mice display increased bone mineral density, which is attributable to defective osteoclast activity rather than a reduction in osteoclast number.[292,296,353,354] This is thought to be primarily due to defective osteoclast actin ring and sealing zone formation following inhibition of signalling via integrins including $\alpha_v\beta_3$.[292-296] At least some of these effects are due to the role of Src as an adapter molecule, as introduction of a kinase-inactive mutant, K295M, which has an ATP-binding domain mutation, partially reverses *Src*$^{-/-}$-induced osteopetrosis; however, Src kinase activity is required to completely reverse the skeletal abnormalities in these mice.[355] Inhibition of Src activity with the pyrrolopyrimidine derivatives CGP77675, CGP76030 and AP23451 reverses IL-1β-, retinoic acid- and PTH-induced hypercalcaemia in murine models, and inhibits bone loss

in ovariecomised rodents, suggesting that inhibition of Src kinase activity may serve as a potential treatment for pathological bone remodelling.[356-358]

In addition to its anti-osteoclastogenic activity, dasatinib, like imatinib, may affect osteoblast activity through inhibition of PDGFR. PDGF is a potent mitogen for osteoblast precursors which also inhibits osteoblast differentiation *in vitro*.[280,289-291] Studies from our laboratory[10] and those of others[16-19], have shown that imatinib activates osteoblast activity, while inhibiting cell proliferation, at least in part through the inhibition of PDGFR. In cultures of human and murine stromal cells and cell lines, treatment with therapeutically-achievable concentrations of imatinib significantly increased mineral deposition[10,17,19] and decreased cell proliferation[10,16-18]. These results suggest that tyrosine kinase inhibitors could inhibit osteoblasts proliferation and activate their differentiation *in vitro*. However, it remains to be seen whether dasatinib has any effects on osteoblast activity.

As dasatinib is a potent inhibitor of tyrosine kinases that are essential for normal bone metabolism, this study investigated the effects of dasatinib on bone remodelling in normal mature Sprague-Dawley rats *in vivo*.

4.2 Results

4.2.1 Imatinib and dasatinib treatment has no effect on body mass in normal rats *in vivo*

To determine the effects of tyrosine kinase inhibition on mature, non-remodelling bone, 9-month-old female Sprague-Dawley rats were treated with imatinib (100 mg/kg), dasatinib (5 mg/kg) or vehicle (10% DMSO/90% PEG 300) by daily oral gavage for up to 12 weeks. Four additional animals received zoledronic acid (100 μg/kg/6 weeks) sub-cutaneously as a positive control for inhibition of osteoclasts.

Treatment with imatinib, dasatinib or zoledronic acid had no effect on total body mass. There were no significant changes in body mass in any treatment group during the 12 weeks of treatment (vehicle, $p = 0.99$; imatinib, $p = 1.00$; dasatinib, $p = 1.00$; zoledronic acid, $p = 1.00$; repeated measures ANOVA with Dunnett's post-test; figure 4.1A). In addition, there were no significant differences in body mass between the treatment groups at any time-point (week 0, $p = 0.13$; week 2, $p = 0.15$; week 4, $p = 0.084$; week 6, $p = 0.48$; week 8, $p = 0.31$; week 10, $p = 0.34$; week 12, $p = 0.48$; one-way ANOVA with Dunnett's post-test; figure 4.1A).

Four animals per group were monitored throughout the experiment for whole body tissue composition by DXA. Using this approach, whole body mass did not change significantly in animals treated with vehicle ($p = 0.12$, repeated measures ANOVA with Dunnett's post-test), imatinib ($p = 0.88$), dasatinib ($p = 0.39$), or zoledronic acid ($p = 0.97$) over the 12 weeks of treatment (figure 4.1B). Similarly, there were no statistically significant changes in lean tissue mass or adipose tissue mass in imatinib-, dasatinib-, zoledronic acid- or vehicle-treated animals at any time-point (data not shown).

4.2.2 The effects of imatinib and dasatinib on the skeleton in normal rats *in vivo*

4.2.2.1 Imatinib and dasatinib have no effect on whole body BMD

Whole body BMD, as determined by DXA, was not altered by treatment with imatinib or dasatinib, relative to controls (figure 4.2). When compared with the vehicle-treated group, there were no significant increases in BMD in the imatinib-, dasatinib- or zoledronic acid-treated groups at any time-point (week 2, $p = 0.62$; week 4, $p = 0.36$; week 6, $p = 0.20$; week 9, $p = 0.39$; week 12, $p = 0.65$; one-way ANOVA with Dunnett's post-test; figure 4.2).

Figure 4.1. Imatinib and dasatinib treatment has no effect on body mass *in vivo*. Nine-month-old Sprague-Dawley rats were treated with imatinib (100 mg/kg), dasatinib (5 mg/kg) or vehicle (10% DMSO/90% PEG 300, v/v) by daily gavage or zoledronic acid (100 μg/kg/6 weeks) by subcutaneous injection. All animals were weighed at the indicated time-points (**A**). Total body mass was monitored in 4 animals per group by DXA at the indicated time-points (**B**). Graphs depict mean ± SEM.

A

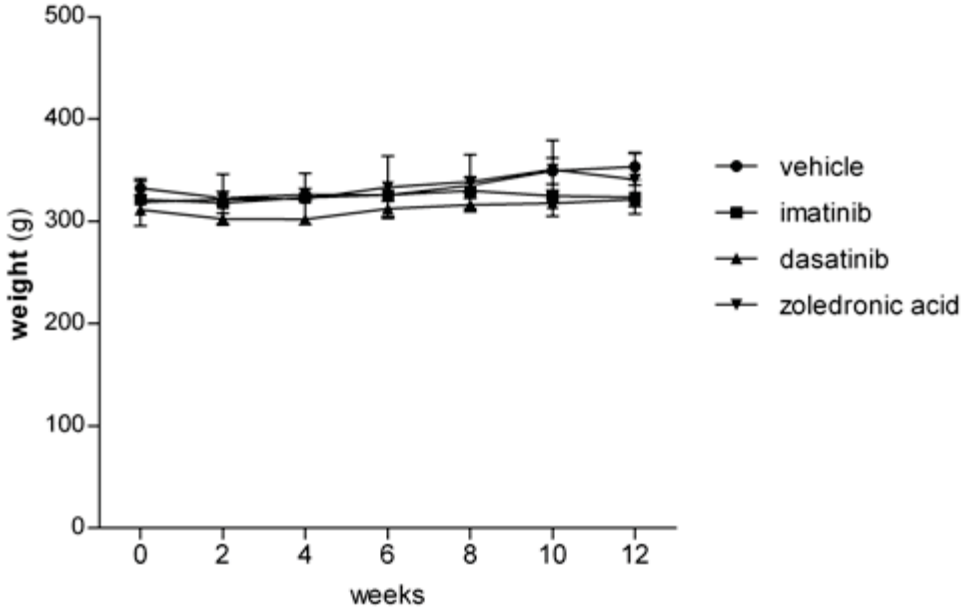
500
400
300
200
100
0
weight (g)
0
2
4
6
8
10
12
weeks
vehicle
imatinib
dasatinib
zoledronic acid

B

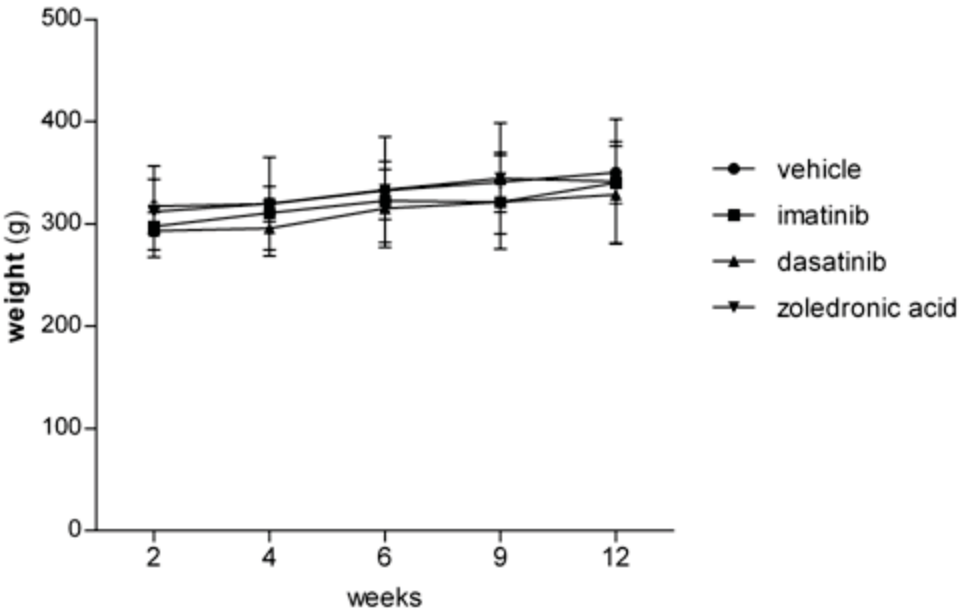
500
400
300
200
100
0
weight (g)
2
4
6
9
12
weeks
vehicle
imatinib
dasatinib
zoledronic acid

Figure 4.2. Imatinib and dasatinib treatment does not result in changes in whole body BMD in normal mature rats. Nine-month-old female Sprague Dawley rats were treated for 12 weeks with imatinib (100 mg/kg/day), dasatinib (5 mg/kg/day), vehicle (10% DMSO/90% PEG 300) or with zoledronic acid (100 μg/kg/6 weeks). Whole body BMD was monitored by DXA at the indicated time-points (n = 4/group). Graph depicts mean ± SEM.

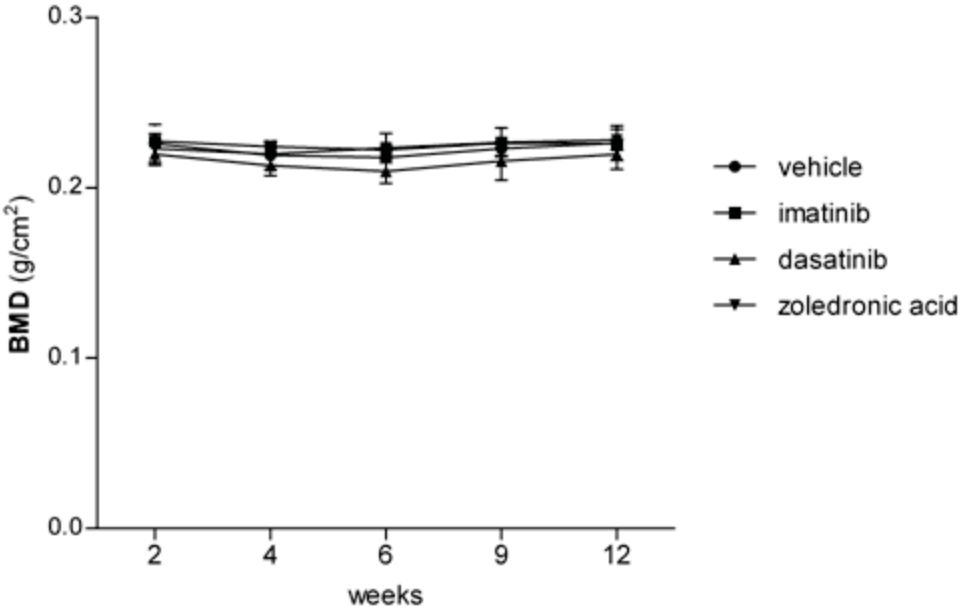
0.3
0.2
0.1
0.0
BMD (g/cm²)
2
4
6
9
12
weeks
vehicle
imatinib
dasatinib
zoledronic acid

4.2.2.2 Dasatinib, but not imatinib, increases trabecular bone volume in vivo

To ensure that the baseline trabecular bone volume was similar in all animals irrespective of the treatment group to which they were assigned, μ-CT analysis was conducted at day 0. No significant differences in trabecular bone parameters were observed at baseline in the dasatinib, imatinib or zoledronic acid groups, relative to the control group (BV/TV, $p = 0.76$; Tb.N, $p = 0.73$; Tb.Th, $p = 0.79$; SMI, $p = 0.64$; Tb.Pf, $p = 0.38$; one-way ANOVA with Dunnett's post-test; figure 4.3).

The effect of imatinib and dasatinib treatment on trabecular bone morphometry was assessed histologically and by μ-CT analysis. As shown in the representative images in figure 4.4 and 4.5, while imatinib had no effect on trabecular bone morphology, 12 weeks of treatment with dasatinib and zoledronic acid resulted in an increase in trabecular bone. Quantitation of trabecular bone morphology by μ-CT revealed that imatinib treatment for up to 12 weeks had no significant effect on trabecular BV/TV, relative to vehicle controls. In contrast, dasatinib treatment increased BV/TV 62% after 12 weeks of treatment, relative to vehicle controls ($p < 0.05$; figure 4.6A). After 12 weeks, dasatinib induced a similar increase in BV/TV as that induced by zoledronic acid (figure 4.6A). There was a trend towards an increase in trabecular BMD (Tb.BMD) in dasatinib- and zoledronic acid-treated animals by 12 weeks of treatment which did not reach statistical significance (figure 4.6B). No change in Tb.BMD was detected in imatinib-treated animals at 4, 8 or 12 weeks (figure 4.6B). Histomorphometric analysis of trabecular architecture revealed similar dasatinib-induced increases in BV/TV as those detected by μ-CT (data not shown).

Quantitative μ-CT analysis revealed that imatinib, dasatinib and zoledronic acid treatment had no significant effect on Tb.N at 4, 8 or 12 weeks of treatment ($p = 0.092$, 0.12 and 0.16, respectively; figure 4.6C). In the vehicle-treated group, there was a significant decrease in Tb.Th after 12 weeks of treatment, relative to the 4 and 8 week cohorts, suggesting a loss of bone with aging[359] ($p < 0.05$; figure 4.6D). In contrast, in the dasatinib- and zoledronic acid-treated animals, there were no significant decreases in Tb.Th over time (figure 4.6D). However, there were no statistically significant differences in Tb.Th in imatinib, dasatinib and zoledronic acid groups when compared with the vehicle group at any time-point (figure 4.6D).

SMI was significantly decreased in the dasatinib-treated animals at 8 and 12 weeks, relative to vehicle-treated controls, indicating a shift to a more plate-like trabecular architecture ($p < 0.05$, figure 4.6E). Similarly, Tb.Pf was significantly decreased by 12 weeks of dasatinib treatment, relative to the control group, indicating an increase in

Figure 4.3. Trabecular morphology at the proximal tibia is similar in all treatment groups at baseline. Prior to the commencement of treatment, animals were anaesthetised and a 4.351 mm long region of trabecular bone, 2.351 mm distal to the growth plate, was analysed by μ-CT. BV/TV (**A**), Tb.N (**B**), Tb.Th (**C**), SMI (**D**), Tb.Pf (**E**). Graphs depict mean ± SEM (vehicle, n = 17; imatinib, n = 12; dasatinib, n = 13; zoledronic acid, n = 2).

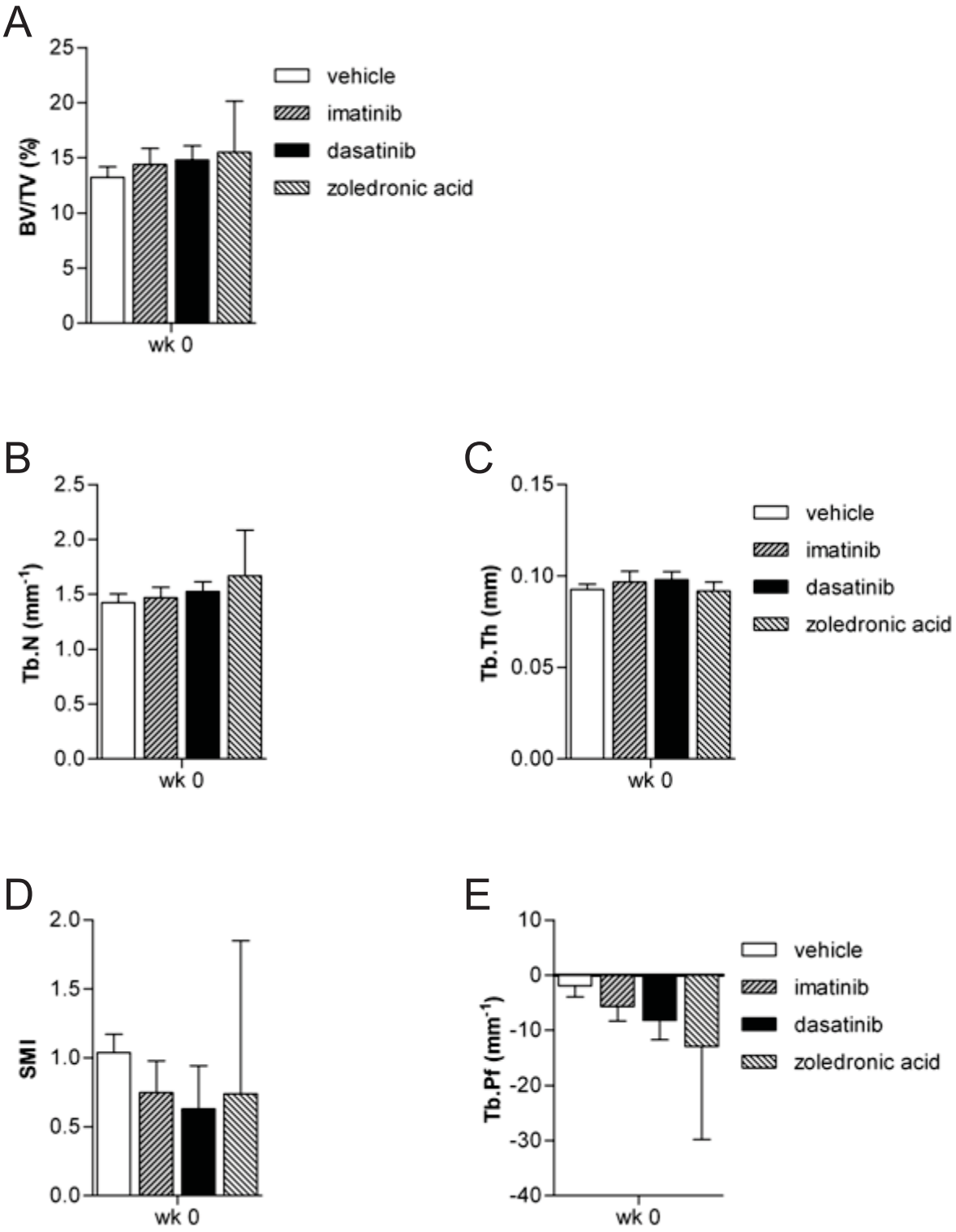
A
BV/TV (%)
25
20
15
10
5
0
wk 0
vehicle
imatinib
dasatinib
zoledronic acid
B
Tb.N (mm-1)
2.5
2.0
1.5
1.0
0.5
0.0
wk 0
C
Tb.Th (mm)
0.15
0.10
0.05
0.00
wk 0
vehicle
imatinib
dasatinib
zoledronic acid
D
SMI
2.0
1.5
1.0
0.5
0.0
wk 0
E
Tb.Pf (mm-1)
10
0
-10
-20
-30
-40
wk 0
vehicle
imatinib
dasatinib
zoledronic acid

Figure 4.4. Histological examination of trabecular bone in normal rats treated with tyrosine kinase inhibitors. Following 12 weeks of treatment with imatinib, dasatinib, vehicle or zoledronic acid, tibiae were collected, embedded in methyl methacrylate and 5 µm sections were stained with von Kossa silver stain then counterstained with haematoxylin and eosin (**A**) or toluidine blue (**B**). Scale bar: 1 mm.

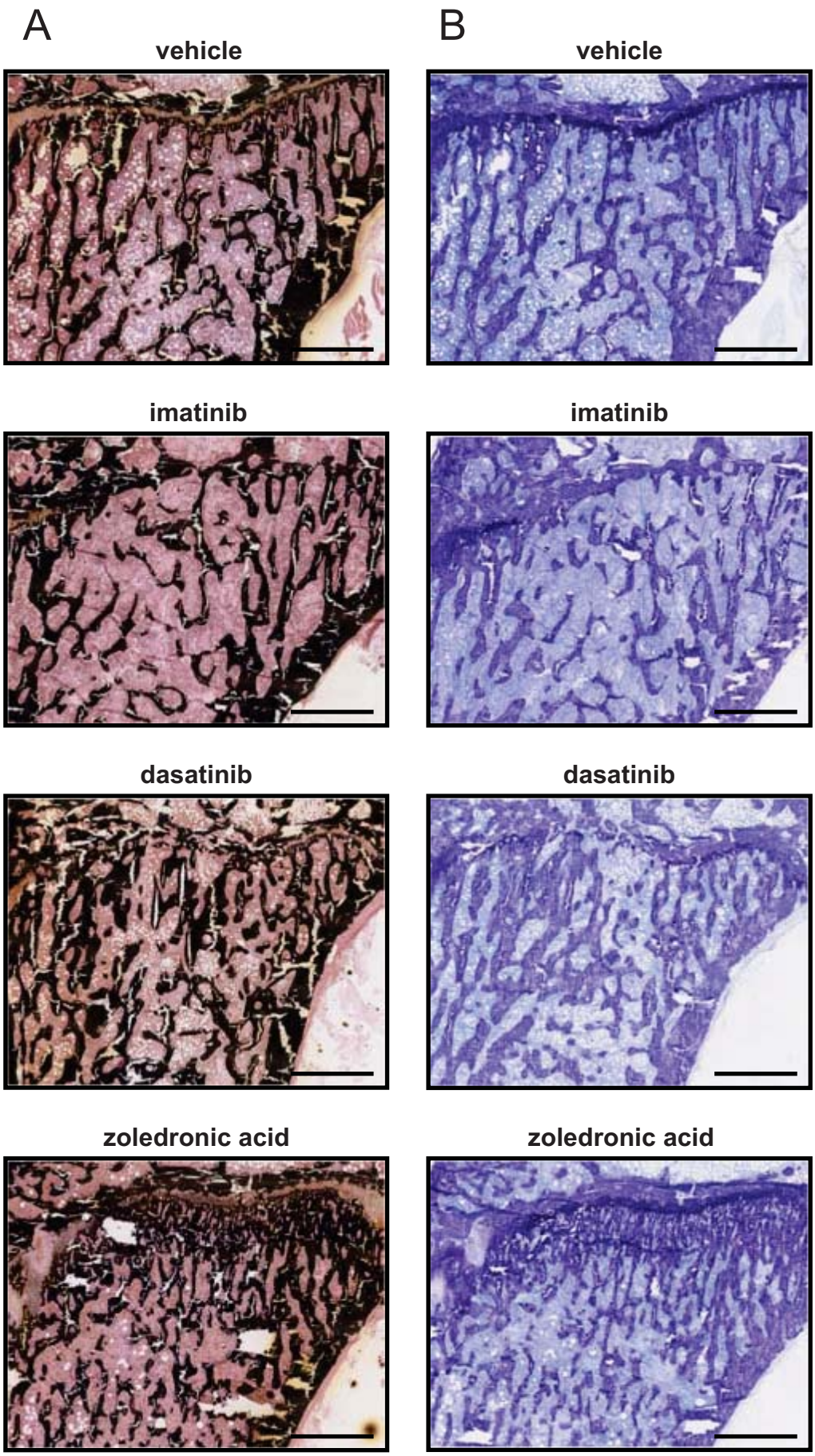
A
B
vehicle
vehicle
imatinib
imatinib
dasatinib
dasatinib
zoledronic acid
zoledronic acid

Figure 4.5. Trabecular bone volume is increased in dasatinib-treated animals. After 12 weeks of treatment, tibiae from imatinib-, dasatinib-, vehicle- or zoledronic acid-treated animals were collected for μ-CT analysis of a 4.351 mm long region of trabecular bone 2.351 mm distal to the growth plate. Cross-sectional 3-dimensional images of representative tibiae from animals treated for 12 weeks are shown.

vehicle

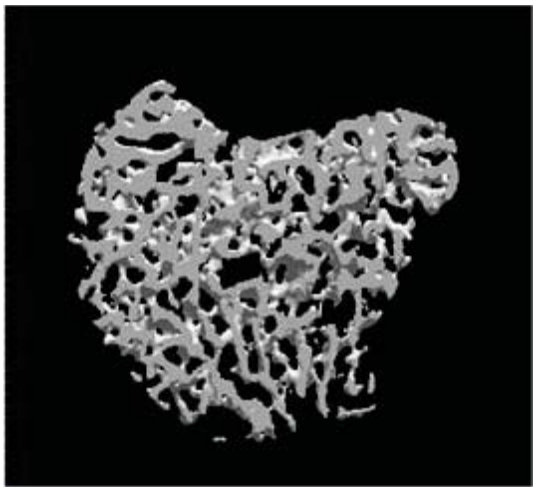

imatinib

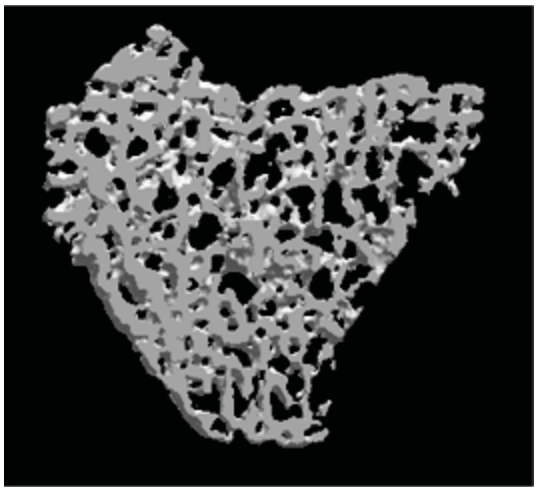

dasatinib

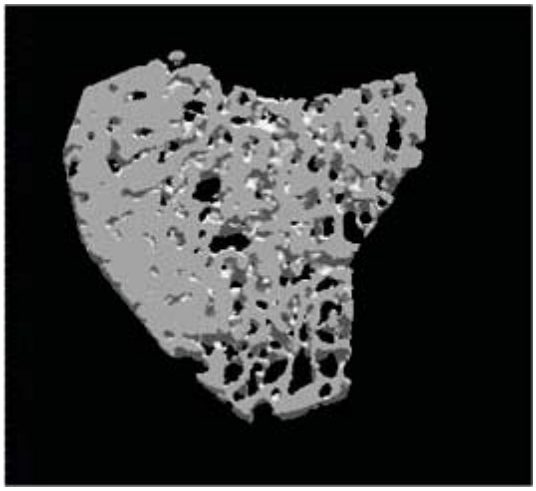

zoledronic acid

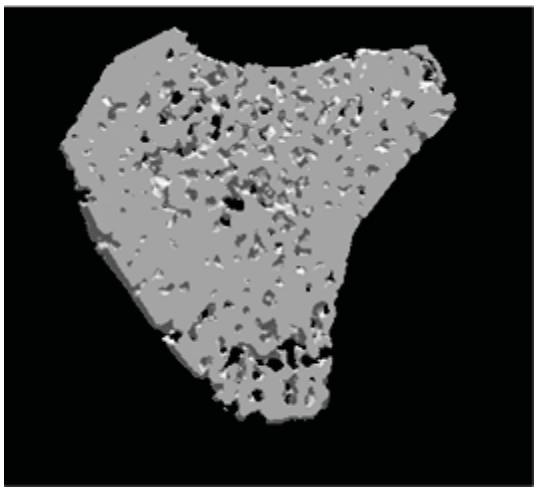

Figure 4.6. Trabecular morphology at the proximal tibia is altered in dasatinib-treated animals. Tibiae from imatinib-, dasatinib- and vehicle-treated animals (4, 8 and 12 weeks) or zoledronic acid-treated animals (12 weeks) were collected for μ-CT analysis of a 4.351 mm long region of trabecular bone 2.351 mm distal to the growth plate. BV/TV (**A**), Tb.BMD (**B**), Tb.N (**C**), Tb.Th (**D**), SMI (**E**), Tb.Pf (**F**). Graphs depict mean ± SEM (n = 4 – 6). * $p < 0.05$, relative to vehicle control at each time-point; ** $p < 0.05$, relative to 4 and 8 week time-points (one-way ANOVA with Dunnett's post-test).

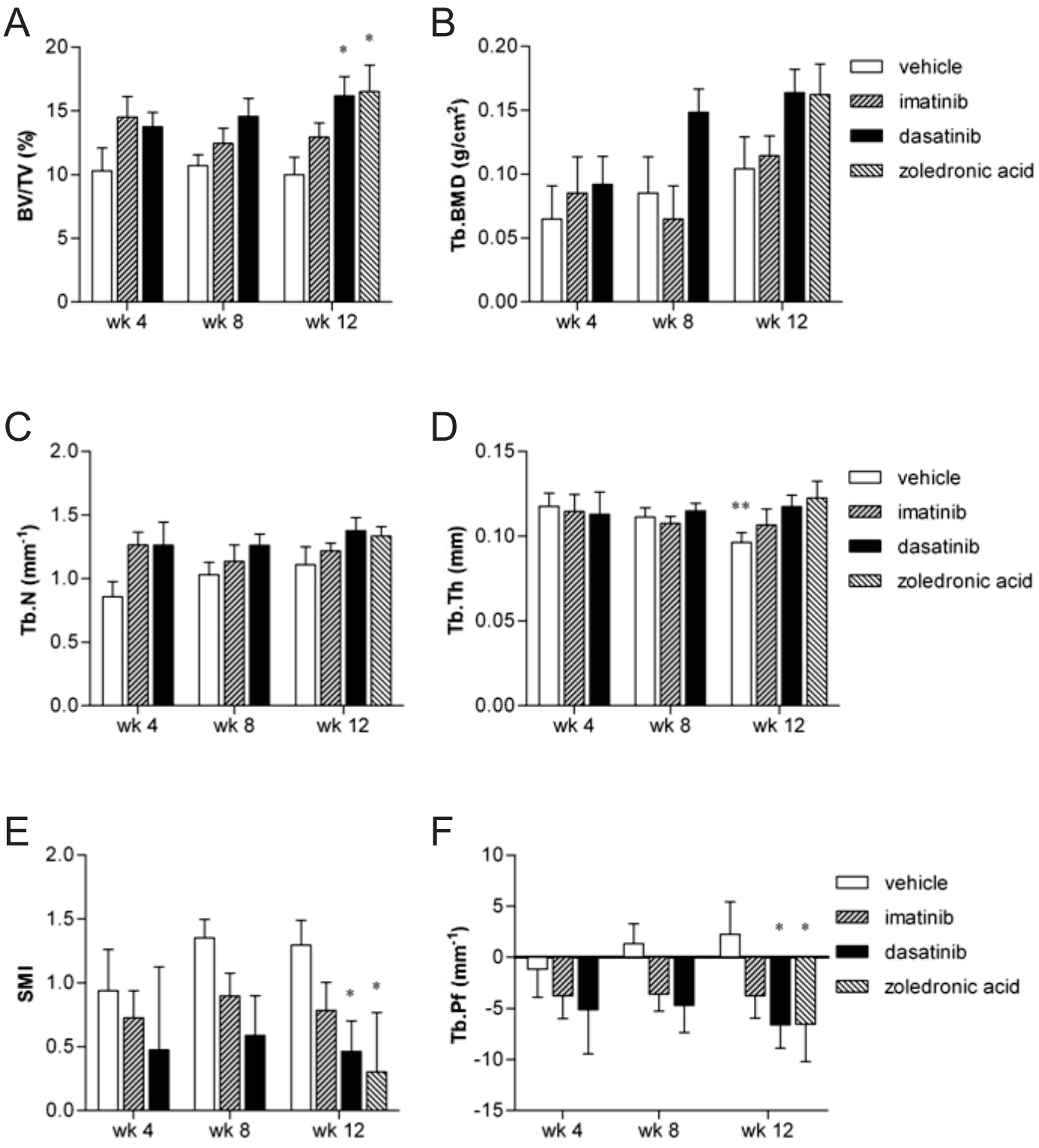
A
BV/TV (%)
20
15
10
5
0
wk 4
wk 8
wk 12
B
Tb.BMD (g/cm²)
0.20
0.15
0.10
0.05
0.00
vehicle
imatinib
dasatinib
zoledronic acid
C
Tb.N (mm⁻¹)
2.0
1.5
1.0
0.5
0.0
D
Tb.Th (mm)
0.15
0.10
0.05
0.00
**
E
SMI
2.0
1.5
1.0
0.5
0.0
F
Tb.Pf (mm⁻¹)
10
5
0
-5
-10
-15

trabecular connectivity ($p < 0.05$, figure 4.6F). Comparable decreases in SMI and Tb.Pf were observed in the zoledronic acid treatment group as were seen in the dasatinib-treated animals ($p < 0.05$), while treatment with imatinib had no effect on these indices (figure 4.6E,F).

4.2.2.3 Dasatinib and imatinib have no effect on cortical bone volume in vivo

To determine the effects of tyrosine kinase inhibition on cortical bone, the tibial diaphyses were analysed by μ-CT. Ct.BV/TV was not altered in the imatinib-, dasatinib- or zoledronic acid-treated animals, relative to vehicle controls, at any of the time-points examined (week 4, $p = 0.70$; week 8, $p = 0.92$; week 12, $p = 0.70$; one-way ANOVA with Dunnett's post-tests; figure 4.7B). Similarly, imatinib-, dasatinib- and zoledronic acid treatment had no significant effect on Ct.Th, relative to vehicle controls (week 4, $p = 0.83$; week 8, $p = 0.81$; week 12, $p = 0.36$; figure 4.7C).

4.2.3 The effects of imatinib and dasatinib on serum biochemistry in normal rats *in vivo*

The effects of tyrosine kinase inhibition on serum biochemistry were assessed after 4, 8 and 12 weeks of treatment. As shown in figure 4.8A, a significant decrease in serum phosphate levels was observed in the dasatinib-treated animals at 4 weeks ($p < 0.05$). Total calcium levels were unchanged by dasatinib at all time-points examined (week 4, $p = 0.32$; week 8, $p = 0.42$; week 12, $p = 0.96$; figure 4.8B). Imatinib treatment had no effect on serum phosphate or calcium levels at any of the time-points examined (figure 4.8A,B).

4.2.4 The effects of imatinib and dasatinib on osteoclasts and osteoblasts *in vivo*

4.2.4.1 The effects of dasatinib and imatinib on osteoclast numbers

Histological analysis was carried out to assess whether tyrosine kinase inhibition affected osteoclast numbers *in vivo*. N.Oc/B.Pm and Oc.S/BS were quantitated in a defined region of secondary spongiosa in TRAP-stained histological sections (figure 4.9A). The number of multinucleated, TRAP-positive osteoclasts were substantially decreased by treatment with dasatinib or zoledronic acid (figure 4.9A). In dasatinib-treated animals, N.Oc/B.Pm at the proximal tibiae was significantly decreased, compared with controls ($p < 0.05$). This decrease in osteoclast numbers was associated with a decrease in Oc.S/BS following 12 weeks of dasatinib treatment, although this did not reach statistical significance (figure 4.9C). Similar decreases in N.Oc/B.Pm and Oc.S/BS were observed in the

Figure 4.7. Cortical morphology at the tibial diaphysis is not altered by tyrosine kinase inhibitor treatment. At 4, 8 and 12 weeks tibiae from imatinib-, dasatinib-, vehicle- or zoledronic acid-treated animals were collected for μ-CT analysis of diaphyseal bone. Cross-sectional 3-dimensional images of representative tibiae from animals treated for 12 weeks are shown (**A**). Cortical bone volume (Ct.BV/TV; **B**) and cortical thickness (Ct.Th; **C**) were analysed at a 1.305 mm long region of cortical bone 13.05 mm distal to the proximal tibial growth plate. Graphs depict mean ± SEM (n = 4 – 6).

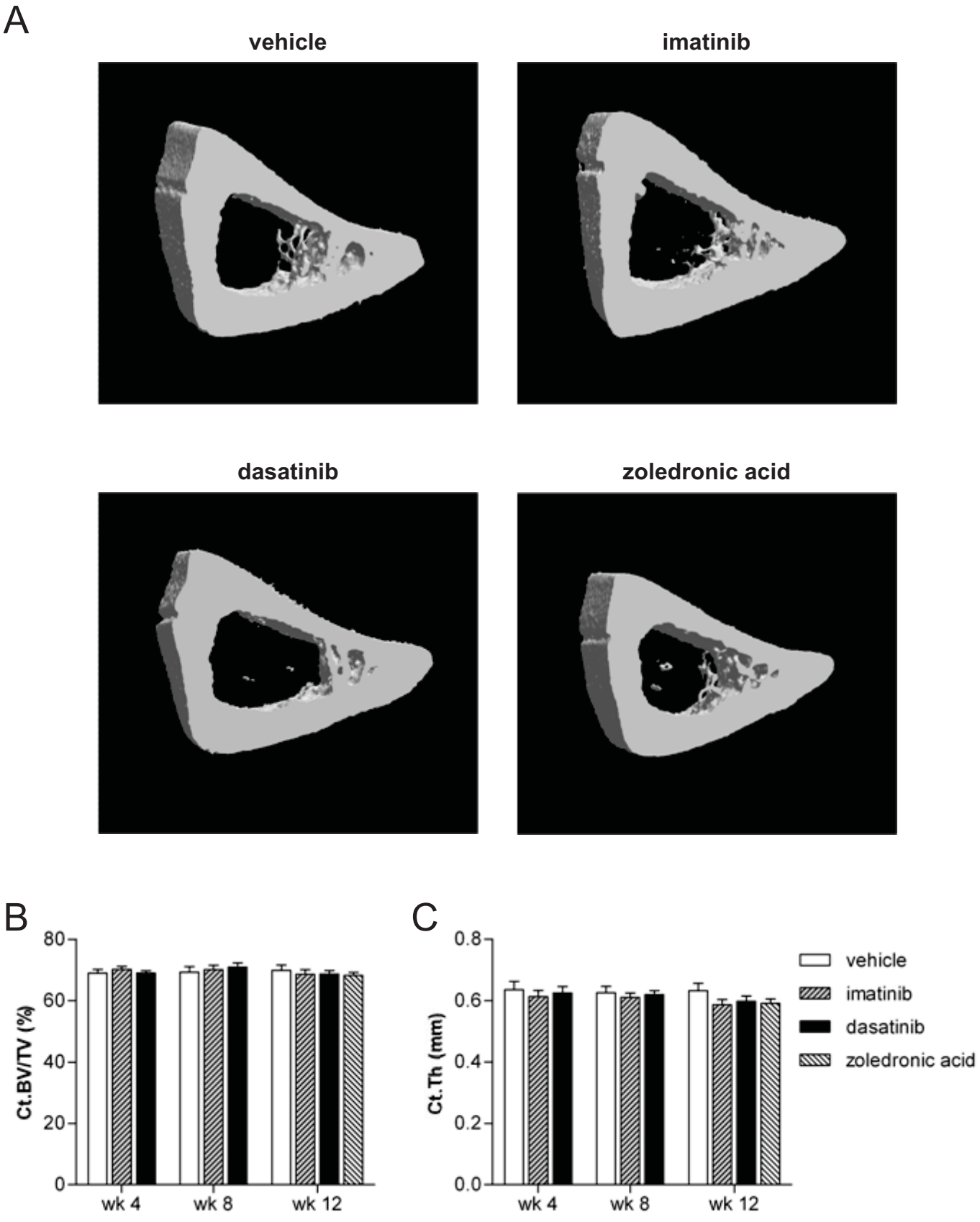
A
vehicle
imatinib
dasatinib
zoledronic acid
B
Ct.BV/TV (%)
80
60
40
20
0
wk 4
wk 8
wk 12
C
Ct.Th (mm)
0.8
0.6
0.4
0.2
0.0
wk 4
wk 8
wk 12
vehicle
imatinib
dasatinib
zoledronic acid

Figure 4.8. The effects of tyrosine kinase inhibitor treatment on serum biochemistry *in vivo*. Blood was collected by cardiac puncture after treatment with imatinib, dasatinib or vehicle (4, 8 or 12 weeks) and serum levels of phosphate (**A**) and calcium (**B**) were determined. Graphs depict mean ± SEM (n = 3 – 6). * $p < 0.05$, relative to vehicle control at each time-point (one-way ANOVA with Dunnett's post-test).

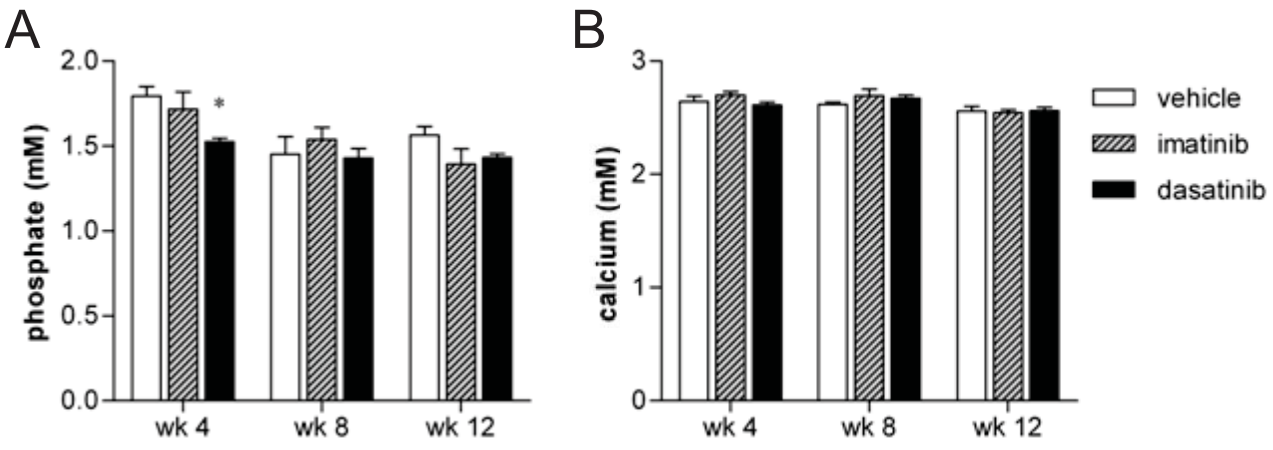
A
2.0
1.5
1.0
0.5
0.0
phosphate (mM)
*
wk 4
wk 8
wk 12
B
3
2
1
0
calcium (mM)
wk 4
wk 8
wk 12
vehicle
imatinib
dasatinib

Figure 4.9. Dasatinib treatment decreases osteoclast numbers *in vivo*. Tibiae were collected, embedded in methyl methacrylate and 5 μm sections were stained for TRAP and counterstained with methyl green. Representative images are shown (**A**). Scale bar: 50 μm. Arrows indicate TRAP-positive multinucleated osteoclasts. N.Oc/B.Pm (**B**) and Oc.S/BS (**C**) were quantitated in a defined region of secondary spongiosa at the proximal tibia. Blood was collected by cardiac puncture after treatment with imatinib, dasatinib or vehicle (4, 8 or 12 weeks) or zoledronic acid (12 weeks only) and serum levels of CTX-1 were quantitated by commercial ELISA (**D**). Graphs depict mean ± SEM ($n = 3 – 6$). * $p < 0.05$, relative to vehicle control (one-way ANOVA with Dunnett's post-test).

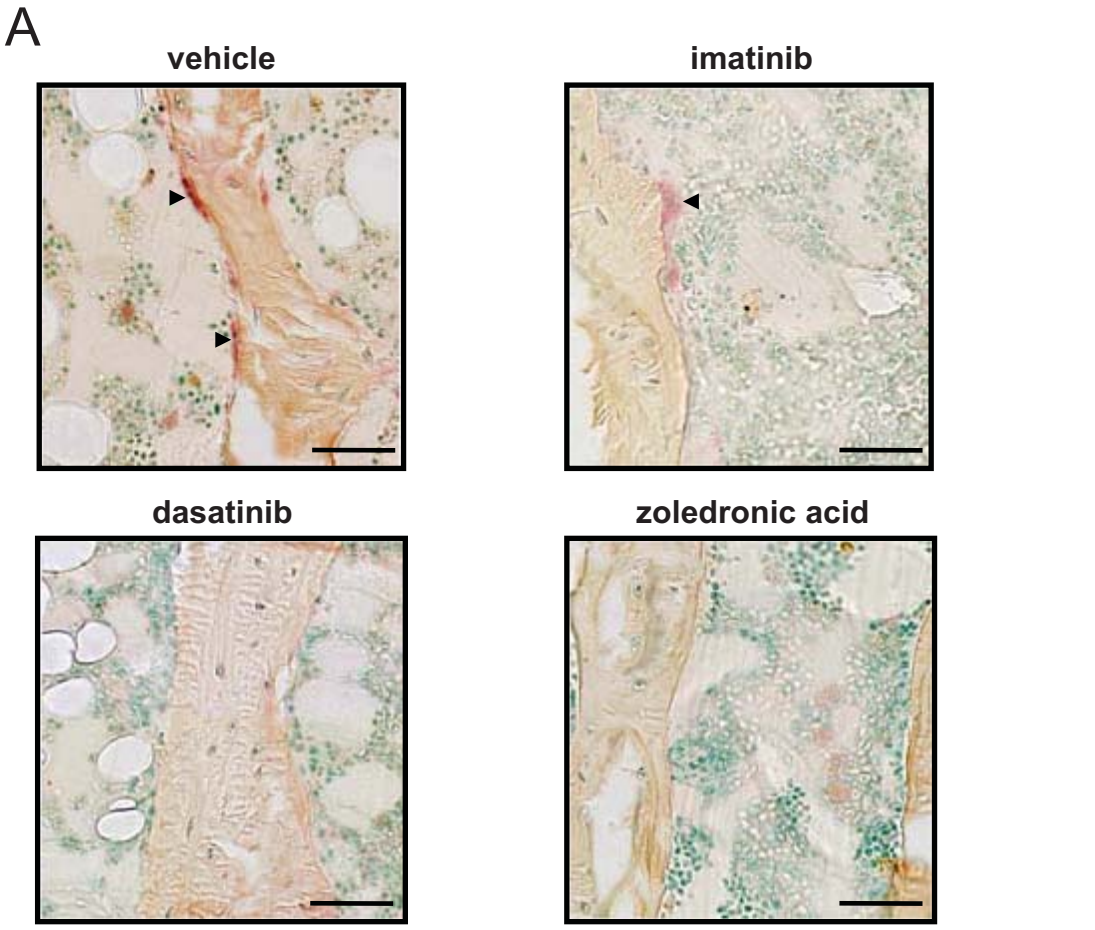
A
vehicle
imatinib
dasatinib
zoledronic acid

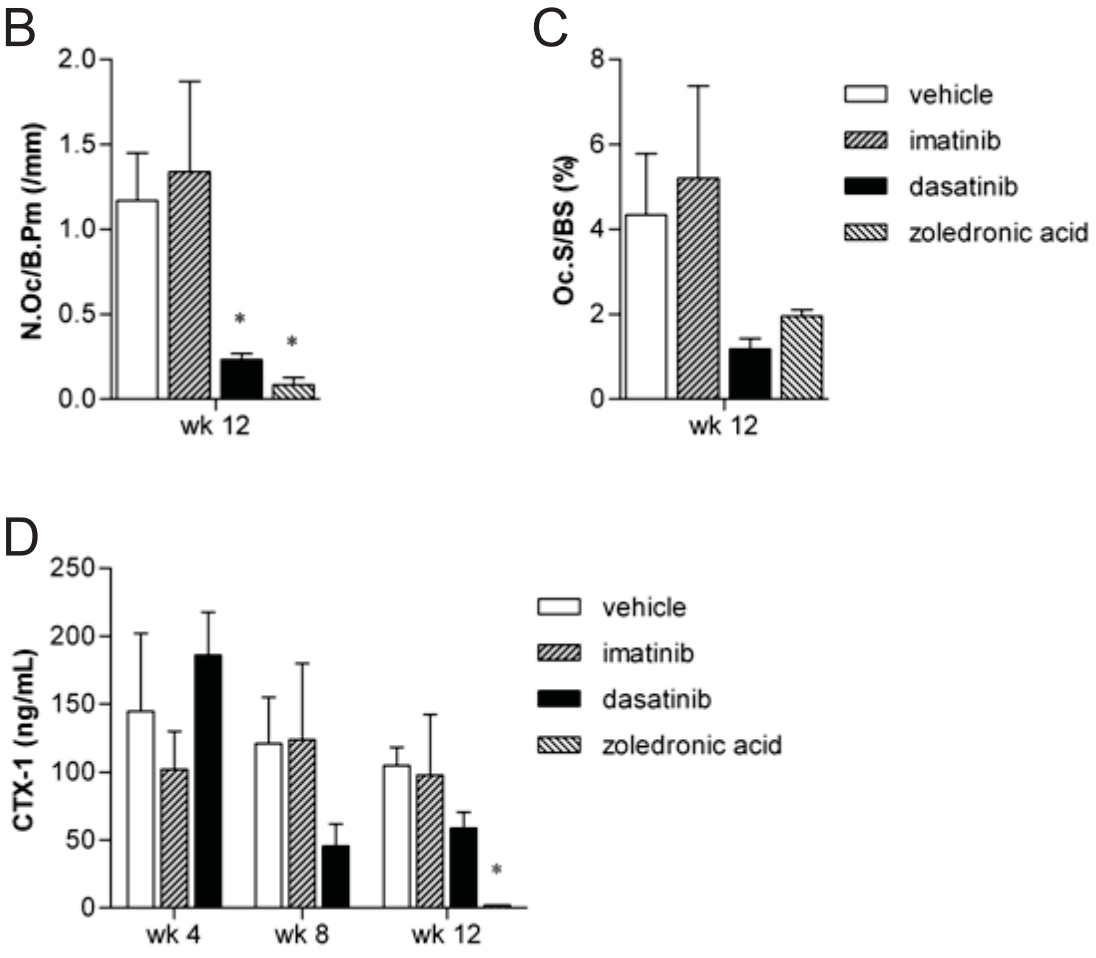
B
N.Oc/B.Pm (/mm)
2.0
1.5
1.0
0.5
0.0
*
*
wk 12
C
Oc.S/BS (%)
8
6
4
2
0
wk 12
vehicle
imatinib
dasatinib
zoledronic acid
D
CTX-1 (ng/mL)
250
200
150
100
50
0
*
wk 4
wk 8
wk 12
vehicle
imatinib
dasatinib
zoledronic acid

zoledronic acid-treated animals (figure 4.9B,C). N.Oc/B.Pm and Oc.S/BS were not significantly altered by treatment with imatinib, when compared with vehicle controls (figure 4.9B,C).

4.2.4.2 The effects on serum levels of the osteoclast marker CTX-1

The effect of tyrosine kinase inhibition on osteoclast activity was investigated by analysing the serum levels of the bone resorption marker CTX-1. While CTX-1 levels were unchanged by imatinib treatment, serum levels of CTX-1 were decreased in the dasatinib-treated group relative to the vehicle controls after 8 and 12 weeks of treatment, although this did not reach statistical significance (figure 4.9D). In animals treated with zoledronic acid for 12 weeks, CTX-1 levels were undetectable ($p < 0.05$; Kruskal-Wallis test with Dunn's post-test; figure 4.9D).

4.2.4.3 The effects of imatinib and dasatinib on osteoblast activity **in vivo**

To determine the effects of tyrosine kinase inhibition on bone formation, rats were injected with calcein 14 days prior to the end of the experiment. Unstained, deplasticised sections of rat tibiae were then used for dynamic measurements of bone formation in a defined area of secondary spongiosa. While imatinib and dasatinib treatment had no effect on calcein labelling, substantially less labelled bone surface was observed in zoledronic acid-treated animals (figure 4.10A). The dynamic measurements of osteoblast activity MS/BS, MAR and BFR were not significantly different from controls in the imatinib- or dasatinib-treated groups (figure 4.10B–D). While a trend towards a decrease in MS/BS, MAR and BFR was observed in the zoledronic acid-treated group, this did not reach statistical significance (figure 4.10B–D).

4.2.4.4 The effects of imatinib and dasatinib on serum markers of osteoblast activity

The serum levels of the bone formation markers osteocalcin and P1NP were measured to further characterise the effects of imatinib and dasatinib on bone formation. Osteocalcin and P1NP levels were not significantly altered by treatment with imatinib, dasatinib or zoledronic acid, when compared with vehicle controls, at any of the examined time-points (figure 4.10E,F).

Figure 4.10. Dasatinib treatment does not affect osteoblast activity *in vivo*. After 10 weeks of treatment, animals were injected with calcein (30 mg/kg) to label the exposed bone surface. After an additional 2 weeks, tibiae were collected, embedded in methyl methacrylate and dynamic histomorphometric measurements were conducted on unstained 5 µm sections. Representative images are shown (**A**). Scale bar: 50 µm. MS/BS (**B**), BFR (**C**) and MAR (**D**) were quantitated in a defined region of secondary spongiosa at the proximal tibia. Blood was collected by cardiac puncture after treatment with imatinib, dasatinib or vehicle (4, 8 or 12 weeks) or zoledronic acid (12 weeks only) and serum levels of osteocalcin (**E**) and P1NP (**F**) were quantitated by commercial ELISA. Graphs depict mean ± SEM (n = 3 – 6).

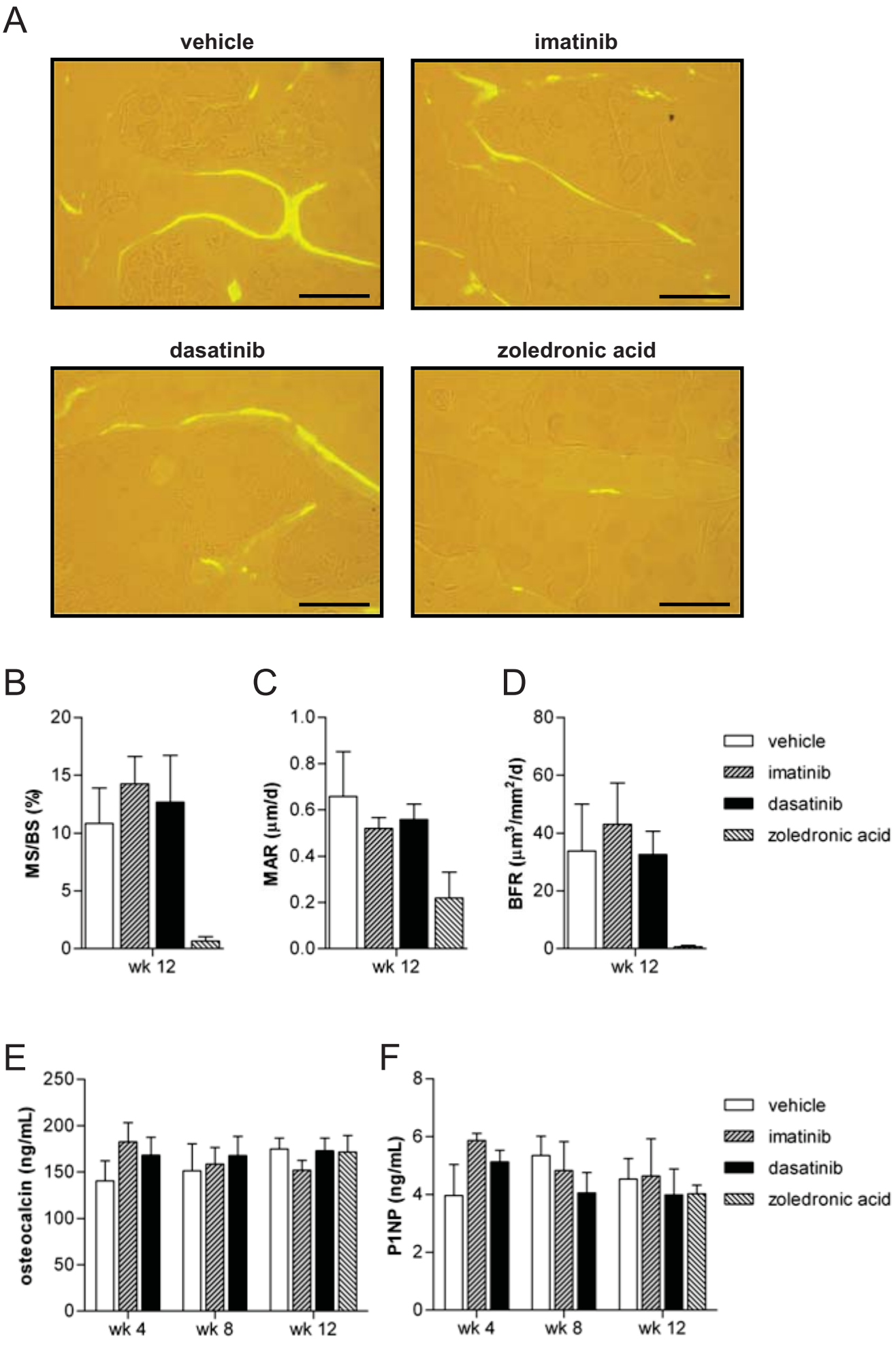
A
vehicle
imatinib
dasatinib
zoledronic acid
B
MS/BS (%)
20
15
10
5
0
wk 12
C
MAR (µm/d)
1.0
0.8
0.6
0.4
0.2
0.0
wk 12
D
BFR (µm³/mm²/d)
80
60
40
20
0
wk 12
vehicle
imatinib
dasatinib
zoledronic acid
E
osteocalcin (ng/mL)
250
200
150
100
50
0
wk 4
wk 8
wk 12
F
P1NP (ng/mL)
8
6
4
2
0
wk 4
wk 8
wk 12
vehicle
imatinib
dasatinib
zoledronic acid

4.2.5 The effects of imatinib and dasatinib on the growth plate

The cartilaginous and trabecular architecture at the proximal tibial growth plate was substantially altered after 12 weeks of imatinib treatment, when compared with controls (figure 4.11). In vehicle-treated controls, the width of the cartilaginous growth plate at the proximal tibia remained constant at all time-points examined ($p = 0.070$, one-way ANOVA; figure 4.11A). In contrast, the width of the growth plate decreased substantially over time in imatinib- and dasatinib-treated animals (figure 4.11A,B). The growth plate was significantly narrower in imatinib-treated group than in the control group after 4, 8 and 12 weeks of treatment ($p < 0.05$; figure 4.11A,B). By 12 weeks of imatinib treatment, the growth plate had almost completely fused and was replaced by trabecular bone (figure 4.11B). In dasatinib-treated animals, the proximal tibial growth plate was significantly narrower than that of vehicle-treated controls after 12 weeks of treatment ($p < 0.05$, figure 4.11A,B). In contrast, at 12 weeks, zoledronic acid treatment induced an increase in growth plate thickness which did not reach statistical significance (figure 4.11A,B).

4.2.6 Pharmacokinetics of imatinib in normal rats

As imatinib had no effect on trabecular morphology in the normal rats used in this study, despite the use of doses previously shown to decrease osteoclast numbers[13], the steady-state serum levels of imatinib were analysed to ascertain whether the levels of imatinib achieved in this study were similar to those achieved in patients undergoing imatinib therapy. Serum was collected at 4, 8 or 12 weeks of imatinib therapy, 26 – 28 hours after the final dose was administered and imatinib levels were quantified by HPLC.

As seen in figure 4.12A, in imatinib-treated rats, the steady-state serum concentration achieved was 2.70 ± 0.68 μM (mean ± SEM; $n = 14$). There was a wide variation in steady-state imatinib concentrations in these normal rats (range: 0.27 – 8.04 μM), consistent with previous data demonstrating high variability in steady-state serum concentrations in imatinib-treated CML patients.[360-362] There were no significant correlation between serum imatinib levels and body mass ($p = 0.18$), BV/TV ($p = 0.77$) or serum CTX-1 levels ($p = 0.95$) in these animals.

To determine the kinetics of imatinib metabolism in mature animals, 7-month-old Sprague-Dawley rats were administered with a single dose of imatinib (100 mg/kg) by gavage and groups of 3 animals were humanely killed and exsanguinated at the nominated time-points (0.5, 1, 2, 4, 8, 12, 24 hours). Serum concentrations of imatinib were determined by HPLC. As shown in figure 4.12B, the maximal serum concentration of

Figure 4.11. The growth plate at the proximal tibia is narrowed in imatinib- and dasatinib-treated animals. After 4, 8 and 12 weeks of treatment, tibiae were collected for histological analysis. Samples were embedded in paraffin and 5 μm sections were stained with safranin O/fast green. Mean growth plate thickness was calculated from measurements taken at 5 equidistant points across the growth plate (**A**). Graph depicts mean ± SEM (n = 3 – 6). * $p < 0.05$ relative to vehicle control at each time-point (one-way ANOVA with Dunnett's post-test). Representative images are shown of safranin O/fast green-stained sections (red, cartilage; green, bone and cytoplasm; purple, nuclei) (**B**). Bar: 100 μm.

A

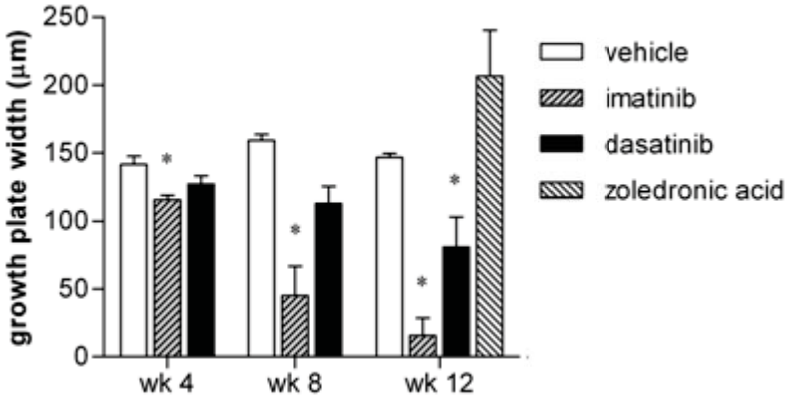
growth plate width (μm)
250
200
150
100
50
0
wk 4
wk 8
wk 12
vehicle
imatinib
dasatinib
zoledronic acid
*
*
*
*

B

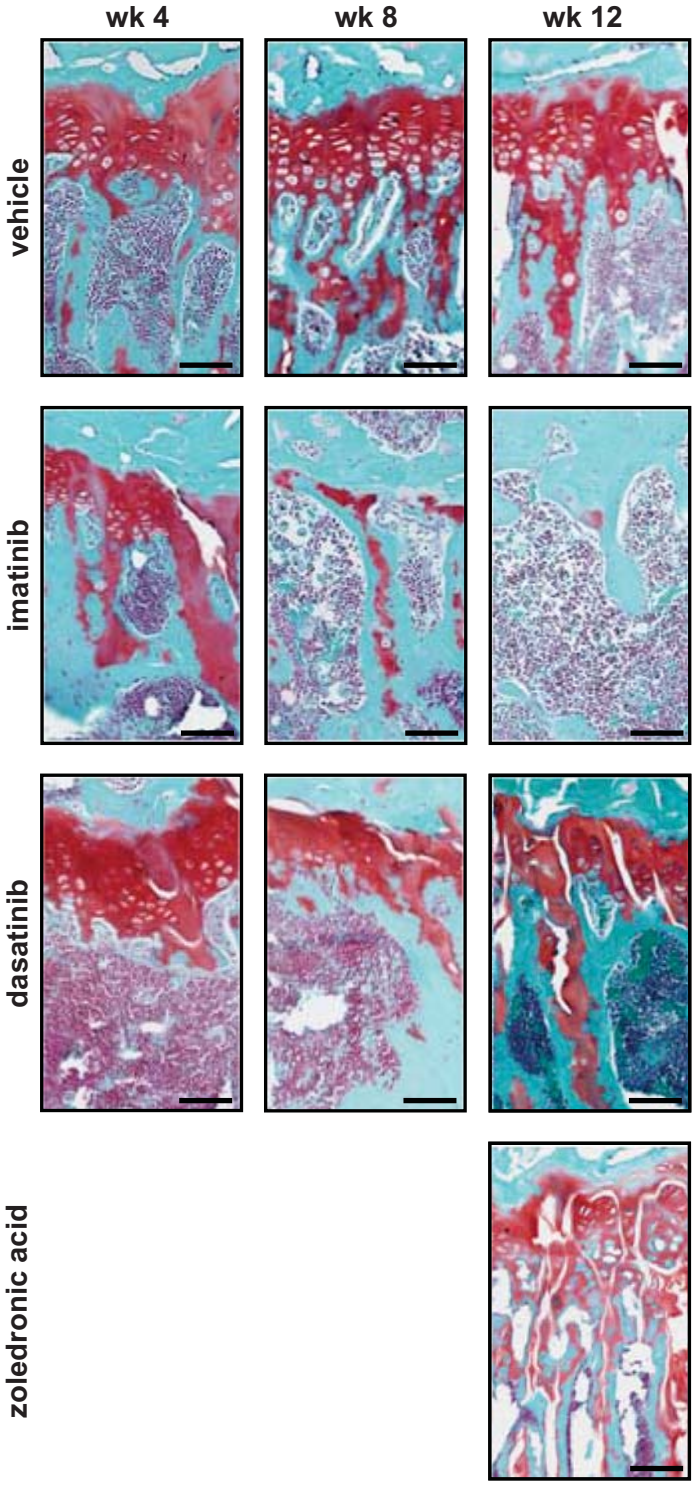
wk 4
wk 8
wk 12
vehicle
imatinib
dasatinib
zoledronic acid

Figure 4.12. Pharmacokinetics of imatinib in mature Sprague-Dawley rats. Nine-month-old female Sprague-Dawley rats were administered with imatinib (100 mg/kg/day) for 4, 8 or 12 weeks. Blood was collected by cardiac bleed 26 – 28 hours following the administration of the final dose. Achieved serum levels of imatinib were analysed by HPLC (**A**). Seven-month-old female Sprague-Dawley rats were administered with imatinib (100 mg/kg) by oral gavage. At the indicated time-points, cardiac blood samples were collected from anaesthetised animals. Sera were analysed for achieved imatinib concentrations by HPLC (**B**). Graphs depict mean ± SEM (**A**, n = 14; **B**, n = 3).

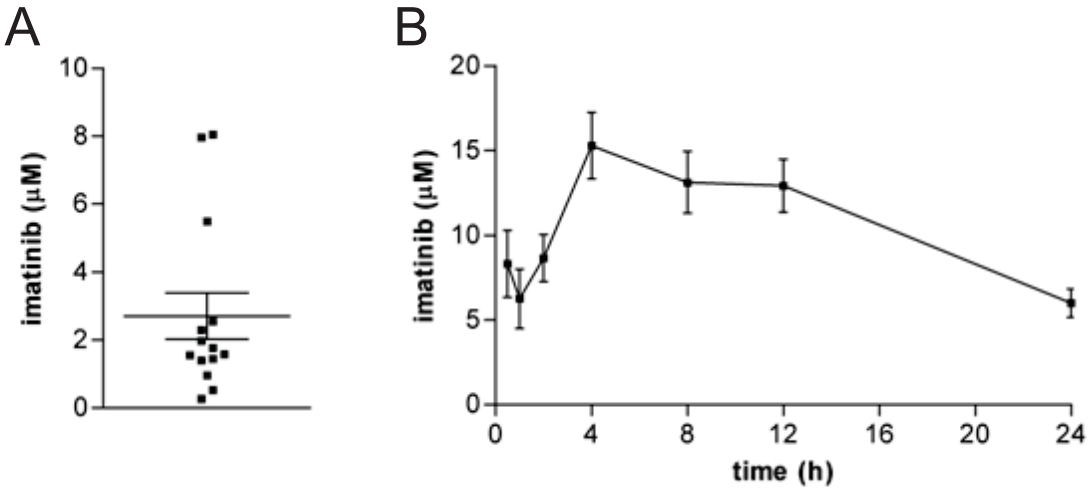
A
B
imatinib (µM)
10
8
6
4
2
0
imatinib (µM)
20
15
10
5
0
0
4
8
12
16
20
24
time (h)

imatinib (C_{max} = 15.29 ± 1.94 μM [mean ± SEM]) was reached 4 hours after drug administration. C_{last} was 5.99 ± 0.84 μM (mean ± SEM), 24 hours following drug administration.

4.3 Discussion

Studies shown here (chapter 3) and previously[5,7,8,10] demonstrate that patients undergoing treatment with imatinib have dysregulated bone remodelling resulting in an overall increase in trabecular bone volume. This is thought to result from inhibition of osteoclast activity and concomitant activation of osteoblast activity by imatinib, through inhibition of Fms and PDGFR, respectively.[10,13,16-19] As dasatinib inhibits PDGFR[348] and may inhibit Fms[237] we examined whether dasatinib could modulate bone remodelling in normal mature Sprague-Dawley rats *in vivo*. While changes in whole body BMD were not observed using DXA, treatment with dasatinib substantially increased trabecular bone volume at the proximal tibia. This was associated with an increase in trabecular connectivity (decreased Tb.Pf) and a change in trabecular architecture from a more rod-like to a more plate-like form (decreased SMI). These changes in trabecular morphology are similar to those observed in imatinib-treated CML patients, shown in chapter 3.

The present study found that serum phosphate levels were transiently decreased in dasatinib-treated rats. In keeping with this observation, grade 3 or 4 hypophosphataemia has been reported in 11% of dasatinib patients.[363] This may be indicative of altered skeletal metabolism, as decreased serum phosphate may be symptomatic of decreased release of bone phosphate stores through inhibition of osteoclastogenesis, as has been suggested for patients undergoing imatinib therapy.[5,10] To our knowledge, there have been no published reports suggesting that changes in bone remodelling occur in CML patients receiving dasatinib. Our current results suggest that the potential affects of dasatinib on bone in patients undertaking long-term treatment need further evaluation.

The changes in bone morphometric parameters in dasatinib-treated animals were similar to those induced by the potent osteoclast inhibitor zoledronic acid. Data presented here suggest that dasatinib, like zoledronic acid, increased bone volume by inhibiting osteoclast activity, as evidenced by a decrease in osteoclast numbers, osteoclast-occupied bone surface and decreased serum CTX-1 levels. Bisphosphonates are used as effective therapeutic agents for diseases characterised by aberrantly increased bone resorption, including osteoporosis, Paget's disease, osteogenesis imperfecta and bone metastatic tumours in breast cancer, prostate cancer and multiple myeloma.[364,365] The similarities in the effects of dasatinib and zoledronic acid on trabecular bone architecture observed in this study suggest that dasatinib may be an effective treatment for diseases characterised by increased osteoclast activity.

Under normal conditions, the bone resorptive activity of osteoclasts and the bone formative activity of osteoblasts are tightly coupled. To this end, osteoclast-deficient transgenic mice have been reported to show decreased osteoblast numbers and activity.[366,367] Similarly, bisphosphonate treatment has been shown to potently decrease osteoclast activity and to concomitantly decrease osteoblast activity in normal rodents *in vivo*.[368,369] Here we found that zoledronic acid treatment significantly decreased osteoclast activity and dynamic bone formation, relative to vehicle-treated controls, suggesting that bone turnover may be inhibited in zoledronic acid-treated animals. However, at the dosing schedule used here, dasatinib treatment of normal rats decreased osteoclast numbers and serum CTX-1 levels but had no effect on BFR and MAR, suggesting that bone turnover was still occurring or that osteoblast and osteoclast activity was uncoupled in these animals. Although dasatinib did not affect osteoblasts *in vivo* at the dose administered, it is likely that dasatinib, like imatinib[10,16-19], can inhibit osteoblast proliferation and stimulate differentiation *in vitro* due to its specificity for PDGFR. This hypothesis will be investigated further in chapter 6.

In contrast to previous results indicating that imatinib treatment increases bone volume in patients undergoing imatinib therapy, imatinib treatment of normal adult rats had no effect on any of the bone parameters investigated here. This is at odds with previously-reported *in vivo* data suggesting that imatinib treatment significantly decreases osteoclast numbers[13] and increased trabecular BMD and bone volume[253,254] in normal mice *in vivo*. In the experiments conducted here, the trough concentrations of imatinib achieved in these normal rats were similar to steady-state serum levels in imatinib-treated patients. These findings suggest that the lack of detectable skeletal response to imatinib observed in these aged rats was not due to insufficient dosing. However, species-specific differences in imatinib transport may affect intracellular imatinib concentrations independent of the achieved serum imatinib level.

While imatinib serum trough concentrations are indicative of response rate in patients[361,362], intracellular concentrations may correlate more strongly with effectiveness (reviewed in [370-372]). Active imatinib uptake into cells is mediated by organic cation transporter-1 (OCT-1).[229,373] In CML patients, OCT-1 expression[231] and activity[230] correlates with clinical response to imatinib. Cellular imatinib efflux is mediated by ABCB1 and ABCG2 (also known as breast cancer resistance protein [BCRP]), with increased expression of ABCB1 reducing intracellular imatinib concentrations and thus decreasing imatinib sensitivity in CML cells *in vitro*.[228,374] Additionally, binding of

imatinib by serum proteins, including α_1-acid glycoprotein, may limit imatinib bioavailability.[227,375,376] Therefore, intracellular imatinib concentrations are not dictated by the achieved serum concentration of drug, as cell membrane influx and efflux pumps and serum protein-binding affect intracellular concentrations independently of achieved serum concentration[227-229,373-376] (reviewed in [370,371]). Although the serum concentrations of imatinib achieved in the rats in this study were comparable to those achieved in patients, species-specific variations in ABCB1, ABCG2 and OCT-1 activity[377-379] or serum protein binding[380] could account for the observed differences in *in vivo* imatinib response.

Despite the fact that imatinib had no effect on bone volume in these aged rats, we observed a significant decrease in cartilaginous growth plate thickness in the imatinib treated animals, relative to the vehicle-treated controls. Dasatinib-treated animals also exhibited significantly narrower growth plates than their vehicle-treated counterparts, although complete growth plate closure did not occur in these animals. In normal growing bone, cartilage thickness at the growth plate is determined by the rate of chondrocyte proliferation, the rate of cartilage deposition by chondrocytes and the lifespan of the cartilage before it is mineralised and replaced by trabecular bone.[147] Longitudinal bone growth, however, is primarily determined by the rate of chondrocyte proliferation.[147] Whilst some targets of imatinib and dasatinib, including PDGFR[381,382], DDR2[383] and Src family kinases[384-386], are important in chondrocyte proliferation and activity, no studies have as yet been carried out to investigate the effects of imatinib and dasatinib on chondrocytes. This will be investigated further in chapter 6.

The putative effects of imatinib and dasatinib on the growth plate may have important implications for the use of imatinib and dasatinib in the paediatric setting. While short-term imatinib therapy has been successful and well-tolerated in children, there is emerging data suggesting that long-term therapy potentially causes side-effects that are specific to the paediatric setting. Three recently-published case studies report decelerated growth in juvenile CML patients undergoing imatinib therapy.[387-389] Mariani *et al*. described an 11-year-old boy who experienced a dramatic reduction in growth rate from 4.3 cm/year to 1.5 cm/year after commencing imatinib therapy.[387] While normal growth recommenced at the onset of puberty, 2 years after imatinib treatment began, the correlation of the onset of growth retardation with onset of imatinib therapy suggested a causative link. A second report described a 6-year-old female whose growth velocity decreased after beginning imatinib-therapy for CML.[388] During 4 years of imatinib therapy, the patient's height increased only marginally, from 114 cm to 121 cm, with a

corresponding decrease in SD score from -0.7 to -2.7. Furthermore, when imatinib therapy ceased, the patient's growth rate rapidly increased. Schmid *et al*. recently reported decreased growth in a female CML patient who commenced treatment with imatinib at age 5.5 years. This patient's height was in the 74th percentile at diagnosis; however, it fell to the 9th percentile after 3 years of imatinib treatment.[389] While these studies suggest that imatinib therapy in pre-pubertal individuals may retard growth, there are currently no preclinical reports suggesting a mechanism for altered growth in imatinib-treated paediatric patients.

To our knowledge, this is the first report to describe a potential mechanism for the observed perturbation of growth seen in some juvenile patients undergoing imatinib therapy. Growth plate closure in normal situations is a marker of cessation of growth, rather than a cause of it.[147] It is not clear from this study whether the rapid acceleration of growth plate closure observed is merely associated with a growth inhibitory effect of imatinib therapy or is a mechanism by which imatinib therapy causes decreased growth. In the three reported cases of delayed growth in imatinib-treated pre-pubescent patients, bone age (based on X-rays of the wrist or hand) was delayed[388,389] or normal[387], suggesting that premature growth plate closure at these sites was not detected. However, this does not rule out the possibility that growth plates were affected at other sites. In any case, the dramatic effect of imatinib on growth plate closure in rats suggests that growth plate morphology should be monitored in juvenile patients undergoing imatinib therapy and should be investigated as a potential mechanism for inhibited growth in pre-pubescent patients receiving imatinib.

Chapter 5

The effects of tyrosine kinase inhibition on osteoclasts *in vitro*

5.1 Introduction

Osteoclast formation and activation is a multistep process which involves (1) monocyte proliferation and commitment to a pre-osteoclast phenotype, (2) differentiation of pre-osteoclasts into multinucleated osteoclasts and (3) osteoclast adhesion, polarisation and bone resorption. This process is tightly regulated both temporally and spatially through the activation of specific signalling pathways.

The activation of the cell membrane receptor RANK is a key step in osteoclast differentiation. Binding of RANKL to RANK facilitates recruitment of TRAF family members which, in turn, activate downstream signalling through IKK1/2 (IκB kinase 1/2)[117,390], JNK[117,390], p38 and ERK (extracellular signal-regulated kinase) (reviewed in [121,391]). IKK1/2 and JNK signalling pathways activate the transcription factors FOS and NFκB, which drive osteoclast differentiation by upregulating the key osteoclastogenic transcription factor NFATc1 (reviewed in [391]). p38 signalling results in activation of the transcription factor Mitf, which controls the expression of key genes with roles in regulating osteoclast activity, including those for TRAP and cathepsin K.[273] Conversely, activation of the Ras/Raf/MEK/ERK pathway downstream of RANK may serve to negatively regulate osteoclastogenesis, as inhibition of MEK activity results in increased osteoclast formation.[392-394]

The activation of Fms in osteoclast precursors plays an important regulatory role in osteoclastogenesis, triggering signalling cascades which lead to increased proliferation, survival, differentiation and cytoskeletal reorganisation. MEK/ERK1/2 signalling downstream of Fms leads to increased cell proliferation through activation of cyclin D1 and D2[395], regulation of osteoclast differentiation via stabilisation of FOS and Mitf[396,397] and increased cell survival through deactivation of Bim (also known as Bcl-2-like 11)[257,398-400]. PI3K (phosphoinositide-3-kinase) signalling downstream of Fms results in deactivation of the cyclin D inhibitors FOXO (forkhead box O) and GSK-3β[256] and in cytoskeletal remodelling via a mechanism involving Rac (Ras-related C3 botulinum toxin substrate 1) and $\alpha_v\beta_3$ integrins (reviewed in [260]).

Src is involved in PI3K signalling downstream of Fms, forming a complex with Fms, PI3K, Cbl (Cas-Br-M ecotropic retroviral transforming sequence) and Grb2 (growth factor receptor-bound protein 2) upon stimulation with M-CSF.[256,401] Additionally, Src is involved in Fms-independent osteoclast adhesion, spreading and actin ring formation following binding of $\alpha_v\beta_3$ integrins to the extracellular matrix *in vitro* (reviewed in [260]). Src may also be involved in cell survival pathways through induction of Akt signalling

downstream of RANK in osteoclasts *in vitro*.[296,402] However, as *Src*$^{-/-}$ mice have similar osteoclast numbers as their wild-type counterparts, it is likely that other signalling pathways compensate for the lack of Src in anti-apoptotic pathways *in vivo*.[296]

Emerging evidence suggests that imatinib and dasatinib can inhibit osteoclast formation and activity. Treatment with imatinib at therapeutic concentrations inhibits the formation of TRAP-positive osteoclasts from human CD14+ peripheral blood mononuclear cells, primary rat bone marrow cells and primary rabbit bone marrow-derived monocytes.[13-15] Preliminary data also suggest osteoclast numbers or activity are decreased in mice[13,253,254] and in CML patients undergoing imatinib treatment (chapter 3 and [5,12]). In addition, data presented in chapter 4 demonstrated that dasatinib treatment decreases osteoclast numbers in normal rats *in vivo*. The importance of Fms and Src in osteoclast formation and function suggests that these kinases may mediate the anti-osteoclastogenic effects of imatinib and dasatinib. However, a direct correlation between the inhibition of M-CSF-induced Fms phosphorylation and osteoclast inhibition by these drugs has not been examined in osteoclasts or osteoclast precursors. While preliminary evidence suggests that dasatinib may inhibit Fms[237], this has not been conclusively demonstrated. Furthermore, other tyrosine kinase targets, including Kit[220], CAII[224] and PDGFR[220], may play a role in the inhibitory effects of imatinib and dasatinib on osteoclasts.

In this chapter, studies were undertaken to examine whether dasatinib, like imatinib, could modulate osteoclast formation and/or activity *in vitro* and whether any such effects were attributable to an inhibition of Src and/or Fms signal transduction. In addition, studies presented in this chapter using the murine monocyte/macrophage cell line RAW 264.7 describe Fms-independent mechanisms responsible for the osteoclast-inhibitory effects of imatinib and dasatinib. The immortal RAW 264.7 cell line was initially isolated from an Abl-positive murine leukaemia virus-infected mouse and has the ability to form osteoclast-like cells *in vitro* in an M-CSF-independent manner, when cultured in the presence of RANKL.[403] As RAW 264.7 cells are not dependent on M-CSF for osteoclastogenesis, they were used as a control to determine whether inhibition of osteoclastogenesis is occurring via inhibition of Fms signalling or by other pathways.

5.2 Results

5.2.1 Osteoclast formation in mBM and rBM cultures is dependent on M-CSF and RANKL

The formation of osteoclasts from monocyte/macrophage precursors *in vitro* is primarily dependent upon two factors: M-CSF and RANKL. Whilst RANKL is essential for the differentiation of monocyte/macrophage precursors into osteoclasts, and for the activity of the mature osteoclasts, M-CSF is essential for the survival of osteoclast precursors and mature osteoclasts. In mBM cultures, addition of rhM-CSF and rhRANKL induces the formation of large, TRAP-positive multinucleated osteoclasts (figure 5.1A,a), whereas cultures supplemented with rhM-CSF alone did not form multinucleated cells and contained fewer TRAP-positive mononucleated cells (figure 5.1A,b). When mBM cells were supplemented with rhRANKL alone, no viable adherent cells were evident after 6 days of culture (figure 5.1A,c), highlighting the role of M-CSF in promoting cell survival. In the presence of rhRANKL, osteoclast formation in mBM and rBM was M-CSF-dose-dependent (figure 5.1B,C).

5.2.2 Imatinib and dasatinib inhibit osteoclastogenesis *in vitro*

5.2.2.1 Therapeutically-achievable concentrations of imatinib and dasatinib inhibit osteoclast formation in vitro

Previous studies from our laboratory have shown that imatinib inhibits human osteoclast formation and activity *in vitro*.[13] To confirm that rat and mouse primary cells were sensitive to imatinib, the effect of imatinib on osteoclast formation and activity in murine bone marrow cultures was examined.

To determine the effects of imatinib on murine osteoclast formation, mBM and rBM cells were cultured with M-CSF and RANKL in the presence of imatinib or vehicle for 6 days. Doses of up to 4 μM imatinib were used in these studies, to reflect the doses which are therapeutically-achievable in patients.[4,322] After the treatment period, the cultures were fixed and stained for the osteoclast marker TRAP and the number of osteoclast-like cells per well was enumerated. In vehicle-treated cultures, addition of rhM-CSF and rhRANKL induced the formation of 108.17 ± 6.32 and 65.83 ± 5.09 TRAP-positive, multinucleated osteoclast per well in mBM and rBM cultures, respectively (figure 5.2A,B). A significant decrease in the number of TRAP-positive, multinucleated cells was observed in mBM cultures treated with 2 μM imatinib and higher ($p < 0.05$; figure 5.4A). In rBM cultures, osteoclast numbers were decreased at concentrations in excess of 1 μM

Figure 5.1. Osteoclast formation in murine BM cultures is dependent on rhM-CSF concentration. mBM (**A**,**B**) or rBM (**C**) cells were cultured at 3.13 x 10^5 cells/cm^2 in 96-well plates in c-α-MEM containing 25 – 100 ng/mL rhM-CSF. Following overnight adhesion, the medium was replaced with c-α-MEM containing rhRANKL (75 ng/mL) and rhM-CSF (25 – 100 ng/mL). Following 6 days of culture, cells were stained for TRAP and TRAP-positive cells with 3 or more nuclei were counted. Representative photos (**A**) of mBM cells cultured with **a** 75 ng/mL rhM-CSF and 75 ng/mL rhRANKL, **b** rhM-CSF alone or **c** rhRANKL alone. Graphs depict mean ± SEM of quadruplicate wells (**B**) or triplicate wells (**C**) from 1 experiment.

A

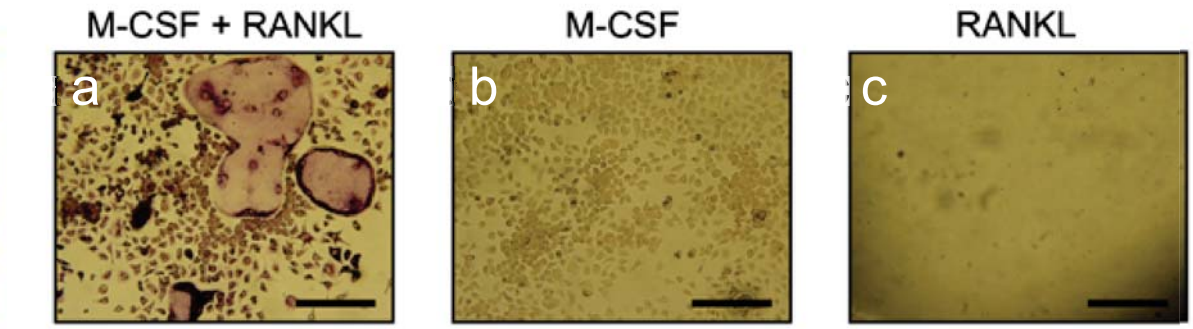
M-CSF + RANKL
M-CSF
RANKL
a
b
c

B

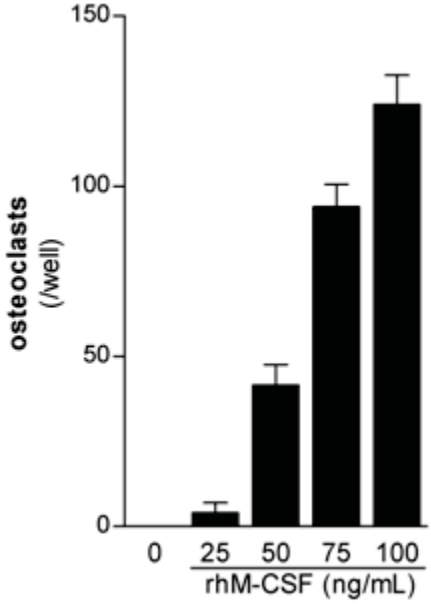
150
100
50
0
osteoclasts
(/well)
0
25
50
75
100
rhM-CSF (ng/mL)

C

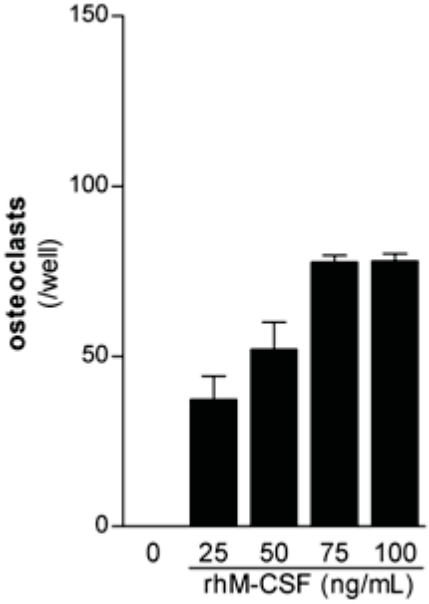
150
100
50
0
osteoclasts
(/well)
0
25
50
75
100
rhM-CSF (ng/mL)

Figure 5.2. Imatinib inhibits the formation of osteoclasts in murine cultures *in vitro*. mBM (**A**) and rBM (**B**) cells were cultured at 3.13 x 10^5 cells/cm^2 in 96-well plates in c-α-MEM containing 75 ng/mL rhM-CSF. Following overnight adhesion, the medium was replaced with c-α-MEM containing rhM-CSF (75 ng/mL) and rhRANKL (75 ng/mL) and imatinib (at the indicated concentrations) containing 0.05% DMSO vehicle or vehicle (0.05% DMSO) alone. After 6 days of treatment, cells were stained for TRAP and a representative photograph of each well was taken at 20 x magnification. Representative photos of 1 of 3 experiments for mBM (**A**) and rBM (**B**) cultures are shown. Scale bars: 200 μm.

A

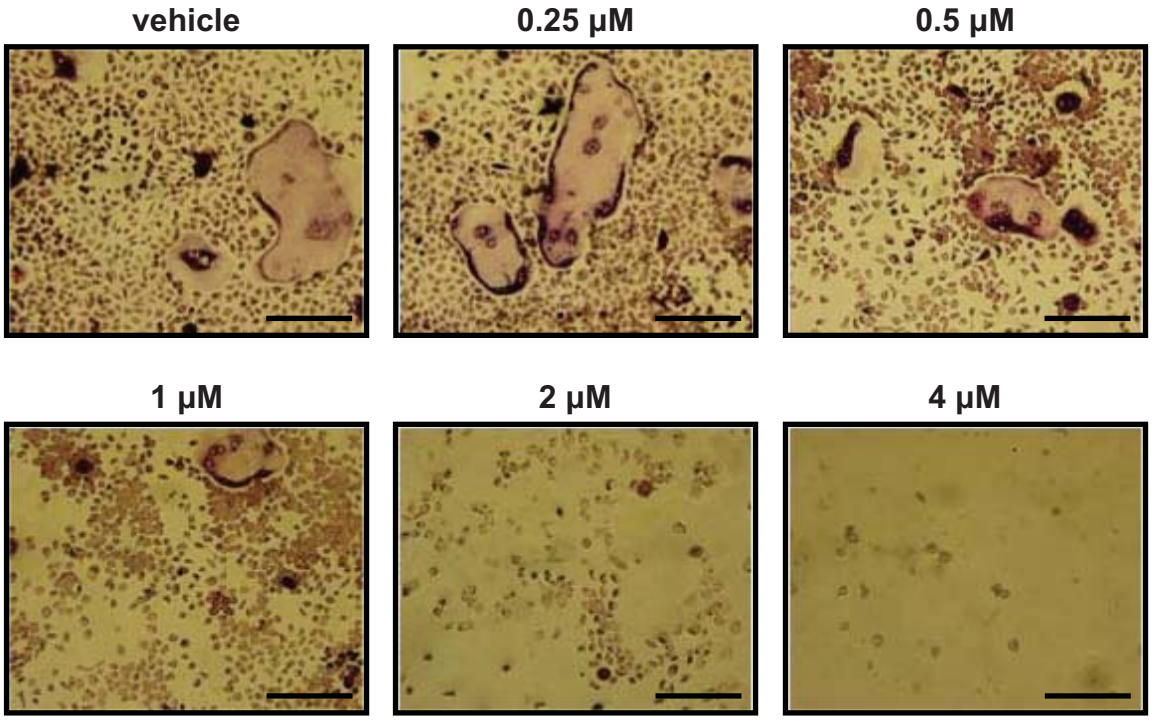
vehicle
0.25 μM
0.5 μM
1 μM
2 μM
4 μM

B

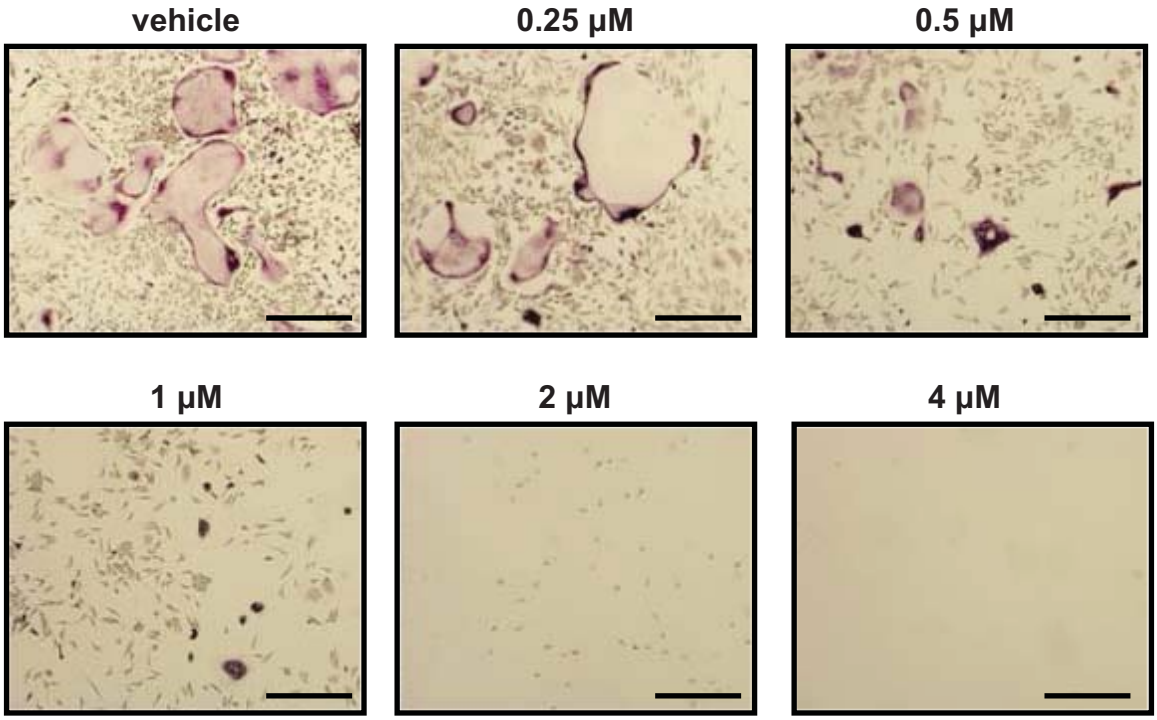
vehicle
0.25 μM
0.5 μM
1 μM
2 μM
4 μM

Figure 5.3. Dasatinib inhibits the formation of osteoclasts in murine cultures *in vitro*. mBM (**A**) and rBM (**B**) cells were cultured at 3.13 x 10^5 cells/cm^2 in 96-well plates in c-α-MEM containing 75 ng/mL rhM-CSF. Following overnight adhesion, the medium was replaced with c-α-MEM containing rhM-CSF (75 ng/mL) and rhRANKL (75 ng/mL) and dasatinib (at the indicated concentrations) or vehicle (0.05% DMSO) alone. After 6 days of treatment, cells were stained for TRAP and a representative photograph of each well was taken at 20 x magnification. Representative photos of 1 of 3 experiments for mBM (**A**) and rBM (**B**) cultures are shown. Scale bars: 200 μm.

A

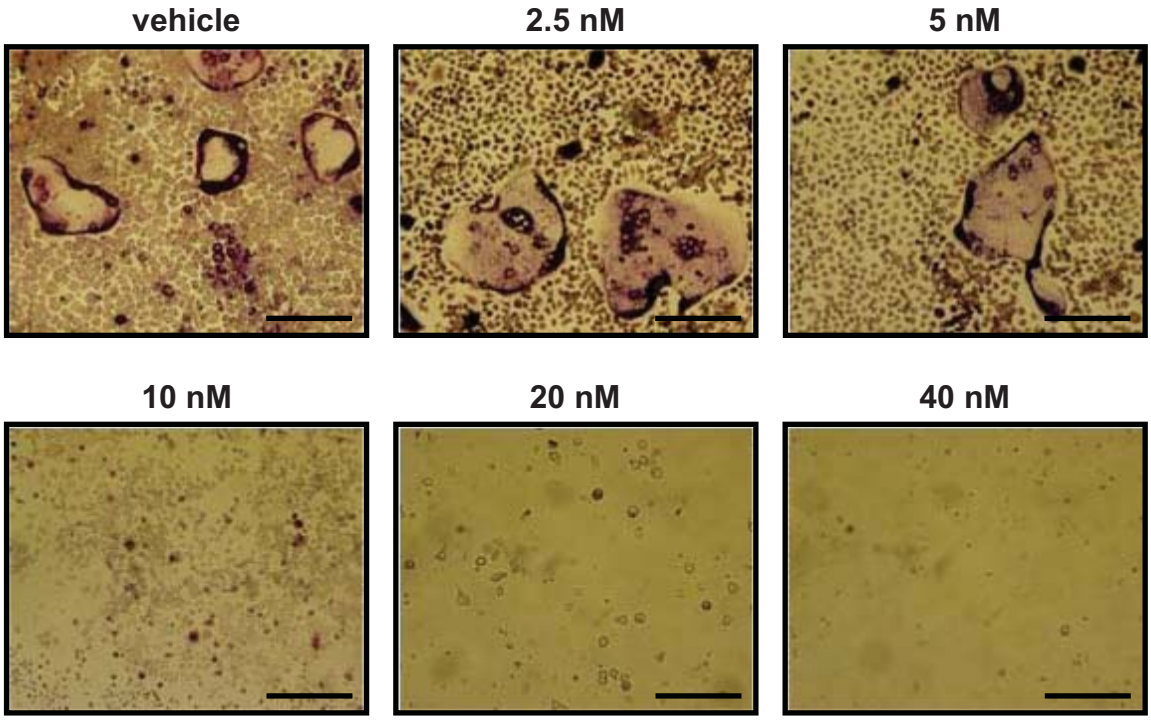
vehicle
2.5 nM
5 nM
10 nM
20 nM
40 nM

B

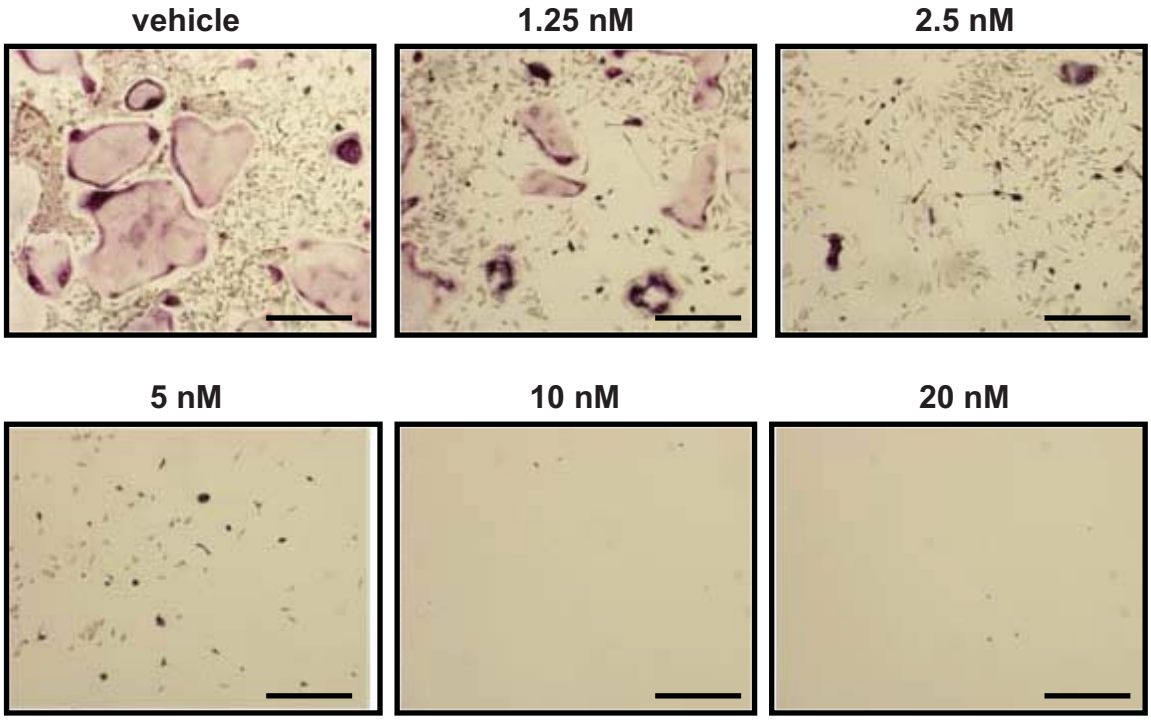
vehicle
1.25 nM
2.5 nM
5 nM
10 nM
20 nM

Figure 5.4. Quantitation of the effects of imatinib and dasatinib on osteoclast formation in murine bone marrow cultures *in vitro*. mBM (**A**) and rBM (**B**) cells were cultured at 3.13 x 10^5 cells/cm^2 in 96-well plates in c-α-MEM containing 75 ng/mL rhM-CSF. Following overnight adhesion, the medium was replaced with c-α-MEM containing rhM-CSF (75 ng/mL) and rhRANKL (75 ng/mL) and imatinib or dasatinib (containing 0.05% DMSO vehicle) or vehicle alone. After 6 days of treatment, cells were stained for TRAP and the number of TRAP-positive cells with 3 or more nuclei per well was enumerated. Graphs depict mean ± SEM of 3 independent experiments. * $p < 0.05$ relative to vehicle control (one-way ANOVA with Dunnett's post-tests).

A

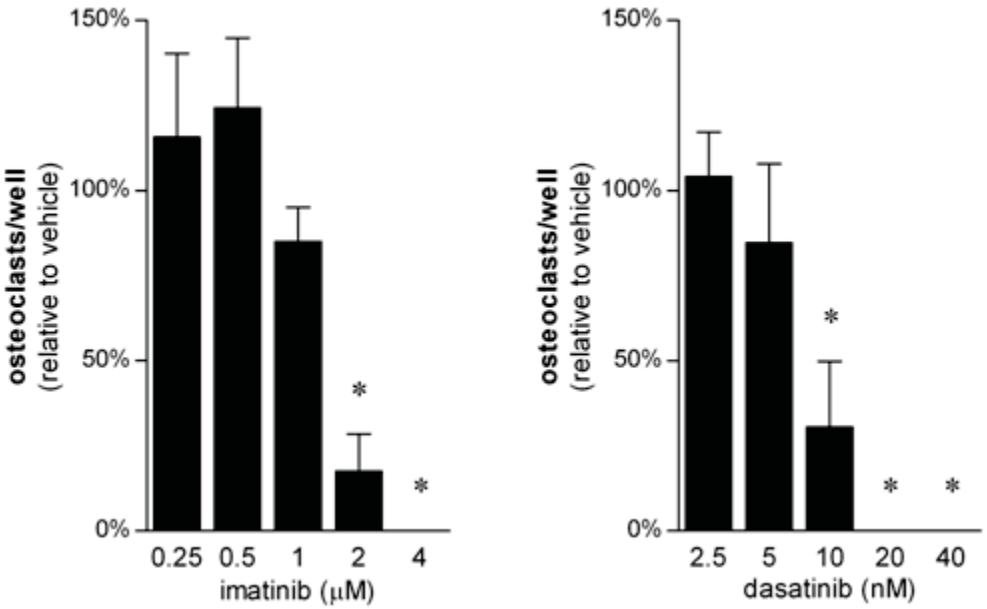
150%
100%
50%
0%
osteoclasts/well
(relative to vehicle)
0.25 0.5 1 2 4
imatinib (μM)
2.5 5 10 20 40
dasatinib (nM)

B

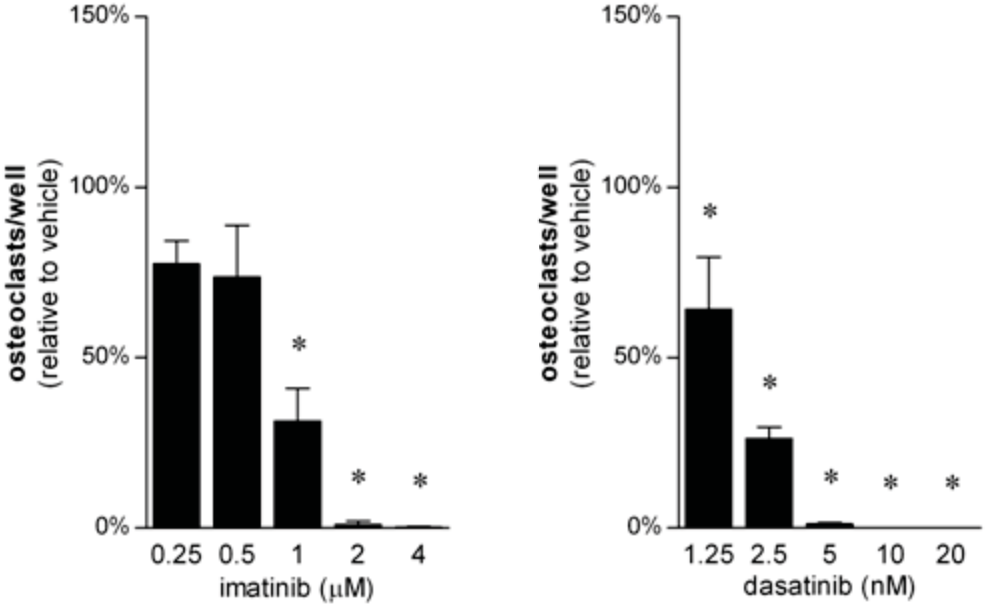
150%
100%
50%
0%
osteoclasts/well
(relative to vehicle)
0.25 0.5 1 2 4
imatinib (μM)
1.25 2.5 5 10 20
dasatinib (nM)

imatinib ($p < 0.05$; figure 5.4B). In both mBM and rBM cultures, osteoclast formation was completely abrogated by treatment with 4 μM imatinib (figure 5.2, 5.4). Osteoclast size was substantially reduced, when compared with controls, following exposure to 1 μM imatinib in mouse and rat culture systems (figure 5.2A,B).

Similar cultures were established to assess whether dasatinib, like imatinib, could inhibit osteoclast formation *in vitro*. In mouse and rat cultures, treatment with therapeutically-relevant concentrations of dasatinib[306] dose-dependently reduced osteoclast formation and size (figure 5.3A). Treatment of mBM cells with 10 nM dasatinib, or more, significantly inhibited the formation of TRAP-positive, multinucleated cells (figure 5.4A). In rBM cultures, the number of osteoclasts formed per well was significantly decreased at concentrations of 1.25 nM dasatinib and greater (figure 5.4B). No osteoclasts were detectable in cultures treated with 20 nM dasatinib (figure 5.3A,B and 5.4A,B).

5.2.2.2 Imatinib and dasatinib inhibit osteoclast activity in vitro

The effect of imatinib and dasatinib on osteoclast activity was also assessed in mBM and rBM cultures using calcium phosphate-coated slides. Culture of mBM and rBM cells with rRANKL and rhM-CSF for 9 days induced the formation of osteoclasts that were able to resorb the mineral substrate (Figure 5.5, 5.6). The mineral was then stained using von Kossa silver stain and the area of the resorption lacunae (clearing in the mineral substrate) was quantitated. The mean area of the mineralised surface resorbed during the 9 days of culture in the vehicle-treated wells was 3.80 ± 0.70% (mBM) and 14.81 ± 3.80% (rBM) (figure 5.5, 5.6). The addition of imatinib at concentrations of 1 μM (mBM; figure 5.7A) or 2 μM (rBM; figure 5.7B) and greater significantly reduced the area of the mineral substrate resorbed. In dasatinib-treated cultures, a significant inhibition of the resorptive activity was observed at 2.5 nM and greater in mBM cultures (figure 5.7A) and 1.25 nM dasatinib and greater in rBM cultures (figure 5.7B).

Bone resorption by osteoclasts depends on their ability to dissolve the mineral substrate and to then digest the collagen matrix. To assess whether imatinib and dasatinib could affect the ability of cultured osteoclasts to resorb a complex bone-like substrate, murine cultures were established on slices of elephant tusk dentine. In vehicle-treated cultures, the area of dentine resorbed was 8.40 ± 1.68%. The effects of imatinib and dasatinib on osteoclastic resorption of dentine slices was similar to the effects of resorption of a calcium-phosphate substrate (figure 5.8A,B). There was a significant decrease in

Figure 5.5. Imatinib inhibits the ability of murine osteoclasts to resorb mineral *in vitro*. mBM (**A**) and rBM (**B**) were cultured 3.13 x 10^5 cells/cm^2 on calcium phosphate-coated slides in 75 ng/mL rhM-CSF. Following overnight adhesion, the cultures were treated with c-α-MEM containing rhM-CSF (75 ng/mL) and rhRANKL (75 ng/mL) supplemented with imatinib (at the indicated concentrations) or vehicle (0.05% DMSO) alone for 9 days. Mineral was stained with silver stain and the slides were photographed at 0.8 x magnification. Images of representative wells from a representative of 3 independent experiments (mBM; **A**) or 2 independent experiments (rBM; **B**) are shown. Scale bar: 2.5 mm.

A

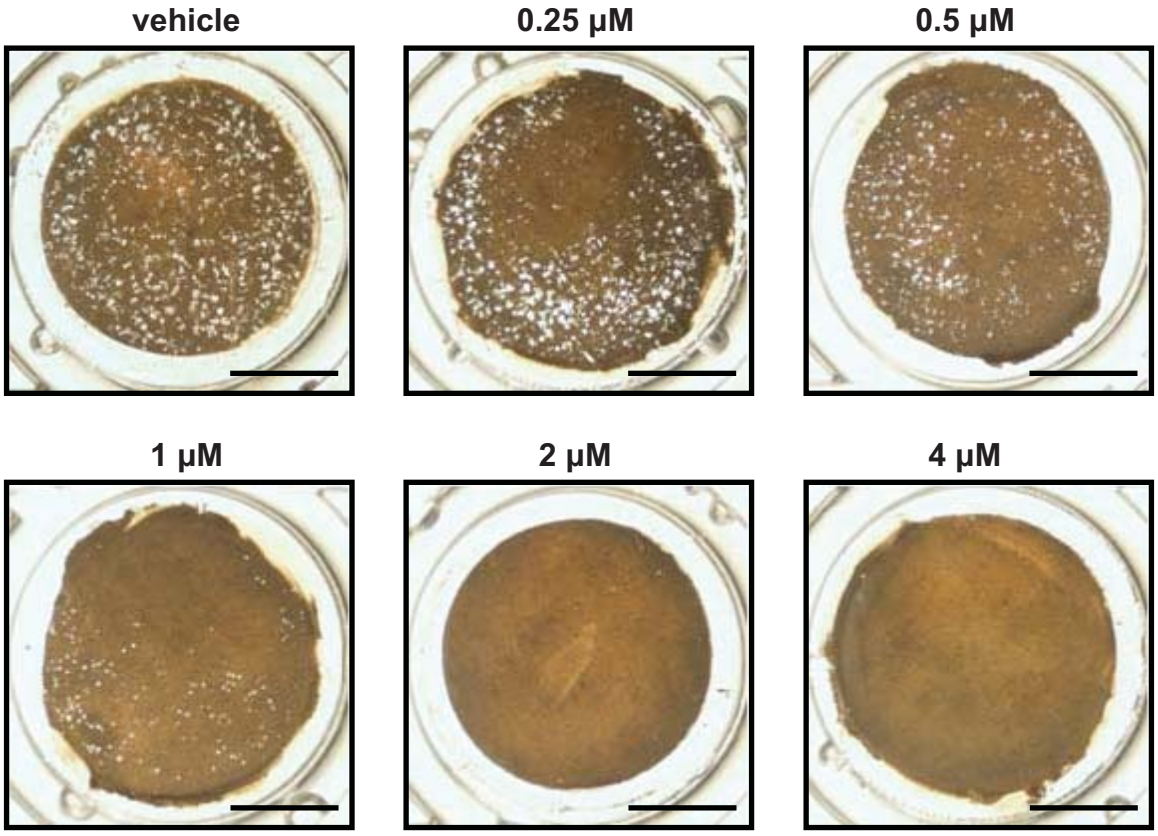
vehicle
0.25 μM
0.5 μM
1 μM
2 μM
4 μM

B

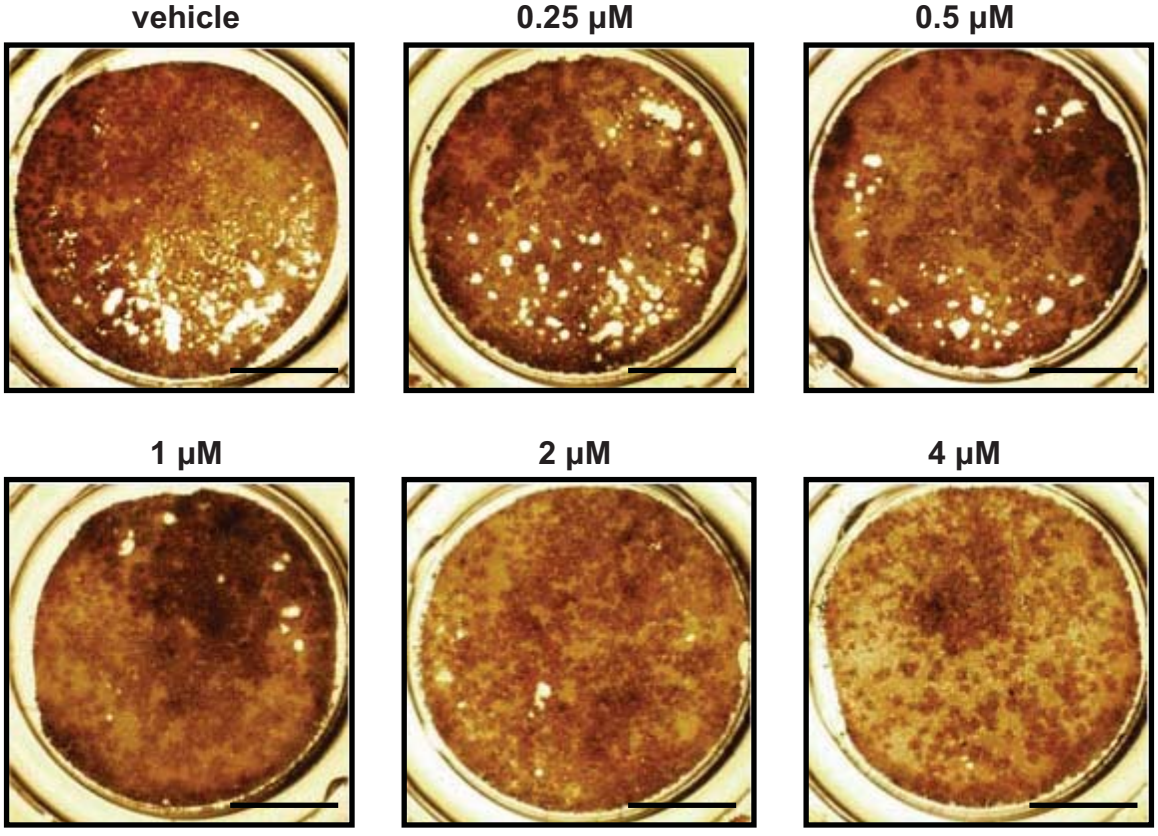
vehicle
0.25 μM
0.5 μM
1 μM
2 μM
4 μM

Figure 5.6. Dasatinib inhibits the ability of murine osteoclasts to resorb mineral *in vitro*. mBM (**A**) and rBM (**B**) were cultured 3.13 x 10^5 cells/cm^2 on calcium phosphate-coated slides in 75 ng/mL rhM-CSF. Following overnight adhesion, the cultures were treated with c-α-MEM containing rhM-CSF (75 ng/mL) and rhRANKL (75 ng/mL) supplemented with dasatinib (at the indicated concentrations) or vehicle (0.05% DMSO) alone for 9 days. Mineral was stained with silver stain and the slides were photographed at 0.8 x magnification. Images of representative wells from a representative of 3 independent experiments (mBM; **A**) or 2 independent experiments (rBM; **B**) are shown. Bar: 2.5 mm.

A

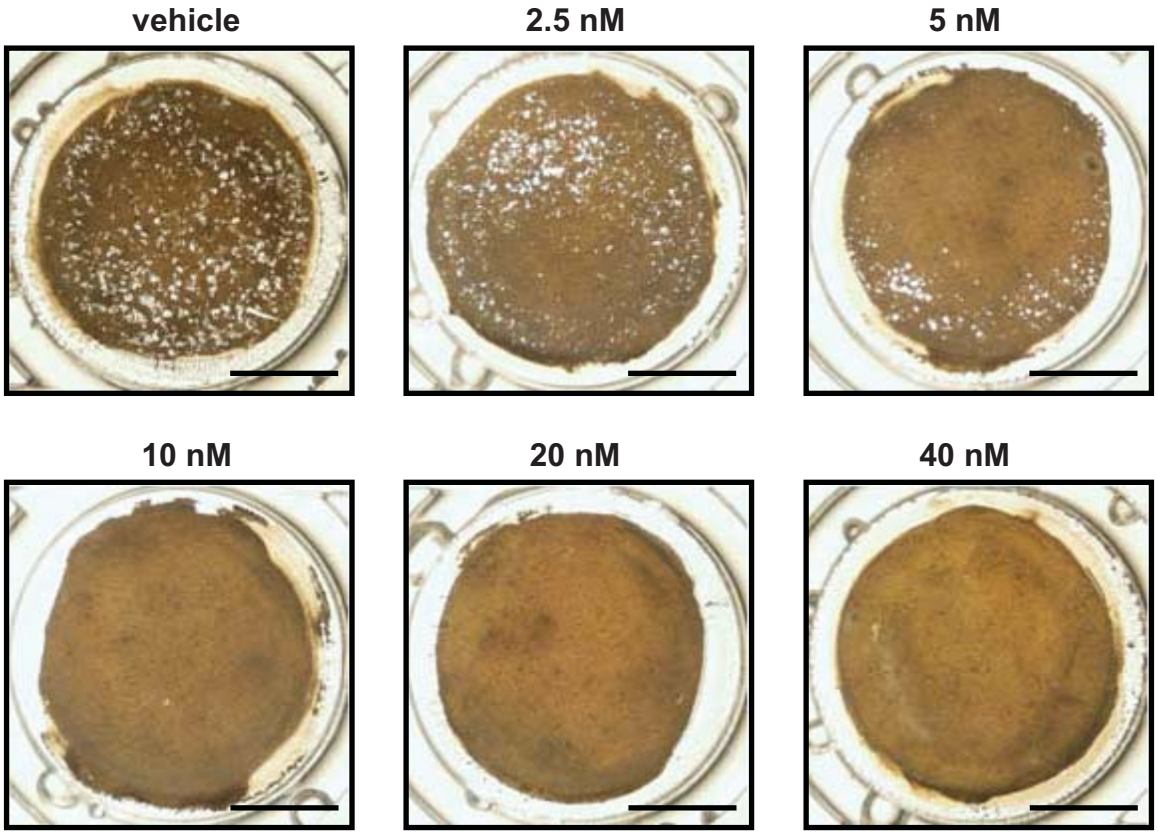
vehicle
2.5 nM
5 nM
10 nM
20 nM
40 nM

B

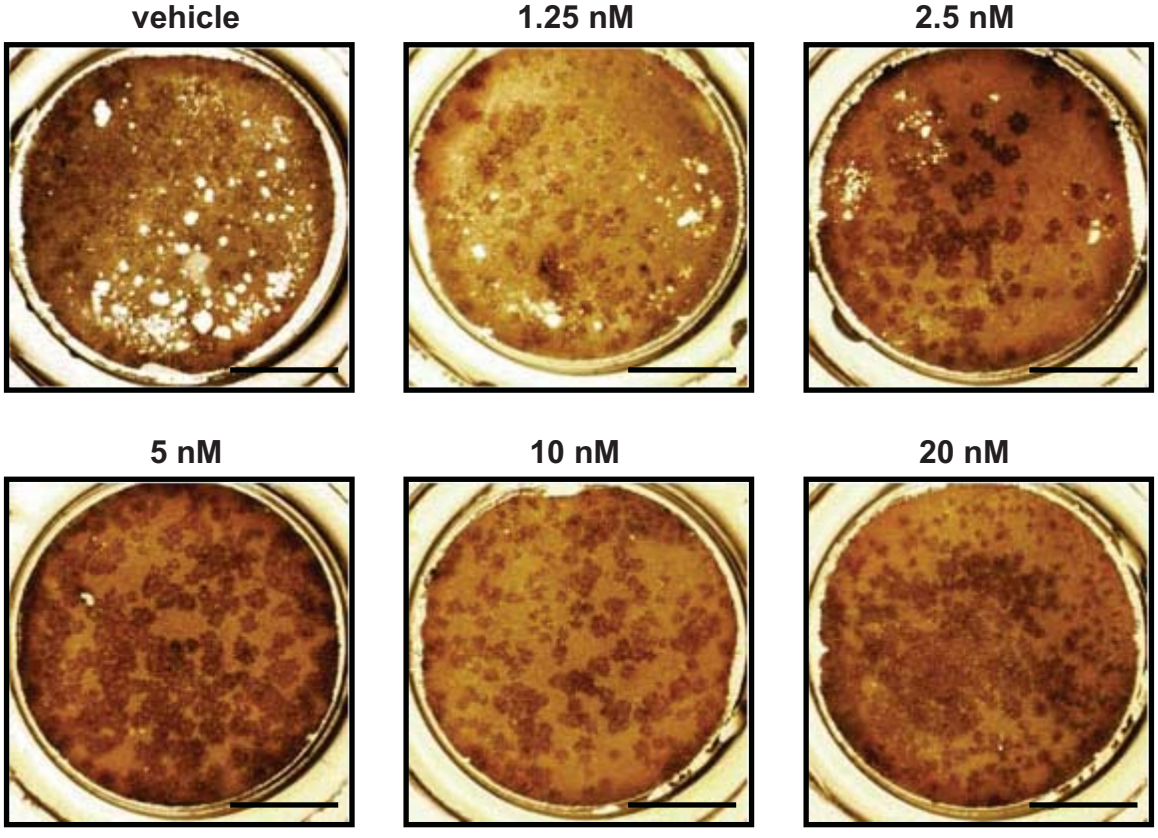
vehicle
1.25 nM
2.5 nM
5 nM
10 nM
20 nM

Figure 5.7. Imatinib and dasatinib inhibit the resorption of calcium phosphate substrates by mBM and rBM cells *in vitro*. mBM (**A**) and rBM (**B**) were cultured on calcium phosphate-coated slides and were treated with c-α-MEM containing rhM-CSF (75 ng/mL) and rhRANKL (75 ng/mL) supplemented with imatinib or dasatinib (containing 0.05% DMSO vehicle) or vehicle alone for 9 days, as shown in figure 5.5 and 5.6. Mineral was stained with silver stain and the area of substrate resorbed (lacunae area) was calculated. Graphs depict mean ± SEM of 3 independent experiments (**A**) or mean ± range of 2 independent experiments (**B**). * $p < 0.05$ relative to vehicle control (one-way ANOVA with Dunnett's post-tests).

A

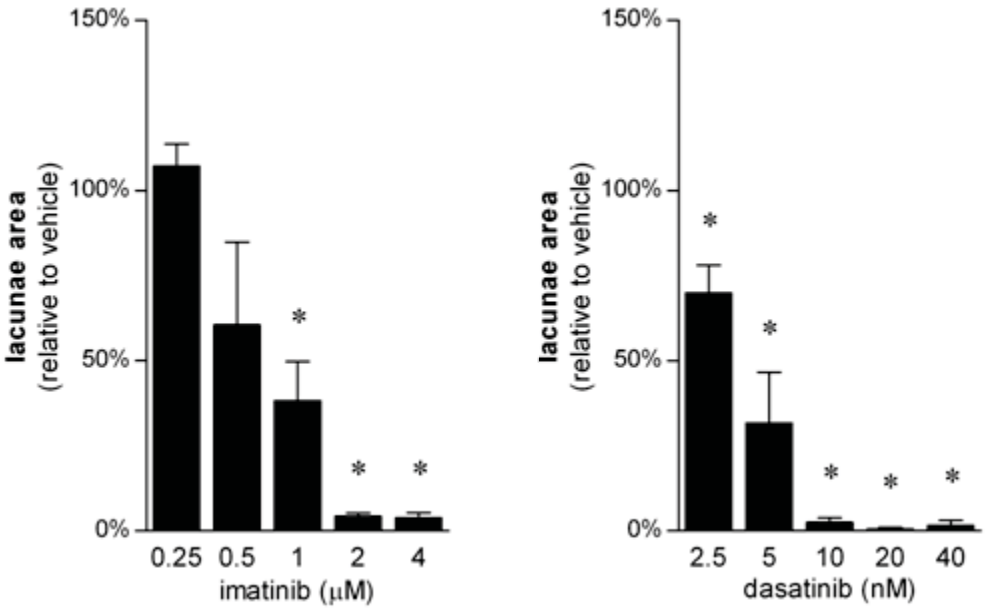
150%
100%
50%
0%
lacunae area
(relative to vehicle)
0.25 0.5 1 2 4
imatinib (μM)
2.5 5 10 20 40
dasatinib (nM)

B

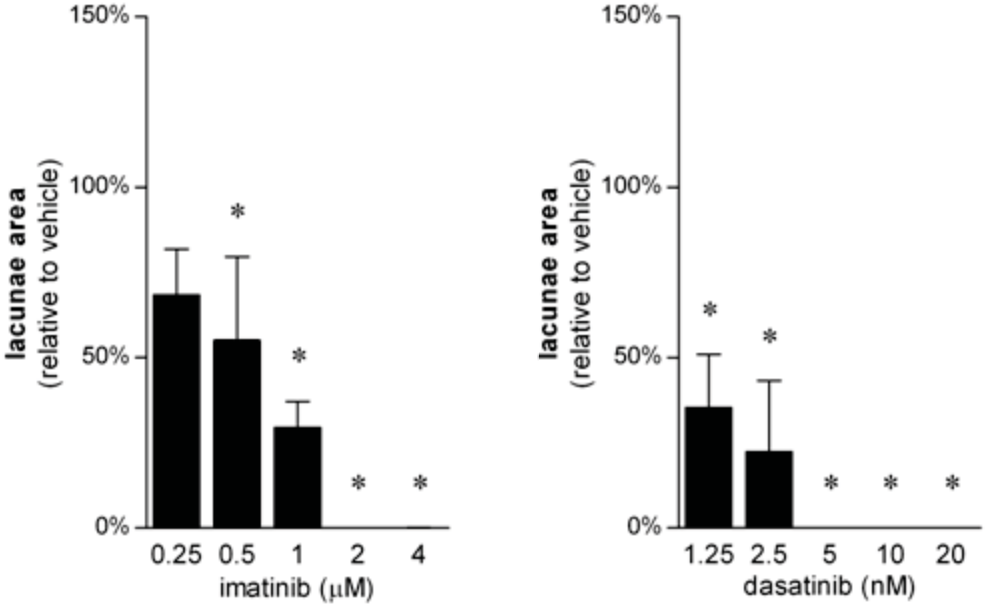
150%
100%
50%
0%
lacunae area
(relative to vehicle)
0.25 0.5 1 2 4
imatinib (μM)
1.25 2.5 5 10 20
dasatinib (nM)

Figure 5.8. Osteoclastic resorption of dentine is inhibited by imatinib and dasatinib *in vitro*. mBM cells were cultured at 3.13 x 10^5 cells/cm^2 on dentine slices in c-α-MEM containing 75 ng/mL rhM-CSF. Following overnight adhesion, the medium was replaced with c-α-MEM containing rhM-CSF (75 ng/mL) and rhRANKL (75 ng/mL) supplemented with imatinib, dasatinib or 0.05% DMSO vehicle. After 9 days of treatment, the dentine slices were stained with toluidine blue and were photographed at 0.8 x magnification. Representative photos of triplicate wells are shown for imatinib (**A**) and dasatinib (**B**). Scale bars: 400 μm.

A

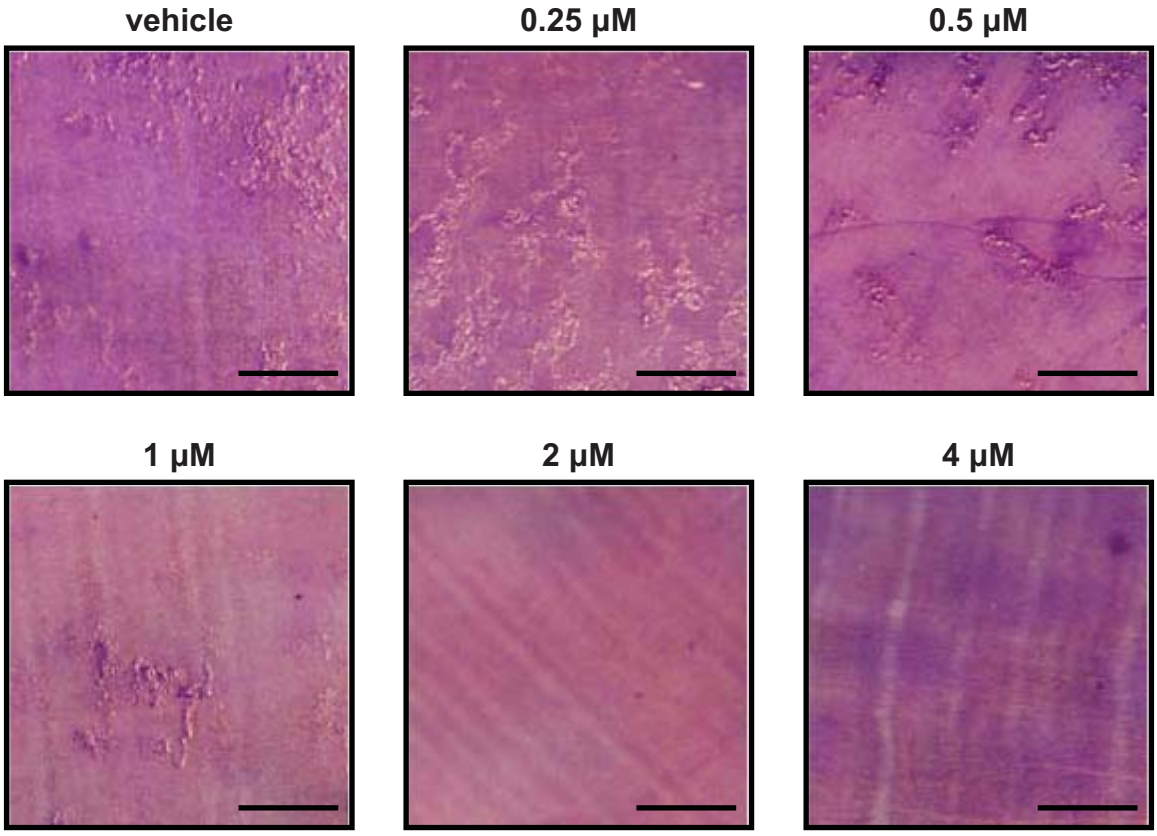
vehicle
0.25 μM
0.5 μM
1 μM
2 μM
4 μM

B

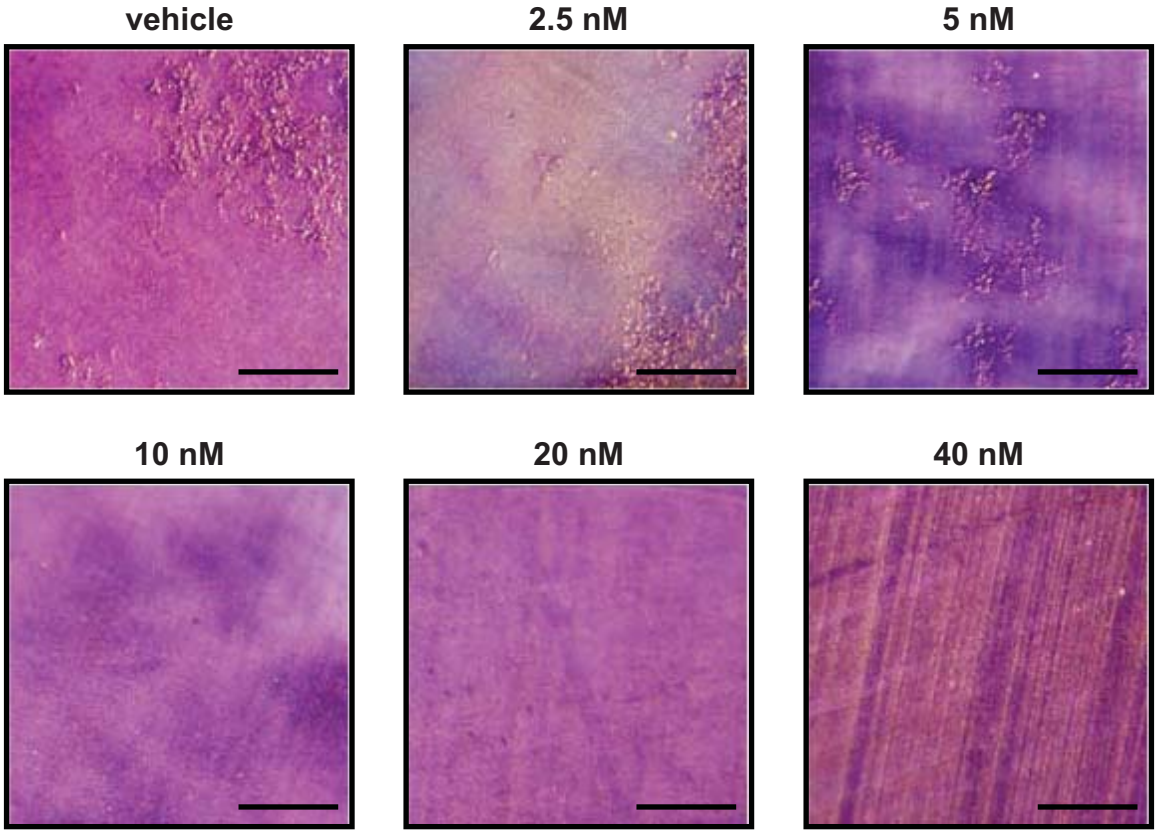
vehicle
2.5 nM
5 nM
10 nM
20 nM
40 nM

mBM osteoclast-mediated bone resorption at concentrations exceeding 1 μM imatinib and 10 nM dasatinib (figure 5.9A,B).

5.2.3 Inhibition of Fms contributes to the anti-osteoclastogenic effects of imatinib and dasatinib *in vitro*

5.2.3.1 M-CSF-dependent survival/proliferation of mBM and rBM cells is inhibited by treatment with imatinib and dasatinib

The importance of M-CSF in the survival of osteoclasts and osteoclast precursors *in vitro* suggested that imatinib and dasatinib may inhibit osteoclastogenesis through inhibition of the M-CSF receptor, Fms. To examine whether imatinib and dasatinib inhibits Fms-dependent cell survival, the effect of imatinib and dasatinib on mBM and rBM cell survival/proliferation was examined. mBM cells were cultured in media containing rhM-CSF and rhRANKL or rhM-CSF alone for 3 days with vehicle, imatinib or dasatinib and the relative number of cells per well was determined via the WST-1 assay. There was no significant difference in the relative number of cells per well in mBM cultures treated with either rhM-CSF alone or rhM-CSF with rhRANKL for 3 days. Addition of 1 μM imatinib and greater significantly decreased the relative number of cells per well in mBM cultures treated with rhM-CSF alone or with rhM-CSF and rhRANKL (figure 5.10A). Dasatinib treatment significantly decreased cell proliferation/survival at concentrations of 2.5 nM and higher in rhM-CSF-treated or rhM-CSF- and rhRANKL-treated mBM cultures (figure 5.10A). In rhM-CSF-stimulated rBM cells, imatinib (0.25 – 4 μM) dose-dependently decreased cell numbers relative to controls after 72 hours (figure 5.10B). Treatment of rhM-CSF-stimulated rBM cells with dasatinib significantly inhibited cell survival/proliferation at concentrations of 2.5 nM and higher (figure 5.10B).

In contrast to the growth inhibitory effects observed in mBM and rBM cultures, the proliferation of the mouse monocyte/macrophage cell line RAW 264.7, which is not dependent on M-CSF for cell survival, was not affected by therapeutically-achievable concentrations of imatinib or dasatinib (figure 5.11A,B). RAW 264.7 cells were treated with imatinib, dasatinib or vehicle for 3 days in complete α-MEM and the WST-1 assay was carried out. While treatment of RAW 264.7 cells with 10 μM imatinib was toxic, imatinib had no effect on cell number at therapeutically-relevant concentrations (up to 5 μM). Dasatinib had no effect on RAW 264.7 cell proliferation/survival at concentrations up to 80 nM ($p = 0.49$; figure 5.11B).

Figure 5.9. Imatinib and dasatinib inhibit dentine resorption by mBM cells *in vitro*. mBM cells were cultured at 3.13 x 10^5 cells/cm^2 on dentine slices in c-α-MEM containing 75 ng/mL rhM-CSF. Following overnight adhesion, the medium was replaced with c-α-MEM containing rhM-CSF (75 ng/mL) and rhRANKL (75 ng/mL) supplemented with imatinib, dasatinib or 0.05% DMSO vehicle. After 9 days of treatment, the area of the dentine was stained with toluidine blue and resorption lacunae was calculated. Graphs depict mean ± SEM of triplicate wells of 1 experiment for imatinib (**A**) and dasatinib (**B**). * $p < 0.05$ relative to vehicle control (one-way ANOVA with Dunnett's post-tests).

A

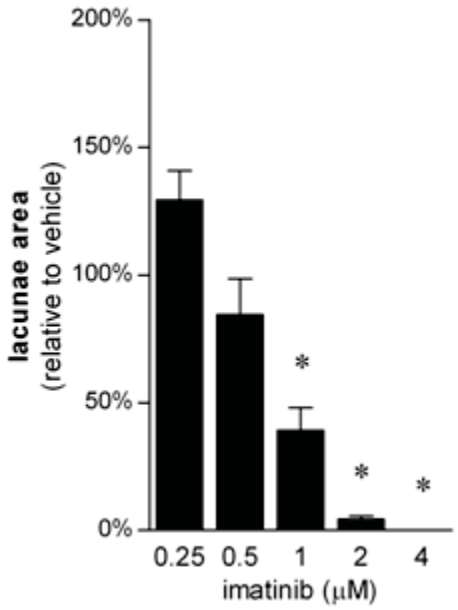
200%
150%
100%
50%
0%
lacunae area
(relative to vehicle)
*
*
*
0.25
0.5
1
2
4
imatinib (μM)

B

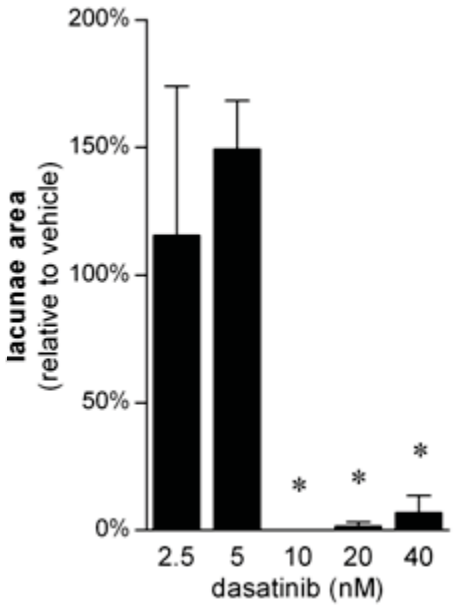
200%
150%
100%
50%
0%
lacunae area
(relative to vehicle)
*
*
*
2.5
5
10
20
40
dasatinib (nM)

Figure 5.10. Imatinib and dasatinib treatment decreases cell numbers in mBM and rBM cultures *in vitro*. mBM (**A**) or rBM (**B**) were seeded at 3.13 x 10^5 cells/cm^2 in 96-well plates in c-α-MEM containing rhM-CSF (75 ng/mL) and were incubated overnight to allow the cells to adhere. The cells were then treated with imatinib, dasatinib or vehicle (0.05% DMSO) in media containing rhM-CSF (75 ng/mL) with or without rhRANKL (75 ng/mL), as indicated. Following 3 days of treatment, relative viable cell number per well was assayed using WST-1. Graphs depict mean ± SEM of 3 experiments (**A**) or mean ± range of 2 experiments (**B**). * $p < 0.05$ relative to vehicle control (one-way ANOVA with Dunnett's post-tests).

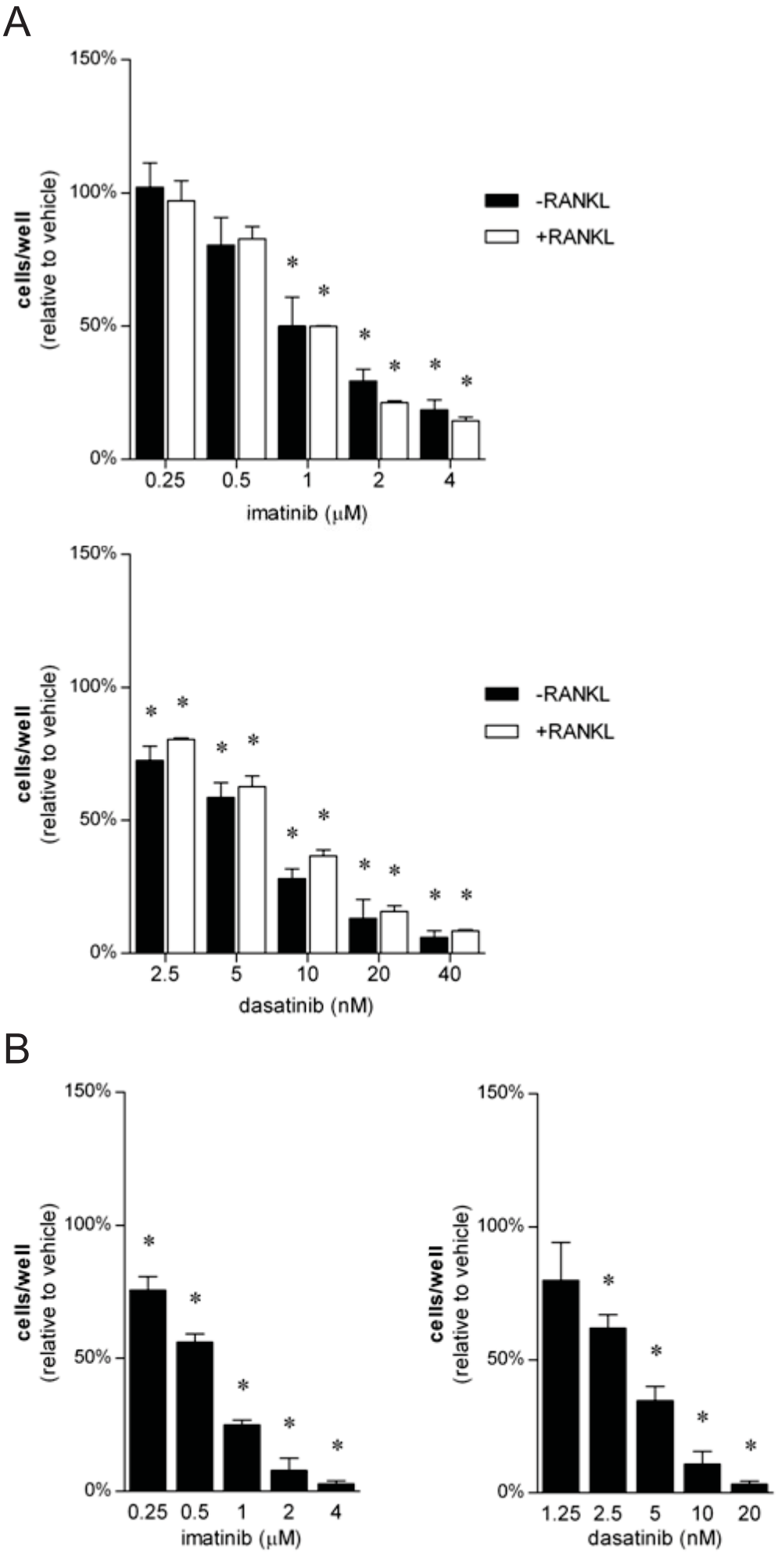
A
150%
100%
50%
0%
cells/well
(relative to vehicle)
-RANKL
+RANKL
0.25
0.5
1
2
4
imatinib (μM)
2.5
5
10
20
40
dasatinib (nM)
B
1.25

Figure 5.11. Therapeutically-achievable concentrations of imatinib and dasatinib have no effect on cell numbers in RAW 264.7 cultures *in vitro*. RAW 264.7 cells were cultured at 9.38 x 10^3 cells/cm^2 in 96-well plates in c-DMEM. Following overnight adhesion, the medium was replaced with c-DMEM containing imatinib (**A**) or dasatinib (**B**) (containing 0.05% DMSO vehicle) or vehicle alone. Following 3 days of treatment, relative viable cell number per well was assayed using the WST-1 assay. Graphs depict mean ± range of 2 independent experiments. * $p < 0.05$ relative to vehicle control (one-way ANOVA with Dunnett's post-tests).

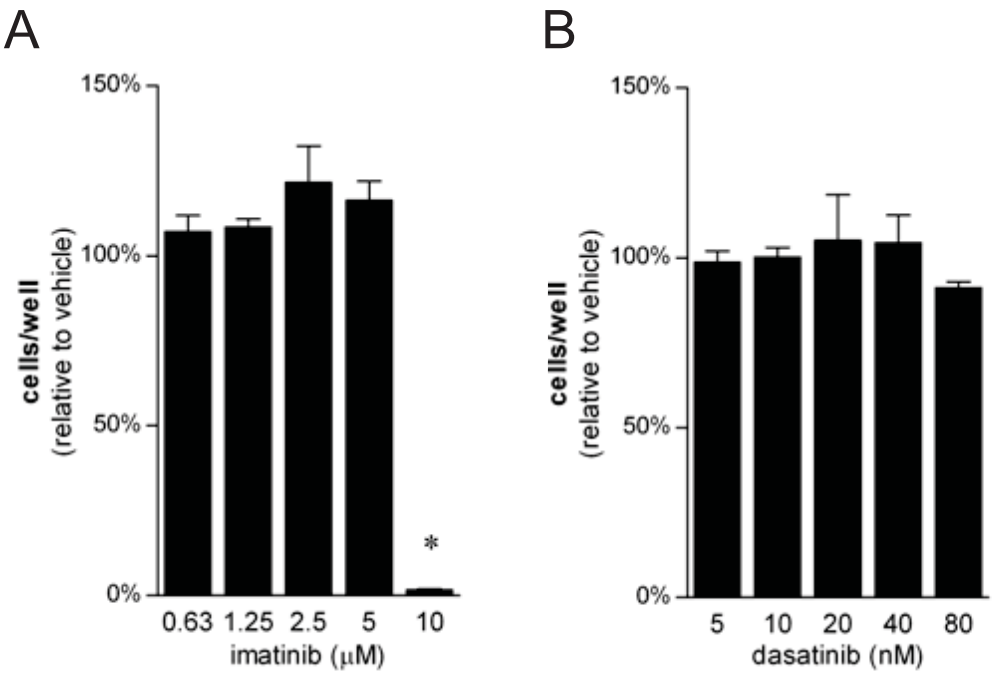
A
150%
100%
50%
0%
cells/well
(relative to vehicle)
*
0.63 1.25 2.5 5 10
imatinib (μM)
B
150%
100%
50%
0%
cells/well
(relative to vehicle)
5 10 20 40 80
dasatinib (nM)

5.2.3.2 Activation of Fms is inhibited by treatment with imatinib and dasatinib in mBM and rBM cells

To determine whether dasatinib, like imatinib, can inhibit signal transduction through Fms, the effect of imatinib and dasatinib on Fms phosphorylation was examined in murine monocyte/macrophage-lineage cells. mBM and rBM cultures were serum-starved in media containing imatinib, dasatinib or vehicle for 2 hours prior to stimulation with rhM-CSF for 5 minutes to activate the Fms receptor. Cell lysates were then subjected to Western blotting and phosphorylated Fms and total Fms proteins were detected with specific antibodies.

Binding of M-CSF to its receptor, Fms, induces dimerisation, trans-autophosphorylation at several intracellular tyrosine residues and binding of cofactors that initiate specific signalling cascades.[255,256,397,404,405] The activated receptor is then endocytosed, ubiquitinated and degraded.[404] Starved mBM and rBM cells that were not stimulated with rhM-CSF showed a complete lack of Fms phosphorylation (figure 5.12, 5.13). In contrast, rhM-CSF-stimulated cultures showed rapid induction of Fms phosphorylation and an increase in the amount of ubiquitinated Fms protein. Pre-treatment of cultures with imatinib inhibited the rhM-CSF-induced Fms phosphorylation at approximately 1 μM imatinib and greater in both mBM and rBM (figure 5.12A,B). Pre-incubation of mBM and rBM cells with dasatinib inhibited rhM-CSF-induced Fms phosphorylation at concentrations of approximately 5 nM and higher (figure 5.13A,B).

5.2.3.3 Sigmoidal dose-response relationship of the inhibition of osteoclastogenesis, M-CSF-dependent cell proliferation/survival and Fms activation **in vitro**

The relationship between the concentrations at which imatinib and dasatinib inhibit osteoclast formation, cell proliferation/survival and Fms signal transduction was investigated by fitting the data to a sigmoidal dose-response curve (figure 5.14A,B).

There was close agreement between the concentrations at which imatinib decreased osteoclast formation, cell numbers and Fms phosphorylation. In mBM cultures, the concentrations of imatinib required to inhibit cell proliferation, osteoclast formation and osteoclast activity by 50% (IC_{50}) were 1.16 μM, 1.46 μM and 0.72 μM, respectively, whilst the IC_{50} for Fms phosphorylation was 1.29 μM imatinib (figure 5.14A). For rBM cells, the IC_{50} for the effects of imatinib on osteoclast formation, osteoclast activity, cell proliferation and Fms activation were 0.53 μM, 0.69 μM, 0.50 μM and 0.55 μM, respectively (figure 5.14A).

Figure 5.12. Imatinib inhibits the M-CSF-induced phosphorylation of Fms in murine bone marrow cultures. mBM (**A**,**B**) or rBM (**C**,**D**) were cultured at 3.13 x 10^5 cells/cm^2 in 60 mm dishes with rhM-CSF (75 ng/mL) for seven days. The cells were starved in sf-α-MEM containing imatinib or vehicle (V; 0.05% DMSO) for 120 minutes prior to stimulation with rhM-CSF (75 ng/mL) for 5 minutes. Cell lysates (75 μg/lane) were resolved on 8% polyacrylamide SDS-PAGE gels, transferred to PVDF and were probed with a specific antibody to phosphorylated Fms (p-Fms) or total Fms. Blots from a representative experiment are shown (n = 2) for mBM (**A**) and rBM (**C**). **I**. ubiquitinated Fms receptor; **II**. mature, hyper-glycosylated Fms receptor; **III**. hypo-glycosylated Fms precursor. Graphs depict the p-Fms band intensity, normalised to total Fms, for mBM (**B**) and rBM (**D**).

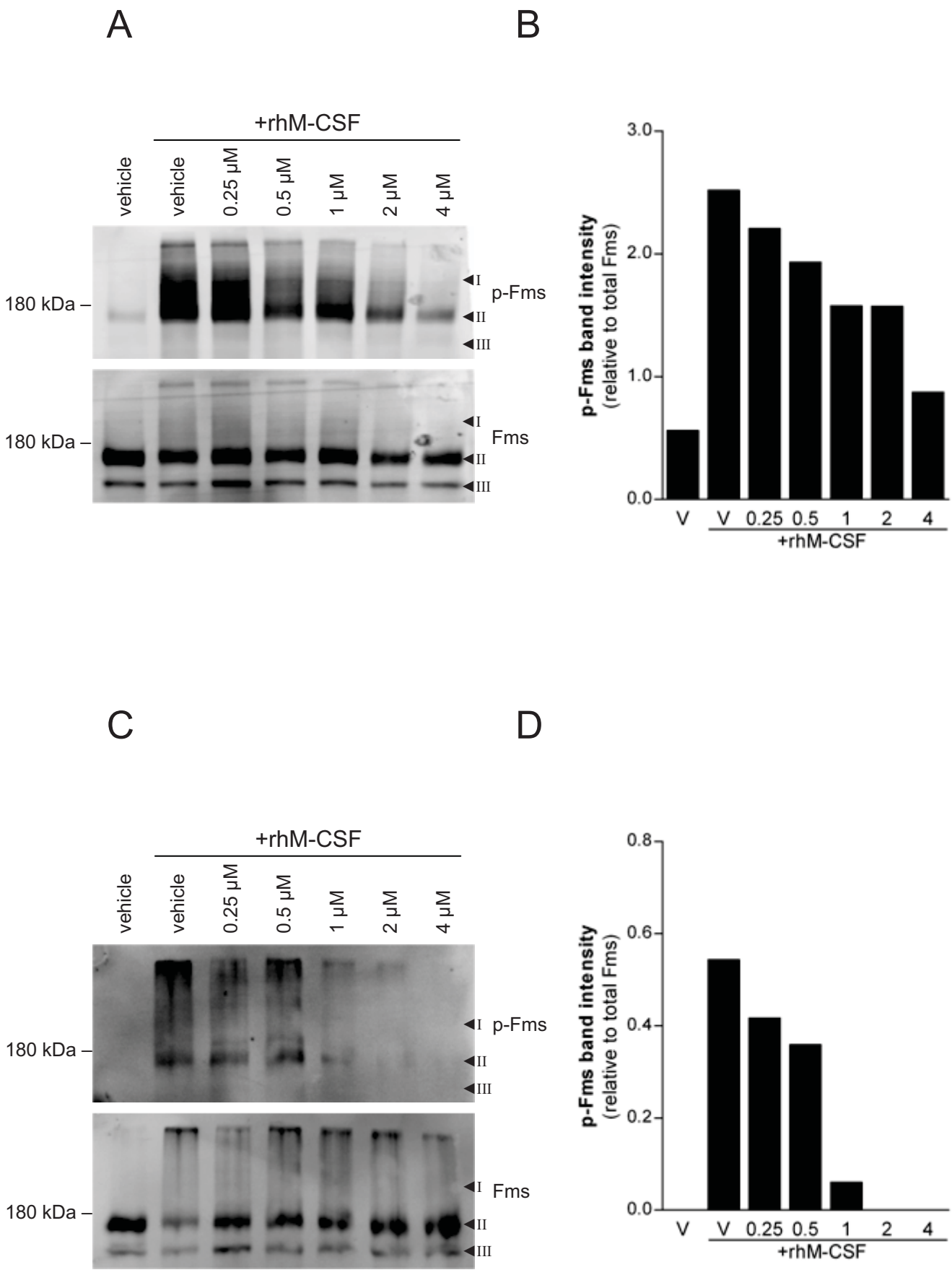
A
+rhM-CSF
vehicle
vehicle
0.25 μM
0.5 μM
1 μM
2 μM
4 μM
180 kDa –
I
II
III
p-Fms
180 kDa –
I
II
III
Fms
B
p-Fms band intensity
(relative to total Fms)
3.0
2.0
1.0
0.0
V
V
0.25
0.5
1
2
4
+rhM-CSF
C
+rhM-CSF
vehicle
vehicle
0.25 μM
0.5 μM
1 μM
2 μM
4 μM
180 kDa –
I
II
III
p-Fms
180 kDa –
I
II
III
Fms
D
p-Fms band intensity
(relative to total Fms)
0.8
0.6
0.4
0.2
0.0
V
V
0.25
0.5
1
2
4
+rhM-CSF

Figure 5.13. Dasatinib inhibits the M-CSF-induced phosphorylation of Fms in mBM and rBM cells. Murine bone marrow cells were cultured at 3.13 x 10^5 cells/cm^2 in 60 mm dishes with rhM-CSF (75 ng/mL) for seven days. The cells were starved in sf-α-MEM containing imatinib, dasatinib or vehicle (V; 0.05% DMSO) for 120 minutes prior to stimulation with rhM-CSF (75 ng/mL) for 5 minutes. Cell lysates (75 μg/lane) were resolved on 8% polyacrylamide SDS-PAGE gels, transferred to PVDF and were probed with a specific antibody to phosphorylated Fms (p-Fms) or total Fms. Blots from a representative experiment are shown (n = 2) for mBM (**A**) and rBM (**C**). **I**. ubiquitinated Fms receptor; **II**. mature, hyper-glycosylated Fms receptor; **III**. hypo-glycosylated Fms precursor. Graphs depict the p-Fms band intensity, normalised to total Fms, for mBM (**B**) and rBM (**D**).

A

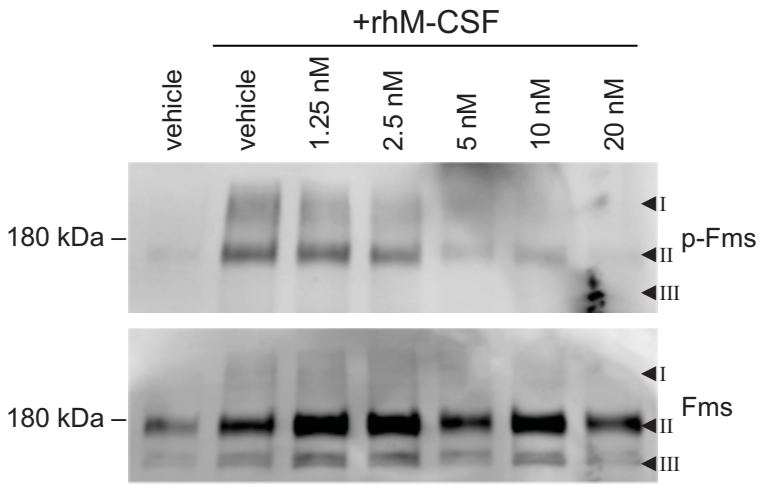
+rhM-CSF
vehicle
vehicle
1.25 nM
2.5 nM
5 nM
10 nM
20 nM
180 kDa –
I
II
III
p-Fms
180 kDa –
I
II
III
Fms

B

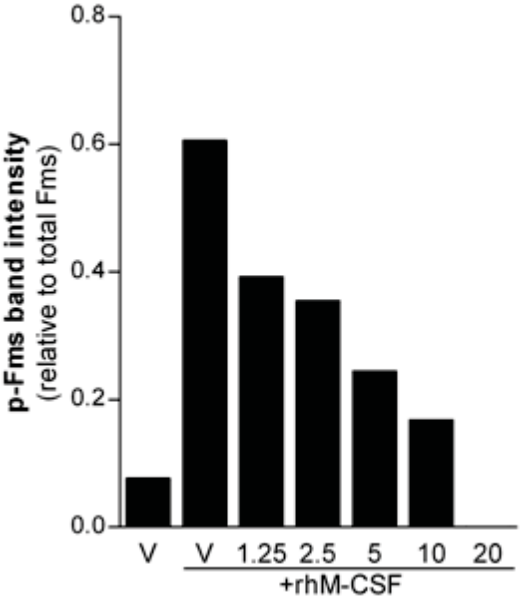
p-Fms band intensity
(relative to total Fms)
0.8
0.6
0.4
0.2
0.0
V
V
1.25
2.5
5
10
20
+rhM-CSF

C

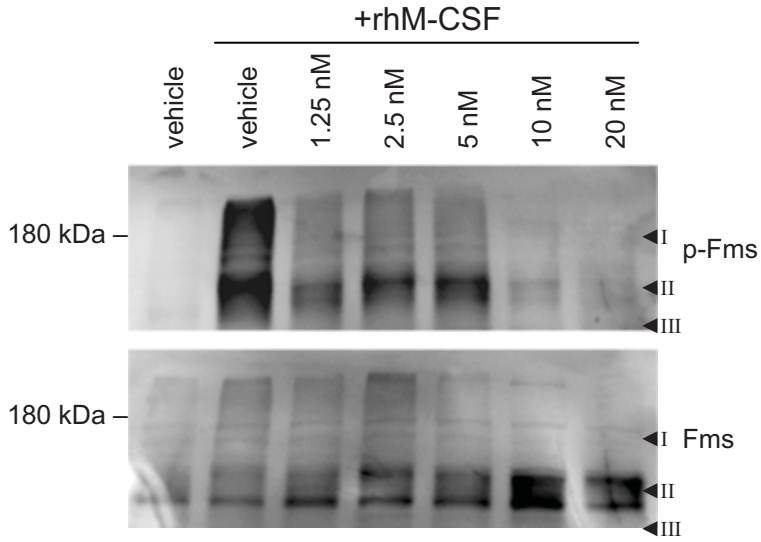
+rhM-CSF
vehicle
vehicle
1.25 nM
2.5 nM
5 nM
10 nM
20 nM
180 kDa –
I
II
III
p-Fms
180 kDa –
I
II
III
Fms

D

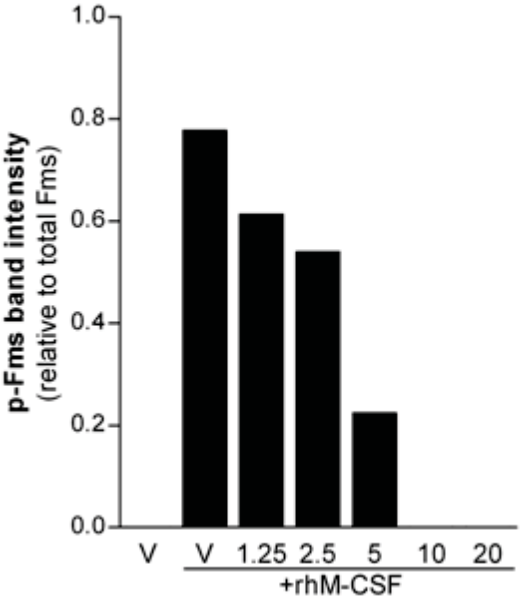
p-Fms band intensity
(relative to total Fms)
1.0
0.8
0.6
0.4
0.2
0.0
V
V
1.25
2.5
5
10
20
+rhM-CSF

Figure 5.14. Sigmoidal curve fit of the inhibitory effects of imatinib and dasatinib of cell proliferation/survival, osteoclastogenesis and Fms phosphorylation. Data for the inhibitory effects of imatinib (**A**) and dasatinib (**B**) on cell survival/proliferation (WST-1), osteoclast formation and activity and M-CSF-induced Fms phosphorylation were plotted to obtain a sigmoidal dose-response curve fits, as shown for mBM (solid lines) and rBM (dashed lines).

A

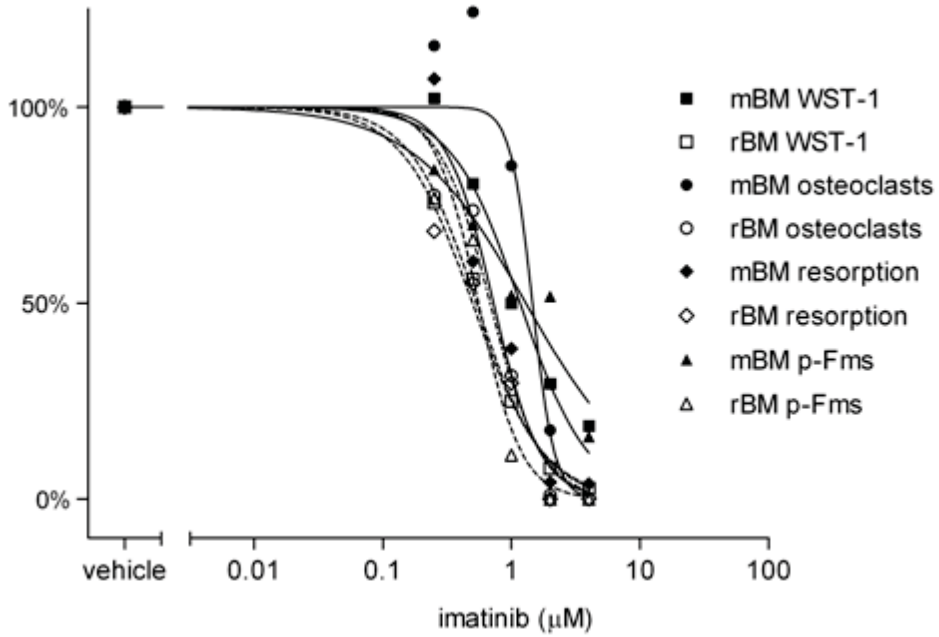
100%
50%
0%
vehicle
0.01
0.1
1
10
100
imatinib (μM)
mBM WST-1
rBM WST-1
mBM osteoclasts
rBM osteoclasts
mBM resorption
rBM resorption
mBM p-Fms
rBM p-Fms

B

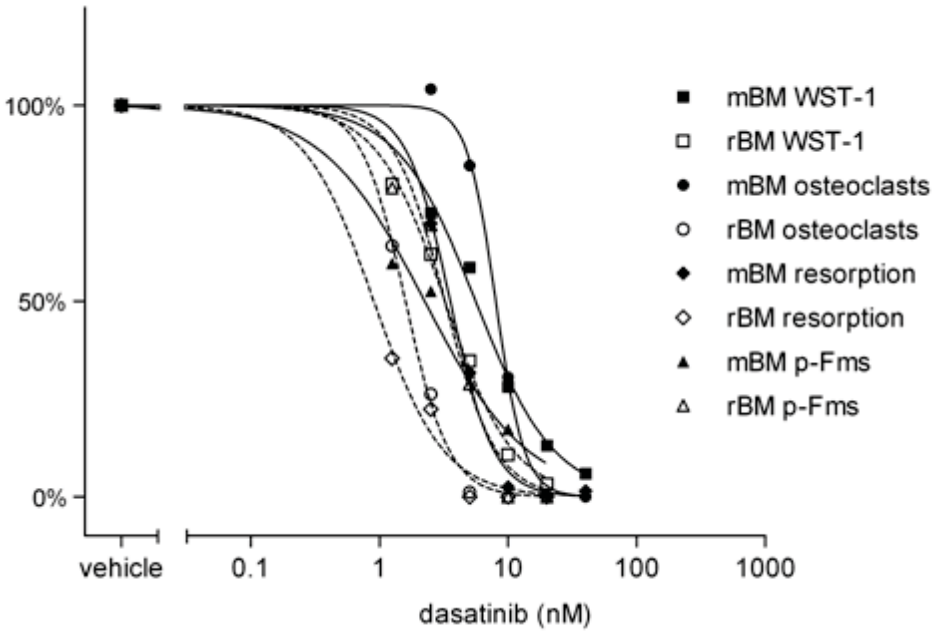
100%
50%
0%
vehicle
0.1
1
10
100
1000
dasatinib (nM)
mBM WST-1
rBM WST-1
mBM osteoclasts
rBM osteoclasts
mBM resorption
rBM resorption
mBM p-Fms
rBM p-Fms

Similarly, dasatinib inhibited osteoclast formation, osteoclast activity, cell survival and Fms activation at similar concentrations in mBM cells, with IC_{50} of 8.00 nM, 3.55 nM, 5.58 nM and 2.24 nM, respectively (figure 5.14B). In dasatinib-treated rBM cultures, the IC_{50} for osteoclast numbers, osteoclast formation, cell numbers and Fms phosphorylation were 1.59 nM, 0.90 nM, 3.23 nM and 3.23 nM, respectively (figure 5.14B).

5.2.3.4 The effects of imatinib and dasatinib on Fms-independent osteoclastogenesis in vitro

While these results suggest that that there is an association between the inhibition of Fms by imatinib and dasatinib and the inhibition of osteoclast formation by these compounds, these inhibitors may also affect osteoclastogenesis through inhibition of other tyrosine kinases. To determine whether imatinib and dasatinib can affect osteoclastogenesis via Fms-independent mechanisms, the RAW 264.7 cell line was utilised.

RAW 264.7 cells were cultured in media supplemented with rhRANKL and imatinib, dasatinib or vehicle for 4 days, after which time the cells were fixed, stained for TRAP and the number of osteoclast-like cells per well was enumerated. In vehicle-treated wells, RAW 264.7 cells formed 210.28 ± 12.39 multinucleated TRAP-positive osteoclast-like cells per well (figure 5.15). In contrast to the effects of imatinib on osteoclast formation and activity in primary murine cells, treatment with imatinib increased osteoclast formation in RAW 264.7 cells (figure 5.15A, 5.16A). The addition of 1.25, 2.5 or 5 μM imatinib to these cultures induced a greater than 2.5-fold increase in the number of osteoclasts formed per well (figure 5.16A). In addition, the osteoclasts formed in the presence of 2.5 and 5 μM imatinib were substantially larger than those formed in wells treated with vehicle alone (figure 5.15A). In cultures treated with 10 μM imatinib, no cells were present (figure 5.15A, 5.16A), an observation which is consistent with WST-1 data suggesting that 10 μM imatinib is toxic to RAW 264.7 cells (figure 5.11A).

In RAW 264.7 cultures established on calcium phosphate-coated slides, treatment with imatinib increased the area of the mineral layer absorbed (figure 5.17A, 5.18A). Treatment with 2.5 and 5 μM imatinib significantly increased the resorptive activity of the cultured RAW 264.7 osteoclasts (figure 5.18A).

In contrast, dasatinib dose-dependently inhibited the formation of osteoclasts in RAW 264.7 cultures (figure 5.15B, 5.16B), in the absence of any effect on cell numbers (figure 5.11B). Treatment with 20 nM dasatinib and higher significantly decreased the formation of multinucleated osteoclasts, with no osteoclast formation occurring in cultures

Figure 5.15. **The effects of protein tyrosine kinase inhibitors on osteoclast-like cell formation in RAW 264.7 cultures *in vitro*. A.** RAW 264.7 cells were cultured at 9.38 x 10^3 cells/cm^2 in 96-well plates in c-DMEM containing 100 ng/mL rhRANKL. Following overnight adhesion, the medium was replaced with c-DMEM containing rhRANKL (100 ng/mL), with imatinib (**A**) or dasatinib (**B**) (containing 0.05% DMSO vehicle) or vehicle alone. Following 3 days of treatment, cells were stained for TRAP and wells were photographed at 20 x magnification. Representative images are shown for cultures treated with imatinib (**A**) and dasatinib (**B**). Bar: 200 μm.

A

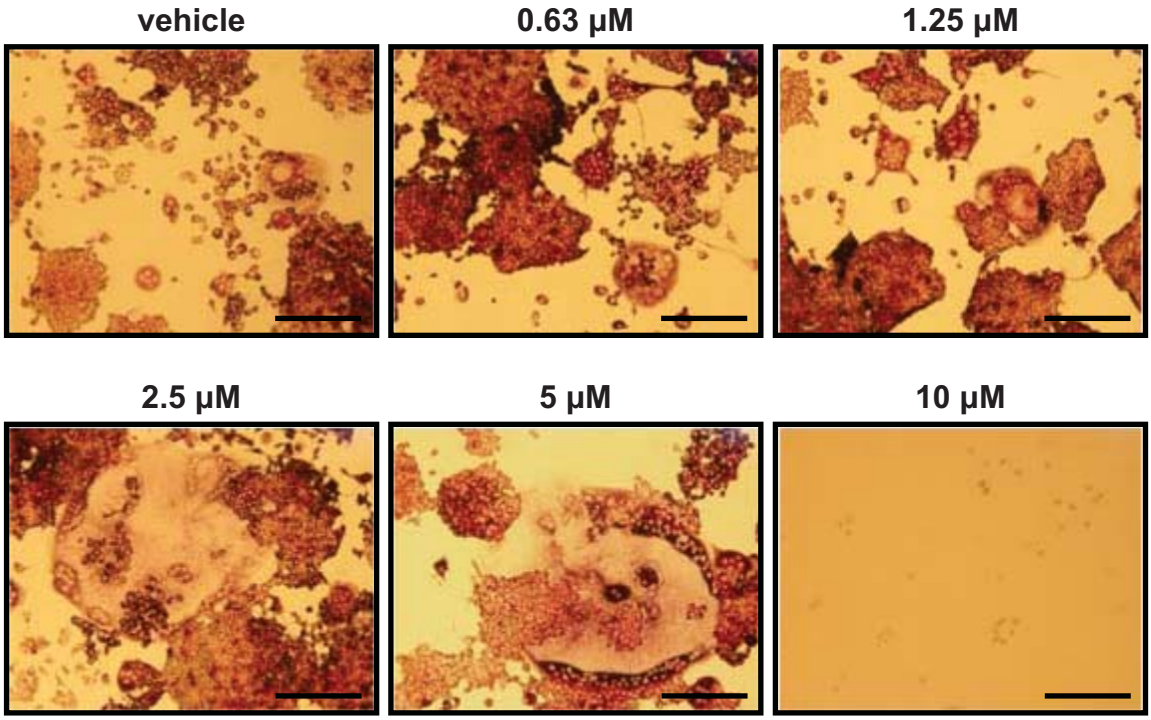
vehicle
0.63 μM
1.25 μM
2.5 μM
5 μM
10 μM

B

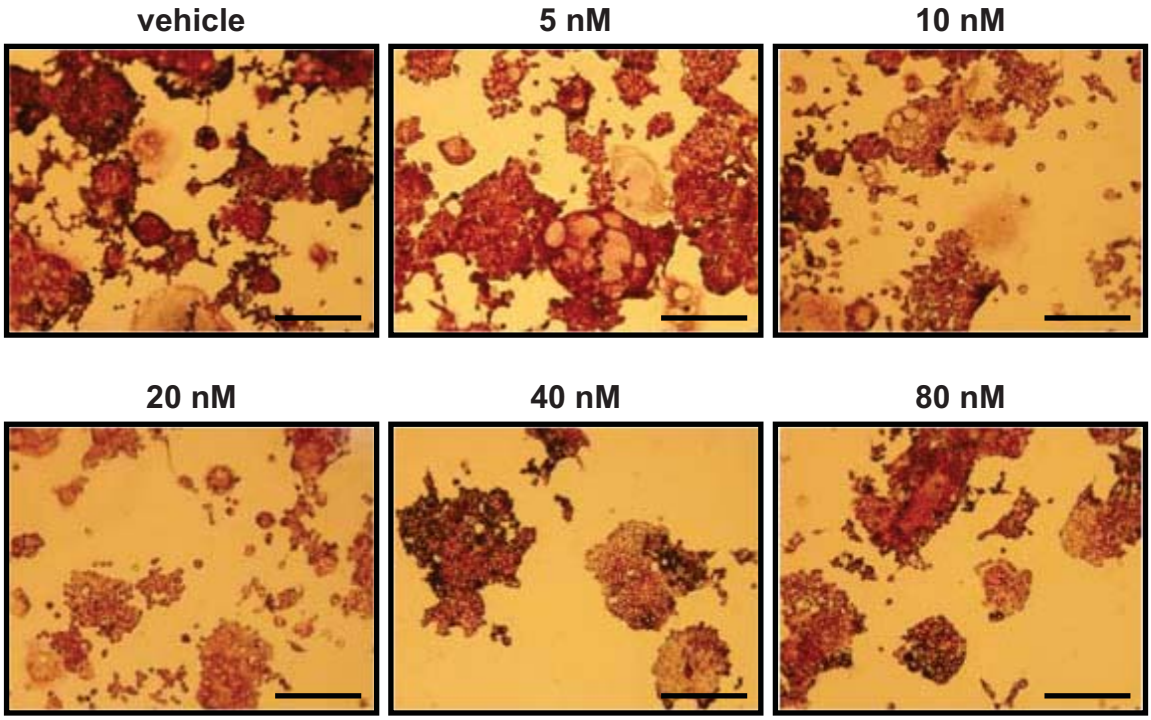
vehicle
5 nM
10 nM
20 nM
40 nM
80 nM

Figure 5.16. Imatinib and dasatinib affect osteoclast formation in RAW 264.7 cultures *in vitro*. RAW 264.7 cells were treated with containing rhRANKL (100 ng/mL) and imatinib (**A**) or dasatinib (**B**) (containing 0.05% DMSO vehicle) or vehicle alone, as described in Figure 5.13. Following 3 days of treatment, cells were stained for TRAP and TRAP-positive cells with 3 or more nuclei were counted. Graphs depict mean ± range of 2 independent experiments. * $p < 0.05$ relative to vehicle control (one-way ANOVA with Dunnett's post-tests).

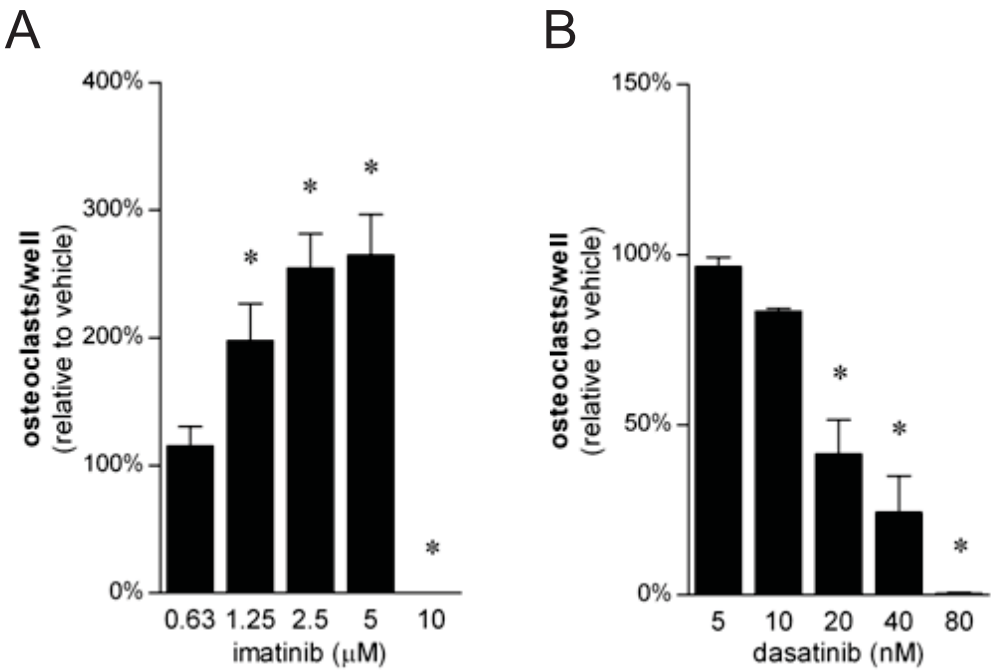
A
400%
300%
200%
100%
0%
osteoclasts/well
(relative to vehicle)
*
*
*
*
0.63
1.25
2.5
5
10
imatinib (μM)
B
150%
100%
50%
0%
osteoclasts/well
(relative to vehicle)
*
*
*
5
10
20
40
80
dasatinib (nM)

Figure 5.17. The effects of protein tyrosine kinase inhibitors on osteoclastic resorption in RAW 264.7 cultures *in vitro*. RAW 264.7 cells were cultured at 9.38×10^3 cells/cm^2 on calcium phosphate-coated slides in c-DMEM containing 100 ng/mL rhRANKL. Following overnight adhesion, the medium was replaced with c-DMEM containing rhRANKL (100 ng/mL) and imatinib (**A**) or dasatinib (**B**) or vehicle alone. After 5 days of treatment, the mineral was stained with von Kossa silver stain and the wells were photographed at 0.8 x magnification. Representative wells from 1 of 2 experiments are shown. Bar: 2.5 mm.

A

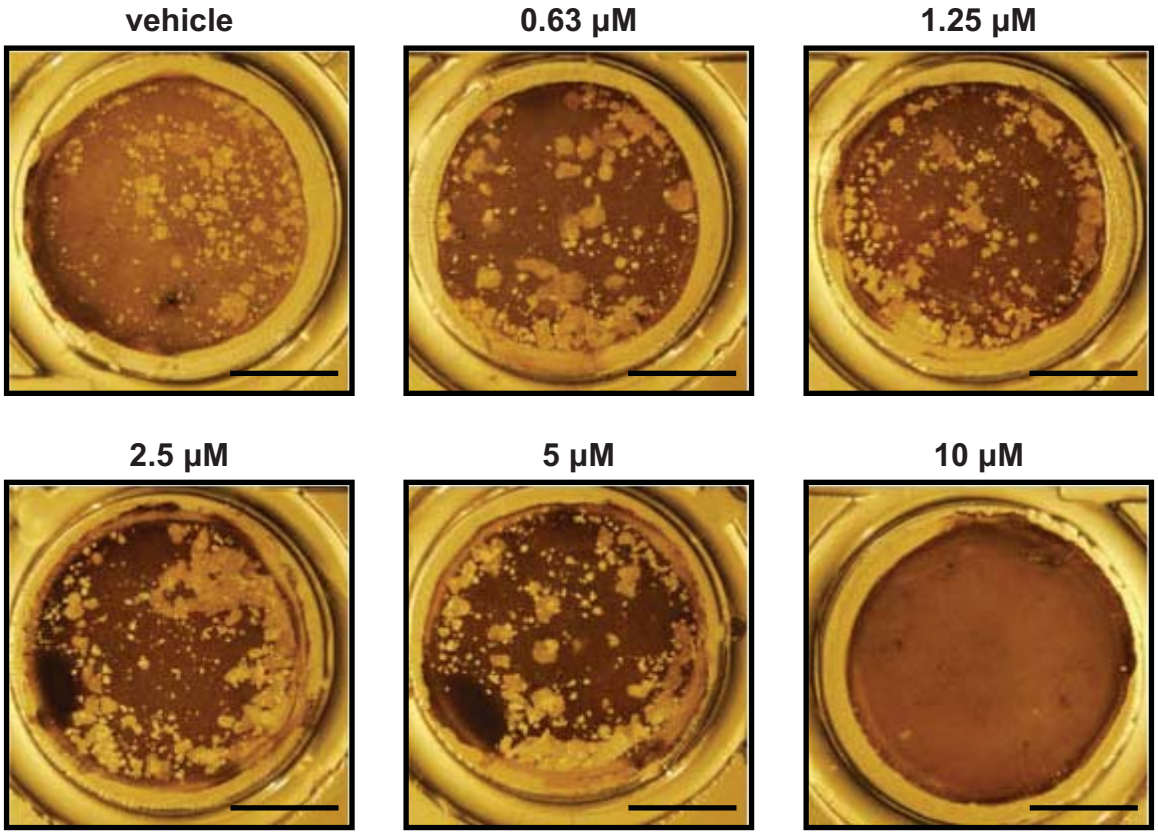
vehicle
0.63 µM
1.25 µM
2.5 µM
5 µM
10 µM

B

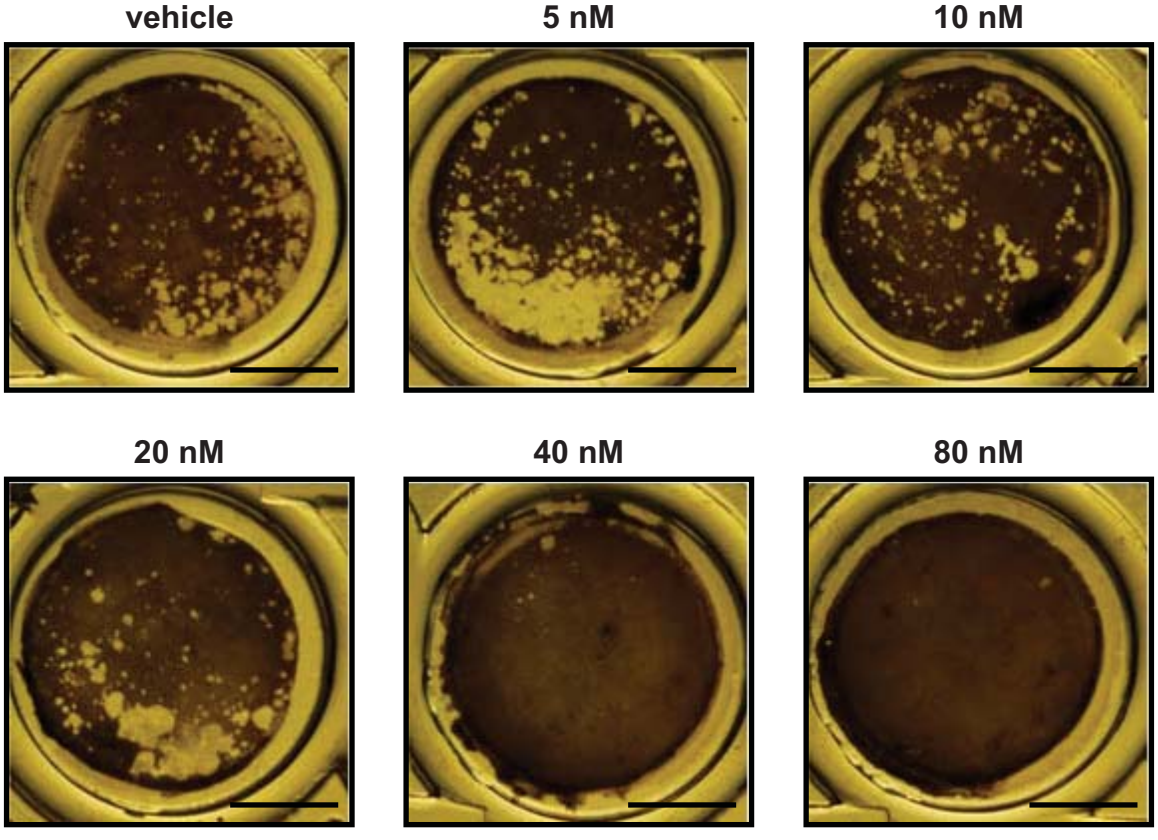
vehicle
5 nM
10 nM
20 nM
40 nM
80 nM

Figure 5.18. The effects of protein tyrosine kinase inhibitors on resorption in RAW 264.7 cultures *in vitro*. RAW 264.7 cells were on calcium phosphate-coated slides in c-DMEM containing 100 ng/mL rhRANKL. Following overnight adhesion, the medium was replaced with c-DMEM containing rhRANKL (100 ng/mL) and imatinib (**A**) or dasatinib (**B**) or vehicle alone. After 5 days of treatment, the area of substrate resorbed was calculated. Graphs depict mean ± range of 2 independent experiments. * $p < 0.05$ relative to vehicle control (one-way ANOVA with Dunnett's post-tests).

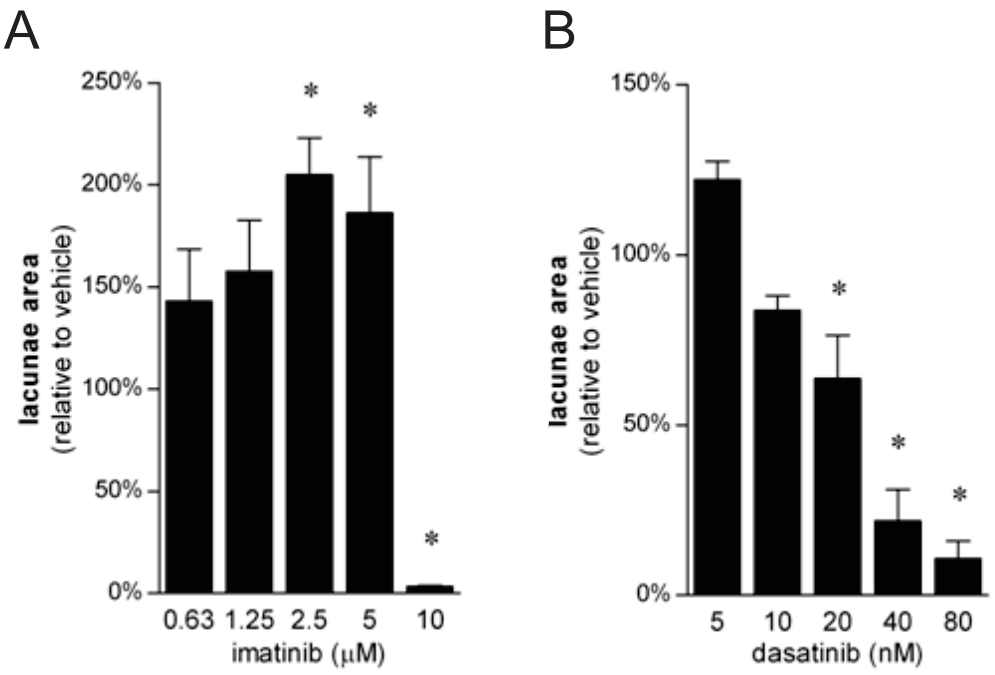
A
250%
200%
150%
100%
50%
0%
lacunae area
(relative to vehicle)
*
*
*
0.63 1.25 2.5 5 10
imatinib (μM)
B
150%
100%
50%
0%
lacunae area
(relative to vehicle)
*
*
*
5 10 20 40 80
dasatinib (nM)

treated with 80 nM dasatinib (figure 5.16B). Similarly, the resorptive activity of RAW 264.7 cells cultured on calcium-phosphate-coated slides was significantly decreased by concentrations of 20 nM dasatinib or more (figure 5.17B, 5.18B).

5.2.4 Inhibition of Src may contribute to the Fms-independent effects of dasatinib on osteoclastogenesis

5.2.4.1 Dasatinib inhibits basal levels of Src phosphorylation

The inhibitory effects of dasatinib on osteoclast formation in RAW 264.7 cultures suggest that dasatinib may inhibit osteoclastogenesis through Fms-independent mechanisms. To examine whether inhibition of Src may contribute to the inhibition of osteoclastogenesis by dasatinib, the concentration at which dasatinib inhibited Src activity in mBM, rBM and RAW 264.7 cells was determined. Cells were serum-starved in the presence of imatinib, dasatinib or vehicle for 2 hours. Cell lysates were subjected to Western blotting and proteins were detected with specific antibodies against total HSP90 or Src phosphorylated at Tyr416.

Starved cells incubated with vehicle alone exhibited basal Src phosphorylation (figure 5.19A–F). Dasatinib treatment dose-dependently decreased basal levels of Src phosphorylation at concentrations of 20 nM and higher in mBM, rBM and RAW 264.7 (figure 5.19A–F).

5.2.4.2 Sigmoidal dose-response relationship of the inhibition of osteoclastogenesis and Src activation in vitro

The relationship between the concentrations at which dasatinib inhibits osteoclast formation and Src phosphorylation was investigated by fitting the data to a sigmoidal dose-response curve (figure 5.20).

The concentration at which dasatinib inhibited Src phosphorylation was 5-fold higher (mBM) and 40-fold higher (rBM) that that was required to inhibit osteoclast activity (figure 5.20). Dasatinib inhibited Src phosphorylation at IC_{50} of 17.15 nM and 35.61 nM in mBM and rBM, respectively (figure 5.20), whereas osteoclast activity in mBM and rBM cultures was inhibited at an IC_{50} of 3.55 nM and 0.90 nM, respectively (figure 5.14B). In contrast, in RAW 264.7 cultures, dasatinib inhibited osteoclast formation and activity and Src activation at similar concentrations (IC_{50} = 19.08 nM, 24.78 nM and 32.02 nM, respectively; figure 5.20).

Figure 5.19. Dasatinib inhibits basal Src phosphorylation in mBM, rBM and RAW 264.7 cultures. mBM (**A**,**B**) or rBM (**C**,**D**) were cultured at 3.13 x 10^5 cells/cm^2 with 75 ng/mL rhM-CSF for 7 days. The cells were starved in sf-α-MEM containing dasatinib or vehicle (V; 0.05% DMSO) for 120 minutes prior to lysis in non-reducing lysis buffer. RAW 264.7 cells (**E**,**F**) were cultured at 9.38 x 10^3 cells/cm^2 in 6-well plates in c-DMEM. Following overnight adhesion, the cells were serum starved in sf-DMEM overnight. The cells were then treated with dasatinib or vehicle for 120 minutes. Cell lysates (30 μg/lane) were resolved on a 10% polyacrylamide SDS-PAGE gel, transferred to PVDF membrane and the membrane was probed with antibodies against phosphorylated Src (p-Src) or HSP90. Representative immunoblots are shown (**A**,**C**,**E**). Graphs depict the p-Src band intensity, normalised to HSP90, of a representative of 2 experiments.

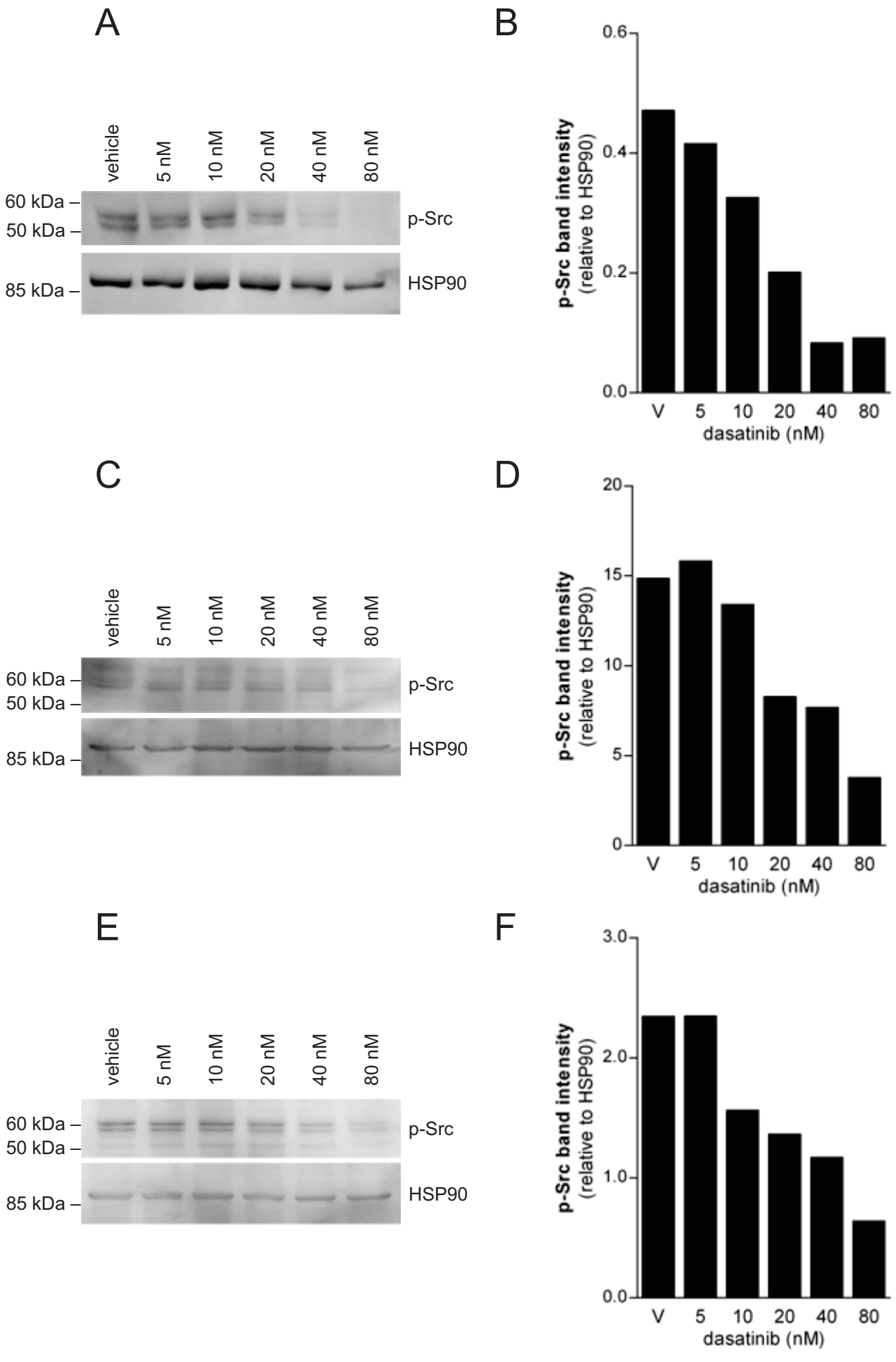
A
vehicle
5 nM
10 nM
20 nM
40 nM
80 nM
60 kDa
50 kDa
85 kDa
p-Src
HSP90
B
p-Src band intensity
(relative to HSP90)
0.6
0.4
0.2
0.0
V
5
10
20
40
80
dasatinib (nM)
C
vehicle
5 nM
10 nM
20 nM
40 nM
80 nM
60 kDa
50 kDa
85 kDa
p-Src
HSP90
D
p-Src band intensity
(relative to HSP90)
20
15
10
5
0
V
5
10
20
40
80
dasatinib (nM)
E
vehicle
5 nM
10 nM
20 nM
40 nM
80 nM
60 kDa
50 kDa
85 kDa
p-Src
HSP90
F
p-Src band intensity
(relative to HSP90)
3.0
2.0
1.0
0.0
V
5
10
20
40
80
dasatinib (nM)

Figure 5.20. Sigmoidal curve fit of the inhibitory effects of dasatinib on osteoclastogenesis and basal Src phosphorylation in RAW 264.7, mBM and rBM cultures. Mean values for the inhibitory effects of dasatinib on osteoclast formation and activity and basal Src phosphorylation were plotted to obtain sigmoidal dose-response curve fits, as shown for mBM (solid lines), rBM (dashed lines) or RAW 264.7 (dotted lines).

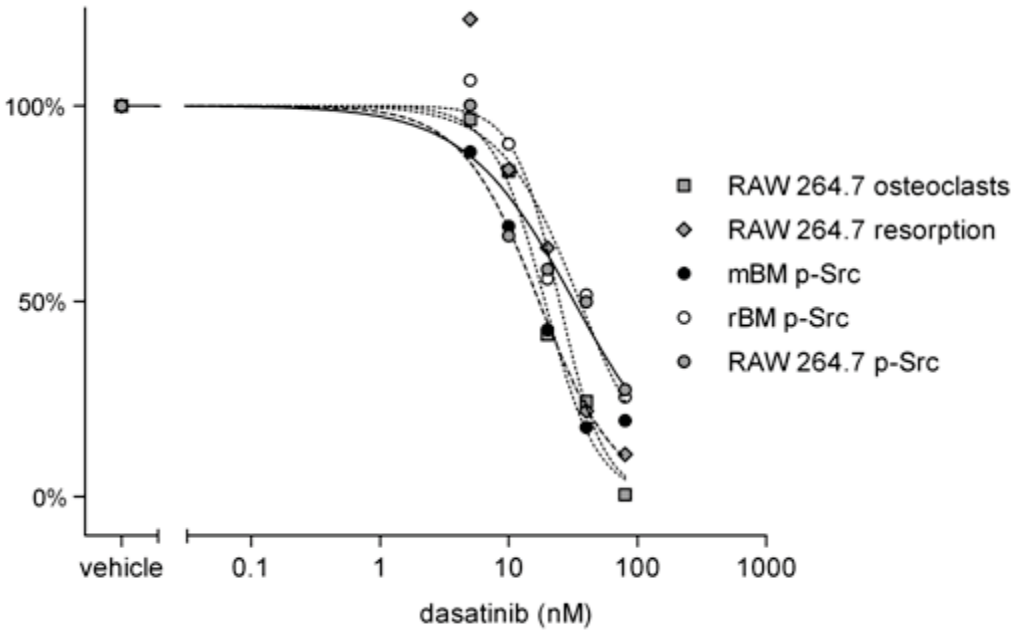
100%
50%
0%
vehicle
0.1
1
10
100
1000
dasatinib (nM)
RAW 264.7 osteoclasts
RAW 264.7 resorption
mBM p-Src
rBM p-Src
RAW 264.7 p-Src

5.2.4.3 The Src inhibitor PP2 inhibits osteoclastogenesis in mBM and RAW 264.7 cultures in vitro

Although it is well-established that Src plays an essential role in osteoclast activity *in vivo*, the role of Src signalling in osteoclast formation *in vitro* is less clear. To determine whether the inhibition of Src kinase activity could alter osteoclast formation in primary murine cells and in RAW 264.7 cells, the Src inhibitor PP2 was used.

As shown in figure 5.21, PP2 dose-dependently inhibits basal Src phosphorylation in mBM (figure 5.21A,B) and RAW 264.7 (figure 5.21C,D) cells at concentrations of approximately 1.25 μM and higher.

mBM cells, cultured with rhRANKL and rhM-CSF to induce osteoclastogenesis, were treated with vehicle or PP2 for 6 days, the cultures were stained for TRAP and the number of osteoclasts per well was enumerated. Treatment with PP2 substantially decreased osteoclast numbers (figure 5.22A), with concentrations of 1.25 μM PP2 and greater significantly reducing the number of osteoclasts per well ($p < 0.05$; figure 5.23A). In RAW 264.7 cells, while there was a non-significant increase in osteoclast numbers at 0.31 and 0.62 μM PP2, the formation of osteoclasts was significantly inhibited by the addition of 2.5 μM PP2 and higher ($p < 0.05$; figure 5.22B, 5.23B).

5.2.5 Inhibition of MEK/ERK signalling does not contribute to the pro-osteoclastogenic effects of imatinib in RAW 264.7 cultures

5.2.5.1 The effects of MEK inhibition on osteoclastogenesis in RAW 264.7 cultures

Inhibition of the MEK/ERK signalling pathway has previously been shown to activate osteoclast formation in RAW 264.7 cells.[392,394] As imatinib has been suggested to inhibit Raf[406], and thus may inhibit MEK/ERK signalling, inhibition of MEK/ERK was investigated as a potential mechanism for the activation of osteoclast formation by imatinib in RAW 264.7 cells.

In RAW 264.7 cultures treated with rhRANKL, the addition of a MEK/ERK1/2 inhibitor, PD098059[407,408], significantly increased both osteoclast formation and the size of the resulting osteoclasts (figure 5.24A). Treatment with concentrations of 1.25 μM PD098059 and higher significantly increased the number of osteoclasts per well in RAW 264.7 cultures, relative to vehicle-treated controls (figure 5.24B).

Figure 5.21. PP2 inhibits basal levels of Src phosphorylation in mBM and RAW 264.7 cells *in vitro*. mBM (**A**,**B**) were cultured at 3.13 x 10^5 cells/cm^2 with 75 ng/mL rhM-CSF for 7 days. The cells were starved in sf-α-MEM containing the Src inhibitor PP2 or vehicle (V; 0.2% DMSO) for 120 minutes prior to preparation of cell lysates. RAW 264.7 cells (**C**,**D**) were cultured at 9.38 x 10^3 cells/cm^2 in 6-well plates in c-DMEM. Following overnight adhesion, the medium was replaced with sf-DMEM and the cells were starved overnight. The cells were then treated with the Src inhibitor PP2 (containing 0.2% DMSO vehicle) or vehicle alone in serum-free media. Following 120 minutes of treatment, cell lysates were prepared and 30 μg of protein per lane were resolved on 10% polyacrylamide SDS-PAGE gels. The protein was transferred to a membrane and the membrane was probed for phosphorylated Src (p-Src) or HSP90. Representative immunoblots are shown (**A**,**C**). Graphs depict the normalised p-Src band intensity of a representative of 2 independent experiments.

A

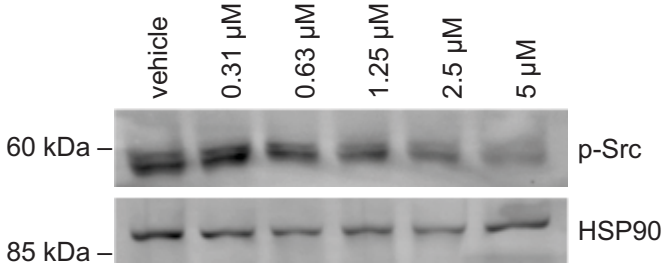
vehicle
0.31 µM
0.63 µM
1.25 µM
2.5 µM
5 µM
60 kDa –
p-Src
85 kDa –
HSP90

B

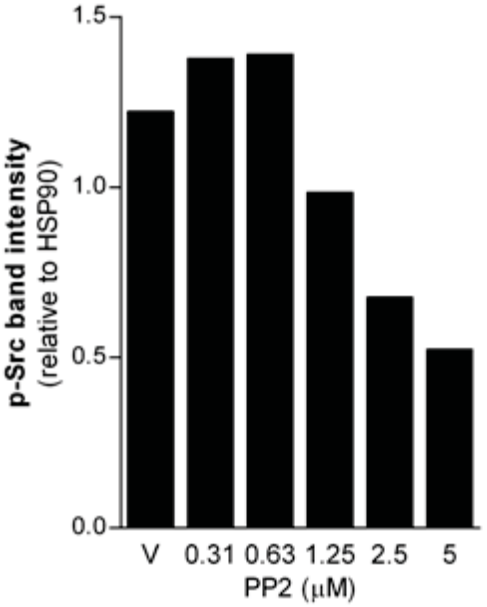
p-Src band intensity
(relative to HSP90)
1.5
1.0
0.5
0.0
V
0.31
0.63
1.25
2.5
5
PP2 (µM)

C

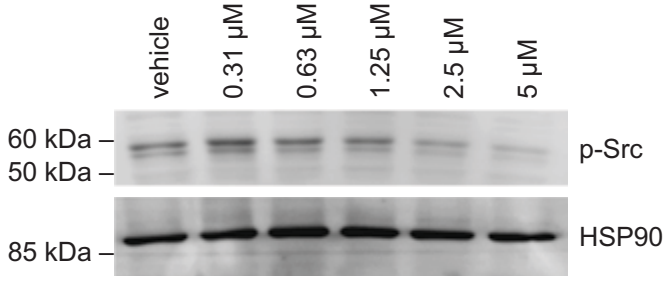
vehicle
0.31 µM
0.63 µM
1.25 µM
2.5 µM
5 µM
60 kDa –
50 kDa –
p-Src
85 kDa –
HSP90

D

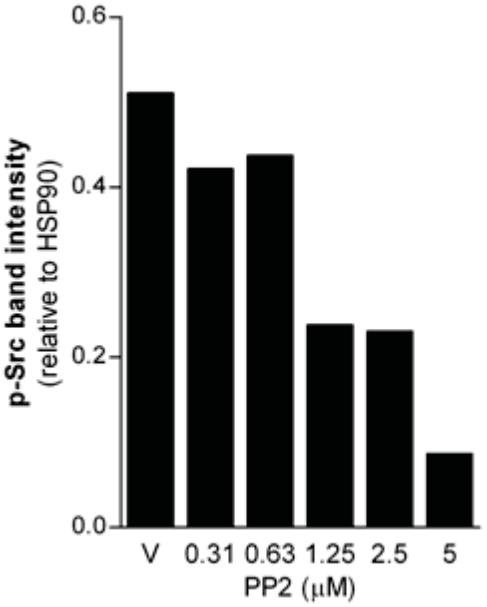
p-Src band intensity
(relative to HSP90)
0.6
0.4
0.2
0.0
V
0.31
0.63
1.25
2.5
5
PP2 (µM)

Figure 5.22. The Src inhibitor PP2 inhibits osteoclast formation in mBM and RAW 264.7 cultures. mBM (**A**) were cultured at 3.13 x 10^5 cells/cm^2 in 96-well plates in c-α-MEM containing 75 ng/mL rhM-CSF. Following overnight adhesion, the medium was replaced with c-α-MEM containing rhM-CSF (75 ng/mL) and rhRANKL (75 ng/mL) and PP2 (containing 0.2% DMSO vehicle) or vehicle alone for 6 days. RAW 264.7 cells (**B**) were seeded at 9.38 x 10^3 cells/cm^2 on 96-well plates in c-DMEM containing 100 ng/mL rhRANKL and were cultured overnight. The cells were then treated with c-DMEM supplemented with rhRANKL and PP2 (containing 0.2% DMSO vehicle) or vehicle for 3 days. After treatment, mBM and RAW 264.7 cultures were stained for TRAP and photographs were taken at 20 x magnification. Representative images from 1 of 2 experiments (**A**) or 1 of 3 experiments (**B**) are shown. Scale bars: 200 μm.

A

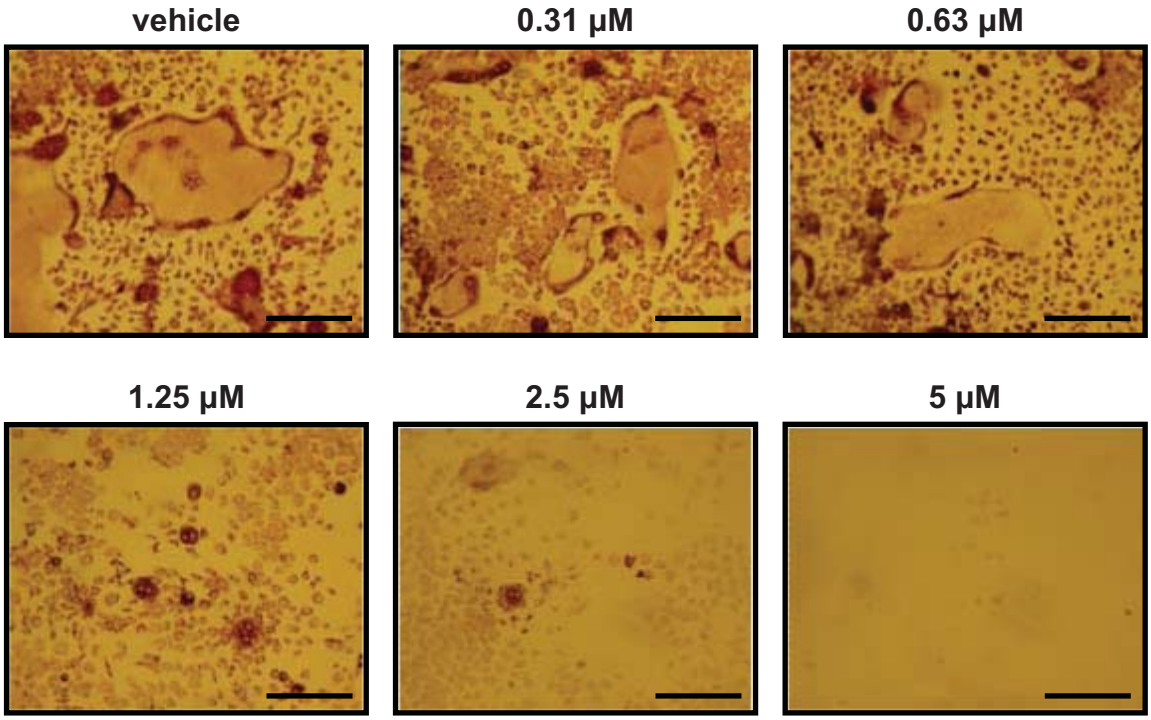
vehicle
0.31 μM
0.63 μM
1.25 μM
2.5 μM
5 μM

B

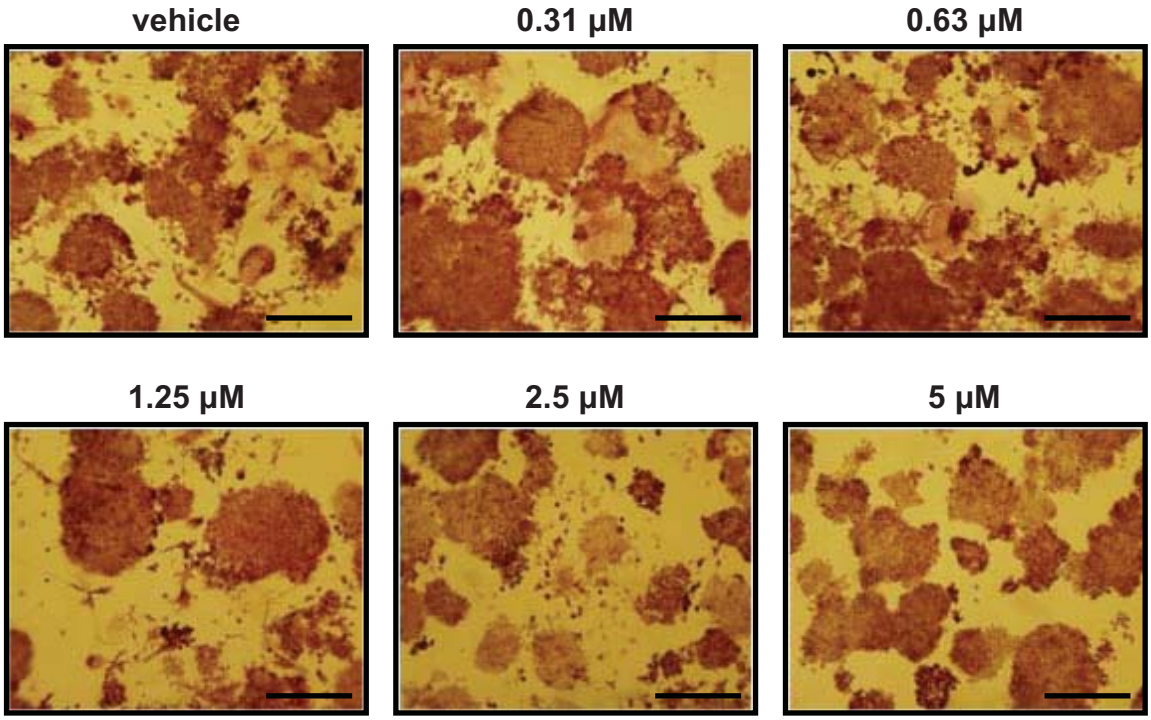
vehicle
0.31 μM
0.63 μM
1.25 μM
2.5 μM
5 μM

Figure 5.23. Enumeration of the effects of PP2 on osteoclast formation in mBM and RAW 264.7 cultures. mBM (**A**) were cultured in c-α-MEM containing rhM-CSF (75 ng/mL) and rhRANKL (75 ng/mL) and PP2 (containing 0.2% DMSO vehicle) or vehicle alone for 6 days. RAW 264.7 cells (**B**) were treated with c-DMEM supplemented with rhRANKL and PP2 (containing 0.2% DMSO vehicle) or vehicle for 3 days. Following treatment, the number of TRAP-positive, multinucleated osteoclast-like cells per well were enumerated. Graphs depict mean ± range of 2 independent experiments (**A**) or mean ± SEM of 3 independent experiments (**B**). * $p < 0.05$ relative to vehicle control (one-way ANOVA with Dunnett's post-tests).

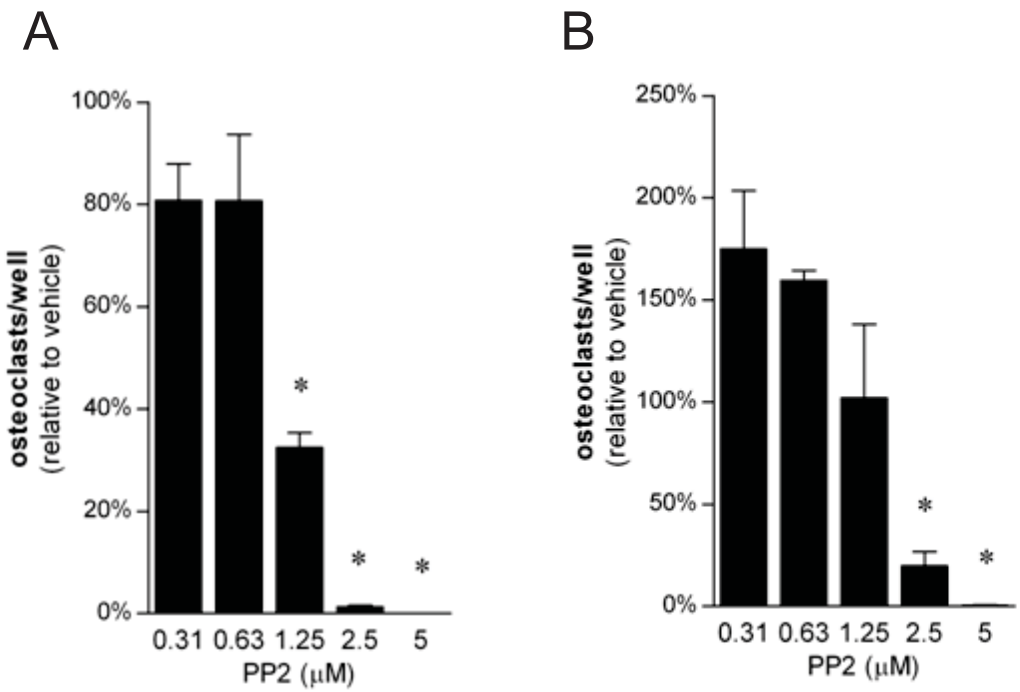
A
B
100%
80%
60%
40%
20%
0%
250%
200%
150%
100%
50%
0%
osteoclasts/well
(relative to vehicle)
*
0.31 0.63 1.25 2.5 5
PP2 (μM)

Figure 5.24. The effects of the MEK/ERK inhibitor PD098059 on osteoclast formation in RAW 264.7 cultures. RAW 264.7 cells were cultured at 9.38 x 10^3 cells/cm^2 in 96-well plates in c-DMEM. Following overnight adhesion, the medium was replaced with c-DMEM supplemented the MEK inhibitor PD098059 or 0.2% DMSO vehicle (V). After 3 days of treatment, the cultures were stained for TRAP and photographs were taken at 20 x magnification. Representative images are shown (**A**). Scale bars: 200 μm. Graph depicts mean ± SEM of 3 independent experiments (**B**). * $p < 0.05$ relative to vehicle control (one-way ANOVA with Dunnett's post-tests).

A

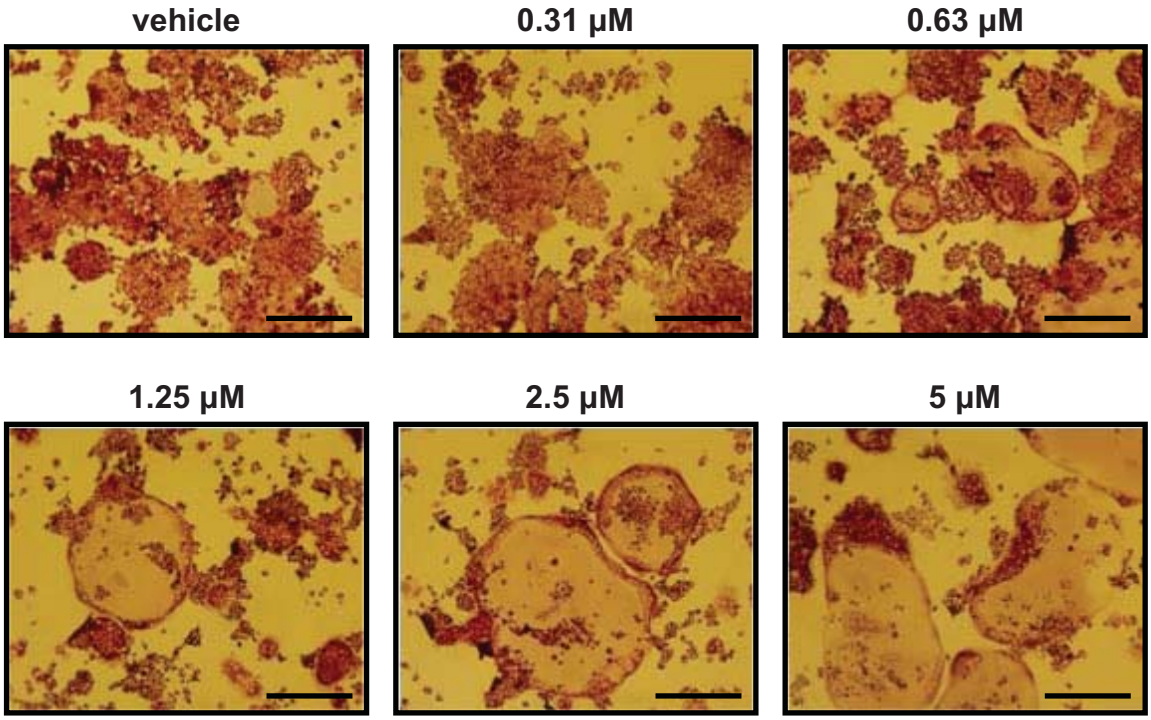
vehicle
0.31 μM
0.63 μM
1.25 μM
2.5 μM
5 μM

B

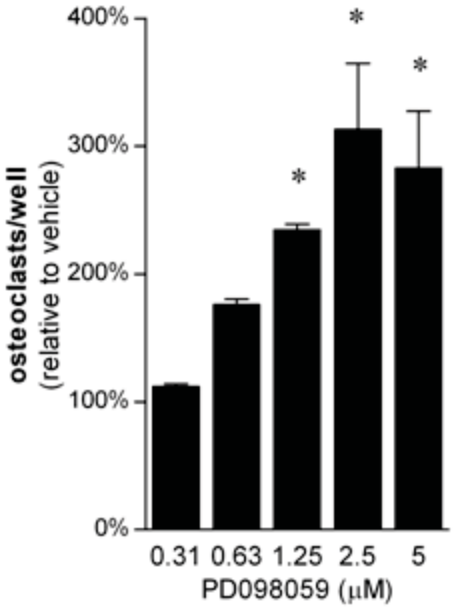
400%
300%
200%
100%
0%
osteoclasts/well
(relative to vehicle)
*
*
*
0.31 0.63 1.25 2.5 5
PD098059 (μM)

5.2.5.2 Imatinib does not inhibit MEK/ERK signalling in RAW 264.7 cells

The effects of imatinib on the MEK/ERK signalling pathway were investigated using Western blotting. RAW 264.7 cells were serum-starved overnight prior to the addition of imatinib or vehicle alone. Western blotting was then carried out with antibodies against phosphorylated ERK1/2 or total ERK1/2. In RAW 264.7, basal phosphorylation of ERK1/2 was detected in vehicle-treated serum-starved cultures (figure 5.25A). The level of basal ERK1/2 phosphorylation was not effected by treatment with imatinib at concentrations up to 10 μM (figure 5.25B), suggesting that MEK/ERK signalling was unaffected by imatinib.

A

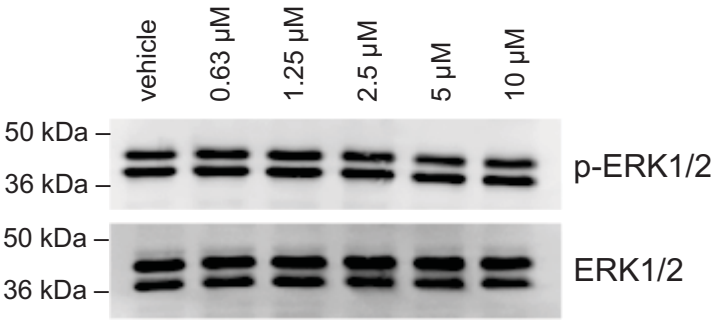
vehicle
0.63 µM
1.25 µM
2.5 µM
5 µM
10 µM
50 kDa –
36 kDa –
p-ERK1/2
50 kDa –
36 kDa –
ERK1/2

B

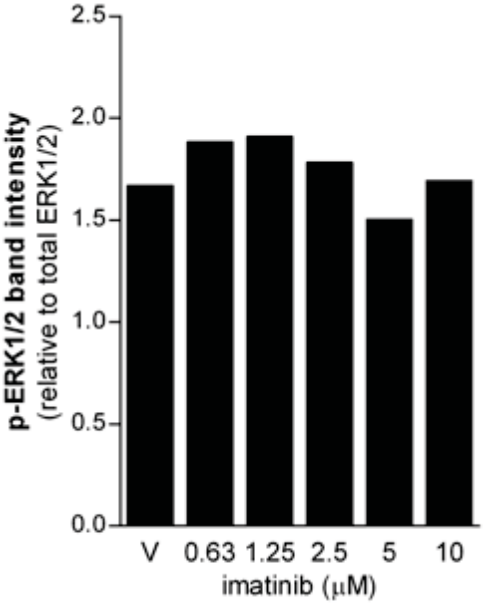
p-ERK1/2 band intensity
(relative to total ERK1/2)
2.5
2.0
1.5
1.0
0.5
0.0
V
0.63
1.25
2.5
5
10
imatinib (µM)

Figure 5.25. Imatinib does not inhibit MEK/ERK signalling in RAW 264.7 cells *in vitro*. RAW 264.7 cells were cultured at 9.38 x 10^3 cells/cm^2 in 6-well plates in c-DMEM. Following overnight adhesion, the cells were starved overnight in sf-DMEM. The cells were then treated with imatinib or vehicle (0.05% DMSO) for 120 minutes. Cell lysates (30 µg/lane) were resolved on 10% polyacrylamide SDS-PAGE, transferred to PVDF and probed with antibodies against phosphorylated ERK1/2 (p-ERK1/2) or HSP90 (**A**). Graphs depict relative pixel intensity of a representative experiment (**B**).

5.3 Discussion

Recently, members of the tyrosine kinase inhibitor family of drugs have been found to have inhibitory effects on osteoclast formation and function. Imatinib decreases osteoclast numbers and activity *in vitro* and *in vivo*, at least in part through inhibition of Fms.[13-15,221] Furthermore, the tyrosine kinase inhibitor nilotinib, which decreases osteoclast numbers *in vitro*, has also been shown to mediate its effects partly via inhibition of Fms.[264] Data presented in chapter 4 suggested that dasatinib, which has overlapping tyrosine kinase targets to imatinib and nilotinib, inhibits osteoclast formation *in vivo*. In this current chapter, a detailed evaluation of the effects of dasatinib on osteoclast formation and function was performed using *in vitro* culture systems. Therapeutic concentrations of dasatinib significantly reduced the formation and activity of osteoclasts from rat and mouse bone marrow mononuclear cells (rBM and mBM) at IC_{50} concentrations of lower than 10 nM dasatinib. A close association between the concentrations at which dasatinib inhibits osteoclast resorptive activity and Fms signalling was observed, suggesting that the inhibition of osteoclast activity in these cultures may be attributable, at least in part, to inhibition of Fms kinase activity. Subsequent to conducting this study, Brownlow *et al*. have also shown that dasatinib inhibits osteoclastogenesis in human peripheral blood monocyte cultures at similar concentrations to that required to inhibit Fms in Fms-transfected Rat2 fibroblasts.[409]

The possibility that dasatinib may also affect osteoclastogenesis via inhibition of Src was investigated. Src is critical for normal osteoclast activity, as is demonstrated in *Src*$^{-/-}$ mice, which are severely osteopetrotic due to an absence of osteoclast activity rather than a reduction in osteoclast number.[292,296,353,354] While the role of Src *in vivo* appears to be primarily responsible for driving osteoclast activity, there is some evidence that inhibition of Src activity may decrease osteoclast formation or survival *in vitro*. The treatment of mouse bone marrow cultures with the Src kinase inhibitors CGP77675, CGP76030 and PP1 decreases osteoclast formation and, in mature osteoclast cultures, increases osteoclast apoptosis.[357] As shown here (figure 5.23), treatment of mBM and RAW 264.7 cells with the Src kinase inhibitor PP2 decreased osteoclast numbers and Src phosphorylation at similar concentrations, suggesting that an inhibition of Src phosphorylation may contribute to decreased osteoclast numbers in these cells *in vitro* (figure 5.22, 5.23). The association between the anti-osteoclastogenic effects of dasatinib and inhibition of Src was also examined in mBM and rBM cells. Dasatinib treatment decreased basal Src phosphorylation at doses 5-fold and 40-fold higher than those required

to inhibit osteoclast activity in mBM and rBM cultures, respectively (figure 5.20). While the precise mechanism(s) remain to be elucidated, these data suggest that dasatinib inhibits *in vitro* osteoclastogenesis at concentrations at which Fms, but not Src, is affected. However, it is not clear to what extent inhibition of Src and Fms contribute to the inhibitory effects of dasatinib on osteoclasts *in vivo*. Fms-independent osteoclast formation and activity was inhibited by dasatinib in RAW 264.7 cultures suggesting that, under some circumstances, inhibition by dasatinib of other tyrosine kinase targets, such as Src and Kit, may have anti-osteoclastogenic effects.

In addition to examining the effects of dasatinib on osteoclastogenesis, in this chapter the anti-osteoclastogenic properties of imatinib in murine cultures were investigated. It has previously been shown that imatinib inhibits the phosphorylation of Fms in response to stimulation with M-CSF in a murine haematopoietic cell line, FDC-Fms, engineered to express human Fms.[13,261] The concentrations of imatinib required to inhibit Fms signalling in this cell line was higher than that shown to inhibit osteoclast activity in human CD14-positive peripheral blood mononuclear cell cultures.[13] This suggested that either imatinib inhibits osteoclast activity in these cells via mechanisms other than inhibition of Fms kinase activity, or that inhibition of Fms by imatinib occurs at lower concentrations in human osteoclasts than in FDC-Fms cells. The effects of imatinib on Fms phosphorylation in osteoclasts or osteoclast precursors have not previously been determined. Therefore, as part of this study, physiologically-relevant Fms-expressing osteoclast precursors derived from primary murine monocyte/macrophage cultures were used to assess the direct effects of imatinib on osteoclastogenesis and Fms phosphorylation. In these primary murine bone marrow cultures, imatinib inhibited Fms phosphorylation and osteoclast formation at similar concentrations (figure 5.14), supporting the theory that inhibition of Fms is responsible for the anti-osteoclastogenic properties of imatinib.

Data presented in chapter 4 indicated that therapeutic concentrations of imatinib had no effect on osteoclasts in normal Sprague-Dawley rats *in vivo*. This contrasts with patient data presented in chapter 3, and preliminary data in mice[13,253,254], which demonstrated decreased osteoclast numbers and activity following imatinib treatment *in vivo*. Although previous studies have shown inhibition of osteoclasts *in vitro* in Lewis rat bone marrow cultures[14] there may be strain-specific effects of these drugs. We have shown here that imatinib is an inhibitor of osteoclastogenesis in Sprague-Dawley rat bone marrow cultures, suggesting that osteoclasts from this rat strain, like others[14], are sensitive to

imatinib *in vivo*. In human CD14-positive peripheral blood mononuclear cell cultures, imatinib inhibits osteoclast activity at doses more than 10-fold lower than it affects osteoclast formation, via a mechanism that is thought to involve down-regulation of RANK expression via inhibition of Fms.[13] However, data shown here (figure 5.4, 5.7) demonstrate that in murine cultures imatinib inhibits osteoclast formation and resorption at similar concentrations. Therefore, higher concentrations of imatinib are required to inhibit murine osteoclast activity than those required to inhibit human osteoclast activity. This may in part explain why no effects on osteoclasts were observed in normal rats *in vivo* (chapter 4) while imatinib treatment resulted in a significant inhibitory effect on osteoclast activity in patients (chapter 3). However, this cannot fully explain the observed disparate effects of imatinib in humans and rats, as osteoclast numbers as well as activity were decreased in imatinib-treated patients, suggesting that the concentration achieved was sufficient to inhibit both osteoclast formation and activity.

We hypothesised that inhibition of tyrosine kinase targets other than Fms, such as CAII[224], may contribute to the inhibitory effects of imatinib on osteoclasts. CAII plays an essential role in osteoclast activity as this enzyme catalyses the reaction which provides that protons required for acidification of the resorption lacunae, allowing dissolution of the mineralised bone matrix.[89-91] Inhibition of this enzyme by imatinib may, therefore, decrease osteoclast activity. However, treatment of Fms-independent RAW 264.7 cells with imatinib resulted in an increase in osteoclast formation and, subsequently, activity. This contrasts with previously published results indicating that therapeutic concentrations of imatinib resulted in a slight decrease in RAW 264.7 osteoclast formation.[17,410] This difference may be due to differences in seeding densities used in each study, as cell density can dramatically alter the osteoclastogenic response of RAW 264.7 cells to kinase inhibitors.[392] As one study has suggested that imatinib may inhibit Raf1[406], we investigated the effects of inhibition of the Ras/Raf/MEK/ERK pathway on RAW 264.7 osteoclastogenesis. While MEK/ERK signalling downstream of Fms is important in osteoclast survival/proliferation[257,395,398-400,411], it has been suggested that MEK/ERK signalling downstream of RANK is a negative regulator of osteoclastogenesis[392-394]. In RAW 264.7 cells, treatment with the MEK1 inhibitors PD098059 or U0126 increases osteoclast formation whilst at very high doses these inhibitors decrease cell proliferation/survival (figure 5.24 and [392,394]). The similarities between the effects of these MEK1 inhibitors and the observed effects of imatinib on RAW 264.7 osteoclastogenesis lead to the hypothesis that inhibition of Raf1 signalling by imatinib may be resulting in

increased osteoclastogenesis. However, imatinib had no effect on Ras/Raf/MEK/ERK signalling in RAW 264.7 cells, as determined by ERK1/2 phosphorylation (figure 5.25), suggesting that imatinib did not inhibit Raf1 in these cells. The potential mechanism for the pro-osteoclastogenic effect of imatinib in RAW 264.7 cells observed here requires further investigation.

In summary, these studies demonstrate that the tyrosine kinase inhibitor dasatinib is a potent inhibitor of osteoclastogenesis *in vitro*, at least in part through an inhibition of Fms signal transduction. In addition, our results show that imatinib-induced inhibition of osteoclast activity and Fms phosphorylation in osteoclast precursors occurs at similar concentrations, supporting the theory that Fms inhibition is an important mechanism in the anti-osteoclastogenic capacity of imatinib.

Chapter 6

The effects of tyrosine kinase inhibition on osteoblasts and chondrocytes *in vitro*

6.1 Introduction

Mesenchymal stem cells are multipotent precursors that have the capacity to differentiate into cells of different lineages, including osteoblasts, chondrocytes, adipocytes and myocytes.[36,37] While the signals involved in the lineage selection process are unclear, it is known that hierarchical expression of transcription factors is involved in driving differentiation down one lineage and limiting commitment to the others. For example, Runx2 and Sox9 are master regulators of osteoblastogenesis and chondrogenesis, driving the expression of lineage-specific genes.[38,39,148-150,156-158]

The differentiation of osteoblasts from mesenchymal stem cells is primarily regulated by the transcription factors Runx2 and Osterix (reviewed in [108]). This process is closely regulated by locally- and systemically-produced hormones and cytokines. Several receptor tyrosine kinases, including IGF receptor[412-414], epidermal growth factor receptor (EGFR)[415-417], FGFR[415,416,418] and PDGFR[280,289-291,415] are involved in the regulation of osteoblast proliferation and differentiation by cytokines. Of these tyrosine kinases, PDGFR has been implicated as a potential mediator of the observed effects of imatinib on osteoblast proliferation and function *in vitro*. PDGF is a potent mitogen for mesenchymal stromal cells and suppresses bone matrix deposition in primary osteoblast cultures.[280,289-291] In human bone explant cultures and in cultures of the murine osteoblast-like cell line MC3T3-E1, treatment with imatinib relieved the inhibitory effects of PDGF on mineralisation[10,17] suggesting that inhibition of PDGFR signalling may be one mechanism whereby imatinib activates osteoblast differentiation. It is likely that dasatinib also inhibits osteoblast proliferation and stimulates differentiation due to its specificity for PDGFR, although this remains to be demonstrated.

As described in chapter 4, treatment of normal mature rats with dasatinib increased trabecular bone volume at the proximal tibia while having no effect on bone formation rate or serum markers of osteoblast activity. Similarly, imatinib had no effect on these indices of osteoblast activity, relative to vehicle-treated controls. One aim of the following study was, therefore, to confirm whether Sprague-Dawley rat osteoblasts are sensitive to imatinib and dasatinib and to determine the effects of PDGFR inhibition on the proliferation and activity of these cells.

Additionally, studies described in chapter 4 found that treatment of normal rats with imatinib and dasatinib significantly reduced growth plate thickness, leading to complete growth plate closure in imatinib-treated animals after 12 weeks. The regulation of longitudinal bone growth is tightly regulated through the coordinated proliferation,

differentiation and activity of epiphyseal growth plate chondrocytes (reviewed by [146]). In normal bone, the rate of chondrocyte proliferation and the size of the resultant hypertrophic chondrocytes are the primary determinants of the rate of longitudinal bone growth[143,145] (reviewed in [419]). Chondrocyte proliferation and maturation is tightly-regulated by autocrine and paracrine signalling via factors including Ihh[159-162], PTHrP[159-162], FGF[180,181] and IGF1[186-189]. The disruption of the activities of any of these factors can cause aberrant bone growth, resulting in a number of human growth disorders.[182-185] In addition to the role of PDGFR in osteoblast activity, PDGFR signalling is also known to regulate chondrocyte proliferation and activity. PDGF-BB treatment has been shown to increase cell proliferation and activity of resting zone chondrocytes derived from Sprague-Dawley rats.[381] Additionally, PDGF-BB increases the proliferation, but not the rate of GAG production per cell, of chondrocytes isolated from bovine occipital cartilage.[382] Imatinib and dasatinib may therefore inhibit chondrocytes through inhibition of PDGFR signalling, although as yet this has not been confirmed experimentally.

In light of the observed effects of dasatinib on bone volume in normal rats, we determined whether dasatinib, like imatinib, could affect osteoblast activity *in vitro*. In addition, the mechanisms involved in the observed effects of imatinib and dasatinib on growth plate closure were investigated using a murine chondrocyte cell line. Furthermore, this study examined whether any effects of imatinib and dasatinib on mesenchymal cell proliferation and activity were attributable to an inhibition of PDGFR signal transduction.

6.2 Results

6.2.1 Imatinib and dasatinib inhibit proliferation and promote mineralisation in murine stromal cell cultures *in vitro*

6.2.1.1 Imatinib and dasatinib inhibit the proliferation of rBMSC

It has previously been demonstrated that the tyrosine kinase inhibitor imatinib mesylate increases osteoblast activity while inhibiting osteoblast proliferation, in cultures of human mesenchymal stromal cells, at least in part due to the inhibition of PDGFR.[10,16,19] In order to confirm that rodent mesenchymal stromal cells are affected by imatinib in a similar manner to human cells, and to determine whether dasatinib can alter osteoblast proliferation and differentiation, primary mesenchymal stromal cells isolated from the long bones of Sprague-Dawley rats (rBMSC) were used.

To determine whether imatinib and dasatinib can inhibit the proliferation of rBMSC, cells were cultured with imatinib, dasatinib or vehicle alone for 2, 4 or 6 days and the relative number of cells per well was determined using the WST-1 assay (figure 6.1A,B). At all time points examined, treatment with imatinib at concentrations of 0.13 μM and higher significantly decreased cell proliferation, relative to vehicle-treated controls (figure 6.1A). Similarly, treatment of rBMSC with 5 nM or more of dasatinib for 2, 4 or 6 days had a significant inhibitory effect on cell proliferation (figure 6.1B). Addition of imatinib at concentrations up to 4 μM, or dasatinib at concentrations up to 160 nM had no further inhibitory effects on cell numbers (data not shown).

6.2.1.2 Therapeutically-achievable concentrations of imatinib and dasatinib activate osteoblast activity in rBMSC cultures

To investigate the potential effects of imatinib and dasatinib on osteoblast activity, the ability of imatinib and dasatinib to drive mineral formation and differentiation was examined in rBMSC cultures. rBMSC were cultured with osteogenic media in the presence of imatinib, dasatinib or vehicle. Control wells were treated with c-α-MEM supplemented with ascorbate. After 42 days of culture, the mineral content of cultures was revealed by alizarin red staining. As shown in figure 6.2A, cells cultured in c-α-MEM supplemented with ascorbate did not form mineralised nodules. However, in cultures treated with osteogenic media the formation of mineralised nodules was evident (figure 6.2B). Treatment with imatinib (4 μM) or dasatinib (80 nM) increased the incidence of mineralised nodules in rBMSC cultures, when compared with vehicle-treated control wells (figure 6.2B,C,D).

Figure 6.1. Imatinib and dasatinib inhibit the proliferation of rBMSC *in vitro*. Rat bone marrow stromal cells (rBMSC) were cultured at 8 x 10^3 cells/cm^2 in 96-well plates in c-α-MEM containing 100 μM ascorbate. After overnight adhesion, the medium was replaced with c-α-MEM containing ascorbate (100 μM) and imatinib (**A**) or dasatinib (**B**) (containing 0.05% DMSO vehicle) or vehicle alone. At the indicated time points, the relative number of cells per well was enumerated using WST-1. Graphs depict mean ± range of 2 independent experiments. * $p < 0.05$ relative to vehicle control at each time point (one-way ANOVA with Dunnett's post-tests).

A

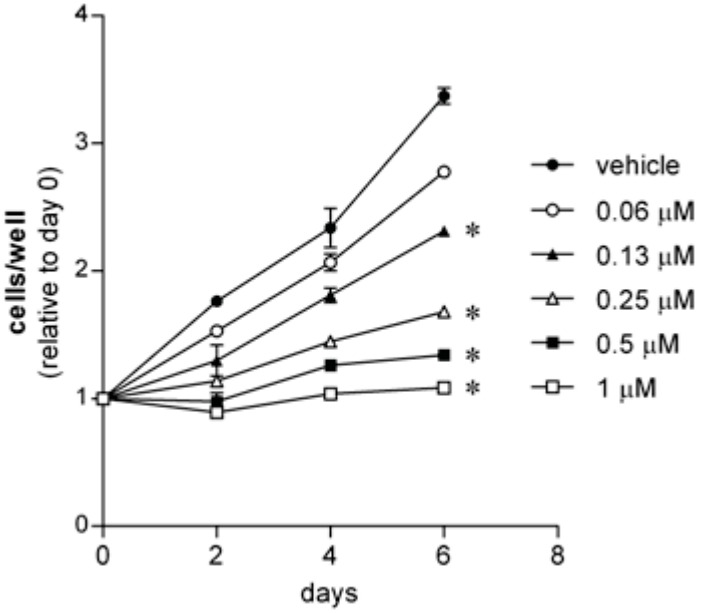
cells/well
(relative to day 0)
days
vehicle
0.06 μM
0.13 μM
0.25 μM
0.5 μM
1 μM
*
*
*
*

B

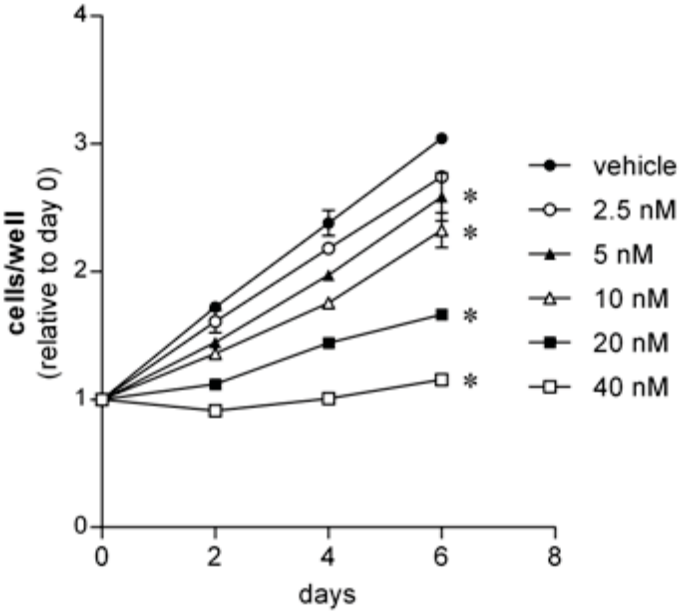
cells/well
(relative to day 0)
days
vehicle
2.5 nM
5 nM
10 nM
20 nM
40 nM
*
*
*
*

Figure 6.2. The effects of imatinib and dasatinib on mineral production by rBMSC *in vitro*. rBMSC were cultured in osteogenic media and imatinib, dasatinib or vehicle. Negative controls, treated with c-α-MEM supplemented with ascorbate, were also included. Following 42 days of treatment, the mineral was stained with alizarin red. Representative images of negative controls (**A**) and cultures treated with vehicle (**B**), 4 μM imatinib (**C**) or 80 nM dasatinib (**D**) are shown. Scale bars: 200 μm.

A

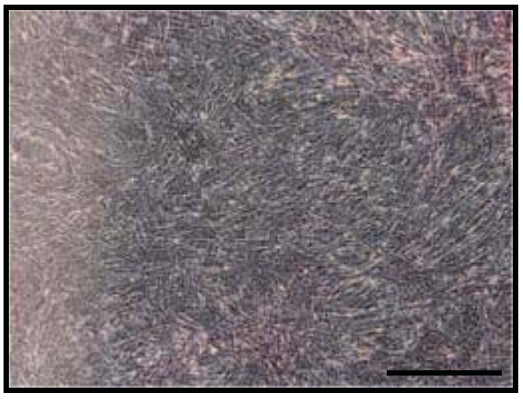

B

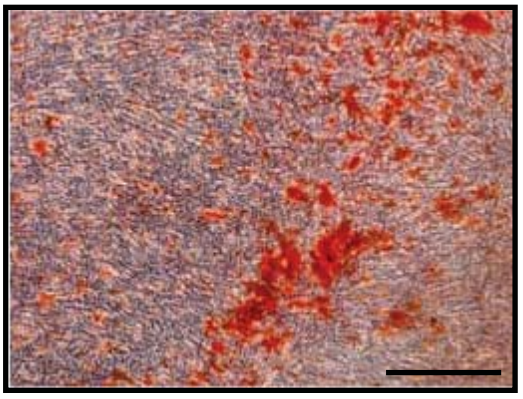

C

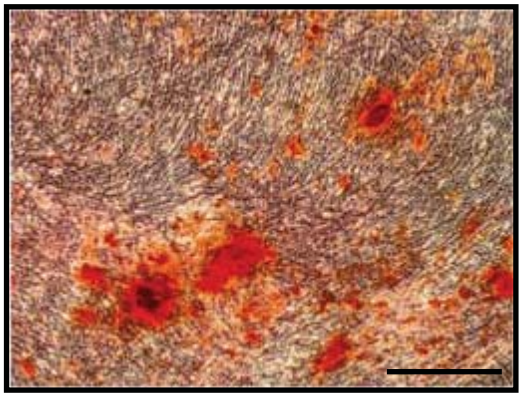

D

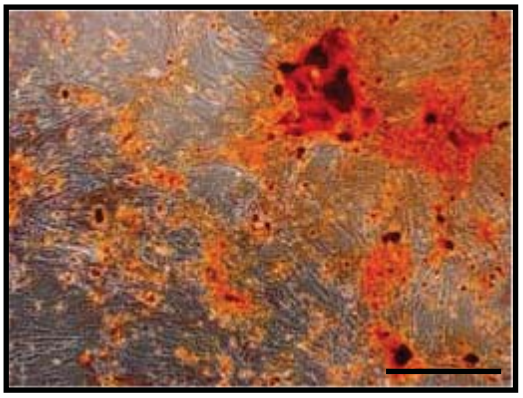

In order to quantitate the amount of mineral produced under different culture conditions, the mineralised matrix was dissolved using hydrochloric acid and the calcium content quantified using a cresolphthalein complexone assay. Calcium levels were normalised to DNA content, to correct for differences in cell numbers between treatments. A significant increase in mineral production, on a per cell basis, in cultures treated with 2 μM imatinib and higher was observed (figure 6.3A). Similarly, treatment with 40 nM dasatinib and higher significantly increased the mineralising activity of the rBMSC by more than 3-fold (figure 6.3B).

6.2.1.3 Imatinib and dasatinib abrogate PDGF-induced phosphorylation of ERK1/2 and Akt in rBMSC cultures

As detailed in sections 6.2.1.1 and 6.2.1.2, imatinib and dasatinib inhibit cell proliferation while stimulating the mineralising activity of primary rat stromal cells. As PDGF is known to be an important inducer of mesenchymal cell proliferation, and an inhibitor of osteoblast activity, the effects of imatinib and dasatinib on PDGFR signalling in rBMSC was examined by Western blot.

rBMSC cultures were serum-starved overnight and then treated for 2 hours with vehicle, imatinib or dasatinib in serum-free media. The cells, where indicated, were stimulated with rhPDGF-BB for 5 minutes prior to the preparation of cell lysates. The extracts were then examined by Western blot to determine the effects of imatinib and dasatinib on PDGF-induced phosphorylation of Akt and ERK1/2. Unstimulated cells displayed no basal phosphorylation of Akt and low levels of basal ERK1/2 phosphorylation (figure 6.4A, 6.5A). Following stimulation with rhPDGF-BB for 5 minutes, there was strong induction of phosphorylation of Akt and ERK1/2. Consistent with the known effects of imatinib on the PDGFR, in the presence of imatinib there was a dose-dependent inhibition of the rhPDGF-BB-induced phosphorylation of Akt and ERK1/2 (figure 6.4A). Quantitation of the intensity of the Akt and ERK1/2 bands, normalised to HSP90, indicates that imatinib at concentration of 0.5 μM and higher inhibited PDGF-induced phosphorylation of Akt and ERK1/2, relative to vehicle controls (figure 6.4B,C). Cells treated with 4 μM imatinib displayed no induction of PDGFR signalling, with similar levels of phosphorylated ERK1/2 and Akt as unstimulated, serum-starved cells (figure 6.4B,C). Pre-treatment with dasatinib at concentrations in excess of 10 nM substantially reduced the activation of ERK1/2 and Akt phosphorylation by rhPDGF-BB treatment (figure 6.5A). Treatment of rBMSC with 40 nM dasatinib completely abrogated

Figure 6.3. Imatinib and dasatinib enhance the mineralisation activity of rBMSC *in vitro*. Murine bone marrow stromal cells were seeded at 2.5 x 10^4 cells/cm^2 in 96-well plates in c-α-MEM containing 100 μM ascorbate and were allowed to adhere overnight. The medium was then replaced with osteogenic media containing imatinib (**A**), dasatinib (**B**) or vehicle. Following 42 days of treatment, mineral was dissolved with HCl and calcium content was calculated using the cresolphthalein complexone assay. Calcium produced per well was corrected for relative cell numbers by determining total DNA content per well. Graphs depicts mean ± range of 2 independent experiments. * $p < 0.05$ relative to vehicle control (one-way ANOVA with Dunnett's post-tests).

A

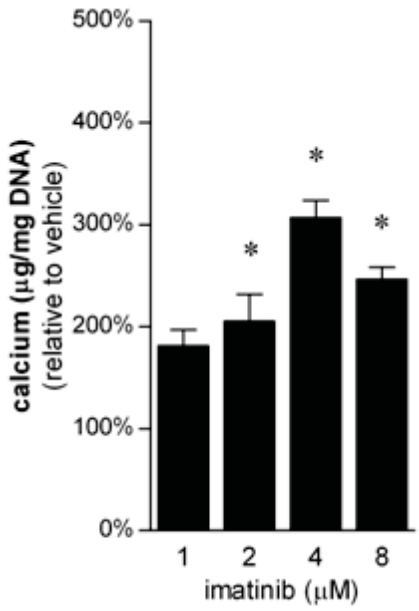
500%
400%
300%
200%
100%
0%
calcium (μg/mg DNA)
(relative to vehicle)
*
*
*
1
2
4
8
imatinib (μM)

B

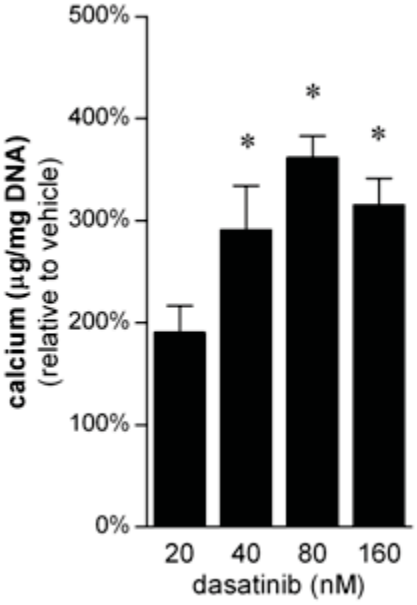
500%
400%
300%
200%
100%
0%
calcium (μg/mg DNA)
(relative to vehicle)
*
*
*
20
40
80
160
dasatinib (nM)

Figure 6.4. Imatinib inhibits PDGFR signalling in rBMSC *in vitro*. rBMSC were cultured at 2.5 x 10^4 cells/cm^2 in 6-well plates in c-α-MEM containing 100 μM ascorbate. After overnight culture, the cells were serum-starved by overnight incubation in sf-α-MEM. The cells were pre-treated for 2 hours with sf-α-MEM containing imatinib or 0.05% DMSO and, where indicated, were then stimulated with rhPDGF-BB (10 ng/mL) for 5 min. Cell lysates (30 μg/lane) were resolved through a 10% polyacrylamide SDS-PAGE gel and the proteins were transferred to PVDF. Phosphorylated Akt (p-Akt) and phosphorylated ERK1/2 (p-ERK1/2), as well as total HSP90, were detected using specific antibodies. Representative images are shown (**A**). Graphs indicate the relative pixel intensity for p-Akt (**B**) and p-ERK1/2 (**C**) normalised to HSP90 from a representative of 2 experiments.

A

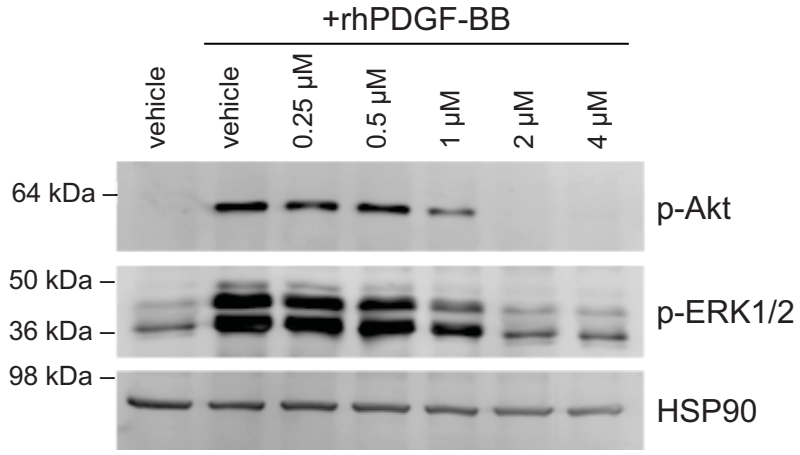
+rhPDGF-BB
vehicle
vehicle
0.25 µM
0.5 µM
1 µM
2 µM
4 µM
64 kDa –
p-Akt
50 kDa –
36 kDa –
p-ERK1/2
98 kDa –
HSP90

B

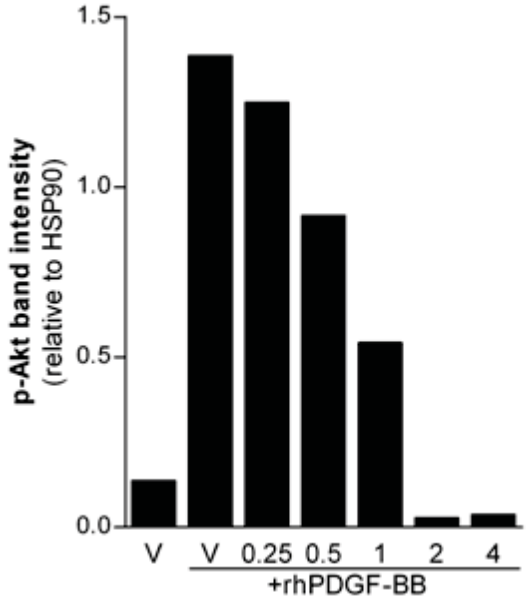
p-Akt band intensity
(relative to HSP90)
1.5
1.0
0.5
0.0
V
V
0.25
0.5
1
2
4
+rhPDGF-BB

C

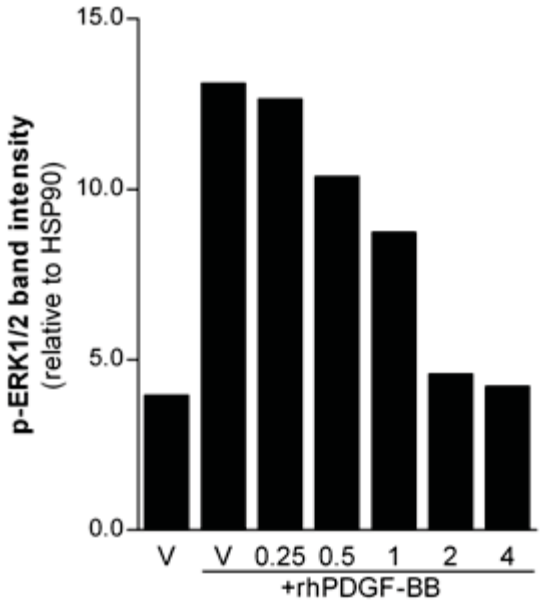
p-ERK1/2 band intensity
(relative to HSP90)
15.0
10.0
5.0
0.0
V
V
0.25
0.5
1
2
4
+rhPDGF-BB

Figure 6.5. Dasatinib inhibits PDGFR signalling in rBMSC *in vitro*. rBMSC were cultured at 2.5 x 10^4 cells/cm^2 in 6-well plates in c-α-MEM containing 100 μM ascorbate. After overnight culture, the cells were serum-starved by overnight incubation in sf-α-MEM. The cells were pre-treated with sf-α-MEM containing dasatinib or 0.05% DMSO and, where indicated, were then stimulated with rhPDGF-BB (10 ng/mL) for 5 min. Cell lysates (30 μg/lane) were resolved through a 10% polyacrylamide SDS-PAGE gel and the proteins were transferred to PVDF. Phosphorylated Akt (p-Akt) and phosphorylated ERK1/2 (p-ERK1/2), as well as total HSP90, were detected using specific antibodies. Representative images are shown (**A**). Graphs indicate the relative pixel intensity for p-Akt (**B**) and p-ERK1/2 (**C**) normalised to HSP90 from a representative of 2 experiments.

A

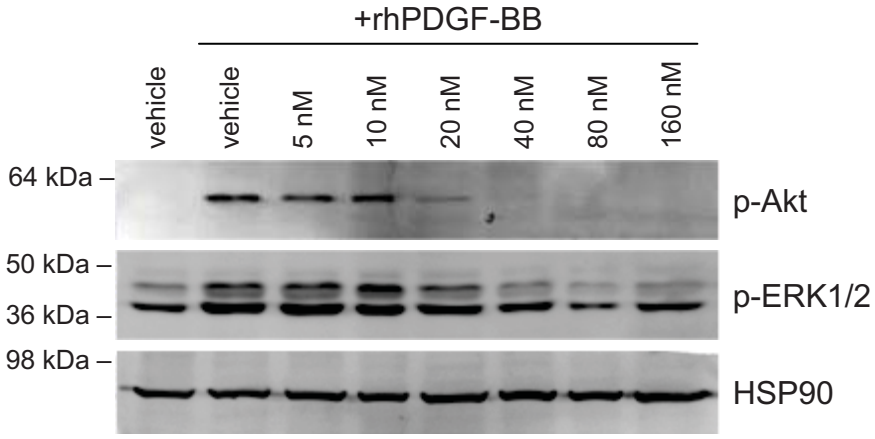
+rhPDGF-BB
vehicle
vehicle
5 nM
10 nM
20 nM
40 nM
80 nM
160 nM
64 kDa –
50 kDa –
36 kDa –
98 kDa –
p-Akt
p-ERK1/2
HSP90

B

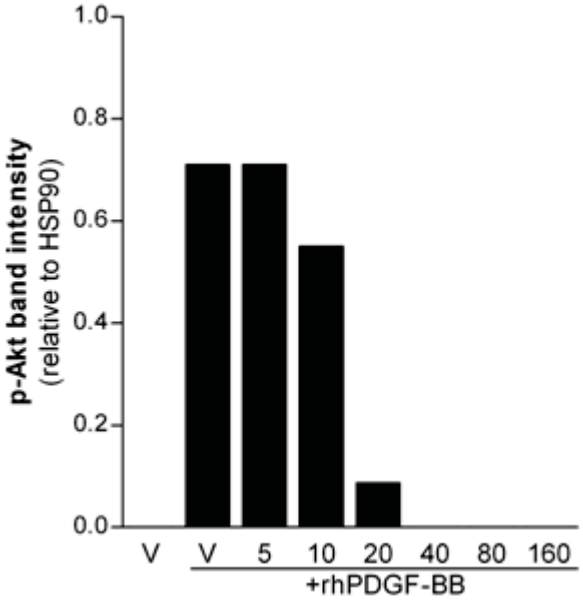
p-Akt band intensity
(relative to HSP90)
1.0
0.8
0.6
0.4
0.2
0.0
V
V
5
10
20
40
80
160
+rhPDGF-BB

C

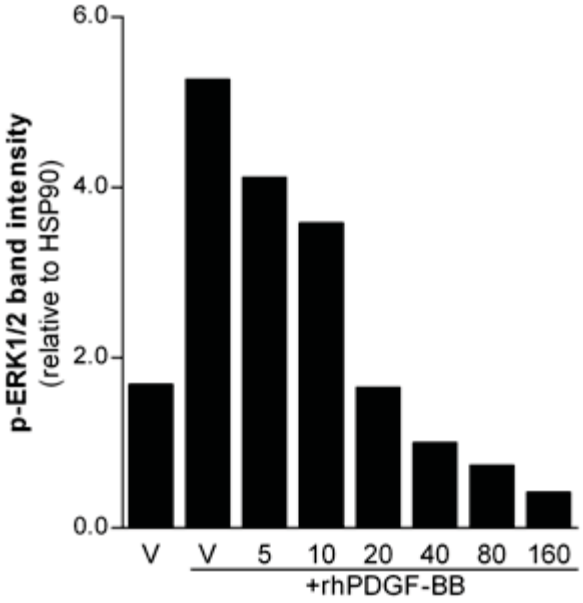
p-ERK1/2 band intensity
(relative to HSP90)
6.0
4.0
2.0
0.0
V
V
5
10
20
40
80
160
+rhPDGF-BB

phosphorylation of Akt in response to PDGF-BB stimulation (figure 6.5B). ERK1/2 phosphorylation was reduced to below baseline levels by treatment with 40 nM dasatinib and higher (6.5C).

6.2.1.4 Sigmoidal dose-response relationship of the inhibition of PDGFR signalling by imatinib and dasatinib and the effects of these inhibitors on rBMSC proliferation

The relationship between the concentrations at which imatinib and dasatinib inhibit PDGFR signalling and proliferation was investigated by fitting the data to a sigmoidal dose-response curve (figure 6.6A,B).

In rBMSC cultures, PDGFR signalling through Akt and ERK1/2 was inhibited at IC_{50} of 0.69 μM and 0.78 μM imatinib, respectively (figure 6.6A). The concentration at which rBMSC proliferation was inhibited was substantially lower, with an IC_{50} of 0.13 μM (figure 6.6A). There was close agreement between the concentrations at which dasatinib inhibited PDGFR signalling and cell proliferation. PDGF-induced phosphorylation of Akt and ERK1/2 was inhibited at IC_{50} of 11.12 nM and 11.85 nM, respectively, while cell proliferation was inhibited at an IC_{50} of 10.74 nM dasatinib.

6.2.1.5 Imatinib and dasatinib inhibit the effects of PDGF-BB on cell proliferation and mineral formation

The potential contribution of inhibition of PDGFR to the effects of imatinib and dasatinib on rBMSC cells was next investigated.

As shown earlier (figure 6.1), treatment of rBMSC with 1 μM imatinib or 40 nM dasatinib for 6 days decreased cell numbers by 60%, relative to vehicle-treated controls, as assessed by WST-1 (figure 6.7A). Addition of 10 ng/mL rhPDGF-BB increased cell proliferation 2-fold, relative to vehicle-treated levels, after 6 days of culture (figure 6.7A). This induction of cell proliferation was significantly inhibited, to levels below that of vehicle treatment alone, by co-treatment with 4 μM imatinib or 40 nM dasatinib (figure 6.7A).

When rBMSC were cultured under osteogenic conditions, the addition of PDGF-BB resulted in a small, non-significant, decrease in mineral formation, on a per cell basis, after 42 days (figure 6.7B). This inhibition was reversed by co-treatment with imatinib (4 μM) or dasatinib (40 nM), with mineral levels in these cultures being similar to those of wells treated with imatinib or dasatinib alone (figure 6.7B).

Figure 6.6. Sigmoidal dose response curve of the effects of imatinib and dasatinib on cell proliferation and PDGFR signalling in rBMSC *in vitro*. Mean values for the inhibitory effects of imatinib (**A**) and dasatinib (**B**) on cell proliferation (WST-1) and PDGF-BB-induced Akt and ERK1/2 phosphorylation in rBMSC were plotted to obtain a sigmoidal dose-response curve fits.

A

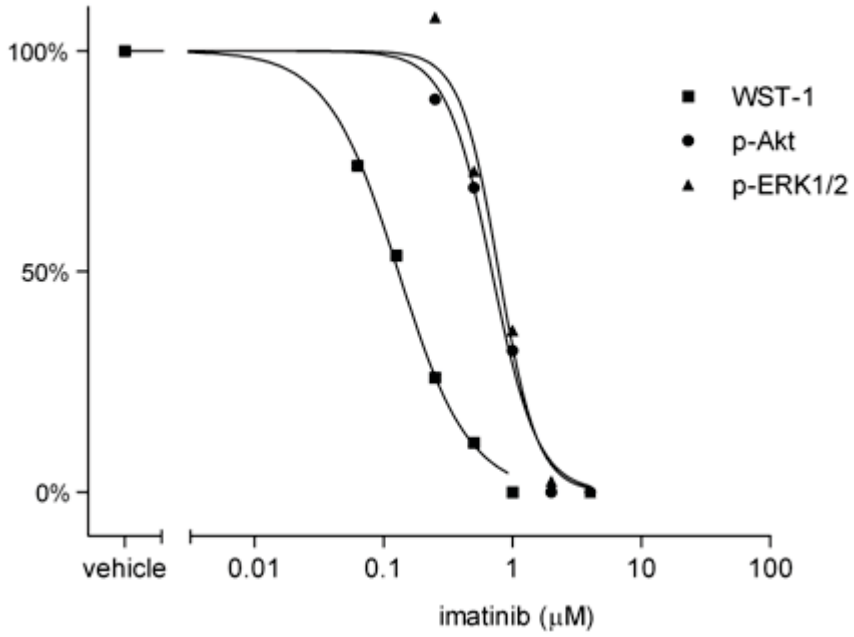
100%
50%
0%
vehicle
0.01
0.1
1
10
100
imatinib (μM)
WST-1
p-Akt
p-ERK1/2

B

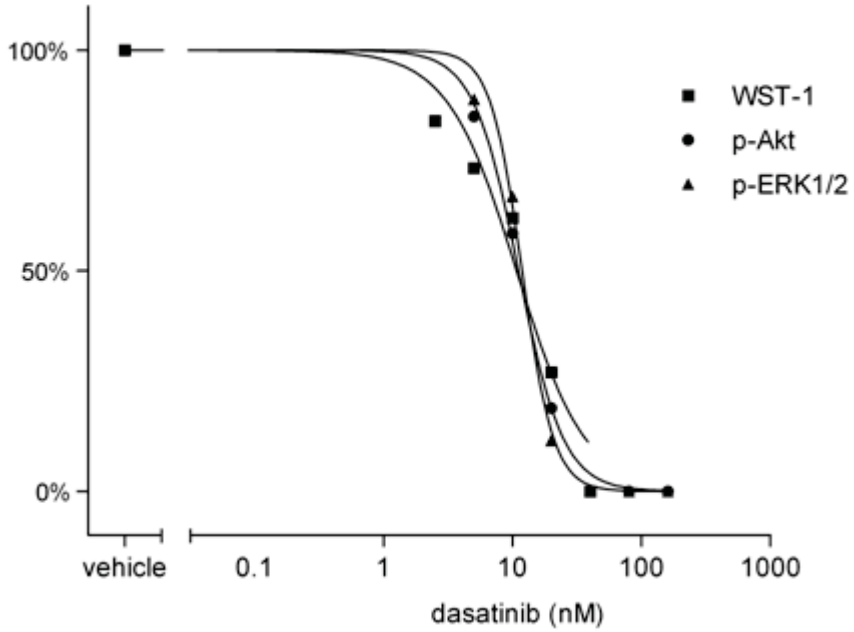
100%
50%
0%
vehicle
0.1
1
10
100
1000
dasatinib (nM)
WST-1
p-Akt
p-ERK1/2

Figure 6.7. Imatinib and dasatinib inhibit the effects of PDGF-BB on cell proliferation and mineral formation in rBMSC cultures. **A**. Murine bone marrow stromal cells were cultured at 8 x 10^3 cells/cm^2 in 96-well plates in c-α-MEM containing 100 μM ascorbate. After overnight adhesion, the medium was replaced with c-α-MEM containing ascorbate (100 μM) and 0.05% DMSO vehicle (V), 1 μM imatinib (I) or 40 nM dasatinib (D). Where indicated, cells were treated with 10 ng/mL rhPDGF-BB for the duration of the experiment. After 6 days of treatment, the relative number of cells per well was enumerated using WST-1. Graph depicts mean ± range of 2 independent experiments. **B**. Murine bone marrow stromal cells were seeded at 2.5 x 10^4 cells/cm^2 in 96-well plates in c-α-MEM containing 100 μM ascorbate and were allowed to adhere overnight. The medium was then replaced with osteogenic media containing imatinib, dasatinib or vehicle and, where indicated, 10 ng/mL rhPDGF-BB. Following 42 days of treatment, mineral was dissolved with HCl and calcium content was calculated using the cresolphthalein complexone assay. Calcium produced per well was corrected for relative cell numbers by determining total DNA content per well. Graphs depict mean ± range of 2 independent experiments. * $p < 0.05$ as indicated (Student's t-test).

A

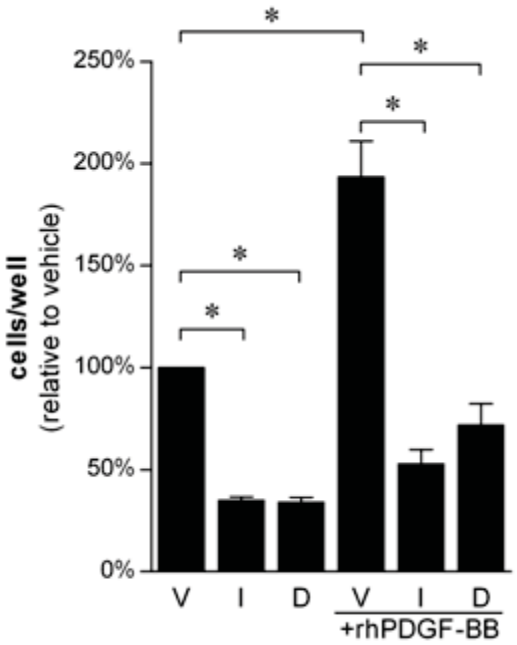
cells/well
(relative to vehicle)
250%
200%
150%
100%
50%
0%
*
V
I
D
V
I
D
+rhPDGF-BB

B

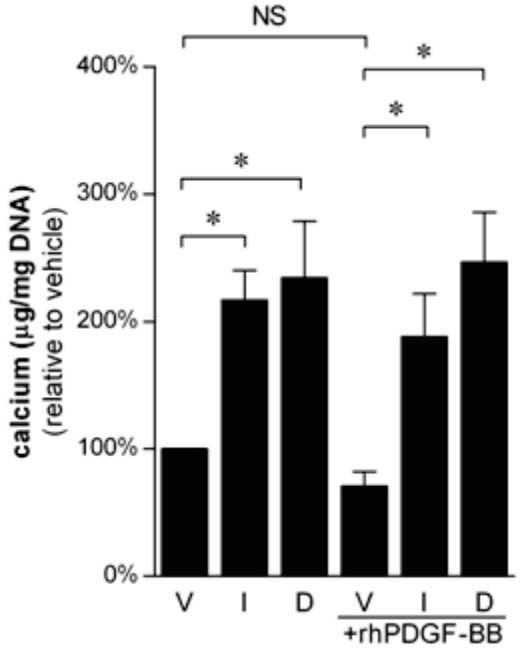
NS
calcium (µg/mg DNA)
(relative to vehicle)
400%
300%
200%
100%
0%
*
V
I
D
V
I
D
+rhPDGF-BB

6.2.2 Imatinib and dasatinib inhibit chondrocyte proliferation and activity *in vitro*

6.2.2.1 Imatinib and dasatinib inhibit the proliferation of ATDC5 cells in vitro

To determine whether tyrosine kinase inhibition can directly affect chondrocyte proliferation or activity, the effects of imatinib and dasatinib on the murine pre-chondrocyte cell line ATDC5[298] were investigated *in vitro.*

To examine the effects of tyrosine kinase inhibition on ATDC5 proliferation, cells were cultured for 2, 4 or 6 days with imatinib, dasatinib or vehicle and the relative number of cells per well was determined by WST-1 assay. In vehicle-treated cultures, cell numbers increased 4-fold during the 6 days of culture. Imatinib dose-dependently decreased cell numbers at all three time points at concentrations of 0.13 μM and higher, with 4 μM imatinib resulting in no detectable cell proliferation, relative to prior to treatment (day 0) (figure 6.8A). Treatment of ATDC5 cells with dasatinib significantly inhibited cell proliferation at concentrations of 2.5 nM and higher after 2, 4 or 6 days (figure 6.8B). Treatment with 40 nM dasatinib completely inhibited cell proliferation over this time period (figure 6.8B).

6.2.2.2 Imatinib and dasatinib inhibit the activity of ATDC5 cells in vitro

The effects of imatinib and dasatinib on chondrocyte activity were next investigated using a GAG-synthesis assay. ATDC5 cultures were treated with 10 ng/mL rhTGF-β1, a known inducer of chondrocyte differentiation and activity.[420-422] Addition of rhTGF-β1 increased GAG production 2.5-fold and 4-fold after 24 and 48 hours, respectively (figure 6.9A-D). Treatment with imatinib, up to 4 μM, or dasatinib, up to 80 nM, had no effect on TGF-β1-induced GAG synthesis after 24 hours (figure 6.9A,B). However, after 48 hours of treatment, there was a significant reduction in GAG production in cultures treated with 1 μM imatinib or more, with an almost 40% reduction in GAG synthesis at 2 and 4 μM imatinib, relative to vehicle controls (figure 6.9C). Similarly, dasatinib treatment for 48 hours significantly decreased TGF-β1-induced GAG synthesis at 40 nM and 80 nM concentrations (figure 6.9D).

To determine whether these inhibitory effects on GAG synthesis were specific to TGF-β1-induction, the effects of dasatinib and imatinib on GAG production in unstimulated ATDC5 cell cultures was examined. After 48 hours of imatinib treatment, a significant decrease in the production of GAG, normalised for cell numbers, was observed at 0.5 μM concentrations and higher (figure 6.10A). On a per cell basis, GAG production

Figure 6.8. Imatinib and dasatinib inhibit cell proliferation in ATDC5 cell cultures *in vitro*. ATDC5 cells (1.56 x 10^4 cells/cm^2) were seeded in 96-well plates in c-α-MEM supplemented with ascorbate (100 μM) and were cultured overnight to allow the cells to adhere. The cells were then treated with imatinib (**A**), dasatinib (**B**) or vehicle (0.5% DMSO) for the indicated periods of time before the relative number of cells per well were determined by WST-1 assay. Graphs depict mean ± range of 2 representative experiments, normalised to vehicle controls. * $p < 0.05$ relative to vehicle control at each time-point (one-way ANOVA with Dunnett's post-tests).

A

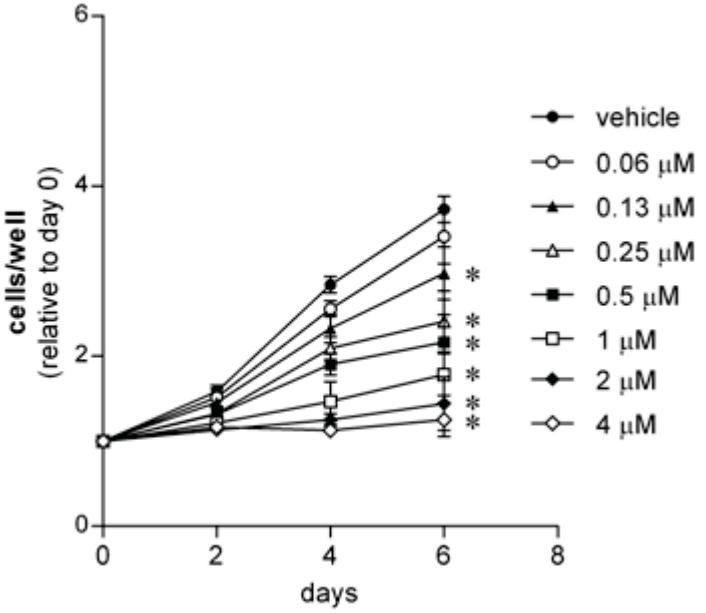
cells/well
(relative to day 0)
days
vehicle
0.06 μM
0.13 μM
0.25 μM
0.5 μM
1 μM
2 μM
4 μM
*
*
*
*
*
*

B

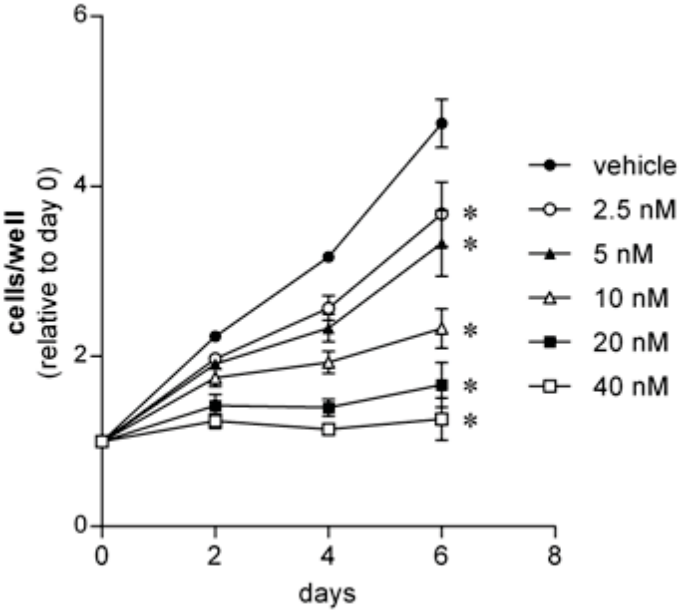
cells/well
(relative to day 0)
days
vehicle
2.5 nM
5 nM
10 nM
20 nM
40 nM
*
*
*
*
*

Figure 6.9. Imatinib and dasatinib inhibits TGF-β1-induced GAG-production in ATDC5 cell cultures *in vitro*. ATDC5 cells (1.56 x 10^5 cells/cm^2) were cultured in 96-well plates in media containing ascorbate-2-phosphate (100 μM). Following overnight adhesion, the cultures were treated with rhTGF-β1 (10 ng/mL) and the indicated doses of imatinib (**A**,**C**) or dasatinib (**B**,**D**) or 0.05% DMSO vehicle. After 24 (**A**,**B**) or 48 (**C**,**D**) hours, treatment media were replaced with media containing 1 μCi $^{35}SO_4$ and the plates were incubated overnight. The matrix was then digested and the amount of $^{35}SO_4$-labelled glycosaminoglycans (GAG) was measured using a scintillation counter. In replicate cultures, cells were digested with papain and the DNA content was measured, as a surrogate marker of cell number. GAG levels were then normalised to DNA content to determine relative GAG production per cell. Graphs depict mean ± SEM of triplicate wells of one experiment, normalised to the rhTGF-β1-treated vehicle control. * $p < 0.05$ relative to the rhTGF-β1-treated vehicle control (one-way ANOVA with Dunnett's post-tests).

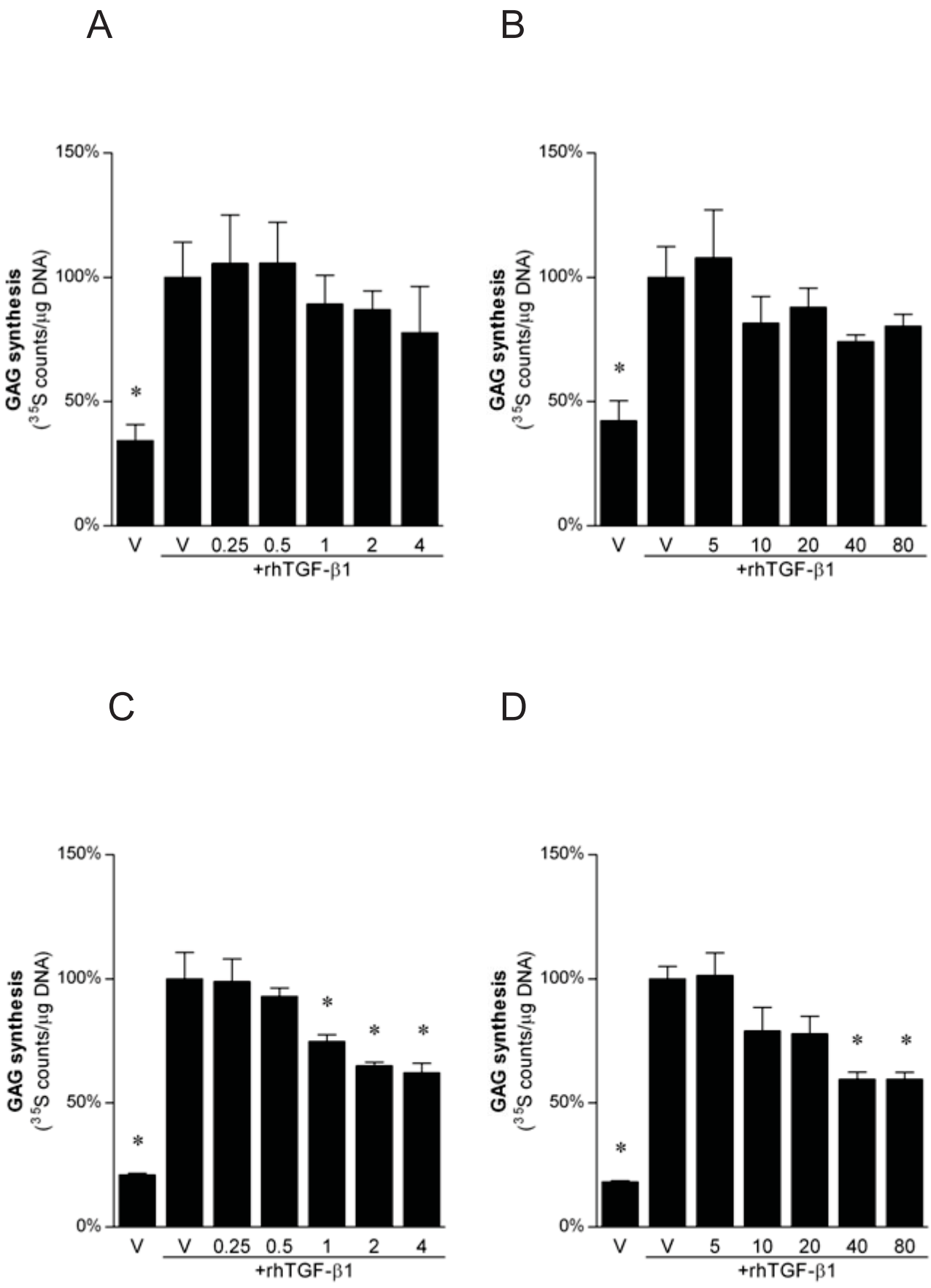
A
B
C
D
GAG synthesis
(^{35}S counts/μg DNA)
150%
100%
50%
0%
*
V
V 0.25 0.5 1 2 4
+rhTGF-β1
V 5 10 20 40 80

Figure 6.10. Imatinib and dasatinib inhibits basal GAG-production in ATDC5 cell cultures *in vitro*. ATDC5 cells (1.56 x 10^5 cells/cm^2) were cultured in 96-well plates in media containing ascorbate (100 μM). Following overnight adhesion, the cultures were treated with the indicated doses of imatinib (**A**) or dasatinib (**B**) or vehicle (0.05% DMSO). After 48 hours, the cells were incubated overnight with 1 μCi $^{35}SO_4$, the matrix was digested and the amount of $^{35}SO_4$-labelled GAG was then measured using a scintillation counter. In replicate cultures, cells were digested and DNA content per well was measured as a surrogate marker of cell number. GAG levels were then normalised to DNA content to determine relative GAG production per cell. Graphs depict mean ± SEM of 3 independent experiments normalised to vehicle controls. * $p < 0.05$ relative to vehicle control (one-way ANOVA with Dunnett's post-tests).

A

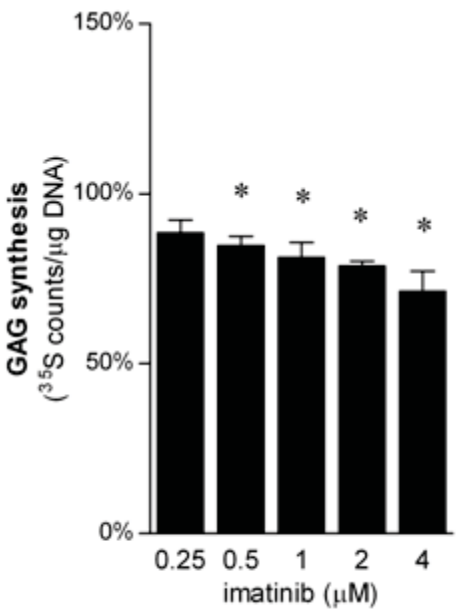
150%
100%
50%
0%
GAG synthesis
(^{35}S counts/μg DNA)
*
*
*
*
0.25
0.5
1
2
4
imatinib (μM)

B

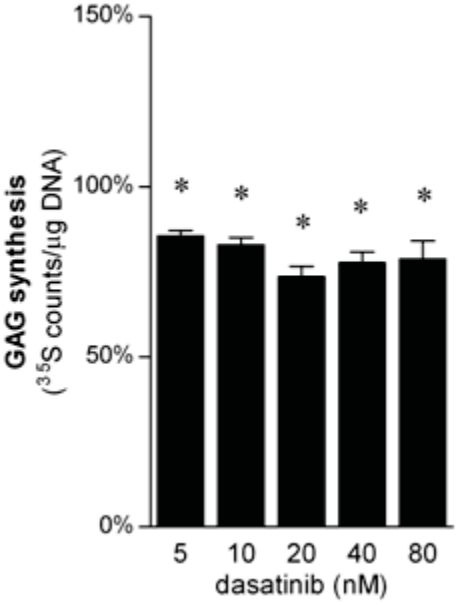
150%
100%
50%
0%
GAG synthesis
(^{35}S counts/μg DNA)
*
*
*
*
*
5
10
20
40
80
dasatinib (nM)

Figure 6.11. Imatinib inhibits PDGFR signalling in ATDC5 cells *in vitro*. ATDC5 cells were cultured at 1.56 x 10^5 cells/cm^2on 6-well plates in c-α-MEM containing 100 μM ascorbate. After overnight culture, the cells were serum-starved by overnight incubation in sf-α-MEM. The cells were pre-treated with sf-α-MEM containing imatinib or 0.05% DMSO prior to stimulation with rhPDGF-BB (10 ng/mL) for 5 min and the cells were then lysed. Cell lysates (30 μg/lane) were resolved through a 10% polyacrylamide SDS-PAGE gel and the proteins were transferred to PVDF. Phosphorylated forms of Akt (p-Akt) and ERK1/2 (p-ERK1/2), as well as total HSP90, were detected using specific antibodies. Representative images are shown (**A**). Graphs indicate the relative pixel intensity for p-Akt (**B**) and p-ERK1/2 (**C**) normalised to HSP90 from a representative of 2 experiments.

A

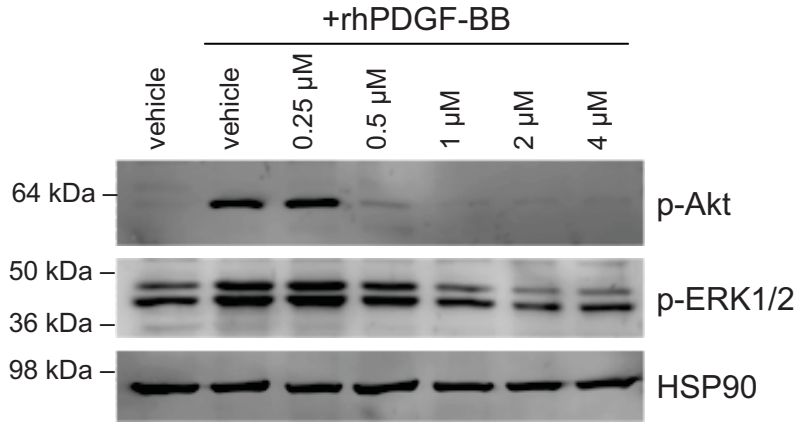
+rhPDGF-BB
vehicle
vehicle
0.25 µM
0.5 µM
1 µM
2 µM
4 µM
64 kDa
p-Akt
50 kDa
36 kDa
p-ERK1/2
98 kDa
HSP90

B

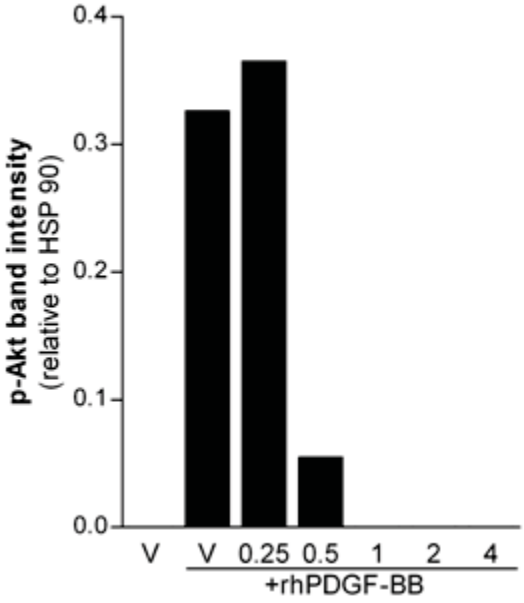
p-Akt band intensity
(relative to HSP 90)
0.4
0.3
0.2
0.1
0.0
V
V
0.25
0.5
1
2
4
+rhPDGF-BB

C

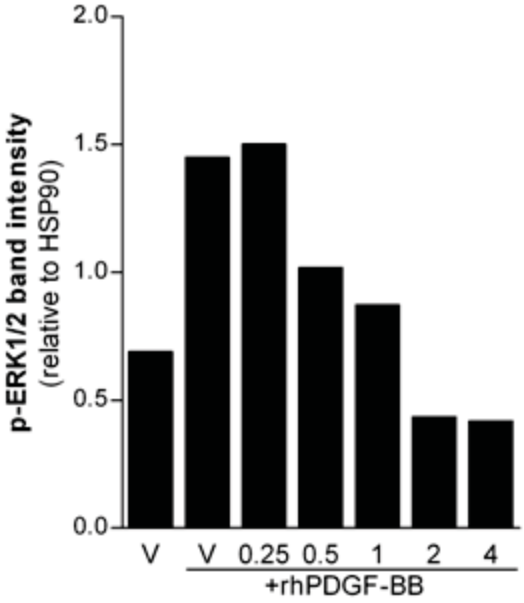
p-ERK1/2 band intensity
(relative to HSP90)
2.0
1.5
1.0
0.5
0.0
V
V
0.25
0.5
1
2
4
+rhPDGF-BB

was significantly inhibited by 5 nM dasatinib and higher, relative to vehicle controls (figure 6.10B).

6.2.2.3 Imatinib and dasatinib abrogate PDGF-induced phosphorylation of ERK1/2 and Akt in ATDC5 cultures

PDGF-BB is a known mitogen for chondrocytes which, in some cases, has been reported to promote chondrocyte activity[381,382] suggesting that imatinib or dasatinib treatment may have direct effects on chondrocyte proliferation and activity through inhibition of PDGFRβ. It was next examined whether inhibition of PDGFRβ contributed to the inhibitory effects of imatinib and dasatinib on ATDC5 proliferation and GAG production.

First, the effects of imatinib and dasatinib on PDGFR receptor signalling through Akt and ERK1/2 were examined by Western blot. ATDC5 cells were serum-starved for 24 hours and either imatinib, dasatinib or vehicle were added to cultures for the final 2 hours of starvation. Where indicated, rhPDGF-BB was added to cultures for 5 minutes prior to the preparation of cell lysates and proteins were detected by Western blot. As shown in figure 6.11 and 6.12, rhPDGF-BB treatment rapidly induced the phosphorylation of Akt and ERK1/2 in ATDC5 cells. Pre-treatment with imatinib or dasatinib dose-dependently inhibited the phosphorylation of Akt and ERK1/2 in response to PDGF-BB (figure 6.11A, 6.12A). Quantitation of the intensity of the bands corresponding to phosphorylated Akt, normalised to HSP90, showed that imatinib at concentrations exceeding 0.25 μM inhibited the induction of PDGFR signalling by rhPDGF-BB (figure 6.11B). Imatinib at concentrations of 0.5 μM and higher inhibited the phosphorylation of ERK1/2 in response to rhPDGF-BB, with 2 μM and 4 μM imatinib decreasing ERK1/2 phosphorylation to levels lower than at baseline (figure 6.11C). Pre-treatment of ATDC5 cells with dasatinib significantly inhibited the induction of Akt and ERK1/2 phosphorylation by rhPDGF-BB treatment (figure 6.12A). Dasatinib at concentrations of 20 nM and 40 nM substantially reduced the induction of Akt and ERK1/2 phosphorylation, relative to the vehicle-treated controls (figure 6.12B,C), with 40 nM dasatinib completely abrogating PDGFR signalling (figure 6.12B,C).

6.2.2.4 Sigmoidal dose-response relationship of the inhibition of chondrocyte proliferation, activity and PDGFR signalling by imatinib and dasatinib

The relationship between the concentrations at which imatinib and dasatinib inhibit PDGFR signalling, cell proliferation and TGF-β1-induced GAG production in ATDC5

Figure 6.12. Dasatinib inhibit PDGFR signalling in ATDC5 cells *in vitro*. ATDC5 cells were cultured at 1.56 x 10^5 cells/cm^2on 6-well plates in c-α-MEM containing 100 μM ascorbate. After overnight culture, the cells were serum-starved by overnight incubation in sf-α-MEM. The cells were pre-treated with sf-α-MEM containing dasatinib or 0.05% DMSO prior to stimulation with rhPDGF-BB (10 ng/mL) for 5 min and the cells were then lysed. Cell lysates (30 μg/lane) were resolved through a 10% polyacrylamide SDS-PAGE gel and the proteins were transferred to PVDF. Phosphorylated forms of Akt and ERK1/2, as well as total HSP90, were detected using specific antibodies. Representative images are shown (**A**). Graphs indicate the relative pixel intensity for phosphorylated Akt (**B**) and phosphorylated ERK1/2 (**C**) normalised to HSP90 from a representative of 2 experiments.

A

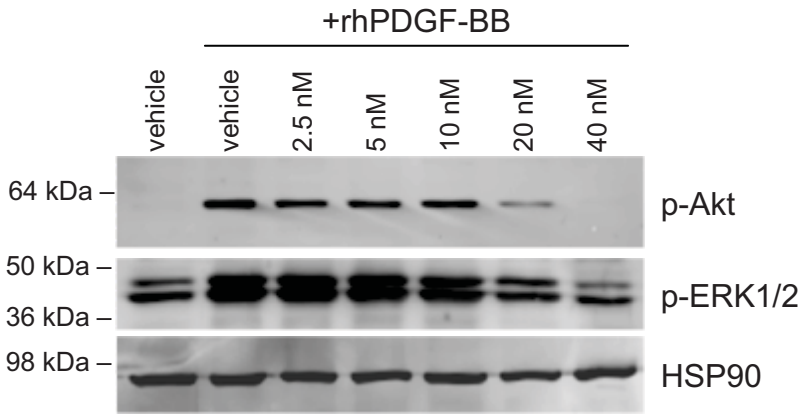
+rhPDGF-BB
vehicle
vehicle
2.5 nM
5 nM
10 nM
20 nM
40 nM
64 kDa –
50 kDa –
36 kDa –
98 kDa –
p-Akt
p-ERK1/2
HSP90

B

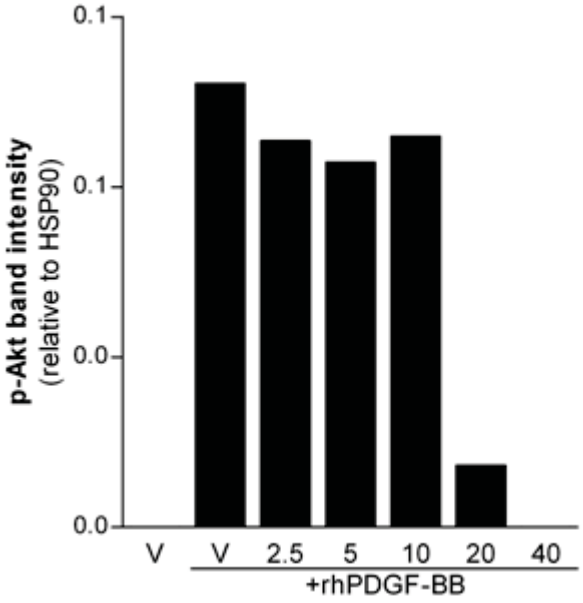
p-Akt band intensity
(relative to HSP90)
0.1
0.1
0.0
0.0
V
V
2.5
5
10
20
40
+rhPDGF-BB

C

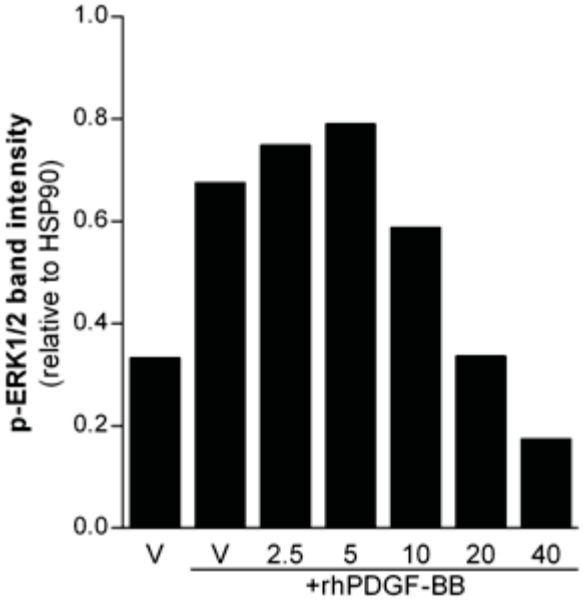
p-ERK1/2 band intensity
(relative to HSP90)
1.0
0.8
0.6
0.4
0.2
0.0
V
V
2.5
5
10
20
40
+rhPDGF-BB

cells was investigated by fitting the data to a sigmoidal dose-response curve (figure 6.13A,B).

Imatinib inhibited PDGFR signalling through Akt and ERK1/2, cell proliferation and GAG production at IC_{50} of 0.37 μM, 0.55 μM, 0.19 μM and 0.75 μM, respectively (figure 6.13A). For dasatinib, the IC_{50} for the inhibition of Akt and ERK1/2 phosphorylation, cell proliferation and GAG synthesis were 5.48 nM, 13.03 nM, 15.07 nM and 13.44 nM, respectively (figure 6.13B).

6.2.2.5 Imatinib and dasatinib inhibit the effects of PDGF-BB on cell proliferation and chondrocyte activity

To determine whether therapeutically-achievable concentrations of imatinib and dasatinib could inhibit the effects of PDGF on chondrocyte proliferation and activity, WST-1 and GAG-synthesis assays were carried out.

Similar to results shown earlier, treatment of ATDC5 cells with imatinib (4 μM) and dasatinib (40 nM) for 6 days significantly decreased the cell numbers, relative to vehicle controls (figure 6.14A). Treatment of ATDC5 cells with PDGF-BB for 6 days increased the number of cells per well by 1.5-fold, compared with vehicle-treated controls (figure 6.14A). This increase in cell proliferation was completely inhibited by co-treatment with imatinib or dasatinib, resulting in cell numbers similar to those in cultures treated with imatinib or dasatinib alone (figure 6.14A).

Treatment of ATDC5 cultures with 4 μM imatinib or 40 nM dasatinib significantly inhibited basal levels of GAG synthesis (figure 6.14B). Under the conditions used here, treatment with rhPDGF-BB for 48 hours induced a 3-fold increase in GAG production, on a per cell basis, relative to untreated controls (figure 6.14B). This stimulatory effect of PDGF-BB was partially inhibited by co-treatment with 4 μM imatinib or 40 nM dasatinib, although levels did not reach those of unstimulated imatinib- or dasatinib-treated cultures (figure 6.14B).

Figure 6.13. Sigmoidal dose response curve of the effects of imatinib and dasatinib on cell proliferation, PDGFR signalling and GAG production in ATDC5 *in vitro*. Mean values for the inhibitory effects of imatinib (**A**) and dasatinib (**B**) on cell proliferation (WST-1), GAG synthesis and PDGF-BB-induced Akt and ERK1/2 phosphorylation in ATDC5 were plotted to obtain a sigmoidal dose-response curve fit.

A

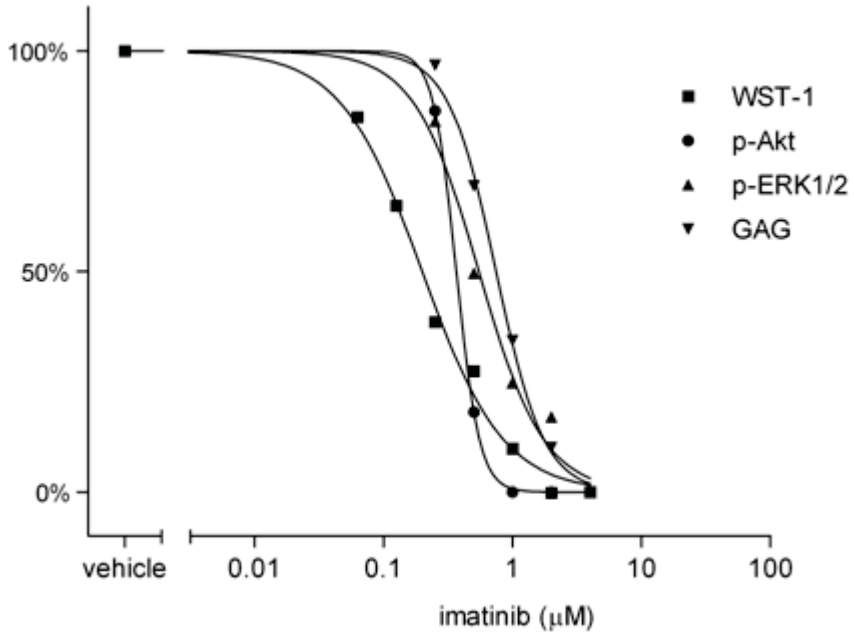
100%
50%
0%
vehicle
0.01
0.1
1
10
100
imatinib (μM)
WST-1
p-Akt
p-ERK1/2
GAG

B

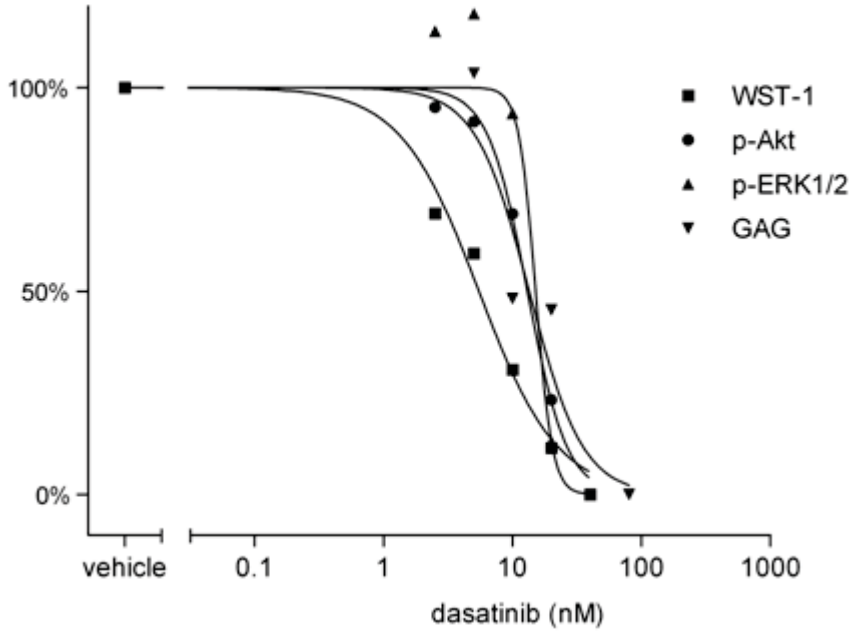
100%
50%
0%
vehicle
0.1
1
10
100
1000
dasatinib (nM)
WST-1
p-Akt
p-ERK1/2
GAG

Figure 6.14. Imatinib and dasatinib inhibit PDGF-BB-induced cell proliferation and GAG production in ATDC5 cell cultures *in vitro*. A. ATDC5 cells (1.56 x 10^4 cells/cm^2) were seeded in 96-well plates in c-α-MEM supplemented with ascorbate (100 μM) and were cultured overnight to allow the cells to adhere. The cells were then treated with 4 μM imatinib, 40 nM dasatinib or vehicle (0.5% DMSO) supplemented, where indicated, with 10 ng/mL PDGF-BB. After 6 days, the relative number of cells per well were determined by WST-1 assay. Graphs depict mean ± range of 2 representative experiments, normalised to vehicle control. **B**. ATDC5 cells were cultured at 1.56 x 10^5 cells/cm^2 overnight in 96-well plates and were then treated with vehicle (V), 4 μM imatinib (I) or 40 nM dasatinib (D) with or without 100 ng/mL recombinant human PDGF-BB. After 48 hours, treatment media were replaced with c-α-MEM containing 1 μCi $^{35}SO_4$ and the plates were incubated overnight. GAG levels and DNA content were quantitated and GAG production per cell was calculated. Graphs depict mean ± SEM of triplicate wells of 1 experiment normalised to vehicle controls. * $p < 0.05$, as indicated (Student's T-tests).

A

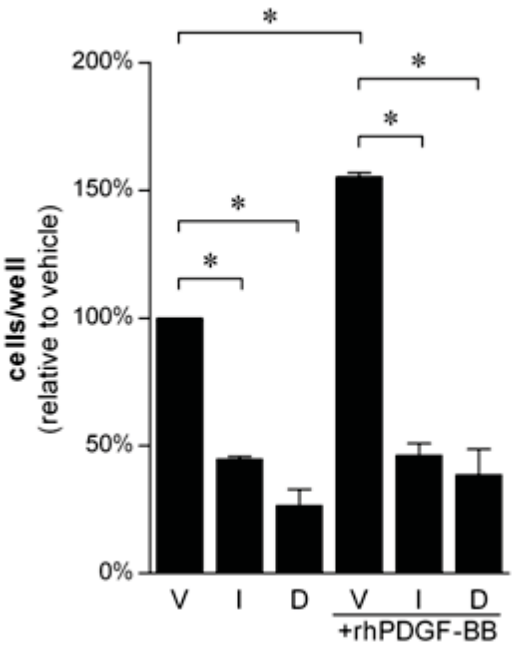
cells/well
(relative to vehicle)
200%
150%
100%
50%
0%
V
I
D
V
I
D
+rhPDGF-BB
*

B

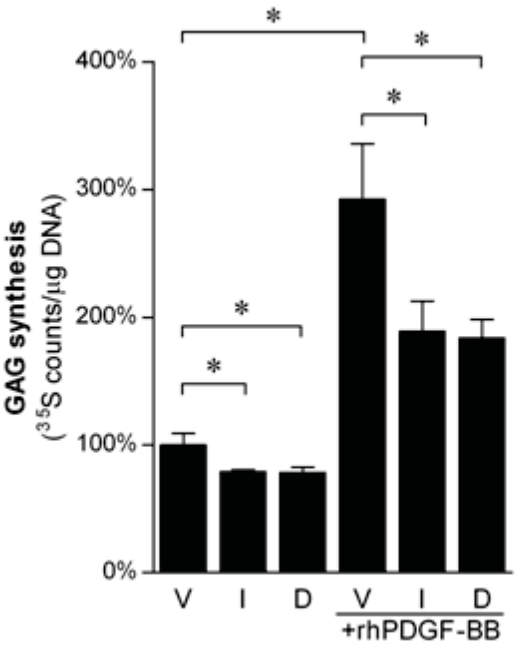
GAG synthesis
(^{35}S counts/µg DNA)
400%
300%
200%
100%
0%
V
I
D
V
I
D
+rhPDGF-BB
*

6.3 Discussion

Previous studies have shown that treatment of human and rodent cells with the tyrosine kinase inhibitor imatinib inhibited cell proliferation and increased mineralised matrix formation *in vitro*. In cultures of human primary stromal cells and cell lines, treatment with imatinib significantly increased mineral deposition[10,17,19] and decreased proliferation of stromal cells[10,16-18]. Similarly, imatinib increased mineralisation[17] and partially inhibited cell proliferation[17,18] in primary rat stromal cells and murine cell lines. We have now confirmed these results in bone marrow stroma isolated from Sprague-Dawley rats. Additionally, the current study has shown that dasatinib inhibits rodent stromal cell proliferation while promoting osteoblast activity (figure 6.2, 6.3). The results presented here have subsequently been confirmed by Lee *et al*. in mouse calvaria-derived stromal cell cultures and the mouse osteoblast-like cell line MC3T3-E1.[423] Although data shown here indicate that dasatinib can increase rat osteoblast activity *in vitro*, in chapter 4 it was found that dasatinib treatment had no effect on serum osteocalcin levels, P1NP levels, BFR or MAR in normal rats *in vivo*, suggesting that dasatinib did not affect osteoblasts at the dose administered. The concentration at which dasatinib activates osteoblast activity *in vitro* is more than 8-fold higher than that required to inhibit osteoclast activity. The concentrations achieved in the *in vivo* study reported in chapter 4 may therefore have been sufficient to inhibit osteoclasts while not reaching the concentrations required to modulate osteoblast function.

The proliferation, differentiation and maturation of osteoblasts are influenced by several receptor and non-receptor tyrosine kinases which are inhibited by imatinib and/or dasatinib. Here we have demonstrated that PDGF-BB treatment stimulated cell proliferation and inhibited mineral production in primary rat stromal cell cultures. This is consistent with previous results indicating that PDGF is an important regulator of osteoblast formation as it enhances osteoblast proliferation while inhibiting osteoblast differentiation *in vitro*.[280,289-291] Results shown here (figure 6.7) and previously[280,289-291], demonstrate that PDGF-BB is a potent mitogen for osteoblast precursors which also inhibits osteoblast differentiation *in vitro*. Previous studies from our laboratory[10] and those of others[16-19], have suggested that the positive effects of imatinib on osteoblast activity may be due to inhibition of PDGFR. In the present study, imatinib and dasatinib reversed the mitogenic effects of PDGF-BB on cell proliferation and counteracted the inhibitory effects of PDGF-BB on mineral deposition. Nevertheless, a direct association between inhibition of PDGFR by imatinib and dasatinib and increased osteoblast activity remains to be

demonstrated. In the studies presented here, the concentrations at which imatinib and dasatinib inhibit PDGFR signalling (1 μM and 10 nM, respectively; figure 6.4, 6.5) were lower than those required to activate mineralising activity in rBMSC cultures (2 μM and 40 nM, respectively; figure 6.3), suggesting that inhibition of other kinases may also be involved in the effects of these tyrosine kinase inhibitors on osteoblasts.

The pro-osteoblastic effects of inhibition of PDGFR by imatinib and dasatinib may be opposed by inhibition of Abl. Abl is a non-receptor tyrosine kinase which is a positive regulator of osteoblast activity. Targeted disruption of *Abl* in mice results in osteoporosis due to decreased osteoblast activity.[284] *In vitro*, Abl-deficient stromal cells synthesise less mineral and express less alkaline phosphatase than wild-type controls, while the proliferative capacity of *Abl*$^{-/-}$ mesenchymal cells is normal.[284] If Abl kinase activity is required for osteoblast activity, the inhibition of Abl and PDGFR by tyrosine kinase inhibitors may have opposing effects on osteoblast activity. Tellingly, the response of *Abl*$^{-/-}$ cells to PDGF-BB treatment is abnormal.[284] While PDGF-BB treatment decreased alkaline phosphatase expression in wild-type osteoblasts by approximately 80%, consistent with the anti-osteoblastic properties of PDGF, Abl-deficient osteoblasts responded less strongly to PDGF, with a 50% decrease in alkaline phosphatase expression in response to PDGF-BB.[284] *Abl*$^{-/-}$ mesenchymal cells had a normal mitogenic response to PDGF-BB, supporting the theory that Abl does not play a role in osteoblast proliferation.

In addition, dasatinib may also affect osteoblasts through inhibition of Src kinase activity. Src has long been known to play an important role in skeletal development, as Src-deficient mice have increased bone density relative to wild-type controls.[353] While this has primarily been attributed to inhibited osteoclast activity[353], activation of osteoblasts in Src-deficient mice may also contribute to the osteopetrotic phenotype. Src-deficient mice have increased mineralising surface and bone formation rates compared with wild-type controls.[424] Cultured *Src*$^{-/-}$ calvarial osteoblasts proliferate more slowly, while producing significantly more mineral, than wild-type controls.[424] Similarly, knockdown of Src expression in mouse osteoblasts *in vitro* inhibits cell proliferation and increases mineral deposition and alkaline phosphatase expression.[423,424] Therefore, inhibition of Src by dasatinib may complement the effects of PDGFR inhibition on osteoblasts.

Dasatinib may also dysregulate bone formation through inhibition of Eph tyrosine kinase activity. Eph receptors are activated by binding to members of the Ephrin family of membrane-bound ligands, inducing conformational changes and Eph kinase-dependent phosphorylation which results in bi-directional signalling in the ligand- and receptor-

bearing cells (reviewed in [425]). While imatinib has no effect on Eph kinase activity[237,426], dasatinib is a potent inhibitor of EphB2[222,237] and EphB4[237,349], which are expressed at high levels in osteoblasts[131]. EphrinB2-EphB4 and EphrinB1-EphB2 interactions are important mediators of cell-cell interactions which up-regulate osteoblast activity.[427,428] Stimulation of murine osteoblast cultures with either EphrinB2 or EphB2 increased osteoblast differentiation *in vitro*, suggesting that forward signalling through EphB4 and reverse signalling through EphrinB1 may play a role in stimulating osteoblast activity.[427,428] Osteoblast-specific deletion of EphrinB1 resulted in stunting due to decreased bone formation rates[428] while osteoblast-specific overexpression of EphB4 resulted in increased bone density and bone formation rates[131]. Similarly, while EphrinB1-deficient osteoblasts exhibit decreased mineralisation rates[428], over-expression of EphB4 increased mineral deposition *in vitro*[131]. These data suggest that inhibition of EphB2 and EphB4 by dasatinib may have additional inhibitory effects osteoblast formation through inhibition of cell-cell signalling.

In addition to confirming the effects of tyrosine kinase inhibition on osteoblasts, the studies presented here demonstrate for the first time that imatinib and dasatinib inhibit the proliferation and activity of chondrocytes *in vitro*. These results may be attributable, at least in part, to inhibition of PDGFR signalling. As demonstrated here (figure 6.14) and previously[381,382] PDGF-BB treatment increases the proliferation and, in some cases, activity of murine and bovine chondrocytes. Imatinib and dasatinib treatment partially reversed the activating effects of PDGFR on the proliferation and activity of the murine chondrocyte cell line ATDC5. The decreased growth plate thickness observed in imatinib and dasatinib-treated normal rats in chapter 4 may therefore be attributable to decreased chondrocyte proliferation and activity through inhibition of PDGFR. However, while the inhibition of PDGFR signalling is likely to contribute to the inhibitory effects of imatinib and dasatinib on chondrocytes, there was a lack of association between the concentration at which chondrocyte proliferation, activity and PDGFR signalling was inhibited, suggesting that other tyrosine kinases may also play a role in the effects of imatinib and dasatinib on chondrogenesis.

The membrane tyrosine kinase receptor DDR2, a recently-identified target of imatinib, but not dasatinib[349], may play a role in the inhibitory effects of imatinib on chondrocytes. In the mouse tibial and femoral growth plates, DDR2 expression is localised to the late-proliferative and hypertrophic zone.[383,429] The expression and kinase activity of DDR2 is activated following binding to collagen II, the most abundant collagen in

cartilage, and collagen X, which is expressed almost exclusively by chondrocytes in the hypertrophic zone.[383,429-433] While the role of DDR2 in growth plate chondrocyte activity is incompletely understood, DDR2 is thought to be important in chondrocyte proliferation. DDR2-deficient animals are stunted due to decreased longitudinal bone growth.[383] The proliferation of growth plate chondrocytes in *DDR2*$^{-/-}$ animals is delayed *in vivo*, resulting in narrowed growth plates, and isolated *DDR2*$^{-/-}$ chondrocytes have decreased proliferation rates *in vitro*.[383] Since DDR2 plays a role in chondrocyte proliferation, the contribution of DDR2 inhibition to the effects of imatinib in chondrogenesis should be investigated further.

Inhibition of Src-family kinases by dasatinib may also result in decreased chondrocyte proliferation. Studies using the Src-family kinase inhibitor PP2 have demonstrated a role for Src-family kinases in chondrocyte proliferation, adhesion and cell spreading. Following the adhesion of chondrocytes to extracellular matrix proteins, Src binds to and activates focal adhesion kinase (FAK), activating signalling pathways that regulate chondrocyte adhesion and spreading.[434,435] Inhibition of Src kinase activity with PP2 prevented murine chondrocyte spreading and attachment to the extracellular matrix proteins fibronectin and bone sialoprotein.[385] Furthermore, treatment of primary mouse mesenchymal cells with PP2 induces the expression of genes involved in early chondrocyte differentiation, suggesting that Src signalling may be involved in pathways that inhibit chondrogenesis.[384,386] PP2 treatment of primary murine chondrocytes also inhibits cell proliferation *in vitro*.[384,386] Thus inhibition of Src-family kinases by dasatinib may contribute to observed inhibition of chondrocyte proliferation in ATDC5 cultures *in vitro* and may counteract the inhibitory affects of dasatinib on chondrocyte activity. However, while *Src*$^{-/-}$ mice have retarded long bone growth, the growth plates of Src-deficient mice are wider than normal[353] suggesting that inhibition of Src alone cannot explain growth plate narrowing observed in normal rats in chapter 4. Other Src-family kinases may be involved in the observed effects of PP2 and dasatinib on chondrocytes *in vitro* or, alternatively, redundancy in the roles of Src family members may compensate for Src-deficiency *in vivo*.

In summary, this study has confirmed previous reports indicating that imatinib increases osteoblast activity while inhibiting cell proliferation in primary rat cultures *in vitro*. Furthermore, data presented here show that dasatinib has similar effects on osteoblast proliferation and activity *in vitro*, via a mechanism that, in part, involves PDGFRβ inhibition. These results, when taken together with the inhibitory effects of imatinib and

dasatinib on osteoclasts shown in chapter 5, suggest decoupling of the bone remodelling process is a likely side-effect of imatinib and dasatinib treatment. Furthermore, this study demonstrates that imatinib and dasatinib can also inhibit chondrocyte proliferation and activity *in vitro*, suggesting a mechanism for the growth plate narrowing observed in imatinib- and dasatinib-treated rats in chapter 4.

Chapter 7

Discussion

7.1 The effects of tyrosine kinase inhibition on skeletal remodelling

When compared with conventional chemotherapeutics, imatinib represented a revolution in the treatment of CML, vastly improving therapeutic efficacy and limiting toxicity.[3,241] However, despite the high rate of complete molecular remission in imatinib-treated chronic phase CML patients[3,241], the persistence of low, undetectable, levels of leukaemic cells can result in relapse after therapy withdrawal.[436-440] The current paradigm therefore suggests that imatinib treatment may need to be continued indefinitely, highlighting the need to assess the off-target consequences of long-term tyrosine kinase inhibition.

The predominant side-effects of imatinib are mild to moderate and include nausea, diarrhoea, rash and oedema.[3,241,320] However, emerging evidence suggests that imatinib treatment may also result in skeletal side-effects, resulting in increased bone volume and density.[10,12,20] While changes in serum markers of bone remodelling have been observed in imatinib-treated CML and GIST patients[5,8,12], effects on osteoclasts and osteoblasts have not been directly investigated in patients. As part of the studies presented in this thesis, it was found that imatinib treatment of CML patients resulted in increased trabecular thickness in iliac crest biopsies and an increase in BMD and BMC at the 33% radius and the tibia and fibula sites after 12 months of treatment. This was associated with a dramatic decrease in osteoclast numbers and serum markers of osteoclast activity, while osteoblast activity was unchanged or slightly increased. The effects of imatinib on histomorphometric parameters suggested that bone formation and resorption were uncoupled in these patients, in favour of osteoblast activity.

Despite the emerging data indicating that imatinib alters bone remodelling, the effect of second-generation tyrosine kinase inhibitors on bone remodelling in CML patients have not been investigated. As part of this project, *in vivo* and *in vitro* models were utilised to demonstrate that dasatinib, like imatinib, can cause dysregulated bone remodelling, primarily through the inhibition of osteoclastogenesis. Treatment of normal, skeletally-mature rats with dasatinib caused an increase in trabecular bone volume which was attributable to an increase in trabecular thickness (chapter 4). This increase in bone volume was associated with a decrease in both osteoclast numbers and serum CTX-1 levels. *In vitro* data, presented in chapter 5, indicated that dasatinib potently inhibits osteoclast formation/survival, leading to a profound decrease in osteoclast activity. This was primarily attributable to a previously unidentified inhibitory activity of dasatinib on Fms. Inhibition of Src activity was not found to contribute substantially to the anti-osteoclastogenic effect of dasatinib *in vitro*.

While *in vitro* data presented in chapter 6 indicated that dasatinib increased osteoblast activity while inhibiting mesenchymal cell proliferation, no detectable effect of dasatinib on osteoblasts was identified in dasatinib-treated rats. Thus, dasatinib had a similar effect on skeletal metabolism in rats as that was observed in imatinib-treated patients; that is, dasatinib inhibited osteoclastogenesis, resulting in an imbalance in bone turnover that favoured osteoblast activity, thereby increasing bone volume. The implications of these results for bone metabolism in patients undergoing dasatinib therapy await further investigation.

The data presented in this thesis highlight the need for studies into the potential long-term consequences of imatinib and dasatinib therapy for bone quality. While the observed increases in trabecular thickness and volume following imatinib and dasatinib treatment is suggestive of increased bone strength[323-325] inhibition of bone turnover may increase bone fragility through the accumulation of microfracture damage.[75,441,442] In healthy bone, the accumulation of microfractures over time is controlled by targeted bone remodelling.[75,441] Abrogation of bone remodelling may therefore increase the degree of skeletal microdamage and lead to bone with decreased mechanical strength.[442] In support of this proposition, studies in beagles have suggested that long-term inhibition of bone turnover by bisphosphonates may result in increased microfracture accumulation and, in some cases, decreased bone strength.[443-445] However, this has not been demonstrated in patients, perhaps because bone turnover is not completely inhibited in patients undergoing bisphosphonate therapy.[446-449] Similarly, the results presented in this thesis suggest that imatinib and dasatinib do not completely abrogate bone turnover, but, rather, shift the balance of bone remodelling towards bone formation. Further studies are required to determine whether accumulation of microfracture damage may be a potential detrimental effect of long-term tyrosine kinase inhibitor therapy.

In addition, tyrosine kinase inhibitors may affect bone healing following fracture via their effects on PDGFR. Expression of PDGF ligands and receptors are up-regulated during callous formation following fracture in humans and rodents, suggesting that PDGFR signalling may play a role in fracture healing.[450-452] Furthermore, conditional deletion of PDGFRβ in mice has been shown to result in abnormal callous formation in a tibial fracture model.[291] In contrast, local administration of rhPDGF-BB at the site of tibial or femoral osteotomy increased the rate of fracture healing in rabbits and rats.[453,454] Further investigation is warranted to determine whether PDGFR inhibition results in aberrant fracture healing in patients undergoing tyrosine kinase inhibitor therapy.

Despite the decrease in osteoclast activity and the increase in trabecular thickness observed in imatinib-treated patients, imatinib treatment was associated with a decrease in BMD and BMC at the femoral neck. This is a concern as BMD is a strong indicator of facture risk. Hip fractures, in particular, are strongly associated with decreased BMD and are a major cause of disability and mortality (reviewed in [334]). While other studies have suggested that BMD at this site is increased following long-term imatinib therapy, relative to age-matched normal controls[20], the decrease in BMD at the femoral neck observed in the prospective study reported herein suggests that the potential loss of cortical bone at this site should be investigated further in longitudinal studies. Monitoring of hip BMD may be required in imatinib-treated patients, particularly in those with low BMD prior to treatment.

7.2 The effects of tyrosine kinase inhibition in paediatric patients

CML is rarely seen in children and accounts for less than 3% of childhood leukaemias.[450,451] Although imatinib is the gold standard therapy for CML in adults, it is only approved for use in paediatric CML when disease recurrence is evident following allogeneic stem cell transplantation, or when paediatric patients exhibit resistance or intolerance to interferon-α therapy. Increasingly, however, imatinib is used as a front-line therapy in paediatric CML patients, especially where HLA-identical sibling donors are not available.[452] Furthermore, dasatinib is now being considered for those children and adolescents that are resistant or intolerant to imatinib when allogeneic transplants are not possible.[453,454]

While short-term imatinib therapy has been successful and well-tolerated in children with chronic-phase CML[455-458], there is emerging information suggesting that long-term therapy may result in side-effects that are specific to the paediatric setting. Three case reports have noted growth retardation in pre-pubescent CML cases, which coincided with the start of imatinib therapy.[387-389] Additionally, a French phase IV trial has recently reported decreased growth in a cohort of 22 children and adolescents (age: 10 months – 17 years) receiving imatinib therapy for chronic-phase CML.[459] Growth rate in this group was significantly lower following imatinib treatment, with a significant decrease in height z-score (median, -0.37; range, -1.09 – +0.14) after 12 months of treatment, compared with baseline.[459] While these studies suggest that imatinib therapy in pre-pubertal individuals

may retard growth, there are currently no preclinical reports suggesting a mechanism for altered growth in imatinib-treated paediatric patients.

In studies presented in chapter 4, it was found that imatinib and dasatinib treatment resulted in accelerated growth plate closure in normal rats *in vivo*. In addition, in chapter 6 it was demonstrated that imatinib and dasatinib inhibit cell proliferation and extracellular matrix synthesis in cultures of chondrocyte-like cells *in vitro*, at least in part through inhibition of PDGFR signalling. We postulate that the retarded growth observed in pre-pubescent CML patients receiving imatinib may be due, in part, to accelerated growth plate narrowing as a consequence of the inhibition of chondrocyte proliferation and activity. However, as yet there is no evidence that imatinib affects the growth plate in patients. Additionally, complete growth plate closure is unlikely to be occurring in imatinib-treated children as, in at least two individuals, growth resumed upon reaching puberty[387] or following cessation of treatment[388].

In normal, healthy individuals, growth plate closure occurs after the cessation of growth, suggesting that is a consequence of growth arrest, rather than a cause of it.[147] Therefore, although inhibition of chondrocyte proliferation and activity may have detrimental effects on growth, the potential that imatinib causes growth retardation through other mechanisms must be considered. A recent study found that in a cohort of 17 imatinib-treated CML patients 25 – 75% had growth hormone (GH) deficiency, as defined by low serum levels of IGF-1 and IGF-binding protein-3 and decreased GH release in response to glucagon or L-DOPA stimulation.[460] However, as an imatinib-naïve CML cohort was not examined in this study, it is unclear whether the observed deficiency was due to treatment or resulted from illness. Nonetheless, the possibility that growth hormone deficiency may contribute to the decreased growth in imatinib-treated patients should be further investigated.

The success of tyrosine kinase inhibitors for the treatment of chronic myeloid leukemia and GIST has resulted in the investigation of the use of these drugs in an increasing number of paediatric disorders. Clinical trials have investigated the use of imatinib in children and adolescents with osteosarcoma, Ewing sarcoma, neuroblastoma, desmoplastic small round cell tumour, synovial sarcoma, GIST, soft tissue tumours and central nervous system tumours.[461-463] Clinical trials are currently underway to investigate the potential efficacy of dasatinib in the treatment of children and adolescents with diffuse intrinsic pontine glioma (National Institutes of Health Clinical Trials Identifier: NCT00996723), Bcr-Abl-positive ALL (NCT00720109), central nervous system tumours,

kidney cancer, liver cancer, lymphoma, neuroblastoma, ovarian cancer, sarcoma, testicular germ cell tumours and other solid tumours (NCT00788125).

Our results suggest that growth plate changes and skeletal metabolism should be monitored in paediatric patients that are undergoing treatment with tyrosine kinase inhibitors. The relative benefit of using imatinib and dasatinib as a frontline treatment for diseases affecting children and adolescents needs to be re-evaluated, taking into account the potential effects of imatinib and dasatinib on growth.

7.3 Potential applications for imatinib and dasatinib in the treatment of tumour-associated bone loss

Tumour associated bone lesions, resulting from metastases or primary tumours, are frequent occurrences in breast and prostate cancer and multiple myeloma and also occur, to a lesser extent, in lung cancer, stomach cancer, bladder cancer, uterine cancer, thyroid cancer, kidney cancer and colon cancer (reviewed in [133]). Bone metastases are the primary cause of morbidity and mortality in breast and prostate cancer, causing spinal cord compression, intractable bone pain, pathological fractures and hypercalcaemia, significantly reducing the quality of life for the patient. Tumour cells residing in the bone marrow produce a number of factors which increase osteoclastic bone resorption[464-468] and either inhibit[469-472] or activate[473,474] osteoblast activity, resulting in lesions that are either predominantly osteolytic or predominantly osteoblastic (reviewed in [133]). However, whether osteolytic or osteoblastic, tumour-associated bone lesions almost universally have an osteolytic component (reviewed in [134]).

Inhibition of osteoclast activity is a proven modality for the palliative treatment of metastatic bone disease. Bisphosphonates, which inhibit osteoclast function and increase the rate of osteoclast apoptosis, are commonly used for the treatment of cancer-associated bone loss.[475-479] Adjuvant bisphosphonate treatment significantly reduces the risk of skeletal morbidity in patients with bone-metastatic breast cancer[480-484], bone-metastatic prostate cancer[485] and multiple myeloma[481,486-488]. However, while effective at reducing the incidence of hypercalcaemia, bone pain and pathological fracture, bisphosphonate treatment is largely palliative, conveying no significant survival advantage.[480-485,487-490]

Despite the success in the use of bisphosphonates in the treatment of tumour-associated bone morbidity, the use of high-dose intravenous bisphosphonates has been associated with infrequent, but significant, side-effects. These include including avascular osteonecrosis of the jaw[491-497] and impaired renal function[252,498-502]. These observations

raise concerns over the prolonged use of high-dose intravenous bisphosphonates as inhibitors of bone resorption. Current guidelines suggest limiting the use of bisphosphonates in patients with renal dysfunction or poor dental hygiene[503-508], suggesting a need for new therapies that can be used in patients for whom bisphosphonates are contraindicated.

The observed effects of imatinib and dasatinib on osteoclast and osteoblast activity provide a rationale for their use in the treatment of conditions in which dysregulated bone remodelling is a feature. A number of studies have examined the effects of imatinib therapy on the growth of breast and prostate tumour cells in the bone marrow environment *in vivo*. In a systemic MDA-MB-231 model of breast cancer bone metastasis[410] and in an intratibial MDA-MB-435 model of tumour-associated bone loss[509], daily imatinib therapy was found to decrease tumour size and tumour-associated osteolysis. Similarly, in animal models of prostate cancer bone metastases, imatinib treatment was shown to decrease tumour burden and associated osteolysis. In an intratibial model of prostate tumour-associated bone loss, treatment with 50 mg/kg imatinib significantly inhibited bone lysis.[510-512] This was associated with reduced tumour incidence, tumour size, tumour cell proliferation and tumour cell apoptosis.[510-512] Additionally, in an animal model of prostate cancer bone metastases, dasatinib treatment decreased tumour burden and tumour-associated bone loss. Similarly, dasatinib (50 mg/kg/day) decreased intratibial LNCaP-C4-2B tumour growth and associated osteolysis, assessed radiographically.[513] BMD was increased by dasatinib treatment in the tumour-bearing and the contralateral limb, compared with untreated controls, suggesting that dasatinib treatment resulted to a generalised increase in bone mass in these animals.

The rationale for these *in vivo* studies has primarily focused on inhibiting tumour cell proliferation and tumour-stroma interactions through the inhibition of paracrine and autocrine growth factor signalling. High concentrations of imatinib may inhibit tumour cell proliferation in some breast and prostate cancer cell lines *in vitro*[514,515] and imatinib therapy has been shown to inhibit the orthotopic growth of MDA-MB-231 breast cancer cells[410]. Similarly, dasatinib has been shown to inhibit the proliferation and/or survival of myeloma cell lines *in vitro* at therapeutically-achievable concentrations[516] and, at high concentrations, to inhibit the proliferation/survival of breast cancer[517] and prostate cancer cell lines[513,518]. In preclinical models, treatment with dasatinib significantly decreased subcutaneous growth of the MM cell line OPM-1[516] and orthotopic growth of the prostate cancer cell line PC3MM2GL[518]. The observed decrease in tumour-associated osteolysis in

intratibial models may therefore result from an indirect effect of imatinib- and dasatinib-mediated tumour cytotoxicity. However, in light of the results presented in this thesis, direct inhibition of osteoclast activity may also contribute to the observed anti-osteolytic effects. Further studies are required to ascertain to what extent direct inhibition of osteolysis by imatinib and dasatinib contributes to the decreased tumour-associated bone loss observed in preclinical models.

Assessing the effects of imatinib on tumour-associated osteolysis in patients is complicated by the fact that few clinical trials have directly examined the impact of imatinib therapy on bone. While some studies have examined the efficacy of imatinib as a treatment for prostate or breast cancer, these have been primarily been carried out in patient populations with non-metastatic disease.[519-523] Additionally, most studies that have been undertaken in patients with bone metastases have not examined indices of bone turnover[524,525], or have been complicated by the patients' concurrent use of bisphosphonates[526]. To date, only one clinical trial has reported the effects of imatinib on bone parameters in bisphosphonate naïve patients with bone metastases.[527] In this study, docetaxol was used alone, or in combination with imatinib, to treat patients with advanced hormone-refractory prostate cancer with bone metastases. Although time to progression was no different between the imatinib and placebo groups during the 42 days of the trial, the level of urinary collagen N-telopeptides was significantly decreased in the imatinib group. While not definitive, these studies suggest that imatinib may decrease bone loss by affecting osteoclast formation/activity.

Furthermore, a recent phase II study has suggested that dasatinib may be an effective anti-osteolytic agent in patients with hormone-refractory prostate cancer.[528] In this study, 41 patients with bone-metastatic prostate cancer received dasatinib therapy for up to 14 months. This included 21 patients who received bisphosphonate treatment prior to the commencement of the study who remained on bisphoshonates during the course of the study. Of the patients receiving dasatinib alone, the majority of patients (18/20) had at least some decrease in the osteoclast marker urinary NTX during the study, with 50% (10/20) achieving a $\geq$ 40% decrease in urinary NTX levels by 12 weeks of treatment. Of the patients who had received bisphosphonates, 11/21 had an additional decrease in urinary NTX during the course of dasatinib treatment, suggesting an additive effect of receiving both dasatinib and bisphosphonate therapy. These data suggest that dasatinib treatment decreases osteolysis in patients with bone-metastatic, hormone-refractory prostate cancer.

The observed effects of imatinib and dasatinib on bone remodelling *in vitro* and *in vivo* suggest that these tyrosine kinase inhibitors may be clinically useful as an inhibitor of osteoclast activity in diseases associated with excessive bone resorption, such as cancer-induced bone loss. Clinical trials should be undertaken to examine the potential clinical efficacy of adjuvant tyrosine kinase inhibitor therapy in patients with osteolytic bone disease.

References

1. Buchdunger E, Zimmermann J, Mett H, Meyer T, Müller M, Druker BJ, Lydon NB. Inhibition of the Abl protein-tyrosine kinase *in vitro* and *in vivo* by a 2-phenylaminopyrimidine derivative. *Cancer Res*. 1996;56(1):100-104.

2. Hochhaus A, Schenk T, Erben P, Ernst T, La Rosée P, Muller MC. Cause and management of therapy resistance. *Best Pract Res Clin Haematol*. 2009;22(3):367-379.

3. O'Brien SG, Guilhot F, Larson RA, Gathmann I, Baccarani M, Cervantes F, Cornelissen JJ, Fischer T, Hochhaus A, Hughes T, Lechner K, Nielsen JL, Rousselot P, Reiffers J, Saglio G, Shepherd J, Simonsson B, Gratwohl A, Goldman JM, Kantarjian H, Taylor K, Verhoef G, Bolton AE, Capdeville R, Druker BJ. Imatinib compared with interferon and low-dose cytarabine for newly diagnosed chronic-phase chronic myeloid leukemia. *N Engl J Med*. 2003;348(11):994-1004.

4. Druker BJ, Talpaz M, Resta DJ, Peng B, Buchdunger E, Ford JM, Lydon NB, Kantarjian H, Capdeville R, Ohno-Jones S, Sawyers CL. Efficacy and safety of a specific inhibitor of the BCR-ABL tyrosine kinase in chronic myeloid leukemia. *N Engl J Med*. 2001;344(14):1031-1037.

5. Berman E, Nicolaides M, Maki RG, Fleisher M, Chanel S, Scheu K, Wilson BA, Heller G, Sauter NP. Altered bone and mineral metabolism in patients receiving imatinib mesylate. *N Engl J Med*. 2006;354(19):2006-2013.

6. Owen S, Hatfield A, Letvak L. Imatinib and altered bone and mineral metabolism. *N Engl J Med*. 2006;355(6):627.

7. Joensuu H, Reichardt P. Imatinib and altered bone and mineral metabolism. *N Engl J Med*. 2006;355(6):628.

8. Grey A, O'Sullivan S, Reid IR, Browett P. Imatinib mesylate, increased bone formation, and secondary hyperparathyroidism. *N Engl J Med*. 2006;355(23):2494-2495.

9. Osorio S, Noblejas AG, Durán A, Steegmann JL. Imatinib mesylate induces hypophosphatemia in patients with chronic myeloid leukemia in late chronic phase, and this effect is associated with response. *Am J Hematol*. 2007;82(5):394-395.

10. Fitter S, Dewar AL, Kostakis P, To LB, Hughes TP, Roberts MM, Lynch K, Vernon-Roberts B, Zannettino ACW. Long-term imatinib therapy promotes bone formation in CML patients. *Blood*. 2008;111(5):2538-2547.

11. Franceschino A, Tornaghi L, Benemacher V, Assouline S, Gambacorti-Passerini C. Alterations in creatine kinase, phosphate and lipid values in patients with chronic myeloid leukemia during treatment with imatinib. *Haematologica*. 2008;93(2):317-318.

12. O'Sullivan S, Horne A, Wattie D, Porteous F, Callon K, Gamble G, Ebeling P, Browett P, Grey A. Decreased bone turnover despite persistent secondary hyperparathyroidism during prolonged treatment with imatinib. *J Clin Endocrinol Metab*. 2009;94(4):1131-1136.

13. Dewar AL, Farrugia AN, Condina MR, Bik To L, Hughes TP, Vernon-Roberts B, Zannettino ACW. Imatinib as a potential antiresorptive therapy for bone disease. *Blood*. 2006;107(11):4334-4337.

14. Ando W, Hashimoto J, Nampei A, Tsuboi H, Tateishi K, Ono T, Nakamura N, Ochi T, Yoshikawa H. Imatinib mesylate inhibits osteoclastogenesis and joint destruction in rats with collagen-induced arthritis (CIA). *J Bone Miner Metab*. 2006;24(4):274-282.

15. El Hajj Dib I, Gallet M, Mentaverri R, Sevenet N, Brazier M, Kamel S. Imatinib mesylate (Gleevec) enhances mature osteoclast apoptosis and suppresses osteoclast bone resorbing activity. *Eur J Pharmacol*. 2006;551(1-3):27-33.

16. Fierro F, Illmer T, Jing D, Schleyer E, Ehninger G, Boxberger S, Bornhäuser M. Inhibition of platelet-derived growth factor receptorβ by imatinib mesylate suppresses proliferation and alters differentiation of human mesenchymal stem cells *in vitro*. *Cell Prolif*. 2007;40(3):355-366.

17. O'Sullivan S, Naot D, Callon K, Porteous F, Horne A, Wattie D, Watson M, Cornish J, Browett P, Grey A. Imatinib Promotes Osteoblast Differentiation by Inhibiting PDGFR Signaling and Inhibits Osteoclastogenesis by Both Direct and Stromal Cell-Dependent Mechanisms. *J Bone Miner Res*. 2007;22(11):1679-1689.

18. Wihlidal P, Karlic H, Pfeilstocker M, Klaushofer K, Varga F. Imatinib mesylate (IM)-induced growth inhibition is associated with production of spliced osteocalcin-mRNA in cell lines. *Leuk Res*. 2008;32(3):437-443.

19. Tibullo D, Giallongo C, La Cava P, Berretta S, Stagno F, Chiarenza A, Conticello C, Palumbo GA, Di Raimondo F. Effects of imatinib mesylate in osteoblastogenesis. *Exp Hematol*. 2009;37(4):461-468.

20. Jönsson S, Olsson B, Ohlsson C, Lorentzon M, Mellström D, Wadenvik H. Increased cortical bone mineralization in imatinib treated patients with chronic myelogenous leukemia. *Haematologica*. 2008;93(7):1101-1103.

21. Blair HC, Zaidi M, Schlesinger PH. Mechanisms balancing skeletal matrix synthesis and degradation. *Biochem J*. 2002;364(Pt 2):329-341.

22. Eastoe JE, Eastoe B. The organic constituents of mammalian compact bone. *Biochem J*. 1954;57(3):453-459.

23. Herring GM. Comparison of Bovine Bone Sialoprotein and Serum Orosomucoid. *Nature*. 1964;201:709.

24. Andrews AT, Herring GM, Kent PW. Some studies on the composition of bovine cortical-bone sialoprotein. *Biochem J*. 1967;104(3):705-715.

25. Triffitt JT, Owen M. Studies on bone matrix glycoproteins. Incorporation of (1-14C)glucosamine and plasma (14C)glycoprotein into rabbit cortical bone. *Biochem J*. 1973;136(1):125-134.

26. Ashton BA, Triffitt JT, Herring GM. Isolation and partial characterization of a glycoprotein from bovine cortical bone. *Eur J Biochem*. 1974;45(2):525-533.

27. Ashton BA, Höhling HJ, Triffitt JT. Plasma proteins present in human cortical bone: enrichment of the alpha2HS-glycoprotein. *Calcif Tissue Res*. 1976;22(1):27-33.

28. Triffitt JT, Gebauer U, Ashton BA, Owen ME, Reynolds JJ. Origin of plasma alpha2HS-glycoprotein and its accumulation in bone. *Nature*. 1976;262(5565):226-227.

29. Termine JD, Kleinman HK, Whitson SW, Conn KM, McGarvey ML, Martin GR. Osteonectin, a bone-specific protein linking mineral to collagen. *Cell*. 1981;26(1 Pt 1):99-105.

30. Horton WA, Dwyer C, Goering R, Dean DC. Immunohistochemistry of types I and II collagen in undecalcified skeletal tissues. *J Histochem Cytochem*. 1983;31(3):417-425.

31. Oldberg Å, Franzén A, Heinegård D. Cloning and sequence analysis of rat bone sialoprotein (osteopontin) cDNA reveals an Arg-Gly-Asp cell-binding sequence. *Proc Natl Acad Sci U S A*. 1986;83(23):8819-8823.

32. Clarke B. Normal bone anatomy and physiology. *Clin J Am Soc Nephrol*. 2008;3 Suppl 3:S131-139.

33. Dudley HR, Spiro D. The fine structure of bone cells. *J Biophys Biochem Cytol*. 1961;11(3):627-649.

34. Scott BL, Pease DC. Electron microscopy of the epiphyseal apparatus. *Anat Rec*. 1956;126(4):465-495.

35. Anderson HC. Matrix vesicles and calcification. *Curr Rheumatol Rep*. 2003;5(3):222-226.

36. Pittenger MF, Mackay AM, Beck SC, Jaiswal RK, Douglas R, Mosca JD, Moorman MA, Simonetti DW, Craig S, Marshak DR. Multilineage potential of adult human mesenchymal stem cells. *Science*. 1999;284(5411):143-147.

37. Wakitani S, Saito T, Caplan AI. Myogenic cells derived from rat bone marrow mesenchymal stem cells exposed to 5-azacytidine. *Muscle Nerve*. 1995;18(12):1417-1426.

38. Komori T, Yagi H, Nomura S, Yamaguchi A, Sasaki K, Deguchi K, Shimizu Y, Bronson RT, Gao Y-H, Inada M, Sato M, Okamoto R, Kitamura Y, Yoshiki S, Kishimoto T. Targeted disruption of Cbfa1 results in a complete lack of bone formation owing to maturational arrest of osteoblasts. *Cell*. 1997;89(5):755-764.

39. Otto F, Thornell AP, Crompton T, Denzel A, Gilmour KC, Rosewell IR, Stamp GW, Beddington RS, Mundlos S, Olsen BR, Selby PB, Owen MJ. Cbfa1, a candidate gene for cleidocranial dysplasia syndrome, is essential for osteoblast differentiation and bone development. *Cell*. 1997;89(5):765-771.

40. Pinson KI, Brennan J, Monkley S, Avery BJ, Skarnes WC. An LDL-receptor-related protein mediates Wnt signalling in mice. *Nature*. 2000;407(6803):535-538.

41. Brault V, Moore R, Kutsch S, Ishibashi M, Rowitch DH, McMahon AP, Sommer L, Boussadia O, Kemler R. Inactivation of the beta-catenin gene by Wnt1-Cre-mediated deletion results in dramatic brain malformation and failure of craniofacial development. *Development*. 2001;128(8):1253-1264.

42. Nakashima K, Zhou X, Kunkel G, Zhang Z, Deng JM, Behringer RR, de Crombrugghe B. The novel zinc finger-containing transcription factor osterix is required for osteoblast differentiation and bone formation. *Cell*. 2002;108(1):17-29.

43. Day TF, Guo X, Garrett-Beal L, Yang Y. Wnt/beta-catenin signaling in mesenchymal progenitors controls osteoblast and chondrocyte differentiation during vertebrate skeletogenesis. *Dev Cell*. 2005;8(5):739-750.

44. Ducy P, Zhang R, Geoffroy V, Ridall AL, Karsenty G. Osf2/Cbfa1: a transcriptional activator of osteoblast differentiation. *Cell*. 1997;89(5):747-754.

45. Bialek P, Kern B, Yang X, Schrock M, Sosic D, Hong N, Wu H, Yu K, Ornitz DM, Olson EN, Justice MJ, Karsenty G. A twist code determines the onset of osteoblast differentiation. *Dev Cell*. 2004;6(3):423-435.

46. Koga T, Matsui Y, Asagiri M, Kodama T, de Crombrugghe B, Nakashima K, Takayanagi H. NFAT and Osterix cooperatively regulate bone formation. *Nat Med*. 2005;11(8):880-885.

47. Logan CY, Nusse R. The Wnt signaling pathway in development and disease. *Annu Rev Cell Dev Biol*. 2004;20:781-810.

48. Siegfried E, Chou T-B, Perrimon N. wingless signaling acts through zeste-white 3, the Drosophila homolog of glycogen synthase kinase-3, to regulate engrailed and establish cell fate. *Cell*. 1992;71(7):1167-1179.

49. Rubinfeld B, Albert I, Porfiri E, Fiol C, Munemitsu S, Polakis P. Binding of GSK3beta to the APC-beta-catenin complex and regulation of complex assembly. *Science*. 1996;272(5264):1023-1026.

50. Bodine PV, Zhao W, Kharode YP, Bex FJ, Lambert A-J, Goad MB, Gaur T, Stein GS, Lian JB, Komm BS. The Wnt antagonist secreted frizzled-related protein-1 is a negative regulator of trabecular bone formation in adult mice. *Mol Endocrinol*. 2004;18(5):1222-1237.

51. Semënov M, Tamai K, He X. SOST is a ligand for LRP5/LRP6 and a Wnt signaling inhibitor. *J Biol Chem*. 2005;280(29):26770-26775.

52. Mukhopadhyay M, Shtrom S, Rodriguez-Esteban C, Chen L, Tsukui T, Gomer L, Dorward DW, Glinka A, Grinberg A, Huang S-P, Niehrs C, Izpisua Belmonte JCI, Westphal H. Dickkopf1 is required for embryonic head induction and limb morphogenesis in the mouse. *Dev Cell*. 2001;1(3):423-434.

53. Li X, Zhang Y, Kang H, Liu W, Liu P, Zhang J, Harris SE, Wu D. Sclerostin binds to LRP5/6 and antagonizes canonical Wnt signaling. *J Biol Chem*. 2005;280(20):19883-19887.

54. Li X, Liu P, Liu W, Maye P, Zhang J, Zhang Y, Hurley M, Guo C, Boskey A, Sun L, Harris SE, Rowe DW, Ke HZ, Wu D. Dkk2 has a role in terminal osteoblast differentiation and mineralized matrix formation. *Nat Genet*. 2005;37(9):945-952.

55. Hu H, Hilton MJ, Tu X, Yu K, Ornitz DM, Long F. Sequential roles of Hedgehog and Wnt signaling in osteoblast development. *Development*. 2005;132(1):49-60.

56. Hill TP, Später D, Taketo MM, Birchmeier W, Hartmann C. Canonical Wnt/beta-catenin signaling prevents osteoblasts from differentiating into chondrocytes. *Dev Cell*. 2005;8(5):727-738.

57. Gong Y, Slee RB, Fukai N, Rawadi G, Roman-Roman S, Reginato AM, Wang H, Cundy T, Glorieux FH, Lev D, Zacharin M, Oexle K, Marcelino J, Suwairi W, Heeger S, Sabatakos G, Apte S, Adkins WN, Allgrove J, Arslan-Kirchner M, Batch JA, Beighton P, Black GC, Boles RG, Boon LM, Borrone C, Brunner HG, Carle GF, Dallapiccola B, De Paepe A, Floege B, Halfhide ML, Hall B, Hennekam RC, Hirose T, Jans A, Jüppner H, Kim CA, Keppler-Noreuil K, Kohlschuetter A, LaCombe D, Lambert M, Lemyre E, Letteboer T, Peltonen L, Ramesar RS, Romanengo M, Somer H, Steichen-Gersdorf E, Steinmann B, Sullivan B, Superti-Furga A, Swoboda W, van den Boogaard M-J, Van Hul W, Vikkula M, Votruba M, Zabel B, Garcia T, Baron R, Olsen BR, Warman ML. LDL receptor-related protein 5 (LRP5) affects bone accrual and eye development. *Cell*. 2001;107(4):513-523.

58. Boyden LM, Mao J, Belsky J, Mitzner L, Farhi A, Mitnick MA, Wu D, Insogna K, Lifton RP. High bone density due to a mutation in LDL-receptor-related protein 5. *N Engl J Med*. 2002;346(20):1513-1521.

59. Little RD, Carulli JP, Del Mastro RG, Dupuis J, Osborne M, Folz C, Manning SP, Swain PM, Zhao S-C, Eustace B, Lappe MM, Spitzer L, Zweier S, Braunschweiger K, Benchekroun Y, Hu X, Adair R, Chee L, FitzGerald MG, Tulig C, Caruso A, Tzellas N, Bawa A, Franklin B, McGuire S, Nogues X, Gong G, Allen KM, Anisowicz A, Morales AJ, Lomedico PT, Recker SM, Van Eerdewegh P, Recker RR, Johnson ML. A mutation in the LDL receptor-related protein 5 gene results in the autosomal dominant high-bone-mass trait. *Am J Hum Genet*. 2002;70(1):11-19.

60. Balemans W, Ebeling M, Patel N, Van Hul E, Olson P, Dioszegi M, Lacza C, Wuyts W, Van Den Ende J, Willems P, Paes-Alves AF, Hill S, Bueno M, Ramos FJ, Tacconi P, Dikkers FG, Stratakis C, Lindpaintner K, Vickery B, Foernzler D, Van Hul W. Increased bone density in sclerosteosis is due to the deficiency of a novel secreted protein (SOST). *Hum Mol Genet*. 2001;10(5):537-543.

61. Staehling-Hampton K, Proll S, Paeper BW, Zhao L, Charmley P, Brown A, Gardner JC, Galas D, Schatzman RC, Beighton P, Papapoulos S, Hamersma H, Brunkow ME. A 52-kb deletion in the SOST-MEOX1 intergenic region on 17q12-q21 is associated with van Buchem disease in the Dutch population. *Am J Med Genet*. 2002;110(2):144-152.

62. Balemans W, Patel N, Ebeling M, Van Hul E, Wuyts W, Lacza C, Dioszegi M, Dikkers FG, Hildering P, Willems PJ, Verheij JB, Lindpaintner K, Vickery B, Foernzler D, Van Hul W. Identification of a 52 kb deletion downstream of the SOST gene in patients with van Buchem disease. *J Med Genet*. 2002;39(2):91-97.

63. Yamaguchi A, Ishizuya T, Kintou N, Wada Y, Katagiri T, Wozney JM, Rosen V, Yoshiki S. Effects of BMP-2, BMP-4, and BMP-6 on osteoblastic differentiation of bone marrow-derived stromal cell lines, ST2 and MC3T3-G2/PA6. *Biochem Biophys Res Commun*. 1996;220(2):366-371.

64. Balint E, Lapointe D, Drissi H, van der Meijden C, Young DW, van Wijnen AJ, Stein JL, Stein GS, Lian JB. Phenotype discovery by gene expression profiling: mapping of biological processes linked to BMP-2-mediated osteoblast differentiation. *J Cell Biochem*. 2003;89(2):401-426.

65. Wan M, Cao X. BMP signaling in skeletal development. *Biochem Biophys Res Commun*. 2005;328(3):651-657.

66. Lee K-S, Kim H-J, Li Q-L, Chi X-Z, Ueta C, Komori T, Wozney JM, Kim E-G, Choi J-Y, Ryoo H-M, Bae S-C. Runx2 is a common target of transforming growth factor beta1 and bone morphogenetic protein 2, and cooperation between Runx2 and Smad5 induces osteoblast-specific gene expression in the pluripotent mesenchymal precursor cell line C2C12. *Mol Cell Biol*. 2000;20(23):8783-8792.

67. Lee M-H, Kwon T-G, Park H-S, Wozney JM, Ryoo H-M. BMP-2-induced Osterix expression is mediated by Dlx5 but is independent of Runx2. *Biochem Biophys Res Commun*. 2003;309(3):689-694.

68. Kogianni G, Noble BS. The biology of osteocytes. *Curr Osteoporos Rep*. 2007;5(2):81-86.

69. Pitsillides AA, Rawlinson SCF, Suswillo RFL, Bourrin S, Zaman G, Lanyon LE. Mechanical strain-induced NO production by bone cells: a possible role in adaptive bone (re)modeling? *FASEB J*. 1995;9(15):1614-1622.

70. Lean JM, Jagger CJ, Chambers TJ, Chow JWM. Increased insulin-like growth factor I mRNA expression in rat osteocytes in response to mechanical stimulation. *Am J Physiol*. 1995;268(2 Pt 1):E318-327.

71. Klein-Nulend J, Semeins CM, Ajubi NE, Nijweide PJ, Burger EH. Pulsating fluid flow increases nitric oxide (NO) synthesis by osteocytes but not periosteal fibroblasts--correlation with prostaglandin upregulation. *Biochem Biophys Res Commun*. 1995;217(2):640-648.

72. Klein-Nulend J, van der Plas A, Semeins CM, Ajubi NE, Frangos JA, Nijweide PJ, Burger EH. Sensitivity of osteocytes to biomechanical stress in vitro. *FASEB J*. 1995;9(5):441-445.

73. Ajubi NE, Klein-Nulend J, Nijweide PJ, Vrijheid-Lammers T, Alblas MJ, Burger EH. Pulsating fluid flow increases prostaglandin production by cultured chicken osteocytes--a cytoskeleton-dependent process. *Biochem Biophys Res Commun*. 1996;225(1):62-68.

74. Lanyon LE. Osteocytes, strain detection, bone modeling and remodeling. *Calcif Tissue Int*. 1993;53 Suppl 1:S102-106.

75. Bentolila V, Boyce TM, Fyhrie DP, Drumb R, Skerry TM, Schaffler MB. Intracortical remodeling in adult rat long bones after fatigue loading. *Bone*. 1998;23(3):275-281.

76. Maejima-Ikeda A, Aoki M, Tsuritani K, Kamioka K, Hiura K, Miyoshi T, Hara H, Takano-Yamamoto T, Kumegawa M. Chick osteocyte-derived protein inhibits osteoclastic bone resorption. *Biochem J*. 1997;322 (Pt 1):245-250.

77. Gu G, Mulari M, Peng Z, Hentunen TA, Väänänen HK. Death of osteocytes turns off the inhibition of osteoclasts and triggers local bone resorption. *Biochem Biophys Res Commun*. 2005;335(4):1095-1101.

78. Noble B. Bone microdamage and cell apoptosis. *Eur Cell Mater*. 2003;6:46-55; discusssion 55.

79. Verborgt O, Gibson GJ, Schaffler MB. Loss of osteocyte integrity in association with microdamage and bone remodeling after fatigue in vivo. *J Bone Miner Res*. 2000;15(1):60-67.

80. Fermor B, Skerry TM. PTH/PTHrP receptor expression on osteoblasts and osteocytes but not resorbing bone surfaces in growing rats. *J Bone Miner Res*. 1995;10(12):1935-1943.

81. Ehrlich PJ, Noble BS, Jessop HL, Stevens HY, Mosley JR, Lanyon LE. The effect of in vivo mechanical loading on estrogen receptor alpha expression in rat ulnar osteocytes. *J Bone Miner Res*. 2002;17(9):1646-1655.

82. Fischman DA, Hay ED. Origin of osteoclasts from mononuclear leucocytes in regenerating newt limbs. *Anat Rec*. 1962;143:329-337.

83. Tinkler SM, Linder JE, Williams DM, Johnson NW. Formation of osteoclasts from blood monocytes during 1 alpha-OH Vit D-stimulated bone resorption in mice. *J Anat*. 1981;133(Pt 3):389-396.

84. Scheven BA, Visser JW, Nijweide PJ. In vitro osteoclast generation from different bone marrow fractions, including a highly enriched haematopoietic stem cell population. *Nature*. 1986;321(6065):79-81.

85. Gonzales F, Karnovsky MJ. Electron microscopy of osteoclasts in healing fracturees of rat bone. *J Biophys Biochem Cytol*. 1961;9:299-316.

86. King GJ, Holtrop ME. Actin-like filaments in bone cells of cultured mouse calvaria as demonstrated by binding to heavy meromyosin. *J Cell Biol*. 1975;66(2):445-451.

87. Ross FP, Chappel J, Alvarez JI, Sander D, Butler WT, Farach-Carson MC, Mintz KA, Robey PG, Teitelbaum SL, Cheresh DA. Interactions between the bone matrix proteins osteopontin and bone sialoprotein and the osteoclast integrin alpha v beta 3 potentiate bone resorption. *J Biol Chem*. 1993;268(13):9901-9907.

88. Minkin C, Jennings JM. Carbonic anhydrase and bone remodeling: sulfonamide inhibition of bone resorption in organ culture. *Science*. 1972;176(38):1031-1033.

89. Laitala T, Väänänen HK. Inhibition of bone resorption in vitro by antisense RNA and DNA molecules targeted against carbonic anhydrase II or two subunits of vacuolar H(+)-ATPase. *J Clin Invest*. 1994;93(6):2311-2318.

90. Lehenkari P, Hentunen TA, Laitala-Leinonen T, Tuukkanen J, Väänänen HK. Carbonic anhydrase II plays a major role in osteoclast differentiation and bone resorption by effecting the steady state intracellular pH and Ca^{2+}. *Exp Cell Res*. 1998;242(1):128-137.

91. Rousselle AV, Heymann D. Osteoclastic acidification pathways during bone resorption. *Bone*. 2002;30(4):533-540.

92. Baron R, Neff L, Louvard D, Courtoy PJ. Cell-mediated extracellular acidification and bone resorption: evidence for a low pH in resorbing lacunae and localization of a 100-kD lysosomal membrane protein at the osteoclast ruffled border. *J Cell Biol*. 1985;101(6):2210-2222.

93. Silver IA, Murrills RJ, Etherington DJ. Microelectrode studies on the acid microenvironment beneath adherent macrophages and osteoclasts. *Exp Cell Res*. 1988;175(2):266-276.

94. Saftig P, Hunziker E, Wehmeyer O, Jones S, Boyde A, Rommerskirch W, Moritz JD, Schu P, von Figura K. Impaired osteoclastic bone resorption leads to osteopetrosis in cathepsin-K-deficient mice. *Proc Natl Acad Sci U S A*. 1998;95(23):13453-13458.

95. Nesbitt SA, Horton MA. Trafficking of matrix collagens through bone-resorbing osteoclasts. *Science*. 1997;276(5310):266-269.

96. Salo J, Lehenkari P, Mulari M, Metsikkö K, Väänänen HK. Removal of osteoclast bone resorption products by transcytosis. *Science*. 1997;276(5310):270-273.

97. Yasuda H, Shima N, Nakagawa N, Yamaguchi K, Kinosaki M, Mochizuki S-I, Tomoyasu A, Yano K, Goto M, Murakami A, Tsuda E, Morinaga T, Higashio K, Udagawa N, Takahashi N, Suda T. Osteoclast differentiation factor is a ligand for osteoprotegerin/osteoclastogenesis-inhibitory factor and is identical to TRANCE/RANKL. *Proc Natl Acad Sci U S A*. 1998;95(7):3597-3602.

98. Lacey DL, Timms E, Tan HL, Kelley MJ, Dunstan CR, Burgess T, Elliott R, Colombero A, Elliott G, Scully S, Hsu H, Sullivan J, Hawkins N, Davy E, Capparelli C, Eli A, Qian Y-X, Kaufman S, Sarosi I, Shalhoub V, Senaldi G, Guo J, Delaney J, Boyle WJ. Osteoprotegerin ligand is a cytokine that regulates osteoclast differentiation and activation. *Cell*. 1998;93(2):165-176.

99. Takahashi N, Udagawa N, Suda T. A new member of tumor necrosis factor ligand family, ODF/OPGL/TRANCE/RANKL, regulates osteoclast differentiation and function. *Biochem Biophys Res Commun*. 1999;256(3):449-455.

100. Dougall WC, Glaccum M, Charrier K, Rohrbach K, Brasel K, De Smedt T, Daro E, Smith J, Tometsko ME, Maliszewski CR, Armstrong A, Shen V, Bain S, Cosman D, Anderson D, Morrissey PJ, Peschon JJ, Schuh J. RANK is essential for osteoclast and lymph node development. *Genes Dev*. 1999;13(18):2412-2424.

101. Kong YY, Yoshida H, Sarosi I, Tan HL, Timms E, Capparelli C, Morony S, Oliveira-dos-Santos AJ, Van G, Itie A, Khoo W, Wakeham A, Dunstan CR, Lacey DL, Mak TW, Boyle WJ, Penninger JM. OPGL is a key regulator of osteoclastogenesis, lymphocyte development and lymph-node organogenesis. *Nature*. 1999;397(6717):315-323.

102. Shevde NK, Bendixen AC, Dienger KM, Pike JW. Estrogens suppress RANK ligand-induced osteoclast differentiation via a stromal cell independent mechanism involving c-Jun repression. *Proc Natl Acad Sci U S A*. 2000;97(14):7829-7834.

103. Simonet WS, Lacey DL, Dunstan CR, Kelley M, Chang M-S, Luthy R, Nguyen HQ, Wooden S, Bennett L, Boone T, Shimamoto G, DeRose M, Elliott R, Colombero A, Tan H-L, Trail G, Sullivan J, Davy E, Bucay N, Renshaw-Gegg L, Hughes TM, Hill D, Pattison W, Campbell P, Sander S, Van G, Tarpley J, Derby P, Lee R, Boyle WJ. Osteoprotegerin: a novel secreted protein involved in the regulation of bone density. *Cell*. 1997;89(2):309-319.

104. Bucay N, Sarosi I, Dunstan CR, Morony S, Tarpley J, Capparelli C, Scully S, Tan HL, Xu W, Lacey DL, Boyle WJ, Simonet WS. Osteoprotegerin-deficient mice develop early onset osteoporosis and arterial calcification. *Genes Dev*. 1998;12(9):1260-1268.

105. Mizuno A, Amizuka N, Irie K, Murakami A, Fujise N, Kanno T, Sato Y, Nakagawa N, Yasuda H, Mochizuki S, Gomibuchi T, Yano K, Shima N, Washida N, Tsuda E, Morinaga T, Higashio K, Ozawa H. Severe osteoporosis in mice lacking osteoclastogenesis inhibitory factor/osteoprotegerin. *Biochem Biophys Res Commun*. 1998;247(3):610-615.

106. Nagai M, Sato N. Reciprocal gene expression of osteoclastogenesis inhibitory factor and osteoclast differentiation factor regulates osteoclast formation. *Biochem Biophys Res Commun*. 1999;257(3):719-723.

107. Fazzalari NL, Kuliwaba JS, Atkins GJ, Forwood MR, Findlay DM. The ratio of messenger RNA levels of receptor activator of nuclear factor κB ligand to osteoprotegerin correlates with bone remodeling indices in normal human cancellous bone but not in osteoarthritis. *J Bone Miner Res*. 2001;16(6):1015-1027.

108. Zaidi M. Skeletal remodeling in health and disease. *Nat Med*. 2007;13(7):791-801.

109. McKercher SR, Torbett BE, Anderson KL, Henkel GW, Vestal DJ, Baribault H, Klemsz M, Feeney AJ, Wu GE, Paige CJ, Maki RA. Targeted disruption of the PU.1 gene results in multiple hematopoietic abnormalities. *Embo J*. 1996;15(20):5647-5658.

110. Tondravi MM, McKercher SR, Anderson K, Erdmann JM, Quiroz M, Maki R, Teitelbaum SL. Osteopetrosis in mice lacking haematopoietic transcription factor PU.1. *Nature*. 1997;386(6620):81-84.

111. Dai XM, Ryan GR, Hapel AJ, Dominguez MG, Russell RG, Kapp S, Sylvestre V, Stanley ER. Targeted disruption of the mouse colony-stimulating factor 1 receptor gene results in osteopetrosis, mononuclear phagocyte deficiency, increased primitive progenitor cell frequencies, and reproductive defects. *Blood*. 2002;99(1):111-120.

112. Arai F, Miyamoto T, Ohneda O, Inada T, Sudo T, Brasel K, Miyata T, Anderson DM, Suda T. Commitment and differentiation of osteoclast precursor cells by the sequential expression of c-Fms and receptor activator of nuclear factor κB (RANK) receptors. *J Exp Med*. 1999;190(12):1741-1754.

113. Cappellen D, Luong-Nguyen NH, Bongiovanni S, Grenet O, Wanke C, Šuša M. Transcriptional program of mouse osteoclast differentiation governed by the macrophage colony-stimulating factor and the ligand for the receptor activator of NFkappa B. *J Biol Chem*. 2002;277(24):21971-21982.

114. Cecchini MG, Dominguez MG, Mocci S, Wetterwald A, Felix R, Fleisch H, Chisholm O, Hofstetter W, Pollard JW, Stanley ER. Role of colony stimulating factor-1 in the establishment and regulation of tissue macrophages during postnatal development of the mouse. *Development*. 1994;120(6):1357-1372.

115. Weilbaecher KN, Motyckova G, Huber WE, Takemoto CM, Hemesath TJ, Xu Y, Hershey CL, Dowland NR, Wells AG, Fisher DE. Linkage of M-CSF signaling to Mitf, TFE3, and the osteoclast defect in Mitf(mi/mi) mice. *Mol Cell*. 2001;8(4):749-758.

116. Darnay BG, Haridas V, Ni J, Moore PA, Aggarwal BB. Characterization of the intracellular domain of receptor activator of NF-kappaB (RANK). Interaction with tumor necrosis factor receptor-associated factors and activation of NF-kappab and c-Jun N-terminal kinase. *J Biol Chem*. 1998;273(32):20551-20555.

117. Galibert L, Tometsko ME, Anderson DM, Cosman D, Dougall WC. The involvement of multiple tumor necrosis factor receptor (TNFR)-associated factors in the signaling mechanisms of receptor activator of NF-kappaB, a member of the TNFR superfamily. *J Biol Chem*. 1998;273(51):34120-34127.

118. Wong BR, Josien R, Lee SY, Vologodskaia M, Steinman RM, Choi Y. The TRAF family of signal transducers mediates NF-kappaB activation by the TRANCE receptor. *J Biol Chem*. 1998;273(43):28355-28359.

119. Gohda J, Akiyama T, Koga T, Takayanagi H, Tanaka S, Inoue J. RANK-mediated amplification of TRAF6 signaling leads to NFATc1 induction during osteoclastogenesis. *Embo J*. 2005;24(4):790-799.

120. Takayanagi H, Kim S, Koga T, Nishina H, Isshiki M, Yoshida H, Saiura A, Isobe M, Yokochi T, Inoue J, Wagner EF, Mak TW, Kodama T, Taniguchi T. Induction and activation of the transcription factor NFATc1 (NFAT2) integrate RANKL signaling in terminal differentiation of osteoclasts. *Dev Cell*. 2002;3(6):889-901.

121. Asagiri M, Takayanagi H. The molecular understanding of osteoclast differentiation. *Bone*. 2007;40(2):251-264.

122. Naito A, Azuma S, Tanaka S, Miyazaki T, Takaki S, Takatsu K, Nakao K, Nakamura K, Katsuki M, Yamamoto T, Inoue J. Severe osteopetrosis, defective interleukin-1 signalling and lymph node organogenesis in TRAF6-deficient mice. *Genes Cells*. 1999;4(6):353-362.

123. Johnson RS, Spiegelman BM, Papaioannou V. Pleiotropic effects of a null mutation in the c-fos proto-oncogene. *Cell*. 1992;71(4):577-586.

124. Asagiri M, Sato K, Usami T, Ochi S, Nishina H, Yoshida H, Morita I, Wagner EF, Mak TW, Serfling E, Takayanagi H. Autoamplification of NFATc1 expression determines its essential role in bone homeostasis. *J Exp Med*. 2005;202(9):1261-1269.

125. Iotsova V, Caamaño J, Loy J, Yang Y, Lewin A, Bravo R. Osteopetrosis in mice lacking NF-kappaB1 and NF-kappaB2. *Nat Med*. 1997;3(11):1285-1289.

126. Franzoso G, Carlson L, Xing L, Poljak L, Shores EW, Brown KD, Leonardi A, Tran T, Boyce BF, Siebenlist U. Requirement for NF-kappaB in osteoclast and B-cell development. *Genes Dev*. 1997;11(24):3482-3496.

127. Matsuo K, Galson DL, Zhao C, Peng L, Laplace C, Wang KZ, Bachler MA, Amano H, Aburatani H, Ishikawa H, Wagner EF. Nuclear factor of activated T-cells (NFAT) rescues osteoclastogenesis in precursors lacking c-Fos. *J Biol Chem*. 2004;279(25):26475-26480.

128. Kim Y, Sato K, Asagiri M, Morita I, Soma K, Takayanagi H. Contribution of nuclear factor of activated T cells c1 to the transcriptional control of immunoreceptor osteoclast-associated receptor but not triggering receptor expressed by myeloid cells-2 during osteoclastogenesis. *J Biol Chem*. 2005;280(38):32905-32913.

129. Crotti TN, Flannery M, Walsh NC, Fleming JD, Goldring SR, McHugh KP. NFATc1 regulation of the human beta3 integrin promoter in osteoclast differentiation. *Gene*. 2006;372:92-102.

130. Parfitt AM. Targeted and nontargeted bone remodeling: relationship to basic multicellular unit origination and progression. *Bone*. 2002;30(1):5-7.

131. Zhao C, Irie N, Takada Y, Shimoda K, Miyamoto T, Nishiwaki T, Suda T, Matsuo K. Bidirectional ephrinB2-EphB4 signaling controls bone homeostasis. *Cell Metab*. 2006;4(2):111-121.

132. Clarke NW, McClure J, George NJ. Morphometric evidence for bone resorption and replacement in prostate cancer. *Br J Urol*. 1991;68(1):74-80.

133. Zannettino ACW. Bone loss, cancer mediated. In: Schwab M, ed. Encyclopedia of Cancer (ed 2): Springer Publishers; 2009:382-385.

134. Seibel MJ. Clinical use of markers of bone turnover in metastatic bone disease. *Nat Clin Pract Oncol*. 2005;2(10):504-517.

135. Nielsen OS, Munro AJ, Tannock IF. Bone metastases: pathophysiology and management policy. *J Clin Oncol*. 1991;9(3):509-524.

136. Kronenberg HM. Developmental regulation of the growth plate. *Nature*. 2003;423(6937):332-336.

137. Olsen BR, Reginato AM, Wang W. Bone development. *Annu Rev Cell Dev Biol*. 2000;16:191-220.

138. Hardingham TE, Fosang AJ. Proteoglycans: many forms and many functions. *FASEB J*. 1992;6(3):861-870.

139. Dodds CS. Row formation and other types of arrangement of cartilage cells in endochondral ossification. *The Anatomical Record*. 1930;46(4):385-399.

140. Dodds GS. Osteoclasts and cartilage removal in endochondral ossification of certain mammals. *American Journal of Anatomy*. 1932;50(1):97-127.

141. Kember NF, Sissons HA. Quantitative histology of the human growth plate. *J Bone Joint Surg Br*. 1976;58-B(4):426-435.

142. Sissons HA, Kember NF. Longitudinal bone growth of the human femur. *Postgrad Med J*. 1977;53(622):433-437.

143. Hunziker EB, Schenk RK. Physiological mechanisms adopted by chondrocytes in regulating longitudinal bone growth in rats. *J Physiol*. 1989;414:55-71.

144. St-Jacques B, Hammerschmidt M, McMahon AP. Indian hedgehog signaling regulates proliferation and differentiation of chondrocytes and is essential for bone formation. *Genes Dev*. 1999;13(16):2072-2086.

145. Wilsman NJ, Farnum CE, Leiferman EM, Fry M, Barreto C. Differential growth by growth plates as a function of multiple parameters of chondrocytic kinetics. *J Orthop Res*. 1996;14(6):927-936.

146. Villemure I, Stokes IA. Growth plate mechanics and mechanobiology. A survey of present understanding. *J Biomech*. 2009;42(12):1793-1803.

147. Parfitt AM. Misconceptions (1): epiphyseal fusion causes cessation of growth. *Bone*. 2002;30(2):337-339.

148. Bi W, Deng JM, Zhang Z, Behringer RR, de Crombrugghe B. Sox9 is required for cartilage formation. *Nat Genet*. 1999;22(1):85-89.

149. Lefebvre V, Behringer RR, de Crombrugghe B. L-Sox5, Sox6 and Sox9 control essential steps of the chondrocyte differentiation pathway. *Osteoarthritis Cartilage*. 2001;9 Suppl A:S69-75.

150. Akiyama H, Lyons JP, Mori-Akiyama Y, Yang X, Zhang R, Zhang Z, Deng JM, Taketo MM, Nakamura T, Behringer RR, McCrea PD, de Crombrugghe B. Interactions between Sox9 and beta-catenin control chondrocyte differentiation. *Genes Dev*. 2004;18(9):1072-1087.

151. Lefebvre V, Huang W, Harley VR, Goodfellow PN, de Crombrugghe B. SOX9 is a potent activator of the chondrocyte-specific enhancer of the pro alpha1(II) collagen gene. *Mol Cell Biol*. 1997;17(4):2336-2346.

152. Lefebvre V, Li P, de Crombrugghe B. A new long form of Sox5 (L-Sox5), Sox6 and Sox9 are coexpressed in chondrogenesis and cooperatively activate the type II collagen gene. *Embo J*. 1998;17(19):5718-5733.

153. Bridgewater LC, Lefebvre V, de Crombrugghe B. Chondrocyte-specific enhancer elements in the Col11a2 gene resemble the Col2a1 tissue-specific enhancer. *J Biol Chem*. 1998;273(24):14998-15006.

154. Sekiya I, Tsuji K, Koopman P, Watanabe H, Yamada Y, Shinomiya K, Nifuji A, Noda M. SOX9 enhances aggrecan gene promoter/enhancer activity and is up-regulated by retinoic acid in a cartilage-derived cell line, TC6. *J Biol Chem*. 2000;275(15):10738-10744.

155. Akiyama H, Chaboissier MC, Martin JF, Schedl A, de Crombrugghe B. The transcription factor Sox9 has essential roles in successive steps of the chondrocyte differentiation pathway and is required for expression of Sox5 and Sox6. *Genes Dev*. 2002;16(21):2813-2828.

156. Inada M, Yasui T, Nomura S, Miyake S, Deguchi K, Himeno M, Sato M, Yamagiwa H, Kimura T, Yasui N, Ochi T, Endo N, Kitamura Y, Kishimoto T, Komori T. Maturational disturbance of chondrocytes in Cbfa1-deficient mice. *Dev Dyn*. 1999;214(4):279-290.

157. Takeda S, Bonnamy JP, Owen MJ, Ducy P, Karsenty G. Continuous expression of Cbfa1 in nonhypertrophic chondrocytes uncovers its ability to induce hypertrophic chondrocyte differentiation and partially rescues Cbfa1-deficient mice. *Genes Dev*. 2001;15(4):467-481.

158. Ueta C, Iwamoto M, Kanatani N, Yoshida C, Liu Y, Enomoto-Iwamoto M, Ohmori T, Enomoto H, Nakata K, Takada K, Kurisu K, Komori T. Skeletal malformations caused by overexpression of Cbfa1 or its dominant negative form in chondrocytes. *J Cell Biol*. 2001;153(1):87-100.

159. Vortkamp A, Lee K, Lanske B, Segre GV, Kronenberg HM, Tabin CJ. Regulation of rate of cartilage differentiation by Indian hedgehog and PTH-related protein. *Science*. 1996;273(5275):613-622.

160. Lanske B, Karaplis AC, Lee K, Luz A, Vortkamp A, Pirro A, Karperien M, Defize LH, Ho C, Mulligan RC, Abou-Samra AB, Jüppner H, Segre GV, Kronenberg HM. PTH/PTHrP receptor in early development and Indian hedgehog-regulated bone growth. *Science*. 1996;273(5275):663-666.

161. van der Eerden BC, Karperien M, Gevers EF, Löwik CW, Wit JM. Expression of Indian hedgehog, parathyroid hormone-related protein, and their receptors in the postnatal growth plate of the rat: evidence for a locally acting growth restraining feedback loop after birth. *J Bone Miner Res*. 2000;15(6):1045-1055.

162. Vortkamp A, Pathi S, Peretti GM, Caruso EM, Zaleske DJ, Tabin CJ. Recapitulation of signals regulating embryonic bone formation during postnatal growth and in fracture repair. *Mech Dev*. 1998;71(1-2):65-76.

163. Bitgood MJ, McMahon AP. Hedgehog and Bmp genes are coexpressed at many diverse sites of cell-cell interaction in the mouse embryo. *Dev Biol*. 1995;172(1):126-138.

164. Koyama E, Leatherman JL, Noji S, Pacifici M. Early chick limb cartilaginous elements possess polarizing activity and express hedgehog-related morphogenetic factors. *Dev Dyn*. 1996;207(3):344-354.

165. Chung U, Kronenberg HM. Parathyroid hormone-related peptide and Indian hedgehog. *Curr Opin Nephrol Hypertens*. 2000;9(4):357-362.

166. Karp SJ, Schipani E, St-Jacques B, Hunzelman J, Kronenberg H, McMahon AP. Indian hedgehog coordinates endochondral bone growth and morphogenesis via parathyroid hormone related-protein-dependent and -independent pathways. *Development*. 2000;127(3):543-548.

167. Lee K, Lanske B, Karaplis AC, Deeds JD, Kohno H, Nissenson RA, Kronenberg HM, Segre GV. Parathyroid hormone-related peptide delays terminal differentiation of chondrocytes during endochondral bone development. *Endocrinology*. 1996;137(11):5109-5118.

168. Amizuka N, Warshawsky H, Henderson JE, Goltzman D, Karaplis AC. Parathyroid hormone-related peptide-depleted mice show abnormal epiphyseal cartilage development and altered endochondral bone formation. *J Cell Biol*. 1994;126(6):1611-1623.

169. Karaplis AC, Luz A, Glowacki J, Bronson RT, Tybulewicz VL, Kronenberg HM, Mulligan RC. Lethal skeletal dysplasia from targeted disruption of the parathyroid hormone-related peptide gene. *Genes Dev*. 1994;8(3):277-289.

170. Karaplis AC, He B, Nguyen MT, Young ID, Semeraro D, Ozawa H, Amizuka N. Inactivating mutation in the human parathyroid hormone receptor type 1 gene in Blomstrand chondrodysplasia. *Endocrinology*. 1998;139(12):5255-5258.

171. Jobert AS, Zhang P, Couvineau A, Bonaventure J, Roume J, Le Merrer M, Silve C. Absence of functional receptors for parathyroid hormone and parathyroid hormone-related peptide in Blomstrand chondrodysplasia. *J Clin Invest*. 1998;102(1):34-40.

172. Zhang P, Jobert AS, Couvineau A, Silve C. A homozygous inactivating mutation in the parathyroid hormone/parathyroid hormone-related peptide receptor causing Blomstrand chondrodysplasia. *J Clin Endocrinol Metab*. 1998;83(9):3365-3368.

173. Sahni M, Ambrosetti DC, Mansukhani A, Gertner R, Levy D, Basilico C. FGF signaling inhibits chondrocyte proliferation and regulates bone development through the STAT-1 pathway. *Genes Dev*. 1999;13(11):1361-1366.

174. Minina E, Kreschel C, Naski MC, Ornitz DM, Vortkamp A. Interaction of FGF, Ihh/Pthlh, and BMP signaling integrates chondrocyte proliferation and hypertrophic differentiation. *Dev Cell*. 2002;3(3):439-449.

175. Naski MC, Colvin JS, Coffin JD, Ornitz DM. Repression of hedgehog signaling and BMP4 expression in growth plate cartilage by fibroblast growth factor receptor 3. *Development*. 1998;125(24):4977-4988.

176. Chen L, Adar R, Yang X, Monsonego EO, Li C, Hauschka PV, Yayon A, Deng CX. Gly369Cys mutation in mouse FGFR3 causes achondroplasia by affecting both chondrogenesis and osteogenesis. *J Clin Invest*. 1999;104(11):1517-1525.

177. Li C, Chen L, Iwata T, Kitagawa M, Fu XY, Deng CX. A Lys644Glu substitution in fibroblast growth factor receptor 3 (FGFR3) causes dwarfism in mice by activation of STATs and ink4 cell cycle inhibitors. *Hum Mol Genet*. 1999;8(1):35-44.

178. Iwata T, Chen L, Li C, Ovchinnikov DA, Behringer RR, Francomano CA, Deng CX. A neonatal lethal mutation in FGFR3 uncouples proliferation and differentiation of growth plate chondrocytes in embryos. *Hum Mol Genet*. 2000;9(11):1603-1613.

179. Iwata T, Li CL, Deng CX, Francomano CA. Highly activated Fgfr3 with the K644M mutation causes prolonged survival in severe dwarf mice. *Hum Mol Genet*. 2001;10(12):1255-1264.

180. Deng C, Wynshaw-Boris A, Zhou F, Kuo A, Leder P. Fibroblast growth factor receptor 3 is a negative regulator of bone growth. *Cell*. 1996;84(6):911-921.

181. Colvin JS, Bohne BA, Harding GW, McEwen DG, Ornitz DM. Skeletal overgrowth and deafness in mice lacking fibroblast growth factor receptor 3. *Nat Genet*. 1996;12(4):390-397.

182. Shiang R, Thompson LM, Zhu YZ, Church DM, Fielder TJ, Bocian M, Winokur ST, Wasmuth JJ. Mutations in the transmembrane domain of FGFR3 cause the most common genetic form of dwarfism, achondroplasia. *Cell*. 1994;78(2):335-342.

183. Bellus GA, Hefferon TW, Ortiz de Luna RI, Hecht JT, Horton WA, Machado M, Kaitila I, McIntosh I, Francomano CA. Achondroplasia is defined by recurrent G380R mutations of FGFR3. *Am J Hum Genet*. 1995;56(2):368-373.

184. Tavormina PL, Rimoin DL, Cohn DH, Zhu Y-Z, Shiang R, Wasmuth JJ. Another mutation that results in the substitution of an unpaired cysteine residue in the extracellular domain of FGFR3 in thanatophoric dysplasia type I. *Hum Mol Genet*. 1995;4(11):2175-2177.

185. Woods KA, Savage MO. Laron syndrome: typical and atypical forms. *Baillieres Clin Endocrinol Metab*. 1996;10(3):371-387.

186. Liu J-P, Baker J, Perkins AS, Robertson EJ, Efstratiadis A. Mice carrying null mutations of the genes encoding insulin-like growth factor I (Igf-1) and type 1 IGF receptor (Igf1r). *Cell*. 1993;75(1):59-72.

187. Worster AA, Brower-Toland BD, Fortier LA, Bent SJ, Williams J, Nixon AJ. Chondrocytic differentiation of mesenchymal stem cells sequentially exposed to transforming growth factor-beta1 in monolayer and insulin-like growth factor-I in a three-dimensional matrix. *J Orthop Res*. 2001;19(4):738-749.

188. Oh CD, Chun JS. Signaling mechanisms leading to the regulation of differentiation and apoptosis of articular chondrocytes by insulin-like growth factor-1. *J Biol Chem*. 2003;278(38):36563-36571.

189. Phornphutkul C, Wu K-Y, Yang X, Chen Q, Gruppuso PA. Insulin-like growth factor-I signaling is modified during chondrocyte differentiation. *J Endocrinol*. 2004;183(3):477-486.

190. Moe SM. Disorders involving calcium, phosphorus, and magnesium. *Prim Care*. 2008;35(2):215-237.

191. Bergwitz C, Jüppner H. Regulation of phosphate homeostasis by PTH, vitamin D, and FGF23. *Annu Rev Med*. 2010;61:91-104.

192. Ma YL, Cain RL, Halladay DL, Yang X, Zeng Q, Miles RR, Chandrasekhar S, Martin TJ, Onyia JE. Catabolic effects of continuous human PTH (1--38) in vivo is associated with sustained stimulation of RANKL and inhibition of osteoprotegerin and gene-associated bone formation. *Endocrinology*. 2001;142(9):4047-4054.

193. Locklin RM, Khosla S, Turner RT, Riggs BL. Mediators of the biphasic responses of bone to intermittent and continuously administered parathyroid hormone. *J Cell Biochem*. 2003;89(1):180-190.

194. Huang JC, Sakata T, Pfleger LL, Bencsik M, Halloran BP, Bikle DD, Nissenson RA. PTH differentially regulates expression of RANKL and OPG. *J Bone Miner Res*. 2004;19(2):235-244.

195. Jilka RL, Weinstein RS, Bellido T, Roberson P, Parfitt AM, Manolagas SC. Increased bone formation by prevention of osteoblast apoptosis with parathyroid hormone. *J Clin Invest*. 1999;104(4):439-446.

196. Dempster DW, Hughes-Begos CE, Plavetic-Chee K, Brandao-Burch A, Cosman F, Nieves J, Neubort S, Lu SS, Iida-Klein A, Arnett T, Lindsay R. Normal human osteoclasts formed from peripheral blood monocytes express PTH type 1 receptors and are stimulated by PTH in the absence of osteoblasts. *J Cell Biochem*. 2005;95(1):139-148.

197. Silver J, Russell J, Sherwood LM. Regulation by vitamin D metabolites of messenger ribonucleic acid for preproparathyroid hormone in isolated bovine parathyroid cells. *Proc Natl Acad Sci U S A*. 1985;82(12):4270-4273.

198. Schuessler M, Astecker N, Herzig G, Vorisek G, Schuster I. Skin is an autonomous organ in synthesis, two-step activation and degradation of vitamin D(3): CYP27 in epidermis completes the set of essential vitamin D(3)-hydroxylases. *Steroids*. 2001;66(3-5):399-408.

199. Lehmann B, Meurer M. Extrarenal sites of calcitriol synthesis: the particular role of the skin. *Recent Results Cancer Res*. 2003;164:135-145.

200. Hollis BW. 25-Hydroxyvitamin D3-1 alpha-hydroxylase in porcine hepatic tissue: subcellular localization to both mitochondria and microsomes. *Proc Natl Acad Sci U S A*. 1990;87(16):6009-6013.

201. Dusso AS, Finch J, Brown A, Ritter C, Delmez J, Schreiner G, Slatopolsky E. Extrarenal production of calcitriol in normal and uremic humans. *J Clin Endocrinol Metab*. 1991;72(1):157-164.

202. Howard GA, Turner RT, Sherrard DJ, Baylink DJ. Human bone cells in culture metabolize 25-hydroxyvitamin D3 to 1,25-dihydroxyvitamin D3 and 24,25-dihydroxyvitamin D3. *J Biol Chem*. 1981;256(15):7738-7740.

203. Ichikawa F, Sato K, Nanjo M, Nishii Y, Shinki T, Takahashi N, Suda T. Mouse primary osteoblasts express vitamin D3 25-hydroxylase mRNA and convert 1 alpha-hydroxyvitamin D3 into 1 alpha,25-dihydroxyvitamin D3. *Bone*. 1995;16(1):129-135.

204. van Driel M, Koedam M, Buurman CJ, Hewison M, Chiba H, Uitterlinden AG, Pols HAP, van Leeuwen JPTM. Evidence for auto/paracrine actions of vitamin D in bone: 1alpha-hydroxylase expression and activity in human bone cells. *FASEB J*. 2006;20(13):2417-2419.

205. Huang DC, Papavasiliou V, Rhim JS, Horst RL, Kremer R. Targeted disruption of the 25-hydroxyvitamin D3 1alpha-hydroxylase gene in ras-transformed keratinocytes demonstrates that locally produced 1alpha,25-dihydroxyvitamin D3 suppresses growth and induces differentiation in an autocrine fashion. *Mol Cancer Res*. 2002;1(1):56-67.

206. Atkins GJ, Anderson PH, Findlay DM, Welldon KJ, Vincent C, Zannettino AC, O'Loughlin PD, Morris HA. Metabolism of vitamin D3 in human osteoblasts: evidence for autocrine and paracrine activities of 1 alpha,25-dihydroxyvitamin D3. *Bone*. 2007;40(6):1517-1528.

207. Wood RJ, Tchack L, Taparia S. 1,25-Dihydroxyvitamin D3 increases the expression of the CaT1 epithelial calcium channel in the Caco-2 human intestinal cell line. *BMC Physiol*. 2001;1:11.

208. Wasserman RH, Taylor AN. Vitamin D3-Induced Calcium-Binding Protein in Chick Intestinal Mucosa. *Science*. 1966;152(3723):791-793.

209. Cai Q, Chandler JS, Wasserman RH, Kumar R, Penniston JT. Vitamin D and adaptation to dietary calcium and phosphate deficiencies increase intestinal plasma membrane calcium pump gene expression. *Proc Natl Acad Sci U S A*. 1993;90(4):1345-1349.

210. Kip SN, Strehler EE. Vitamin D3 upregulates plasma membrane Ca2+-ATPase expression and potentiates apico-basal Ca2+ flux in MDCK cells. *Am J Physiol Renal Physiol*. 2004;286(2):F363-369.

211. Xu H, Bai L, Collins JF, Ghishan FK. Age-dependent regulation of rat intestinal type IIb sodium-phosphate cotransporter by 1,25-(OH)(2) vitamin D(3). *Am J Physiol Cell Physiol*. 2002;282(3):C487-493.

212. Horwood NJ, Elliott J, Martin TJ, Gillespie MT. Osteotropic agents regulate the expression of osteoclast differentiation factor and osteoprotegerin in osteoblastic stromal cells. *Endocrinology*. 1998;139(11):4743-4746.

213. Weinstein RS, Underwood JL, Hutson MS, DeLuca HF. Bone histomorphometry in vitamin D-deficient rats infused with calcium and phosphorus. *Am J Physiol*. 1984;246(6 Pt 1):E499-505.

214. Underwood JL, DeLuca HF. Vitamin D is not directly necessary for bone growth and mineralization. *Am J Physiol*. 1984;246(6 Pt 1):E493-498.

215. Amling M, Priemel M, Holzmann T, Chapin K, Rueger JM, Baron R, Demay MB. Rescue of the skeletal phenotype of vitamin D receptor-ablated mice in the setting of normal mineral ion homeostasis: formal histomorphometric and biomechanical analyses. *Endocrinology*. 1999;140(11):4982-4987.

216. Bouillon R, Verstuyf A, Mathieu C, Van Cromphaut S, Masuyama R, Dehaes P, Carmeliet G. Vitamin D resistance. *Best Pract Res Clin Endocrinol Metab*. 2006;20(4):627-645.

217. Weisberg E, Manley PW, Breitenstein W, Bruggen J, Cowan-Jacob SW, Ray A, Huntly B, Fabbro D, Fendrich G, Hall-Meyers E, Kung AL, Mestan J, Daley GQ, Callahan L, Catley L, Cavazza C, Azam M, Neuberg D, Wright RD, Gilliland DG, Griffin JD. Characterization of AMN107, a selective inhibitor of native and mutant Bcr-Abl. *Cancer Cell*. 2005;7(2):129-141.

218. Okuda K, Weisberg E, Gilliland DG, Griffin JD. ARG tyrosine kinase activity is inhibited by STI571. *Blood*. 2001;97(8):2440-2448.

219. Day E, Waters B, Spiegel K, Alnadaf T, Manley PW, Buchdunger E, Walker C, Jarai G. Inhibition of collagen-induced discoidin domain receptor 1 and 2 activation by imatinib, nilotinib and dasatinib. *Eur J Pharmacol*. 2008;599(1-3):44-53.

220. Buchdunger E, Cioffi CL, Law N, Stover D, Ohno-Jones S, Druker BJ, Lydon NB. Abl protein-tyrosine kinase inhibitor STI571 inhibits *in vitro* signal transduction mediated by c-kit and platelet-derived growth factor receptors. *J Pharmacol Exp Ther*. 2000;295(1):139-145.

221. Dewar AL, Cambareri AC, Zannettino ACW, Miller BL, Doherty KV, Hughes TP, Lyons AB. Macrophage colony-stimulating factor receptor c-fms is a novel target of imatinib. *Blood*. 2005;105(8):3127-3132.

222. Rix U, Hantschel O, Dürnberger G, Remsing Rix LL, Planyavsky M, Fernbach NV, Kaupe I, Bennett KL, Valent P, Colinge J, Köcher T, Superti-Furga G. Chemical

proteomic profiles of the BCR-ABL inhibitors imatinib, nilotinib, and dasatinib reveal novel kinase and nonkinase targets. *Blood*. 2007;110(12):4055-4063.

223. Winger JA, Hantschel O, Superti-Furga G, Kuriyan J. The structure of the leukemia drug imatinib bound to human quinone reductase 2 (NQO2). *BMC Struct Biol*. 2009;9:7.

224. Parkkila S, Innocenti A, Kallio H, Hilvo M, Scozzafava A, Supuran CT. The protein tyrosine kinase inhibitors imatinib and nilotinib strongly inhibit several mammalian α-carbonic anhydrase isoforms. *Bioorg Med Chem Lett*. 2009;19(15):4102-4106.

225. Talpaz M, Silver RT, Druker BJ, Goldman JM, Gambacorti-Passerini C, Guilhot F, Schiffer CA, Fischer T, Deininger MWN, Lennard AL, Hochhaus A, Ottmann OG, Gratwohl A, Baccarani M, Stone R, Tura S, Mahon FX, Fernandes-Reese S, Gathmann I, Capdeville R, Kantarjian HM, Sawyers CL. Imatinib induces durable hematologic and cytogenetic responses in patients with accelerated phase chronic myeloid leukemia: results of a phase 2 study. *Blood*. 2002;99(6):1928-1937.

226. Sawyers CL, Hochhaus A, Feldman E, Goldman JM, Miller CB, Ottmann OG, Schiffer CA, Talpaz M, Guilhot F, Deininger MWN, Fischer T, O'Brien SG, Stone RM, Gambacorti-Passerini CB, Russell NH, Reiffers JJ, Shea TC, Chapuis B, Coutre S, Tura S, Morra E, Larson RA, Saven A, Peschel C, Gratwohl A, Mandelli F, Ben-Am M, Gathmann I, Capdeville R, Paquette RL, Druker BJ. Imatinib induces hematologic and cytogenetic responses in patients with chronic myelogenous leukemia in myeloid blast crisis: results of a phase II study. *Blood*. 2002;99(10):3530-3539.

227. Gambacorti-Passerini C, Barni R, le Coutre P, Zucchetti M, Cabrita G, Cleris L, Rossi F, Gianazza E, Brueggen J, Cozens R, Pioltelli P, Pogliani E, Corneo G, Formelli F, D'Incalci M. Role of alpha1 acid glycoprotein in the in vivo resistance of human BCR-ABL(+) leukemic cells to the abl inhibitor STI571. *J Natl Cancer Inst*. 2000;92(20):1641-1650.

228. Mahon FX, Belloc F, Lagarde V, Chollet C, Moreau-Gaudry F, Reiffers J, Goldman JM, Melo JV. MDR1 gene overexpression confers resistance to imatinib mesylate in leukemia cell line models. *Blood*. 2003;101(6):2368-2373.

229. White DL, Saunders VA, Dang P, Engler J, Zannettino AC, Cambareri AC, Quinn SR, Manley PW, Hughes TP. OCT-1-mediated influx is a key determinant of the intracellular uptake of imatinib but not nilotinib (AMN107): reduced OCT-1 activity is the cause of low in vitro sensitivity to imatinib. *Blood*. 2006;108(2):697-704.

230. White DL, Saunders VA, Dang P, Engler J, Venables A, Zrim S, Zannettino A, Lynch K, Manley PW, Hughes T. Most CML patients who have a suboptimal response to imatinib have low OCT-1 activity: higher doses of imatinib may overcome the negative impact of low OCT-1 activity. *Blood*. 2007;110(12):4064-4072.

231. Wang L, Giannoudis A, Lane S, Williamson P, Pirmohamed M, Clark RE. Expression of the uptake drug transporter hOCT1 is an important clinical determinant of

the response to imatinib in chronic myeloid leukemia. *Clin Pharmacol Ther*. 2008;83(2):258-264.

232. Roumiantsev S, Shah NP, Gorre ME, Nicoll J, Brasher BB, Sawyers CL, Van Etten RA. Clinical resistance to the kinase inhibitor STI-571 in chronic myeloid leukemia by mutation of Tyr-253 in the Abl kinase domain P-loop. *Proc Natl Acad Sci U S A*. 2002;99(16):10700-10705.

233. Shah NP, Nicoll JM, Nagar B, Gorre ME, Paquette RL, Kuriyan J, Sawyers CL. Multiple BCR-ABL kinase domain mutations confer polyclonal resistance to the tyrosine kinase inhibitor imatinib (STI571) in chronic phase and blast crisis chronic myeloid leukemia. *Cancer Cell*. 2002;2(2):117-125.

234. Hochhaus A, Kreil S, Corbin AS, La Rosée P, Muller MC, Lahaye T, Hanfstein B, Schoch C, Cross NC, Berger U, Gschaidmeier H, Druker BJ, Hehlmann R. Molecular and chromosomal mechanisms of resistance to imatinib (STI571) therapy. *Leukemia*. 2002;16(11):2190-2196.

235. Shah NP, Tran C, Lee FY, Chen P, Norris D, Sawyers CL. Overriding imatinib resistance with a novel ABL kinase inhibitor. *Science*. 2004;305(5682):399-401.

236. O'Hare T, Walters DK, Stoffregen EP, Jia T, Manley PW, Mestan J, Cowan-Jacob SW, Lee FY, Heinrich MC, Deininger MWN, Druker BJ. *In vitro* activity of Bcr-Abl inhibitors AMN107 and BMS-354825 against clinically relevant imatinib-resistant Abl kinase domain mutants. *Cancer Res*. 2005;65(11):4500-4505.

237. Melnick JS, Janes J, Kim S, Chang JY, Sipes DG, Gunderson D, Jarnes L, Matzen JT, Garcia ME, Hood TL, Beigi R, Xia G, Harig RA, Asatryan H, Yan SF, Zhou Y, Gu X-J, Saadat A, Zhou V, King FJ, Shaw CM, Su AI, Downs R, Gray NS, Schultz PG, Warmuth M, Caldwell JS. An efficient rapid system for profiling the cellular activities of molecular libraries. *Proc Natl Acad Sci U S A*. 2006;103(9):3153-3158.

238. Hochhaus A, Kantarjian HM, Baccarani M, Lipton JH, Apperley JF, Druker BJ, Facon T, Goldberg SL, Cervantes F, Niederwieser D, Silver RT, Stone RM, Hughes TP, Muller MC, Ezzeddine R, Countouriotis AM, Shah NP. Dasatinib induces notable hematologic and cytogenetic responses in chronic-phase chronic myeloid leukemia after failure of imatinib therapy. *Blood*. 2007;109(6):2303-2309.

239. Talpaz M, Shah NP, Kantarjian H, Donato N, Nicoll J, Paquette R, Cortes J, O'Brien S, Nicaise C, Bleickardt E, Blackwood-Chirchir MA, Iyer V, Chen TT, Huang F, Decillis AP, Sawyers CL. Dasatinib in imatinib-resistant Philadelphia chromosome-positive leukemias. *N Engl J Med*. 2006;354(24):2531-2541.

240. Weisberg E, Manley PW, Cowan-Jacob SW, Hochhaus A, Griffin JD. Second generation inhibitors of BCR-ABL for the treatment of imatinib-resistant chronic myeloid leukaemia. *Nat Rev Cancer*. 2007;7(5):345-356.

241. Druker BJ, Guilhot F, O'Brien SG, Gathmann I, Kantarjian H, Gattermann N, Deininger MWN, Silver RT, Goldman JM, Stone RM, Cervantes F, Hochhaus A, Powell BL, Gabrilove JL, Rousselot P, Reiffers J, Cornelissen JJ, Hughes T, Agis H, Fischer T, Verhoef G, Shepherd J, Saglio G, Gratwohl A, Nielsen JL, Radich JP, Simonsson B, Taylor K, Baccarani M, So C, Letvak L, Larson RA. Five-year follow-up of patients receiving imatinib for chronic myeloid leukemia. *N Engl J Med*. 2006;355(23):2408-2417.

242. Van Glabbeke M, Verweij J, Casali PG, Simes J, Le Cesne A, Reichardt P, Issels R, Judson IR, van Oosterom AT, Blay JY. Predicting toxicities for patients with advanced gastrointestinal stromal tumours treated with imatinib: a study of the European Organisation for Research and Treatment of Cancer, the Italian Sarcoma Group, and the Australasian Gastro-Intestinal Trials Group (EORTC-ISG-AGITG). *Eur J Cancer*. 2006;42(14):2277-2285.

243. Kitiyakara C, Atichartakarn V. Renal failure associated with a specific inhibitor of BCR-ABL tyrosine kinase, STI 571. *Nephrol Dial Transplant*. 2002;17(4):685-687.

244. Pou M, Saval N, Vera M, Saurina A, Sole M, Cervantes F, Botey A. Acute renal failure secondary to imatinib mesylate treatment in chronic myeloid leukemia. *Leuk Lymphoma*. 2003;44(7):1239-1241.

245. François H, Coppo P, Hayman JP, Fouqueray B, Mougenot B, Ronco P. Partial fanconi syndrome induced by imatinib therapy: a novel cause of urinary phosphate loss. *Am J Kidney Dis*. 2008;51(2):298-301.

246. Gafter-Gvili A, Ram R, Gafter U, Shpilberg O, Raanani P. Renal failure associated with tyrosine kinase inhibitors--case report and review of the literature. *Leuk Res*. 2009;34(1):123-127.

247. Vora A, Bhutani M, Sharma A, Raina V. Severe tumor lysis syndrome during treatment with STI 571 in a patient with chronic myelogenous leukemia accelerated phase. *Ann Oncol*. 2002;13(11):1833-1834.

248. Dann EJ, Fineman R, Rowe JM. Tumor lysis syndrome after STI571 in Philadelphia chromosome-positive acute lymphoblastic leukemia. *J Clin Oncol*. 2002;20(1):354-355.

249. Ali R, Ozkalemkas F, Ozkan A, Ozcelik T, Ozkocaman V, Akdag I, Ozan U, Tunali A. Tumour lysis syndrome with acute renal failure during imatinib therapy. *Leuk Res*. 2007;31(4):573-574.

250. Cheer SM, Noble S. Zoledronic acid. *Drugs*. 2001;61(6):799-805.

251. Peter R, Mishra V, Fraser WD. Severe hypocalcaemia after being given intravenous bisphosphonate. *BMJ*. 2004;328(7435):335-336.

252. Tanvetyanon T, Stiff PJ. Management of the adverse effects associated with intravenous bisphosphonates. *Ann Oncol*. 2006;17(6):897-907.

253. Boehme J, Suttorp M, Fischer R, Bornhäeuser M. Influence of imatinib on bone remodeling in juvenile mice [abstract]. *J Bone Miner Res*. 2008;23:S189.

254. Suttorp M, Boehme J, Vaitl J, Mosch B, Pursche S, Jung R, Bergmann R, Fischer R, Pietzsch J, Bornhäeuser M, Gasser JA. Side effects on the heart and skeleton of growing mice attributed to chronic imatinib exposure [abstract]. *Blood*. 2008;112:Abstract 1100.

255. Insogna KL, Sahni M, Grey AB, Tanaka S, Horne WC, Neff L, Mitnick M, Levy JB, Baron R. Colony-stimulating factor-1 induces cytoskeletal reorganization and c-*src*-dependent tyrosine phosphorylation of selected cellular proteins in rodent osteoclasts. *J Clin Invest*. 1997;100(10):2476-2485.

256. Grey A, Chen Y, Paliwal I, Carlberg K, Insogna K. Evidence for a functional association between phosphatidylinositol 3-kinase and c-src in the spreading response of osteoclasts to colony-stimulating factor-1. *Endocrinology*. 2000;141(6):2129-2138.

257. Glantschnig H, Fisher JE, Wesolowski G, Rodan GA, Reszka AA. M-CSF, TNFα and RANK ligand promote osteoclast survival by signaling through mTOR/S6 kinase. *Cell Death Differ*. 2003;10(10):1165-1177.

258. Dewar AL, Domaschenz RM, Doherty KV, Hughes TP, Lyons AB. Imatinib inhibits the *in vitro* development of the monocyte/macrophage lineage from normal human bone marrow progenitors. *Leukemia*. 2003;17(9):1713-1721.

259. Dewar AL, Doherty KV, Hughes TP, Lyons AB. Imatinib inhibits the functional capacity of cultured human monocytes. *Immunol Cell Biol*. 2005;83(1):48-56.

260. Ross FP, Teitelbaum SL. $\alpha_v\beta_3$ and macrophage colony-stimulating factor: partners in osteoclast biology. *Immunol Rev*. 2005;208(1):88-105.

261. Taylor JR, Brownlow N, Domin J, Dibb NJ. FMS receptor for M-CSF (CSF-1) is sensitive to the kinase inhibitor imatinib and mutation of Asp-802 to Val confers resistance. *Oncogene*. 2006;25(1):147-151.

262. Guo J, Marcotte PA, McCall JO, Dai Y, Pease LJ, Michaelides MR, Davidsen SK, Glaser KB. Inhibition of phosphorylation of the colony-stimulating factor-1 receptor (c-Fms) tyrosine kinase in transfected cells by ABT-869 and other tyrosine kinase inhibitors. *Mol Cancer Ther*. 2006;5(4):1007-1013.

263. Chase A, Schultheis B, Kreil S, Baxter J, Hidalgo-Curtis C, Jones A, Zhang L, Grand FH, Melo JV, Cross NC. Imatinib sensitivity as a consequence of a CSF1R-Y571D mutation and CSF1/CSF1R signaling abnormalities in the cell line GDM1. *Leukemia*. 2009;23(2):358-364.

264. Brownlow N, Russell AE, Saravanapavan H, Wiesmann M, Murray JM, Manley PW, Dibb NJ. Comparison of nilotinib and imatinib inhibition of FMS receptor signaling, macrophage production and osteoclastogenesis. *Leukemia*. 2008;22(3):649-652.

265. Yoshida H, Hayashi S, Kunisada T, Ogawa M, Nishikawa S, Okamura H, Sudo T, Shultz LD, Nishikawa S. The murine mutation osteopetrosis is in the coding region of the macrophage colony stimulating factor gene. *Nature*. 1990;345(6274):442-444.

266. Niida S, Kaku M, Amano H, Yoshida H, Kataoka H, Nishikawa S, Tanne K, Maeda N, Nishikawa S-I, Kodama H. Vascular endothelial growth factor can substitute for macrophage colony-stimulating factor in the support of osteoclastic bone resorption. *J Exp Med*. 1999;190(2):293-298.

267. Huang EJ, Nocka KH, Buck J, Besmer P. Differential expression and processing of two cell associated forms of the kit-ligand: KL-1 and KL-2. *Mol Biol Cell*. 1992;3(3):349-362.

268. Gattei V, Aldinucci D, Quinn JM, Degan M, Cozzi M, Perin V, Iuliis AD, Juzbasic S, Improta S, Athanasou NA, Ashman LK, Pinto A. Human osteoclasts and preosteoclast cells (FLG 29.1) express functional c-kit receptors and interact with osteoblast and stromal cells via membrane-bound stem cell factor. *Cell Growth Differ*. 1996;7(6):753-763.

269. Broxmeyer HE, Maze R, Miyazawa K, Carow C, Hendrie PC, Cooper S, Hangoc G, Vadhan-Raj S, Lu L. The kit receptor and its ligand, steel factor, as regulators of hemopoiesis. *Cancer Cells*. 1991;3(12):480-487.

270. Demulder A, Suggs SV, Zsebo KM, Scarcez T, Roodman GD. Effects of stem cell factor on osteoclast-like cell formation in long-term human marrow cultures. *J Bone Miner Res*. 1992;7(11):1337-1344.

271. Chae HJ, Park RK, Kang JS, Shin HS, Kim SC, Chung HT, Son DW, Ko KI, Kim JB, Park YC, Kim HR. Effect of stem cell factor, interleukin-6, nitric oxide and transforming growth factor-beta on the osteoclast differentiation induced by 1 alpha,25-(OH)2D3 in primary murine bone marrow cultures. *Pharmacol Toxicol*. 1998;82(5):223-229.

272. van't Hof RJ, von Lindern M, Nijweide PJ, Beug H. Stem cell factor stimulates chicken osteoclast activity in vitro. *FASEB J*. 1997;11(4):287-293.

273. Mansky KC, Sankar U, Han J, Ostrowski MC. Microphthalmia transcription factor is a target of the p38 MAPK pathway in response to receptor activator of NF-kappa B ligand signaling. *J Biol Chem*. 2002;277(13):11077-11083.

274. Steingrimsson E, Moore KJ, Lamoreux ML, Ferre-D'Amare AR, Burley SK, Zimring DC, Skow LC, Hodgkinson CA, Arnheiter H, Copeland NG, et al. Molecular basis of mouse microphthalmia (mi) mutations helps explain their developmental and phenotypic consequences. *Nat Genet*. 1994;8(3):256-263.

275. Moore KJ. Insight into the microphthalmia gene. *Trends Genet*. 1995;11(11):442-448.

276. Sly WS, Hewett-Emmett D, Whyte MP, Yu YS, Tashian RE. Carbonic anhydrase II deficiency identified as the primary defect in the autosomal recessive syndrome of osteopetrosis with renal tubular acidosis and cerebral calcification. *Proc Natl Acad Sci U S A*. 1983;80(9):2752-2756.

277. Lewis SE, Erickson RP, Barnett LB, Venta PJ, Tashian RE. *N*-ethyl-*N*-nitrosourea-induced null mutation at the mouse *Car-2* locus: an animal model for human carbonic anhydrase II deficiency syndrome. *Proc Natl Acad Sci U S A*. 1988;85(6):1962-1966.

278. Margolis DS, Szivek JA, Lai L-W, Lien YH. Phenotypic characteristics of bone in carbonic anhydrase II-deficient mice. *Calcif Tissue Int*. 2008;82(1):66-76.

279. Cochran DL, Rouse CA, Lynch SE, Graves DT. Effects of platelet-derived growth factor isoforms on calcium release from neonatal mouse calvariae. *Bone*. 1993;14(1):53-58.

280. Hock JM, Canalis E. Platelet-derived growth factor enhances bone cell replication, but not differentiated function of osteoblasts. *Endocrinology*. 1994;134(3):1423-1428.

281. Zhang Z, Chen J, Jin D. Platelet-derived growth factor (PDGF)-BB stimulates osteoclastic bone resorption directly: the role of receptor β. *Biochem Biophys Res Commun*. 1998;251(1):190-194.

282. Franchimont N, Canalis E. Platelet-derived growth factor stimulates the synthesis of interleukin-6 in cells of the osteoblast lineage. *Endocrinology*. 1995;136(12):5469-5475.

283. Abboud SL, Pinzani M. Peptide growth factors stimulate macrophage colony-stimulating factor in murine stromal cells. *Blood*. 1991;78(1):103-109.

284. Li B, Boast S, de los Santos K, Schieren I, Quiroz M, Teitelbaum SL, Tondravi MM, Goff SP. Mice deficient in Abl are osteoporotic and have defects in osteoblast maturation. *Nat Genet*. 2000;24(3):304-308.

285. Xie JF, Stroumza J, Graves DT. IL-1 down-regulates platelet-derived growth factor-α receptor gene expression at the transcriptional level in human osteoblastic cells. *J Immunol*. 1994;153(1):378-383.

286. Graves DT, Owen AJ, Antoniades HN. Evidence that a human osteosarcoma cell line which secretes a mitogen similar to platelet-derived growth factor requires growth factors present in platelet-poor plasma. *Cancer Res*. 1983;43(1):83-87.

287. Canalis E, Varghese S, McCarthy TL, Centrella M. Role of platelet derived growth factor in bone cell function. *Growth Regul*. 1992;2(4):151-155.

288. Yu X, Hsieh SC, Bao W, Graves DT. Temporal expression of PDGF receptors and PDGF regulatory effects on osteoblastic cells in mineralizing cultures. *Am J Physiol*. 1997;272(5):C1709-1716.

289. Kubota K, Sakikawa C, Katsumata M, Nakamura T, Wakabayashi K. Platelet-derived growth factor BB secreted from osteoclasts acts as an osteoblastogenesis inhibitory factor. *J Bone Miner Res*. 2002;17(2):257-265.

290. Chaudhary LR, Hofmeister AM, Hruska KA. Differential growth factor control of bone formation through osteoprogenitor differentiation. *Bone*. 2004;34(3):402-411.

291. Tokunaga A, Oya T, Ishii Y, Motomura H, Nakamura C, Ishizawa S, Fujimori T, Nabeshima Y, Umezawa A, Kanamori M, Kimura T, Sasahara M. PDGF receptor beta is a potent regulator of mesenchymal stromal cell function. *J Bone Miner Res*. 2008;23(9):1519-1528.

292. Lowe C, Yoneda T, Boyce BF, Chen H, Mundy GR, Soriano P. Osteopetrosis in Src-deficient mice is due to an autonomous defect of osteoclasts. *Proc Natl Acad Sci U S A*. 1993;90(10):4485-4489.

293. Tanaka S, Amling M, Neff L, Peyman A, Uhlmann E, Levy JB, Baron R. c-Cbl is downstream of c-Src in a signalling pathway necessary for bone resorption. *Nature*. 1996;383(6600):528-531.

294. Abu-Amer Y, Ross FP, Schlesinger P, Tondravi MM, Teitelbaum SL. Substrate recognition by osteoclast precursors induces C-src/microtubule association. *J Cell Biol*. 1997;137(1):247-258.

295. Nakamura I, Jimi E, Duong LT, Sasaki T, Takahashi N, Rodan GA, Suda T. Tyrosine phosphorylation of $p130^{Cas}$ is involved in actin organization in osteoclasts. *J Biol Chem*. 1998;273(18):11144-11149.

296. Xing L, Venegas AM, Chen A, Garrett-Beal L, Boyce BF, Varmus HE, Schwartzberg PL. Genetic evidence for a role for Src family kinases in TNF family receptor signaling and cell survival. *Genes Dev*. 2001;15(2):241-253.

297. Raschke WC, Baird S, Ralph P, Nakoinz I. Functional macrophage cell lines transformed by Abelson leukemia virus. *Cell*. 1978;15(1):261-267.

298. Atsumi T, Miwa Y, Kimata K, Ikawa Y. A chondrogenic cell line derived from a differentiating culture of AT805 teratocarcinoma cells. *Cell Differ Dev*. 1990;30(2):109-116.

299. Wani MR, Fuller K, Kim NS, Choi Y, Chambers T. Prostaglandin E2 cooperates with TRANCE in osteoclast induction from hemopoietic precursors: synergistic activation of differentiation, cell spreading, and fusion. *Endocrinology*. 1999;140(4):1927-1935.

300. Labarca C, Piagen K. A simple, rapid, and sensitive DNA assay procedure. *Anal Biochem*. 1980;102(2):344-352.

301. Esko JD. Special considerations for proteoglycans and glycosaminoglycans and their purification. In: Ausubel F, Brent R, Kingston B, et al., eds. Current Protocols in Molecular Biology. New York: Greene Publishing and Wiley-Interscience 1993:17.12.11–17.12.19.

302. Sawyers CL. Chronic myeloid leukemia. *N Engl J Med.* 1999;340(17):1330-1340.

303. Horton JA, Bariteau JT, Loomis RM, Strauss JA, Damron TA. Ontogeny of skeletal maturation in the juvenile rat. *Anat Rec (Hoboken)*. 2008;291(3):283-292.

304. Labrinidis A, Hay S, Liapis V, Ponomarev V, Findlay DM, Evdokiou A. Zoledronic acid inhibits both the osteolytic and osteoblastic components of osteosarcoma lesions in a mouse model. *Clin Cancer Res*. 2009;15(10):3451-3461.

305. Wolff NC, Randle DE, Egorin MJ, Minna JD, Ilaria RL, Jr. Imatinib mesylate efficiently achieves therapeutic intratumor concentrations in vivo but has limited activity in a xenograft model of small cell lung cancer. *Clin Cancer Res*. 2004;10(10):3528-3534.

306. Wang X, Hochhaus A, Kantarjian HM, Agrawal S, Roy A, Pfister M, Chen T, Bleickardt E, Nicaise C, Shah N. Dasatinib pharmacokinetics and exposure-response (E-R): Relationship to safety and efficacy in patients (pts) with chronic myeloid leukemia (CML) [abstract]. *Journal of Clinical Oncology*. 2008;26(S1):abstr 3590.

307. Kamath AV, Wang J, Lee FY, Marathe PH. Preclinical pharmacokinetics and in vitro metabolism of dasatinib (BMS-354825): a potent oral multi-targeted kinase inhibitor against SRC and BCR-ABL. *Cancer Chemother Pharmacol*. 2008;61(3):365-376.

308. Oostendorp RL, Buckle T, Beijnen JH, van Tellingen O, Schellens JH. The effect of P-gp (Mdr1a/1b), BCRP (Bcrp1) and P-gp/BCRP inhibitors on the in vivo absorption, distribution, metabolism and excretion of imatinib. *Invest New Drugs*. 2009;27(1):31-40.

309. Lagas JS, van Waterschoot RA, van Tilburg VA, Hillebrand MJ, Lankheet N, Rosing H, Beijnen JH, Schinkel AH. Brain accumulation of dasatinib is restricted by P-glycoprotein (ABCB1) and breast cancer resistance protein (ABCG2) and can be enhanced by elacridar treatment. *Clin Cancer Res*. 2009;15(7):2344-2351.

310. Perilli E, Baruffaldi F, Bisi MC, Cristofolini L, Cappello A. A physical phantom for the calibration of three-dimensional X-ray microtomography examination. *J Microsc*. 2006;222(2):124-134.

311. McNeil PJ, Durbridge TC, Parkinson IH, Moore RJ. Simple method for the simultaneous demonstration of formation and resorption in undecalcified bone embedded in methyl methacrylate. *J Histotechnol*. 1997;20(4):307-311.

312. Vanderkerken K, Asosingh K, Willems A, De Raeve H, Couck P, Gorus F, Croucher P, Van Camp B. The 5TMM murine model of multiple myeloma. In: Brown RD, Ho PJ, eds. Multiple Myeloma: Methods and Protocols. Vol. 113. Totowa, NJ, USA: Humana Press; 2005:191-205.

313. Gronthos S, Zannettino AC, Hay SJ, Shi S, Graves SE, Kortesidis A, Simmons PJ. Molecular and cellular characterisation of highly purified stromal stem cells derived from human bone marrow. *J Cell Sci*. 2003;116(Pt 9):1827-1835.

314. Nordin BE, Morris HA, Need AG, Horowitz M, Robertson WG. Relationship between plasma calcium fractions, other bone-related variables, and serum follicle-stimulating hormone levels in premenopausal, perimenopausal, and postmenopausal women. *Am J Obstet Gynecol*. 1990;163(1 Pt 1):140-145.

315. Silver RT, Woolf SH, Hehlmann R, Appelbaum FR, Anderson J, Bennett C, Goldman JM, Guilhot F, Kantarjian HM, Lichtin AE, Talpaz M, Tura S. An evidence-based analysis of the effect of busulfan, hydroxyurea, interferon, and allogeneic bone marrow transplantation in treating the chronic phase of chronic myeloid leukemia: developed for the American Society of Hematology. *Blood*. 1999;94(5):1517-1536.

316. Hehlmann R, Heimpel H, Hasford J, Kolb HJ, Pralle H, Hossfeld DK, Queisser W, Loffler H, Hochhaus A, Heinze B, et al. Randomized comparison of interferon-alpha with busulfan and hydroxyurea in chronic myelogenous leukemia. The German CML Study Group. *Blood*. 1994;84(12):4064-4077.

317. Allan NC, Richards SM, Shepherd PC. UK Medical Research Council randomised, multicentre trial of interferon-alpha n1 for chronic myeloid leukaemia: improved survival irrespective of cytogenetic response. The UK Medical Research Council's Working Parties for Therapeutic Trials in Adult Leukaemia. *Lancet*. 1995;345(8962):1392-1397.

318. Ohnishi K, Ohno R, Tomonaga M, Kamada N, Onozawa K, Kuramoto A, Dohy H, Mizoguchi H, Miyawaki S, Tsubaki K, et al. A randomized trial comparing interferon-alpha with busulfan for newly diagnosed chronic myelogenous leukemia in chronic phase. *Blood*. 1995;86(3):906-916.

319. Interferon alfa-2a as compared with conventional chemotherapy for the treatment of chronic myeloid leukemia. The Italian Cooperative Study Group on Chronic Myeloid Leukemia. *N Engl J Med*. 1994;330(12):820-825.

320. Hochhaus A, Druker B, Sawyers C, Guilhot F, Schiffer CA, Cortes J, Niederwieser DW, Gambacorti-Passerini C, Stone RM, Goldman J, Fischer T, O'Brien SG, Reiffers JJ, Mone M, Krahnke T, Talpaz M, Kantarjian HM. Favorable long-term follow-up results over 6 years for response, survival, and safety with imatinib mesylate therapy in chronic-phase chronic myeloid leukemia after failure of interferon-alpha treatment. *Blood*. 2008;111(3):1039-1043.

321. Mauro MJ, Deininger MW. Management of drug toxicities in chronic myeloid leukaemia. *Best Pract Res Clin Haematol*. 2009;22(3):409-429.

322. Peng B, Hayes M, Resta D, Racine-Poon A, Druker BJ, Talpaz M, Sawyers CL, Rosamilia M, Ford J, Lloyd P, Capdeville R. Pharmacokinetics and pharmacodynamics of imatinib in a phase I trial with chronic myeloid leukemia patients. *J Clin Oncol*. 2004;22(5):935-942.

323. Kleerekoper M, Villanueva AR, Stanciu J, Rao DS, Parfitt AM. The role of three-dimensional trabecular microstructure in the pathogenesis of vertebral compression fractures. *Calcif Tissue Int*. 1985;37(6):594-597.

324. Ikeda S, Morishita Y, Tsutsumi H, Ito M, Shiraishi A, Arita S, Akahoshi S, Narusawa K, Nakamura T. Reductions in bone turnover, mineral, and structure associated with mechanical properties of lumbar vertebra and femur in glucocorticoid-treated growing minipigs. *Bone*. 2003;33(5):779-787.

325. Teo JCM, Si-Hoe KM, Keh JEL, S.H. T. Correlation of cancellous bone microarchitectural parameters from microCT to CT number and bone mechanical properties. *Mat Sci Eng C*. 2007;27:333-339.

326. Parisien MV, McMahon D, Pushparaj N, Dempster DW. Trabecular architecture in iliac crest bone biopsies: infra-individual variability in structural parameters and changes with age. *Bone*. 1988;9(5):289-295.

327. Bonucci E, Ballanti P, Della Rocca C, Milani S, Lo Cascio V, Imbimbo B. Technical variability of bone histomorphometric measurements. *Bone Miner*. 1990;11(2):177-186.

328. Chappard C, Marchadier A, Benhamou L. Interindividual and intraspecimen variability of 3-D bone microarchitectural parameters in iliac crest biopsies imaged by conventional micro-computed tomography. *J Bone Miner Metab*. 2008;26(5):506-513.

329. Olah AJ. Quantitative relations between osteoblasts and osteoid in primary hyperparathyroidism, intestinal malabsorption ad renal osteodystrophy. *Virchows Arch A Pathol Pathol Anat*. 1973;358(4):301-308.

330. Mosekilde L. Primary hyperparathyroidism and the skeleton. *Clin Endocrinol (Oxf)*. 2008;69(1):1-19.

331. Byers PD, Smith R. Quantitative histology of bone in hyperparathyroidism. Its relation to clinical features, x-ray, and biochemistry. *Q J Med.* 1971;40(160):471-486.

332. Eriksen EF, Steiniche T, Mosekilde L, Melsen F. Histomorphometric analysis of bone in metabolic bone disease. *Endocrinol Metab Clin North Am*. 1989;18(4):919-954.

333. Christiansen P, Steiniche T, Vesterby A, Mosekilde L, Hessov I, Melsen F. Primary hyperparathyroidism: iliac crest trabecular bone volume, structure, remodeling, and balance evaluated by histomorphometric methods. *Bone*. 1992;13(1):41-49.

334. Cummings SR, Melton LJ. Epidemiology and outcomes of osteoporotic fractures. *Lancet*. 2002;359(9319):1761-1767.

335. Lanyon LE. Functional strain as a determinant for bone remodeling. *Calcif Tissue Int*. 1984;36 Suppl 1:S56-61.

336. Rubin CT, Lanyon LE. Regulation of bone mass by mechanical strain magnitude. *Calcif Tissue Int*. 1985;37(4):411-417.

337. Carter DR. Mechanical loading histories and cortical bone remodeling. *Calcif Tissue Int*. 1984;36 Suppl 1:S19-24.

338. Christiansen P, Steiniche T, Brockstedt H, Mosekilde L, Hessov I, Melsen F. Primary hyperparathyroidism: iliac crest cortical thickness, structure, and remodeling evaluated by histomorphometric methods. *Bone*. 1993;14(5):755-762.

339. Guo CY, Thomas WE, al-Dehaimi AW, Assiri AM, Eastell R. Longitudinal changes in bone mineral density and bone turnover in postmenopausal women with primary hyperparathyroidism. *J Clin Endocrinol Metab*. 1996;81(10):3487-3491.

340. Jowsey J. Bone histology and hyperparathyroidism. *Clin Endocrinol Metab*. 1974;3(2):267-284.

341. Frydecka I, Bieniek J, Brodzka W. Osteolytic lesion in chronic myelogenous leukaemia. *Folia Haematol Int Mag Klin Morphol Blutforsch*. 1984;111(5):610-613.

342. Thiele J, Hoeppner B, Wienhold S, Schneider G, Fischer R, Zankovich R. Osteoclasts and bone remodeling in chronic myeloproliferative disorders. A histochemical and morphometric study on trephine biopsies in 165 patients. *Pathol Res Pract*. 1989;184(6):591-599.

343. Kwong YL, Ng IO, Leung SY. Osteolytic skeletal lesions in chronic myeloid leukemia. *Pathology*. 1990;22(2):124-125.

344. Nadal E, Cervantes F, Rosinol L, Talarn C, Montserrat E. Hypercalcemia as the presenting feature of t-cell lymphoid blast crisis of ph-positive chronic myeloid leukemia. *Leuk Lymphoma*. 2001;41(1-2):203-206.

345. Maloisel F, Favre G, Mahmal L, Zamfir A, Andres E. Isolated lytic bone lesion as extramedullary disease in chronic myelogenous leukemia: a report of three new cases. *Eur J Intern Med*. 2005;16(4):288-290.

346. Schabel SI, Tyminski L, Holland RD, Rittenberg GM. The skeletal manifestations of chronic myelogenous leukemia. *Skeletal Radiol*. 1980;5(3):145-149.

347. Tokarski JS, Newitt JA, Chang CY, Cheng JD, Wittekind M, Kiefer SE, Kish K, Lee FY, Borzillerri R, Lombardo LJ, Xie D, Zhang Y, Klei HE. The structure of Dasatinib (BMS-354825) bound to activated ABL kinase domain elucidates its inhibitory activity against imatinib-resistant ABL mutants. *Cancer Res*. 2006;66(11):5790-5797.

348. Lombardo LJ, Lee FY, Chen P, Norris D, Barrish JC, Behnia K, Castaneda S, Cornelius LA, Das J, Doweyko AM, Fairchild C, Hunt JT, Inigo I, Johnston K, Kamath A, Kan D, Klei H, Marathe P, Pang S, Peterson R, Pitt S, Schieven GL, Schmidt RJ, Tokarski

J, Wen M-L, Wityak J, Borzilleri RM. Discovery of N-(2-chloro-6-methyl- phenyl)-2-(6-(4-(2-hydroxyethyl)- piperazin-1-yl)-2-methylpyrimidin-4- ylamino)thiazole-5-carboxamide (BMS-354825), a dual Src/Abl kinase inhibitor with potent antitumor activity in preclinical assays. *J Med Chem*. 2004;47(27):6658-6661.

349. Bantscheff M, Eberhard D, Abraham Y, Bastuck S, Boesche M, Hobson S, Mathieson T, Perrin J, Raida M, Rau C, Reader V, Sweetman G, Bauer A, Bouwmeester T, Hopf C, Kruse U, Neubauer G, Ramsden N, Rick J, Kuster B, Drewes G. Quantitative chemical proteomics reveals mechanisms of action of clinical ABL kinase inhibitors. *Nat Biotechnol*. 2007;25(9):1035-1044.

350. Nam S, Kim D, Cheng JQ, Zhang S, Lee JH, Buettner R, Mirosevich J, Lee FY, Jove R. Action of the Src family kinase inhibitor, dasatinib (BMS-354825), on human prostate cancer cells. *Cancer Res*. 2005;65(20):9185-9189.

351. Wiktor-Jedrzejczak W, Bartocci A, Ferrante AW, Jr., Ahmed-Ansari A, Sell KW, Pollard JW, Stanley ER. Total absence of colony-stimulating factor 1 in the macrophage-deficient osteopetrotic (op/op) mouse. *Proc Natl Acad Sci U S A*. 1990;87(12):4828-4832.

352. Yang M, Mailhot G, MacKay CA, Mason-Savas A, Aubin J, Odgren PR. Chemokine and chemokine receptor expression during colony stimulating factor-1-induced osteoclast differentiation in the toothless osteopetrotic rat: a key role for CCL9 (MIP-1gamma) in osteoclastogenesis in vivo and in vitro. *Blood*. 2006;107(6):2262-2270.

353. Soriano P, Montgomery C, Geske R, Bradley A. Targeted disruption of the c-src proto-oncogene leads to osteopetrosis in mice. *Cell*. 1991;64(4):693-702.

354. Boyce BF, Yoneda T, Lowe C, Soriano P, Mundy GR. Requirement of pp60c-src expression for osteoclasts to form ruffled borders and resorb bone in mice. *J Clin Invest*. 1992;90(4):1622-1627.

355. Schwartzberg PL, Xing L, Hoffmann O, Lowell CA, Garrett L, Boyce BF, Varmus HE. Rescue of osteoclast function by transgenic expression of kinase-deficient Src in *src*-/- mutant mice. *Genes Dev*. 1997;11(21):2835-2844.

356. Missbach M, Jeschke M, Feyen J, Müller K, Glatt M, Green J, Šuša M. A novel inhibitor of the tyrosine kinase Src suppresses phosphorylation of its major cellular substrates and reduces bone resorption in vitro and in rodent models in vivo. *Bone*. 1999;24(5):437-449.

357. Recchia I, Rucci N, Funari A, Migliaccio S, Taranta A, Longo M, Kneissel M, Šuša M, Fabbro D, Teti A. Reduction of c-Src activity by substituted 5,7-diphenyl-pyrrolo[2,3-*d*]-pyrimidines induces osteoclast apoptosis in vivo and in vitro. Involvement of ERK1/2 pathway. *Bone*. 2004;34(1):65-79.

358. Boyce BF, Xing L, Yao Z, Shakespeare WC, Wang Y, Metcalf CA, 3rd, Sundaramoorthi R, Dalgarno DC, Iuliucci JD, Sawyer TK. Future anti-catabolic therapeutic targets in bone disease. *Ann N Y Acad Sci*. 2006;1068:447-457.

359. Perrien DS, Akel NS, Dupont-Versteegden EE, Skinner RA, Siegel ER, Suva LJ, Gaddy D. Aging alters the skeletal response to disuse in the rat. *Am J Physiol Regul Integr Comp Physiol*. 2007;292(2):R988-996.

360. Peng B, Lloyd P, Schran H. Clinical pharmacokinetics of imatinib. *Clin Pharmacokinet*. 2005;44(9):879-894.

361. Picard S, Titier K, Etienne G, Teilhet E, Ducint D, Bernard MA, Lassalle R, Marit G, Reiffers J, Begaud B, Moore N, Molimard M, Mahon FX. Trough imatinib plasma levels are associated with both cytogenetic and molecular responses to standard-dose imatinib in chronic myeloid leukemia. *Blood*. 2007;109(8):3496-3499.

362. Larson RA, Druker BJ, Guilhot F, O'Brien SG, Riviere GJ, Krahnke T, Gathmann I, Wang Y. Imatinib pharmacokinetics and its correlation with response and safety in chronic-phase chronic myeloid leukemia: a subanalysis of the IRIS study. *Blood*. 2008;111(8):4022-4028.

363. Carpiuc KT, Stephens JM, S.Y. L, Botteman MF. Incidence of grade 3/4 adverse events in imatinib resistant/intolerant chronic phase CML (CP-CML): A comparison of nilotinib and dasatinib [abstract]. *Journal of Clinical Oncology*. 2007;25(18S):17501.

364. Coleman RE. Bisphosphonates: clinical experience. *Oncologist*. 2004;9 Suppl 4:14-27.

365. Russell RG, Xia Z, Dunford JE, Oppermann U, Kwaasi A, Hulley PA, Kavanagh KL, Triffitt JT, Lundy MW, Phipps RJ, Barnett BL, Coxon FP, Rogers MJ, Watts NB, Ebetino FH. Bisphosphonates: an update on mechanisms of action and how these relate to clinical efficacy. *Ann N Y Acad Sci*. 2007;1117:209-257.

366. Koga T, Inui M, Inoue K, Kim S, Suematsu A, Kobayashi E, Iwata T, Ohnishi H, Matozaki T, Kodama T, Taniguchi T, Takayanagi H, Takai T. Costimulatory signals mediated by the ITAM motif cooperate with RANKL for bone homeostasis. *Nature*. 2004;428(6984):758-763.

367. Sims NA, Jenkins BJ, Nakamura A, Quinn JM, Li R, Gillespie MT, Ernst M, Robb L, Martin TJ. Interleukin-11 receptor signaling is required for normal bone remodeling. *J Bone Miner Res*. 2005;20(7):1093-1102.

368. Pataki A, Muller K, Green JR, Ma YF, Li QN, Jee WS. Effects of short-term treatment with the bisphosphonates zoledronate and pamidronate on rat bone: a comparative histomorphometric study on the cancellous bone formed before, during, and after treatment. *Anat Rec*. 1997;249(4):458-468.

369. Pozzi S, Vallet S, Mukherjee S, Cirstea D, Vaghela N, Santo L, Rosen E, Ikeda H, Okawa Y, Kiziltepe T, Schoonmaker J, Xie W, Hideshima T, Weller E, Bouxsein ML, Munshi NC, Anderson KC, Raje N. High-dose zoledronic acid impacts bone remodeling with effects on osteoblastic lineage and bone mechanical properties. *Clin Cancer Res*. 2009;15(18):5829-5839.

370. Gambacorti-Passerini C, Piazza R, D'Incalci M. Bcr-Abl mutations, resistance to imatinib, and imatinib plasma levels. *Blood*. 2003;102(5):1933-1934.

371. Gambacorti-Passerini CB, Gunby RH, Piazza R, Galietta A, Rostagno R, Scapozza L. Molecular mechanisms of resistance to imatinib in Philadelphia-chromosome-positive leukaemias. *Lancet Oncol*. 2003;4(2):75-85.

372. Cortes JE, Egorin MJ, Guilhot F, Molimard M, Mahon FX. Pharmacokinetic/pharmacodynamic correlation and blood-level testing in imatinib therapy for chronic myeloid leukemia. *Leukemia*. 2009;23(9):1537-1544.

373. Thomas J, Wang L, Clark RE, Pirmohamed M. Active transport of imatinib into and out of cells: implications for drug resistance. *Blood*. 2004;104(12):3739-3745.

374. Burger H, van Tol H, Boersma AW, Brok M, Wiemer EA, Stoter G, Nooter K. Imatinib mesylate (STI571) is a substrate for the breast cancer resistance protein (BCRP)/ABCG2 drug pump. *Blood*. 2004;104(9):2940-2942.

375. Gambacorti-Passerini C, Zucchetti M, Russo D, Frapolli R, Verga M, Bungaro S, Tornaghi L, Rossi F, Pioltelli P, Pogliani E, Alberti D, Corneo G, D'Incalci M. Alpha1 acid glycoprotein binds to imatinib (STI571) and substantially alters its pharmacokinetics in chronic myeloid leukemia patients. *Clin Cancer Res*. 2003;9(2):625-632.

376. Larghero J, Leguay T, Mourah S, Madelaine-Chambrin I, Taksin AL, Raffoux E, Bastie JN, Degos L, Berthaud P, Marolleau JP, Calvo F, Chomienne C, Mahon FX, Rousselot P. Relationship between elevated levels of the alpha 1 acid glycoprotein in chronic myelogenous leukemia in blast crisis and pharmacological resistance to imatinib (Gleevec) in vitro and in vivo. *Biochem Pharmacol*. 2003;66(10):1907-1913.

377. Bleasby K, Castle JC, Roberts CJ, Cheng C, Bailey WJ, Sina JF, Kulkarni AV, Hafey MJ, Evers R, Johnson JM, Ulrich RG, Slatter JG. Expression profiles of 50 xenobiotic transporter genes in humans and pre-clinical species: a resource for investigations into drug disposition. *Xenobiotica*. 2006;36(10-11):963-988.

378. Hilgendorf C, Ahlin G, Seithel A, Artursson P, Ungell AL, Karlsson J. Expression of thirty-six drug transporter genes in human intestine, liver, kidney, and organotypic cell lines. *Drug Metab Dispos*. 2007;35(8):1333-1340.

379. Kim IW, Booth-Genthe C, Ambudkar SV. Relationship between drugs and functional activity of various mammalian P-glycoproteins (ABCB1). *Mini Rev Med Chem*. 2008;8(3):193-200.

380. Kretz O, Weiss HM, Schumacher MM, Gross G. In vitro blood distribution and plasma protein binding of the tyrosine kinase inhibitor imatinib and its active metabolite, CGP74588, in rat, mouse, dog, monkey, healthy humans and patients with acute lymphatic leukaemia. *Br J Clin Pharmacol*. 2004;58(2):212-216.

381. Kieswetter K, Schwartz Z, Alderete M, Dean DD, Boyan BD. Platelet derived growth factor stimulates chondrocyte proliferation but prevents endochondral maturation. *Endocrine*. 1997;6(3):257-264.

382. Weiser L, Bhargava M, Attia E, Torzilli PA. Effect of serum and platelet-derived growth factor on chondrocytes grown in collagen gels. *Tissue Eng*. 1999;5(6):533-544.

383. Labrador JP, Azcoitia V, Tuckermann J, Lin C, Olaso E, Manes S, Bruckner K, Goergen JL, Lemke G, Yancopoulos G, Angel P, Martinez C, Klein R. The collagen receptor DDR2 regulates proliferation and its elimination leads to dwarfism. *EMBO Rep*. 2001;2(5):446-452.

384. Bursell L, Woods A, James CG, Pala D, Leask A, Beier F. Src kinase inhibition promotes the chondrocyte phenotype. *Arthritis Res Ther*. 2007;9(5):R105.

385. Gill KS, Beier F, Goldberg HA. Rho-ROCK signaling differentially regulates chondrocyte spreading on fibronectin and bone sialoprotein. *Am J Physiol Cell Physiol*. 2008;295(1):C38-49.

386. Pala D, Kapoor M, Woods A, Kennedy L, Liu S, Chen S, Bursell L, Lyons KM, Carter DE, Beier F, Leask A. Focal adhesion kinase/Src suppresses early chondrogenesis: central role of CCN2. *J Biol Chem*. 2008;283(14):9239-9247.

387. Mariani S, Giona F, Basciani S, Brama M, Gnessi L. Low bone density and decreased inhibin-B/FSH ratio in a boy treated with imatinib during puberty. *Lancet*. 2008;372(9633):111-112.

388. Kimoto T, Inoue M, Kawa K. Growth deceleration in a girl treated with imatinib. *Int J Hematol*. 2009;89(2):251-252.

389. Schmid H, Jaeger BA, Lohse J, Suttorp M. Longitudinal growth retardation in a prepubertal girl with chronic myeloid leukemia on long-term treatment with imatinib. *Haematologica*. 2009;94(8):1177-1179.

390. Anderson DM, Maraskovsky E, Billingsley WL, Dougall WC, Tometsko ME, Roux ER, Teepe MC, DuBose RF, Cosman D, Galibert L. A homologue of the TNF receptor and its ligand enhance T-cell growth and dendritic-cell function. *Nature*. 1997;390(6656):175-179.

391. Boyle WJ, Simonet WS, Lacey DL. Osteoclast differentiation and activation. *Nature*. 2003;423(6937):337-342.

392. Hotokezaka H, Sakai E, Kanaoka K, Saito K, Matsuo K, Kitaura H, Yoshida N, Nakayama K. U0126 and PD98059, specific inhibitors of MEK, accelerate differentiation of RAW264.7 cells into osteoclast-like cells. *J Biol Chem*. 2002;277(49):47366-47372.

393. Matsumoto M, Sudo T, Saito T, Osada H, Tsujimoto M. Involvement of p38 mitogen-activated protein kinase signaling pathway in osteoclastogenesis mediated by receptor activator of NF-kappa B ligand (RANKL). *J Biol Chem*. 2000;275(40):31155-31161.

394. Inami K, Sawai H, Yakushiji K, Katao Y, Matsumoto N, Domae N. Augmentation of TNF-induced osteoclast differentiation by inhibition of ERK and activation of p38: similiar intracellular signaling between RANKL- and TNF-induced osteoclast differentation. *Orthodontic Waves*. 2008;67:150-156.

395. Dey A, She H, Kim L, Boruch A, Guris DL, Carlberg K, Sebti SM, Woodley DT, Imamoto A, Li W. Colony-stimulating factor-1 receptor utilizes multiple signaling pathways to induce cyclin D2 expression. *Mol Biol Cell*. 2000;11(11):3835-3848.

396. Csar XF, Wilson NJ, McMahon KA, Marks DC, Beecroft TL, Ward AC, Whitty GA, Kanangasundarum V, Hamilton JA. Proteomic analysis of macrophage differentiation. p46/52(Shc) Tyrosine phosphorylation is required for CSF-1-mediated macrophage differentiation. *J Biol Chem*. 2001;276(28):26211-26217.

397. Yeung YG, Stanley ER. Proteomic approaches to the analysis of early events in colony-stimulating factor-1 signal transduction. *Mol Cell Proteomics*. 2003;2(11):1143-1155.

398. Reszka AA, Halasy-Nagy JM, Masarachia PJ, Rodan GA. Bisphosphonates act directly on the osteoclast to induce caspase cleavage of mst1 kinase during apoptosis. A link between inhibition of the mevalonate pathway and regulation of an apoptosis-promoting kinase. *J Biol Chem*. 1999;274(49):34967-34973.

399. Akiyama T, Bouillet P, Miyazaki T, Kadono Y, Chikuda H, Chung UI, Fukuda A, Hikita A, Seto H, Okada T, Inaba T, Sanjay A, Baron R, Kawaguchi H, Oda H, Nakamura K, Strasser A, Tanaka S. Regulation of osteoclast apoptosis by ubiquitylation of proapoptotic BH3-only Bcl-2 family member Bim. *Embo J*. 2003;22(24):6653-6664.

400. Sugatani T, Hruska KA. Akt1/Akt2 and mammalian target of rapamycin/Bim play critical roles in osteoclast differentiation and survival, respectively, whereas Akt is dispensable for cell survival in isolated osteoclast precursors. *J Biol Chem*. 2005;280(5):3583-3589.

401. Elsegood CL, Zhuo Y, Wesolowski GA, Hamilton JA, Rodan GA, Duong le T. M-CSF induces the stable interaction of cFms with $\alpha_V\beta_3$ integrin in osteoclasts. *Int J Biochem Cell Biol*. 2006;38(9):1518-1529.

402. Wong BR, Besser D, Kim N, Arron JR, Vologodskaia M, Hanafusa H, Choi Y. TRANCE, a TNF family member, activates Akt/PKB through a signaling complex involving TRAF6 and c-Src. *Mol Cell*. 1999;4(6):1041-1049.

403. Vincent C, Kogawa M, Findlay DM, Atkins GJ. The generation of osteoclasts from RAW 264.7 precursors in defined, serum-free conditions. *J Bone Miner Metab*. 2009;27(1):114-119.

404. Downing JR, Rettenmier CW, Sherr CJ. Ligand-induced tyrosine kinase activity of the colony-stimulating factor 1 receptor in a murine macrophage cell line. *Mol Cell Biol*. 1988;8(4):1795-1799.

405. Novak U, Harpur AG, Paradiso L, Kanagasundaram V, Jaworowski A, Wilks AF, Hamilton JA. Colony-stimulating factor 1-induced STAT1 and STAT3 activation is accompanied by phosphorylation of Tyk2 in macrophages and Tyk2 and JAK1 in fibroblasts. *Blood*. 1995;86(8):2948-2956.

406. Deininger MWN, Buchdunger E, Druker BJ. The development of imatinib as a therapeutic agent for chronic myeloid leukemia. *Blood*. 2005;105(7):2640-2653.

407. Alessi DR, Cuenda A, Cohen P, Dudley DT, Saltiel AR. PD 098059 is a specific inhibitor of the activation of mitogen-activated protein kinase kinase in vitro and in vivo. *J Biol Chem*. 1995;270(46):27489-27494.

408. Dudley DT, Pang L, Decker SJ, Bridges AJ, Saltiel AR. A synthetic inhibitor of the mitogen-activated protein kinase cascade. *Proc Natl Acad Sci U S A*. 1995;92(17):7686-7689.

409. Brownlow N, Mol C, Hayford C, Ghaem-Maghami S, Dibb NJ. Dasatinib is a potent inhibitor of tumour-associated macrophages, osteoclasts and the FMS receptor. *Leukemia*. 2009;23(3):590-594.

410. Hiraga T, Nakamura H. Imatinib mesylate suppresses bone metastases of breast cancer by inhibiting osteoclasts through the blockade of c-Fms signals. *Int J Cancer*. 2009;124(1):215-222.

411. Miyazaki T, Katagiri H, Kanegae Y, Takayanagi H, Sawada Y, Yamamoto A, Pando MP, Asano T, Verma IM, Oda H, Nakamura K, Tanaka S. Reciprocal role of ERK and NF-κB pathways in survival and activation of osteoclasts. *J Cell Biol*. 2000;148(2):333-342.

412. Canalis E. Effect of insulinlike growth factor I on DNA and protein synthesis in cultured rat calvaria. *J Clin Invest*. 1980;66(4):709-719.

413. Birnbaum RS, Bowsher RR, Wiren KM. Changes in IGF-I and -II expression and secretion during the proliferation and differentiation of normal rat osteoblasts. *J Endocrinol*. 1995;144(2):251-259.

414. Zhang M, Xuan S, Bouxsein ML, von Stechow D, Akeno N, Faugere MC, Malluche H, Zhao G, Rosen CJ, Efstratiadis A, Clemens TL. Osteoblast-specific knockout of the insulin-like growth factor (IGF) receptor gene reveals an essential role of IGF signaling in bone matrix mineralization. *J Biol Chem*. 2002;277(46):44005-44012.

415. Satomura K, Derubeis AR, Fedarko NS, Ibaraki-O'Connor K, Kuznetsov SA, Rowe DW, Young MF, Gehron Robey P. Receptor tyrosine kinase expression in human bone marrow stromal cells. *J Cell Physiol*. 1998;177(3):426-438.

416. Nakayama K, Tamura Y, Suzawa M, Harada S, Fukumoto S, Kato M, Miyazono K, Rodan GA, Takeuchi Y, Fujita T. Receptor tyrosine kinases inhibit bone morphogenetic protein-Smad responsive promoter activity and differentiation of murine MC3T3-E1 osteoblast-like cells. *J Bone Miner Res*. 2003;18(5):827-835.

417. Kratchmarova I, Blagoev B, Haack-Sorensen M, Kassem M, Mann M. Mechanism of divergent growth factor effects in mesenchymal stem cell differentiation. *Science*. 2005;308(5727):1472-1477.

418. Rodan SB, Wesolowski G, Thomas KA, Yoon K, Rodan GA. Effects of acidic and basic fibroblast growth factors on osteoblastic cells. *Connect Tissue Res*. 1989;20(1-4):283-288.

419. Ballock RT, O'Keefe RJ. The biology of the growth plate. *J Bone Joint Surg Am*. 2003;85-A(4):715-726.

420. Hiraki Y, Inoue H, Hirai R, Kato Y, Suzuki F. Effect of transforming growth factor beta on cell proliferation and glycosaminoglycan synthesis by rabbit growth-plate chondrocytes in culture. *Biochim Biophys Acta*. 1988;969(1):91-99.

421. O'Keefe RJ, Puzas JE, Brand JS, Rosier RN. Effects of transforming growth factor-beta on matrix synthesis by chick growth plate chondrocytes. *Endocrinology*. 1988;122(6):2953-2961.

422. Redini F, Galera P, Mauviel A, Loyau G, Pujol JP. Transforming growth factor beta stimulates collagen and glycosaminoglycan biosynthesis in cultured rabbit articular chondrocytes. *FEBS Lett*. 1988;234(1):172-176.

423. Lee YC, Huang CF, Murshed M, Chu K, Araujo JC, Ye X, Decrombrugghe B, Yu-Lee LY, Gallick GE, Lin SH. Src family kinase/abl inhibitor dasatinib suppresses proliferation and enhances differentiation of osteoblasts. *Oncogene*. 2010;Prepublished on March 15, 2010 as DOI 10.1038/onc.2010.73.

424. Marzia M, Sims NA, Voit S, Migliaccio S, Taranta A, Bernardini S, Faraggiana T, Yoneda T, Mundy GR, Boyce BF, Baron R, Teti A. Decreased c-Src expression enhances osteoblast differentiation and bone formation. *J Cell Biol*. 2000;151(2):311-320.

425. Edwards CM, Mundy GR. Eph receptors and ephrin signaling pathways: a role in bone homeostasis. *Int J Med Sci*. 2008;5(5):263-272.

426. Fabian MA, Biggs WH, 3rd, Treiber DK, Atteridge CE, Azimioara MD, Benedetti MG, Carter TA, Ciceri P, Edeen PT, Floyd M, Ford JM, Galvin M, Gerlach JL, Grotzfeld RM, Herrgard S, Insko DE, Insko MA, Lai AG, Lelias JM, Mehta SA, Milanov ZV,

Velasco AM, Wodicka LM, Patel HK, Zarrinkar PP, Lockhart DJ. A small molecule-kinase interaction map for clinical kinase inhibitors. *Nat Biotechnol*. 2005;23(3):329-336.

427. Allan EH, Hausler KD, Wei T, Gooi JH, Quinn JM, Crimeen-Irwin B, Pompolo S, Sims NA, Gillespie MT, Onyia JE, Martin TJ. EphrinB2 regulation by PTH and PTHrP revealed by molecular profiling in differentiating osteoblasts. *J Bone Miner Res*. 2008;23(8):1170-1181.

428. Xing W, Kim J, Wergedal J, Chen ST, Mohan S. Ephrin B1 regulates bone marrow stromal cell differentiation and bone formation by influencing TAZ transactivation via complex formation with NHERF1. *Mol Cell Biol*. 2010;30(3):711-721.

429. Leitinger B, Kwan AP. The discoidin domain receptor DDR2 is a receptor for type X collagen. *Matrix Biol*. 2006;25(6):355-364.

430. Shrivastava A, Radziejewski C, Campbell E, Kovac L, McGlynn M, Ryan TE, Davis S, Goldfarb MP, Glass DJ, Lemke G, Yancopoulos GD. An orphan receptor tyrosine kinase family whose members serve as nonintegrin collagen receptors. *Mol Cell*. 1997;1(1):25-34.

431. Vogel W, Gish GD, Alves F, Pawson T. The discoidin domain receptor tyrosine kinases are activated by collagen. *Mol Cell*. 1997;1(1):13-23.

432. Leitinger B, Steplewski A, Fertala A. The D2 period of collagen II contains a specific binding site for the human discoidin domain receptor, DDR2. *J Mol Biol*. 2004;344(4):993-1003.

433. Xu L, Peng H, Wu D, Hu K, Goldring MB, Olsen BR, Li Y. Activation of the discoidin domain receptor 2 induces expression of matrix metalloproteinase 13 associated with osteoarthritis in mice. *J Biol Chem*. 2005;280(1):548-555.

434. Calalb MB, Polte TR, Hanks SK. Tyrosine phosphorylation of focal adhesion kinase at sites in the catalytic domain regulates kinase activity: a role for Src family kinases. *Mol Cell Biol*. 1995;15(2):954-963.

435. Gemba T, Valbracht J, Alsalameh S, Lotz M. Focal adhesion kinase and mitogen-activated protein kinases are involved in chondrocyte activation by the 29-kDa amino-terminal fibronectin fragment. *J Biol Chem*. 2002;277(2):907-911.

436. Mahon F-X, Huguet F, Etienne G, Réa D, Cayuela J-M, Marit G, Gardembas M, Reiffers J, Rousselot P. Imatinib mesylate discontinuation in patients with chronic myelogenous leukemia in complete molecular remission: an update follow up. *Blood*. 2008;108:2154.

437. Rousselot P, Huguet F, Rea D, Legros L, Cayuela JM, Maarek O, Blanchet O, Marit G, Gluckman E, Reiffers J, Gardembas M, Mahon FX. Imatinib mesylate discontinuation in patients with chronic myelogenous leukemia in complete molecular remission for more than 2 years. *Blood*. 2007;109(1):58-60.

438. Ross DM, Hughes TP. How complete is "complete" molecular response in imatinib-treated chronic myeloid leukemia? *Leuk Lymphoma*. 2008;49(7):1230-1231.

439. Ross DM, Grigg A, Schwarer A, Arthur C, Loftus K, Mills AK, Filshie R, Columbus R, Reynolds J, Seymour JF, Branford S, Hughes T. The majority of chronic myeloid leukaemia patients who cease imatinib after achieving a sustained complete molecular response (CMR) remain in CMR, and any relapses occur early. *Blood*. 2008;112:1102.

440. Mahon F, Rea D, Guilhot F, Legros L, Guilhot J, Aton E, Dulucq J, Reiffers J, Rousselot P. Persistence of complete molecular remission in chronic myeloid leukemia after imatinib discontinuation: interim analysis of the STIM trial. *Journal of Clinical Oncology*. 2009;27(15s):7084.

441. Mori S, Burr DB. Increased intracortical remodeling following fatigue damage. *Bone*. 1993;14(2):103-109.

442. Burr DB, Forwood MR, Fyhrie DP, Martin RB, Schaffler MB, Turner CH. Bone microdamage and skeletal fragility in osteoporotic and stress fractures. *J Bone Miner Res*. 1997;12(1):6-15.

443. Mashiba T, Turner CH, Hirano T, Forwood MR, Johnston CC, Burr DB. Effects of suppressed bone turnover by bisphosphonates on microdamage accumulation and biomechanical properties in clinically relevant skeletal sites in beagles. *Bone*. 2001;28(5):524-531.

444. Mashiba T, Hirano T, Turner CH, Forwood MR, Johnston CC, Burr DB. Suppressed bone turnover by bisphosphonates increases microdamage accumulation and reduces some biomechanical properties in dog rib. *J Bone Miner Res*. 2000;15(4):613-620.

445. Komatsubara S, Mori S, Mashiba T, Ito M, Li J, Kaji Y, Akiyama T, Miyamoto K, Cao Y, Kawanishi J, Norimatsu H. Long-term treatment of incadronate disodium accumulates microdamage but improves the trabecular bone microarchitecture in dog vertebra. *J Bone Miner Res*. 2003;18(3):512-520.

446. Bone HG, Greenspan SL, McKeever C, Bell N, Davidson M, Downs RW, Emkey R, Meunier PJ, Miller SS, Mulloy AL, Recker RR, Weiss SR, Heyden N, Musliner T, Suryawanshi S, Yates AJ, Lombardi A. Alendronate and estrogen effects in postmenopausal women with low bone mineral density. Alendronate/Estrogen Study Group. *J Clin Endocrinol Metab*. 2000;85(2):720-726.

447. Eriksen EF, Melsen F, Sod E, Barton I, Chines A. Effects of long-term risedronate on bone quality and bone turnover in women with postmenopausal osteoporosis. *Bone*. 2002;31(5):620-625.

448. Ste-Marie LG, Sod E, Johnson T, Chines A. Five years of treatment with risedronate and its effects on bone safety in women with postmenopausal osteoporosis. *Calcif Tissue Int*. 2004;75(6):469-476.

449. Devogelaer JP, Brown JP, Burckhardt P, Meunier PJ, Goemaere S, Lippuner K, Body JJ, Samsioe G, Felsenberg D, Fashola T, Sanna L, Ortmann CE, Trechsel U, Krasnow J, Eriksen EF, Garnero P. Zoledronic acid efficacy and safety over five years in postmenopausal osteoporosis. *Osteoporos Int*. 2007;18(9):1211-1218.

450. Castro-Malaspina H, Schaison G, Briere J, Passe S, Pasquier A, Tanzer J, Jacquillat C, Bernard J. Philadelphia chromosome-positive chronic myelocytic leukemia in children. Survival and prognostic factors. *Cancer*. 1983;52(4):721-727.

451. Kaatsch P. Epidemiology of childhood cancer. *Cancer Treat Rev*. 2010;36(4):277-285.

452. Burke MJ, Willert J, Desai S, Kadota R. The treatment of pediatric Philadelphia positive (Ph+) leukemias in the imatinib era. *Pediatr Blood Cancer*. 2009;53(6):992-995.

453. Zwaan MC, Rizzari C, van der Velden VHJ, Beverloo B, den Boer ML, Baruchel A, Mechinaud F, Lancaster D, Matloub Y, Derreumaux D, Pieters R, Kearns P. Dasatinib in children and adolescents with relapsed or refractory leukemia: interim results of the CA180-018 phase I study from the ITCC Consortium. *Blood*. 2008;112:3241.

454. Aplenc R, Strauss LC, Shusterman S, Ingle AM, Agrawal S, Sun J, Wright JJ, Blaney SM, P.C. A. Pediatric phase I trial and pharmacokinetic (PK) study of dasatinib: A report from the Children's Oncology Group Phase I Consortium. *Journal of Clinical Oncology*. 2008;26:3591.

455. Millot F, Guilhot J, Nelken B, Leblanc T, De Bont ES, Bekassy AN, Gadner H, Sufliarska S, Stary J, Gschaidmeier H, Guilhot F, Suttorp M. Imatinib mesylate is effective in children with chronic myelogenous leukemia in late chronic and advanced phase and in relapse after stem cell transplantation. *Leukemia*. 2006;20(2):187-192.

456. Champagne MA, Fu C, Chang M, Cooley L, Heerema NA, Wood C, French ME, Smith FO, Bernstein ML. Imatinib in children with newly diagnosed chronic phase chronic myelogenous leukemia (CP CML): AAML0123 COG study [abstract]. *Blood*. 2006;108:2140.

457. Giona F, Putti MC, Moleti ML, Nanni M, Testi AM, Varotto S, Gottardi EM, De Vellis A, Nunes V, Diverio D, Leszl A, Saglio G, Foà R. Imatinib mesylate induces high complete cytogenetic and molecular response rates in children and adolescents with Philadelphia chromosome-positive (Ph+) chronic myelogenous leukemia (CML) in chronic phase (CP) [abstract]. *Blood*. 2008;122:4273.

458. Suttorp M, Thiede C, Tauer JT, Roettgers S, Sedlacek P, Harbott J. Chronic myeloid leukemia in pediatrics - first results from study CML-PAED II [abstract]. *Blood*. 2009;114:342.

459. Millot F, Baruchel A, Guilhot J, Petit A, Leblanc T, Bertrand Y, Mazingue F, Patrick L, Vérité C, Berthoux C, Galambrun C, Bernard F, Yacouben K, Bordigoni P, Edan C, Reguerre Y, Couillaud G, Cayuela J-M, Guilhot F. Imatinib is efficient but has a

negative impact on growth in children with previously untreated chronic myelogenous leukaemia (CML) in early chronic phase (CP): results of the French national phase IV trial [abstract]. *Blood*. 2009;114:863.

460. Kebapcilar L, Bilgir O, Alacacioglu I, Payzin B, Bilgir F, Oner P, Sari I, Calan M, Binicier O. Does imatinib mesylate therapy cause growth hormone deficiency? *Med Princ Pract*. 2009;18(5):360-363.

461. Petain A, Kattygnarath D, Azard J, Chatelut E, Delbaldo C, Geoerger B, Barrois M, Seronie-Vivien S, LeCesne A, Vassal G. Population pharmacokinetics and pharmacogenetics of imatinib in children and adults. *Clin Cancer Res*. 2008;14(21):7102-7109.

462. Bond M, Bernstein ML, Pappo A, Schultz KR, Krailo M, Blaney SM, Adamson PC. A phase II study of imatinib mesylate in children with refractory or relapsed solid tumors: a Children's Oncology Group study. *Pediatr Blood Cancer*. 2008;50(2):254-258.

463. Baruchel S, Sharp JR, Bartels U, Hukin J, Odame I, Portwine C, Strother D, Fryer C, Halton J, Egorin MJ, Reis RM, Martinho O, Stempak D, Hawkins C, Gammon J, Bouffet E. A Canadian paediatric brain tumour consortium (CPBTC) phase II molecularly targeted study of imatinib in recurrent and refractory paediatric central nervous system tumours. *Eur J Cancer*. 2009;45(13):2352-2359.

464. Southby J, Kissin MW, Danks JA, Hayman JA, Moseley JM, Henderson MA, Bennett RC, Martin TJ. Immunohistochemical localization of parathyroid hormone-related protein in human breast cancer. *Cancer Res*. 1990;50(23):7710-7716.

465. Powell GJ, Southby J, Danks JA, Stillwell RG, Hayman JA, Henderson MA, Bennett RC, Martin TJ. Localization of parathyroid hormone-related protein in breast cancer metastases: increased incidence in bone compared with other sites. *Cancer Res*. 1991;51(11):3059-3061.

466. Guise TA, Yin JJ, Taylor SD, Kumagai Y, Dallas M, Boyce BF, Yoneda T, Mundy GR. Evidence for a causal role of parathyroid hormone-related protein in the pathogenesis of human breast cancer-mediated osteolysis. *J Clin Invest*. 1996;98(7):1544-1549.

467. Choi SJ, Cruz JC, Craig F, Chung H, Devlin RD, Roodman GD, Alsina M. Macrophage inflammatory protein 1-alpha is a potential osteoclast stimulatory factor in multiple myeloma. *Blood*. 2000;96(2):671-675.

468. Bryden AA, Hoyland JA, Freemont AJ, Clarke NW, George NJ. Parathyroid hormone related peptide and receptor expression in paired primary prostate cancer and bone metastases. *Br J Cancer*. 2002;86(3):322-325.

469. Tian E, Zhan F, Walker R, Rasmussen E, Ma Y, Barlogie B, Shaughnessy JD, Jr. The role of the Wnt-signaling antagonist DKK1 in the development of osteolytic lesions in multiple myeloma. *N Engl J Med*. 2003;349(26):2483-2494.

470. Politou MC, Heath DJ, Rahemtulla A, Szydlo R, Anagnostopoulos A, Dimopoulos MA, Croucher PI, Terpos E. Serum concentrations of Dickkopf-1 protein are increased in patients with multiple myeloma and reduced after autologous stem cell transplantation. *Int J Cancer*. 2006;119(7):1728-1731.

471. Yaccoby S, Ling W, Zhan F, Walker R, Barlogie B, Shaughnessy JD, Jr. Antibody-based inhibition of DKK1 suppresses tumor-induced bone resorption and multiple myeloma growth in vivo. *Blood*. 2007;109(5):2106-2111.

472. Heath DJ, Chantry AD, Buckle CH, Coulton L, Shaughnessy JD, Jr., Evans HR, Snowden JA, Stover DR, Vanderkerken K, Croucher PI. Inhibiting Dickkopf-1 (Dkk1) removes suppression of bone formation and prevents the development of osteolytic bone disease in multiple myeloma. *J Bone Miner Res*. 2009;24(3):425-436.

473. Nelson JB, Hedican SP, George DJ, Reddi AH, Piantadosi S, Eisenberger MA, Simons JW. Identification of endothelin-1 in the pathophysiology of metastatic adenocarcinoma of the prostate. *Nat Med*. 1995;1(9):944-949.

474. Nelson JB, Chan-Tack K, Hedican SP, Magnuson SR, Opgenorth TJ, Bova GS, Simons JW. Endothelin-1 production and decreased endothelin B receptor expression in advanced prostate cancer. *Cancer Res*. 1996;56(4):663-668.

475. Eaton CL, Coleman RE. Pathophysiology of bone metastases from prostate cancer and the role of bisphosphonates in treatment. *Cancer Treat Rev*. 2003;29(3):189-198.

476. Mystakidou K, Katsouda E, Stathopoulou E, Vlahos L. Approaches to managing bone metastases from breast cancer: the role of bisphosphonates. *Cancer Treat Rev*. 2005;31(4):303-311.

477. Harousseau JL, Dreyling M. Multiple myeloma: ESMO clinical recommendations for diagnosis, treatment and follow-up. *Ann Oncol*. 2009;20 Suppl 4:97-99.

478. Terpos E, Sezer O, Croucher PI, Garcia-Sanz R, Boccadoro M, San Miguel J, Ashcroft J, Blade J, Cavo M, Delforge M, Dimopoulos MA, Facon T, Macro M, Waage A, Sonneveld P. The use of bisphosphonates in multiple myeloma: recommendations of an expert panel on behalf of the European Myeloma Network. *Ann Oncol*. 2009;20(8):1303-1317.

479. Cardoso F, Castiglione M. Locally recurrent or metastatic breast cancer: ESMO clinical recommendations for diagnosis, treatment and follow-up. *Ann Oncol*. 2009;20 Suppl 4:15-18.

480. Theriault RL, Lipton A, Hortobagyi GN, Leff R, Gluck S, Stewart JF, Costello S, Kennedy I, Simeone J, Seaman JJ, Knight RD, Mellars K, Heffernan M, Reitsma DJ. Pamidronate reduces skeletal morbidity in women with advanced breast cancer and lytic bone lesions: a randomized, placebo-controlled trial. Protocol 18 Aredia Breast Cancer Study Group. *J Clin Oncol*. 1999;17(3):846-854.

481. Berenson JR, Rosen LS, Howell A, Porter L, Coleman RE, Morley W, Dreicer R, Kuross SA, Lipton A, Seaman JJ. Zoledronic acid reduces skeletal-related events in patients with osteolytic metastases. *Cancer*. 2001;91(7):1191-1200.

482. Body JJ, Diel IJ, Lichinitser MR, Kreuser ED, Dornoff W, Gorbunova VA, Budde M, Bergstrom B. Intravenous ibandronate reduces the incidence of skeletal complications in patients with breast cancer and bone metastases. *Ann Oncol*. 2003;14(9):1399-1405.

483. Body JJ, Diel IJ, Lichinitzer M, Lazarev A, Pecherstorfer M, Bell R, Tripathy D, Bergstrom B. Oral ibandronate reduces the risk of skeletal complications in breast cancer patients with metastatic bone disease: results from two randomised, placebo-controlled phase III studies. *Br J Cancer*. 2004;90(6):1133-1137.

484. Diel IJ, Body JJ, Lichinitser MR, Kreuser ED, Dornoff W, Gorbunova VA, Budde M, Bergstrom B. Improved quality of life after long-term treatment with the bisphosphonate ibandronate in patients with metastatic bone disease due to breast cancer. *Eur J Cancer*. 2004;40(11):1704-1712.

485. Saad F, Gleason DM, Murray R, Tchekmedyian S, Venner P, Lacombe L, Chin JL, Vinholes JJ, Goas JA, Chen B. A randomized, placebo-controlled trial of zoledronic acid in patients with hormone-refractory metastatic prostate carcinoma. *J Natl Cancer Inst*. 2002;94(19):1458-1468.

486. Lahtinen R, Laakso M, Palva I, Virkkunen P, Elomaa I. Randomised, placebo-controlled multicentre trial of clodronate in multiple myeloma. Finnish Leukaemia Group. *Lancet*. 1992;340(8827):1049-1052.

487. McCloskey EV, Dunn JA, Kanis JA, MacLennan IC, Drayson MT. Long-term follow-up of a prospective, double-blind, placebo-controlled randomized trial of clodronate in multiple myeloma. *Br J Haematol*. 2001;113(4):1035-1043.

488. Musto P, Falcone A, Sanpaolo G, Bodenizza C, Cascavilla N, Melillo L, Scalzulli PR, Dell'Olio M, La Sala A, Mantuano S, Nobile M, Carella AM. Pamidronate reduces skeletal events but does not improve progression-free survival in early-stage untreated myeloma: results of a randomized trial. *Leuk Lymphoma*. 2003;44(9):1545-1548.

489. Hortobagyi GN, Theriault RL, Porter L, Blayney D, Lipton A, Sinoff C, Wheeler H, Simeone JF, Seaman J, Knight RD. Efficacy of pamidronate in reducing skeletal complications in patients with breast cancer and lytic bone metastases. Protocol 19 Aredia Breast Cancer Study Group. *N Engl J Med*. 1996;335(24):1785-1791.

490. Lipton A, Theriault RL, Hortobagyi GN, Simeone J, Knight RD, Mellars K, Reitsma DJ, Heffernan M, Seaman JJ. Pamidronate prevents skeletal complications and is effective palliative treatment in women with breast carcinoma and osteolytic bone metastases: long term follow-up of two randomized, placebo-controlled trials. *Cancer*. 2000;88(5):1082-1090.

491. Bamias A, Kastritis E, Bamia C, Moulopoulos LA, Melakopoulos I, Bozas G, Koutsoukou V, Gika D, Anagnostopoulos A, Papadimitriou C, Terpos E, Dimopoulos MA. Osteonecrosis of the jaw in cancer after treatment with bisphosphonates: incidence and risk factors. *J Clin Oncol*. 2005;23(34):8580-8587.

492. Woo SB, Hellstein JW, Kalmar JR. Narrative review: bisphosphonates and osteonecrosis of the jaws. *Ann Intern Med*. 2006;144(10):753-761.

493. Van den Wyngaert T, Huizing MT, Vermorken JB. Bisphosphonates and osteonecrosis of the jaw: cause and effect or a post hoc fallacy? *Ann Oncol*. 2006;17(8):1197-1204.

494. Dimopoulos MA, Kastritis E, Anagnostopoulos A, Melakopoulos I, Gika D, Moulopoulos LA, Bamia C, Terpos E, Tsionos K, Bamias A. Osteonecrosis of the jaw in patients with multiple myeloma treated with bisphosphonates: evidence of increased risk after treatment with zoledronic acid. *Haematologica*. 2006;91(7):968-971.

495. Estilo CL, Van Poznak CH, Wiliams T, Bohle GC, Lwin PT, Zhou Q, Riedel ER, Carlson DL, Schoder H, Farooki A, Fornier M, Halpern JL, Tunick SJ, Huryn JM. Osteonecrosis of the maxilla and mandible in patients with advanced cancer treated with bisphosphonate therapy. *Oncologist*. 2008;13(8):911-920.

496. Ibrahim T, Barbanti F, Giorgio-Marrano G, Mercatali L, Ronconi S, Vicini C, Amadori D. Osteonecrosis of the jaw in patients with bone metastases treated with bisphosphonates: a retrospective study. *Oncologist*. 2008;13(3):330-336.

497. Filleul O, Crompot E, Saussez S. Bisphosphonate-induced osteonecrosis of the jaw: a review of 2,400 patient cases. *J Cancer Res Clin Oncol*. 2010;Prepublished on May 29, 2010 as DOI 10.1007/s00432-010-0907-7.

498. Bounameaux HM, Schifferli J, Montani JP, Jung A, Chatelanat F. Renal failure associated with intravenous diphosphonates. *Lancet*. 1983;1(8322):471.

499. Markowitz GS, Appel GB, Fine PL, Fenves AZ, Loon NR, Jagannath S, Kuhn JA, Dratch AD, D'Agati VD. Collapsing focal segmental glomerulosclerosis following treatment with high-dose pamidronate. *J Am Soc Nephrol*. 2001;12(6):1164-1172.

500. Rosen LS, Gordon D, Kaminski M, Howell A, Belch A, Mackey J, Apffelstaedt J, Hussein M, Coleman RE, Reitsma DJ, Seaman JJ, Chen BL, Ambros Y. Zoledronic acid versus pamidronate in the treatment of skeletal metastases in patients with breast cancer or osteolytic lesions of multiple myeloma: a phase III, double-blind, comparative trial. *Cancer J*. 2001;7(5):377-387.

501. Markowitz GS, Fine PL, Stack JI, Kunis CL, Radhakrishnan J, Palecki W, Park J, Nasr SH, Hoh S, Siegel DS, D'Agati VD. Toxic acute tubular necrosis following treatment with zoledronate (Zometa). *Kidney Int*. 2003;64(1):281-289.

502. Chang JT, Green L, Beitz J. Renal failure with the use of zoledronic acid. *N Engl J Med*. 2003;349(17):1676-1679; discussion 1676-1679.

503. Berenson JR, Hillner BE, Kyle RA, Anderson K, Lipton A, Yee GC, Biermann JS. American Society of Clinical Oncology clinical practice guidelines: the role of bisphosphonates in multiple myeloma. *J Clin Oncol*. 2002;20(17):3719-3736.

504. Lacy MQ, Dispenzieri A, Gertz MA, Greipp PR, Gollbach KL, Hayman SR, Kumar S, Lust JA, Rajkumar SV, Russell SJ, Witzig TE, Zeldenrust SR, Dingli D, Bergsagel PL, Fonseca R, Reeder CB, Stewart AK, Roy V, Dalton RJ, Carr AB, Kademani D, Keller EE, Viozzi CF, Kyle RA. Mayo clinic consensus statement for the use of bisphosphonates in multiple myeloma. *Mayo Clin Proc*. 2006;81(8):1047-1053.

505. Dunstan CR, Felsenberg D, Seibel MJ. Therapy insight: the risks and benefits of bisphosphonates for the treatment of tumor-induced bone disease. *Nat Clin Pract Oncol*. 2007;4(1):42-55.

506. Kyle RA, Yee GC, Somerfield MR, Flynn PJ, Halabi S, Jagannath S, Orlowski RZ, Roodman DG, Twilde P, Anderson K. American Society of Clinical Oncology 2007 clinical practice guideline update on the role of bisphosphonates in multiple myeloma. *J Clin Oncol*. 2007;25(17):2464-2472.

507. Aapro M, Abrahamsson PA, Body JJ, Coleman RE, Colomer R, Costa L, Crino L, Dirix L, Gnant M, Gralow J, Hadji P, Hortobagyi GN, Jonat W, Lipton A, Monnier A, Paterson AH, Rizzoli R, Saad F, Thurlimann B. Guidance on the use of bisphosphonates in solid tumours: recommendations of an international expert panel. *Ann Oncol*. 2008;19(3):420-432.

508. Dickinson M, Prince HM, Kirsa S, Zannettino A, Gibbs SD, Mileshkin L, O'Grady J, Seymour JF, Szer J, Horvath N, Joshua DE. Osteonecrosis of the jaw complicating bisphosphonate treatment for bone disease in multiple myeloma: an overview with recommendations for prevention and treatment. *Intern Med J*. 2009;39(5):304-316.

509. Chelouche Lev D, Kim SJ, Onn A, Stone V, Nam DH, Yazici S, Fidler IJ, Price JE. Inhibition of platelet-derived growth factor receptor signaling restricts the growth of human breast cancer in the bone of nude mice. *Clin Cancer Res*. 2005;11(1):306-314.

510. Uehara H, Kim SJ, Karashima T, Shepherd DL, Fan D, Tsan R, Killion JJ, Logothetis C, Mathew P, Fidler IJ. Effects of blocking platelet-derived growth factor-receptor signaling in a mouse model of experimental prostate cancer bone metastases. *J Natl Cancer Inst*. 2003;95(6):458-470.

511. Kim SJ, Uehara H, Yazici S, Langley RR, He J, Tsan R, Fan D, Killion JJ, Fidler IJ. Simultaneous blockade of platelet-derived growth factor-receptor and epidermal growth factor-receptor signaling and systemic administration of paclitaxel as therapy for human prostate cancer metastasis in bone of nude mice. *Cancer Res*. 2004;64(12):4201-4208.

512. Kim SJ, Uehara H, Yazici S, He J, Langley RR, Mathew P, Fan D, Fidler IJ. Modulation of bone microenvironment with zoledronate enhances the therapeutic effects of STI571 and paclitaxel against experimental bone metastasis of human prostate cancer. *Cancer Res*. 2005;65(9):3707-3715.

513. Koreckij T, Nguyen H, Brown LG, Yu EY, Vessella RL, Corey E. Dasatinib inhibits the growth of prostate cancer in bone and provides additional protection from osteolysis. *Br J Cancer*. 2009;101(2):263-268.

514. Kubler HR, van Randenborgh H, Treiber U, Wutzler S, Battistel C, Lehmer A, Wagenpfeil S, Hartung R, Paul R. In vitro cytotoxic effects of imatinib in combination with anticancer drugs in human prostate cancer cell lines. *Prostate*. 2005;63(4):385-394.

515. Brama M, Basciani S, Cherubini S, Mariani S, Migliaccio S, Arizzi M, Rosano G, Spera G, Gnessi L. Osteoblast-conditioned medium promotes proliferation and sensitizes breast cancer cells to imatinib treatment. *Endocr Relat Cancer*. 2007;14(1):61-72.

516. Coluccia AM, Cirulli T, Neri P, Mangieri D, Colanardi MC, Gnoni A, Di Renzo N, Dammacco F, Tassone P, Ribatti D, Gambacorti-Passerini C, Vacca A. Validation of PDGFRbeta and c-Src tyrosine kinases as tumor/vessel targets in patients with multiple myeloma: preclinical efficacy of the novel, orally available inhibitor dasatinib. *Blood*. 2008;112(4):1346-1356.

517. Choi YL, Bocanegra M, Kwon MJ, Shin YK, Nam SJ, Yang JH, Kao J, Godwin AK, Pollack JR. LYN is a mediator of epithelial-mesenchymal transition and a target of dasatinib in breast cancer. *Cancer Res*. 2010;70(6):2296-2306.

518. Park SI, Zhang J, Phillips KA, Araujo JC, Najjar AM, Volgin AY, Gelovani JG, Kim SJ, Wang Z, Gallick GE. Targeting SRC family kinases inhibits growth and lymph node metastases of prostate cancer in an orthotopic nude mouse model. *Cancer Res*. 2008;68(9):3323-3333.

519. Breccia M, De Cuia MR, D'Elia GM, Francesca B, Mandelli F, Alimena G. Response of prostate cancer during imatinib therapy in a patient with chronic myeloid leukemia. *Haematologica*. 2004;89(7):e68-e69.

520. Rao K, Goodin S, Levitt MJ, Dave N, Shih WJ, Lin Y, Capanna T, Doyle-Lindrud S, Juvidian P, DiPaola RS. A phase II trial of imatinib mesylate in patients with prostate specific antigen progression after local therapy for prostate cancer. *Prostate*. 2005;62(2):115-122.

521. Lin AM, Rini BI, Weinberg V, Fong K, Ryan CJ, Rosenberg JE, Fong L, Small EJ. A phase II trial of imatinib mesylate in patients with biochemical relapse of prostate cancer after definitive local therapy. *BJU Int*. 2006;98(4):763-769.

522. Mathew P, Pisters LL, Wood CG, Papadopoulos JN, Williams DL, Thall PF, Wen S, Horne E, Oborn CJ, Langley R, Fidler IJ, Pettaway CA. Neoadjuvant platelet derived

growth factor receptor inhibitor therapy combined with docetaxel and androgen ablation for high risk localized prostate cancer. *J Urol*. 2009;181(1):81-87.

523. Bajaj GK, Zhang Z, Garrett-Mayer E, Drew R, Sinibaldi V, Pili R, Denmeade SR, Carducci MA, Eisenberger MA, DeWeese TL. Phase II study of imatinib mesylate in patients with prostate cancer with evidence of biochemical relapse after definitive radical retropubic prostatectomy or radiotherapy. *Urology*. 2007;69(3):526-531.

524. Modi S, Seidman AD, Dickler M, Moasser M, D'Andrea G, Moynahan ME, Menell J, Panageas KS, Tan LK, Norton L, Hudis CA. A phase II trial of imatinib mesylate monotherapy in patients with metastatic breast cancer. *Breast Cancer Res Treat*. 2005;90(2):157-163.

525. Cristofanilli M, Morandi P, Krishnamurthy S, Reuben JM, Lee BN, Francis D, Booser DJ, Green MC, Arun BK, Pusztai L, Lopez A, Islam R, Valero V, Hortobagyi GN. Imatinib mesylate (Gleevec) in advanced breast cancer-expressing C-Kit or PDGFR-β: clinical activity and biological correlations. *Ann Oncol*. 2008;19(10):1713-1719.

526. Tiffany NM, Wersinger EM, Garzotto M, Beer TM. Imatinib mesylate and zoledronic acid in androgen-independent prostate cancer. *Urology*. 2004;63(5):934-939.

527. Mathew P, Thall PF, Bucana CD, Oh WK, Morris MJ, Jones DM, Johnson MM, Wen S, Pagliaro LC, Tannir NM, Tu SM, Meluch AA, Smith L, Cohen L, Kim SJ, Troncoso P, Fidler IJ, Logothetis CJ. Platelet-derived growth factor receptor inhibition and chemotherapy for castration-resistant prostate cancer with bone metastases. *Clin Cancer Res*. 2007;13(19):5816-5824.

528. Yu EY, Wilding G, Posadas E, Gross M, Culine S, Massard C, Morris MJ, Hudes G, Calabro F, Cheng S, Trudel GC, Paliwal P, Sternberg CN. Phase II study of dasatinib in patients with metastatic castration-resistant prostate cancer. *Clin Cancer Res*. 2009;15(23):7421-7428.